

November 2011

Morpho-physiological analysis of interneuronal populations in the rat piriform cortex before and after kindling induced epilepsy

Cezar Gavrilovici

The University of Western Ontario

Supervisor

Dr. Michael O. Poulter

The University of Western Ontario

Graduate Program in Physiology

A thesis submitted in partial fulfillment of the requirements for the degree in Doctor of Philosophy

© Cezar Gavrilovici 2011

Follow this and additional works at: <https://ir.lib.uwo.ca/etd>



Part of the [Cellular and Molecular Physiology Commons](#)

Recommended Citation

Gavrilovici, Cezar, "Morpho-physiological analysis of interneuronal populations in the rat piriform cortex before and after kindling induced epilepsy" (2011). *Electronic Thesis and Dissertation Repository*. 310.

<https://ir.lib.uwo.ca/etd/310>

This Dissertation/Thesis is brought to you for free and open access by Scholarship@Western. It has been accepted for inclusion in Electronic Thesis and Dissertation Repository by an authorized administrator of Scholarship@Western. For more information, please contact tadam@uwo.ca, wlsadmin@uwo.ca.

MORPHO-PHYSIOLOGICAL ANALYSIS OF INTERNEURONAL
POPULATIONS IN THE RAT PIRIFORM CORTEX BEFORE AND AFTER
KINDLING INDUCED EPILEPSY.

(Spine title: Kindling induced alterations in piriform cortex)

(Thesis format: Integrated-Article)

by

Cezar N. Gavrilovici

Graduate Program in Physiology

A thesis submitted in partial fulfillment
of the requirements for the degree of
Doctor of Philosophy

The School of Graduate and Postdoctoral Studies
The University of Western Ontario
London, Ontario, Canada

© Cezar Gavrilovici 2011

THE UNIVERSITY OF WESTERN ONTARIO
School of Graduate and Postdoctoral Studies

CERTIFICATE OF EXAMINATION

Supervisor

Dr. Michael Poulter

Examiners

Dr. Peter Carlen

Supervisory Committee

Dr. Stan Leung

Dr. Arthur Brown

Dr. Stephen Sims

Dr. Wei-Yang Lu

Dr. Donglin Bai

Dr. Susanne Schmid

The thesis by

Cezar Nicolae Gavrilovici

entitled:

**MORPHO-PHYSIOLOGICAL ANALYSIS OF INTERNEURONAL
POPULATIONS IN THE RAT PIRIFORM CORTEX BEFORE AND
AFTER KINDLING INDUCED EPILEPSY**

is accepted in partial fulfillment of the
requirements for the degree of
Doctor of Philosophy

Date

Chair of the Thesis Examination Board

ABSTRACT

The piriform cortex (PC) is involved in olfactory sensory processing, associative learning tasks and is highly seizurogenic. Understanding how interneurons participate in these behaviours, especially their contribution in epileptogenic mechanisms, is hampered by an incomplete understanding of their functional and morphological diversity. The hypothesis in this work is that kindling-induced epilepsy alters the firing properties of PC interneuronal populations. Altered/impaired interneuronal firing could lead to abnormal processing in the PC and epileptogenesis. Therefore it was important to first identify and describe interneuronal morpho-functional properties in the unkindled brain and then to assess the electrophysiological parameters following kindling.

Based on interneuronal calcium-binding protein content, immunohistochemical analysis of PC showed that the four distinct interneuronal populations (calretinin, calbindin, parvalbumin, and parvalbumin/calbindin containing interneurons) had distinct layer localizations, preferred dendritic arborization patterns and specific innervations onto interneurons and pyramidal cells.

Whole cell patch-clamp recordings of PC interneuronal populations indicated a large heterogeneity of firing patterns that could be classified into five main patterns ranging from non-adapting very high frequency (NAvHF) to various degrees of spiking adaptation: adapting high frequency (AHF), adapting low frequency (ALF), strongly adapting low frequency (sALF), and weakly adapting low frequency (wALF). This high firing variability in the PC suggests that different interneuronal populations might have distinct functional means to control and regulate the olfactory network processing, memory coding and/or generation of oscillatory activities. However, after kindling, NAvHF and wALF

firing patterns were absent. These changes were correlated to an increased K^+ current in multipolar cells. This result was confirmed by quantitative real time polymerase chain reaction (QPCR) and immunohistochemistry studies indicating an increased expression of a voltage-gated potassium channel Kv1.6 after kindling. Thus, kindling-induced alteration of interneuronal firing properties, especially the absence of NAvHF firing behaviour, might reduce the efficacy of inhibition on the pyramidal cells leading to increased disinhibition and/or altered oscillatory activities in the PC.

Overall, this work provides a morpho-functional analysis of PC interneuronal populations indicating a high complexity of innervation and firing behaviours. It also shows for the first time that kindling induces alterations of interneuronal firing patterns that might be responsible for epileptogenesis in this area.

KEYWORDS: piriform cortex; interneuron; temporal lobe epilepsy; kindling; calcium-binding proteins; firing pattern; immunohistochemistry; whole cell recordings.

CO-AUTHORSHIP

Chapter 2 entitled “Diverse interneuron population have highly specific interconnectivity in the rat piriform cortex” was previously published in *Journal of Comparative Neurology*, 2010, **518**:1570-88 (Co-authored by C. Gavrilovici, S. D’Alfonso and M.O. Poulter). Immunohistochemistry was performed by S. D’Alfonso and C. Gavrilovici. Data analysis and writing were performed by C. Gavrilovici.

Chapter 3 entitled: “Diverse interneuron firing modes between layers of the rat piriform cortex“ was co-authored by C. Gavrilovici and M.O. Poulter. All experimental work, data analysis and writing were performed by C. Gavrilovici.

Chapter 4 entitled “Kindling-induced alterations of interneuronal firing pattern in the piriform cortex“ was co-authored by C. Gavrilovici, E. Pollock, M. Everest and M.O. Poulter. QPCR was performed by M. Everest. Immunohistochemistry was performed by E. Pollock. All other experimental work, data analysis and writing were performed by C. Gavrilovici.

ACKNOWLEDGEMENTS

The author would like to thank Dr. Michael Poulter for guidance and support throughout this project; to his advisory committee members, Dr. Stephen Sims, Dr. Stan Leung and Dr. Arthur Brown for valuable suggestions and their availability.

Special thanks must be also addressed to those who helped my work, provided assistance or just for their friendship during these years: Sabrina D'Alfonso, Douglas Salgado, Chris Drummond Main, Arash Kia, Michelle Everest, Zeinab Birjandian, Fiona Simpson, Emily Pollock, Vladimir Zhurov and Deborah Andersen.

Finally, I would like to thank my family for their unconditional love and patience.

I acknowledge the financial support from the Ontario Graduate Studentship (OGS).

TABLE OF CONTENTS

| | |
|--|----------|
| Certificate of examination | ii |
| Abstract | iii |
| Co-Authorship | v |
| Acknowledgements | vi |
| Table of Contents | vii |
| List of Figures | xii |
| List of Tables | xv |
| Abbreviations | xvi |
| | |
| CHAPTER 1. General introduction and thesis overview | 1 |
| 1.1 Piriform cortex | 1 |
| 1.1.1 PC divisions and heterogeneity | 1 |
| 1.1.2 Laminar organization of PC | 3 |
| 1.1.3 Inhibitory processes in PC | 3 |
| 1.1.3.1 General characteristics of interneurons | 4 |
| 1.1.3.2 Molecular markers of PC interneurons | 5 |
| 1.1.3.3 Firing properties of PC interneurons | 5 |
| 1.1.3.4 Feedback and feedforward circuits in piriform cortex | 6 |
| 1.1.3.5 Dendritic and somatic inhibitory postsynaptic potentials in the piriform cortex | 7 |
| 1.2 Epilepsy | 8 |
| 1.2.1 Temporal lobe epilepsy | 9 |
| 1.2.2 Animal models of temporal lobe epilepsy | 11 |
| 1.2.3 Post status models | 12 |

| | | |
|---|--|-----------|
| 1.2.4 | Kindling model of epilepsy | 13 |
| 1.2.4.1 | Kindling model characteristics and classification of clinical manifestations | 13 |
| 1.2.4.2 | Kindling-induced structural brain changes | 14 |
| 1.2.4.3 | Kindling-induced alterations of excitatory and inhibitory synaptic transmission | 14 |
| 1.2.4.4 | Kindling-induced alterations in voltage gated receptor properties | 16 |
| 1.2.4.5 | Advantages and limitations of kindling model | 16 |
| 1.3 | Piriform cortex involvement in limbic seizures | 17 |
| 1.3.1 | Piriform cortex anatomical connection to other limbic structures | 17 |
| 1.3.2 | Neuronal activation and metabolic rate studies in the piriform cortex | 18 |
| 1.3.3 | Afterdischarge events, interictal spikes, spontaneous bursting in the piriform cortex | 18 |
| 1.3.4 | Lesional studies underlying the importance of PC in epileptogenesis | 19 |
| 1.4 | GABAergic system and epilepsy | 20 |
| 1.4.1 | GABA receptors | 20 |
| 1.4.2 | GABA _A receptor alterations in genetic models of epilepsy | 21 |
| 1.4.3 | GABAergic interneurons and epilepsy | 22 |
| 1.5 | Thesis outline | 23 |
| 1.6 | References | 25 |
| | | |
| CHAPTER 2. Diverse interneuron populations have highly specific interconnectivity in the rat piriform cortex | | 40 |
| 2.1 | Introduction | 40 |
| 2.2 | Methods | 42 |
| 2.2.1 | Tissue preparation and fixation | 42 |

| | | |
|--|--|---------------|
| 2.2.2 | Antigen retrieval and immunohistochemistry | 43 |
| 2.2.3 | Antibodies | 44 |
| 2.2.4 | Image acquisition | 47 |
| 2.2.5 | Image processing and analysis | 49 |
| 2.2.5.1 | Interneuron localization in PC | 49 |
| 2.2.5.2 | CBP colocalization | 49 |
| 2.2.5.3 | Dendritic arborization of interneurons defined by neurochemical content | 50 |
| 2.2.5.4 | Innervation of interneurons defined by neurochemical content and coexpression | 51 |
| 2.2.6 | Cell nomenclature | 53 |
| 2.3 | Results | 53 |
| 2.3.1 | Interneuron localization in PC | 53 |
| 2.3.2 | CBP colocalization | 57 |
| 2.3.3 | Morphological characterization of interneurons defined by neurochemical content | 60 |
| 2.3.4 | Innervation of interneurons defined by neurochemical content and coexpression | 67 |
| 2.4 | Discussion | 74 |
| 2.5 | References | 83 |
| CHAPTER 3. Diverse interneuron firing modes between layers of the rat piriform cortex | | 89 |
| 3.1 | Introduction | 89 |
| 3.2 | Methods | 91 |
| 3.2.1 | Tissue preservation, slicing procedures and maintenance | 91 |
| 3.2.2 | Electrophysiology | 91 |
| 3.2.3 | Cluster analysis & statistics | 92 |
| 3.2.4 | Histochemistry | 93 |

| | |
|---|------------|
| 3.2.5 Image acquisition and morphological reconstruction of patched neurons | 97 |
| 3.3 Results | 98 |
| 3.3.1 High frequency spiking interneurons | 99 |
| 3.3.2 Low firing frequency interneurons | 100 |
| 3.3.3 Intra-layer localization analysis | 108 |
| 3.3.4 Comparison of firing patterns with morphological attributes | 111 |
| 3.4 Discussion | 116 |
| 3.4.1 Comparison of aPC spiking patterns to those found in other cortical and limbic regions | 116 |
| 3.4.2 How do these firing patterns control the activity of the aPC? | 117 |
| 3.4.3 Morphological and functional correlations | 119 |
| 3.5 References | 122 |
| | |
| CHAPTER 4. Kindling-induced alterations of interneuronal firing pattern in the piriform cortex | 127 |
| 4.1 Introduction | 127 |
| 4.2 Methods | 129 |
| 4.2.1 Animals and surgery | 129 |
| 4.2.1.1 Electrode implantation | 129 |
| 4.2.1.2 Kindling and slice preparation | 129 |
| 4.2.2 Electrophysiology | 130 |
| 4.2.3 Cluster analysis & statistics | 132 |
| 4.2.4 Histochemistry | 132 |
| 4.2.4.1 Image acquisition and morphological reconstruction of patched neurons | 132 |
| 4.2.4.2 Parvalbumin/Kv1.6 colocalization | 134 |
| 4.2.5 RT-QPCR | 135 |
| 4.3 Results | 137 |

| | | |
|-------------------------|---|------------|
| 4.3.1 | Intra-layer localization analysis | 144 |
| 4.3.2 | Comparison of firing patterns with morphological attributes | 148 |
| 4.3.3 | Kindling-induced alteration of voltage-gated K ⁺ channels | 148 |
| 4.4 | Discussion | 157 |
| 4.5 | References | 161 |
| | | |
| CHAPTER 5. | General discussion | 165 |
| 5.1 | Morphological analysis of PC interneuronal populations | 166 |
| 5.2 | Electrophysiological study of PC interneuronal populations | 168 |
| 5.3 | Kindling induced alterations in the firing pattern of interneuronal populations | 169 |
| 5.4 | Further studies | 173 |
| 5.5 | References | 175 |
| | | |
| Appendix A. | Gene table for RT² Profiler™ rat PCR Array | 179 |
| Appendix B. | Ethics approval (rat) | 183 |
| Appendix C. | Copyright license agreement | 184 |
| Curriculum Vitae | | 189 |

LIST OF FIGURES

| | |
|---|----|
| Fig. 2.1 Example of the raw data showing two channels of images and the colocalized channel (white), which was added after appropriate thresholding of the magenta and green channels. | 48 |
| Fig. 2.2 General distribution of calcium-binding protein (CBP) interneurons in the piriform cortex. | 55 |
| Fig. 2.3 Calcium-binding protein immunoreactive (CBP-IR) cell distribution in each layer of the piriform cortex. | 58 |
| Fig. 2.4 Parvalbumin/calbindin (PV/CB) colocalization in the piriform cortex. | 59 |
| Fig. 2.5 Parvalbumin/calretinin (PV-CR) colocalization in the piriform cortex. | 61 |
| Fig. 2.6 Calbindin dendritic arborization in L3 of the piriform cortex. | 62 |
| Fig. 2.7 Parvalbumin dendritic arborization in the piriform cortex. | 63 |
| Fig. 2.8 Calretinin dendritic arborization in the piriform cortex. | 64 |
| Fig. 2.9 Calbindin-, parvalbumin-, and parvalbumin/calbindin-expressing nerve terminal distribution in the piriform cortex. | 71 |
| Fig. 2.10 Calretinin nerve terminal distribution in the piriform cortex. | 73 |
| Fig. 2.11 Hypothetical circuit indicating the contribution of calcium-binding protein immunoreactive (CBP-IR) interneurons to the feedback inhibition loop of piriform cortex. | 79 |
| Fig. 2.12 Hypothetical circuit indicating the contribution of calcium-binding protein immunoreactive (CBP-IR) interneurons to the feed-forward inhibition loop of piriform cortex. | 80 |
| Fig. 2.13 Inhibitory innervations on the calcium-binding protein immunoreactive (CBP-IR) interneurons of piriform cortex. | 81 |
| Fig. 3.1 Cluster analysis of electrophysiological properties of rat aPC interneuronal populations before kindling-induced epilepsy. | 95 |

| | |
|--|-----|
| Fig. 3.2 Firing pattern classification and terminology. | 96 |
| Fig. 3.3 Distribution of the five types of firing patterns in the anterior piriform cortex of rat | 101 |
| Fig. 3.4 Electrophysiological properties of non-adapting very high frequency (NAvHF) cell type. | 103 |
| Fig. 3.5 Electrophysiological properties of adapting high frequency (AHF) cell type. | 104 |
| Fig. 3.6 Firing properties of adapting low frequency (ALF) cell type. | 105 |
| Fig. 3.7 Firing properties of strongly adapting low frequency (sALF) cell type. | 107 |
| Fig. 3.8 Firing properties of weakly adapting low frequency (wALF) cell type. | 109 |
| Fig 3.9 Layer distribution of the five firing groups in the anterior piriform cortex. | 110 |
| Fig. 3.10 Correlation between the firing pattern types and interneuronal morphology in the anterior piriform cortex. | 112 |
| Fig. 3.11 Localization and morphologies of predominant firing patterns groups within the anterior piriform cortex. | 113 |
| Fig. 3.12 Firing properties of cells recorded using K ⁺ methanesulfonate are similar to those recorded in K ⁺ gluconate electrode solution. | 115 |
| Fig. 4.1 Cluster analysis of electrophysiological properties of rat aPC interneuronal populations after kindling-induced epilepsy. | 139 |
| Fig. 4.2 Distribution of the three types of firing patterns in the anterior piriform cortex of rat after kindling-induced epilepsy. | 140 |
| Fig. 4.3 Electrophysiological properties of adapting high frequency (AHF) cell type. | 142 |
| Fig. 4.4 Firing properties of adapting low frequency (ALF) cell type. | 143 |

| | |
|---|-----|
| Fig. 4.5 Firing properties of strongly adapting low frequency (sALF) cell type. | 145 |
| Fig. 4.6 Layer distribution of the three firing groups in the anterior piriform cortex. | 146 |
| Fig. 4.7 Correlation between the firing pattern types and interneuronal morphology in the anterior piriform cortex. | 149 |
| Fig. 4.8 Gabazine effect on firing patterns of piriform cortex interneurons. | 153 |
| Fig. 4.9 The voltage-dependent K^+ current in PC interneurons before and after kindling. | 154 |
| Fig. 4.10 Delta CT analysis of four voltage-gated potassium channels mRNA expression in rat anterior piriform cortex before and after kindling-induced epilepsy. | 155 |
| Fig. 4.11 Parvalbumin/Kv 1.6 colocalization in rat anterior piriform cortex before and after kindling-induced epilepsy. | 156 |

LIST OF TABLES

| | |
|--|-----|
| Table 2.1 Primary antibodies used in the study. | 46 |
| Table 2.2. Distribution of calcium-binding protein immunoreactive cells in the rat piriform cortex layers. | 56 |
| Table 2.3 Mean ratio of horizontal to vertical dendritic arborization length and dendritic shape of calcium-binding protein cells in layers 2-3 of rat piriform cortex. | 66 |
| Table 2.4 Percentages of GABA Transporter Type 1 (GAT-1)-immunoreactive terminals colocalized with calcium-binding proteins in the rat piriform cortex. | 68 |
| Table 2.5 Innervation target of calcium-binding protein immunoreactive interneurons of piriform cortex. | 72 |
| Table 3.1 Electrophysiological properties of the five types of interneuronal firing groups in the anterior piriform cortex. | 102 |
| Table 3.2 Firing group distribution across the anterior piriform cortex layers. | 106 |
| Table 3.3 Layer distribution of the three main morphological interneuronal types of piriform cortex. | 114 |
| Table 4.1 Electrophysiological properties of the five types of interneuronal firing groups in the anterior piriform cortex in amygdala kindled rats. | 141 |
| Table 4.2 Firing group distribution across the anterior piriform cortex layers in amygdala kindled rats. | 147 |
| Table 4.3 Firing distribution of the three main morphological interneuronal types of piriform cortex in amygdala kindled rats. | 150 |

ABBREVIATIONS

| | |
|-------------------|--|
| AHF | adapting high frequency |
| ALF | adapting low frequency |
| AMPA | α -amino-3-hydroxy-5-methylisoxazole-4-propionate |
| aPC | anterior piriform cortex |
| CB | calbindin |
| CBP | calcium-binding protein |
| CR | calretinin |
| CNS | central nervous system |
| FF | firing frequency |
| FS | fast spiking |
| GABA _A | gamma-amino butyric acid type A receptor |
| GAT-1 | gamma-amino butyric acid (GABA) transporter 1 |
| Π_R | interspike interval ratio |
| IR | immunoreactive |
| ISI | interspike interval |
| I_t | threshold current |
| L1 | layer 1 |
| L2 | layer 2 |
| L3 | layer 3 |
| LOT | lateral olfactory tract |
| mm | millimeter |
| mM | millimolar |
| mV | millivolt |
| M Ω | megaohm |
| NAvHF | Non-adapting very high frequency |
| NMDA | N-methyl-D-aspartate |
| NTs | nerve terminals |
| pA | picoampere |
| PC | piriform cortex |
| pPC | posterior piriform cortex |
| PV | parvalbumin |
| PV/CB | parvalbumin/calbindin |
| QPCR | quantitative real time polymerase chain reaction |
| R_i | input resistance |
| RMP | resting membrane potential |
| sALF | strongly adapting low frequency |
| wALF | weakly adapting low frequency |

Chapter 1. General introduction and thesis overview

1.1 Piriform cortex

The olfactory system has shown a dramatic increase in size in ancestral mammals, indicating the importance of this sensory modality for survival and reproduction (Rowe *et al.*, 2011). However, in the course of phylogeny, in newer species, especially in primates (monkeys and humans), the size of olfactory structures including olfactory cortex were reduced as the neocortex expanded and differentiated (Herrick, 1933; Striedter, 2003). The primary olfactory cortex represents the areas of cerebral cortex receiving direct input from the olfactory bulb. Olfactory input, comprised of axons of mitral and tufted cells of the olfactory bulb, is carried through the lateral olfactory tract and delivered in various structures including piriform cortex, anterior olfactory nucleus, anterior cortical nucleus of amygdale, periamygdaloid complex and entorhinal cortex. However, the main area involved in olfactory perception and discrimination is represented by the piriform cortex (PC) (Neville & Haberly, 2004).

1.1.1 Piriform cortex divisions and heterogeneity

The PC has a relatively simple three layered structure (paleocortex) and is located at the basolateral surface of the forebrain ventral to the rhinal fissure in rodents (Paxinos & Watson, 1986) and near the junction between frontal and temporal lobe in primates (Price, 1990).

Although the PC is usually divided in two parts, anterior and posterior PC, a central part of the PC has also been delineated (Haberly & Price, 1978) and suggested to play a role in the epileptic network (Lehmann *et al.*, 1998; Schwabe *et al.*, 2000). Structural differences between different divisions of rodent PC suggest a functional specialization of PC's anteroposterior axis. For example, association fibers (collaterals of pyramidal cells targeting apical dendrites of other pyramidal cells within the PC) have a different predominance: rostrocaudal fibers were more

numerous and originated mainly from layer 2 (L2) while the caudorostral ones were less prominent and originated mainly from layer 3 (L3) (Haberly & Price, 1978; Datiche *et al.*, 1996). Also, connections from and to other brain areas indicate a marked difference between anterior and posterior PC. For example, input from the amygdala terminates mainly in posterior PC (pPC); however only lighter connections from the basolateral amygdala to the anterior PC (aPC) have been described (Wilson & Barkai, 2010). As well, extensive backprojections from the PC to olfactory bulb originate from the aPC while only a reduced number arise from the pPC (Haberly & Price, 1978). Asymmetry in commissural fibers connections has also been described; specifically the anterior olfactory nucleus connects primarily to the contralateral anterior PC, while the pPC receive main commissural input from the contralateral aPC (Wilson & Barkai, 2010).

Other structural differences consist of an increased density of GABAergic neurons in the central PC (Loscher *et al.*, 1998); a gradual decrease of the lateral olfactory tract; and a different layer thickness along the anteroposterior axis of the PC (Haberly & Price, 1978). Stimulation of the lateral olfactory tract (LOT), a major input to the PC, can activate all parts of the PC, however the rate of activation of the aPC and pPC is different. Specifically, it was shown that short collaterals from the LOT activate the aPC first and nearly synchronous while longer and unmyelinated LOT collaterals activate the pPC sequentially (Ketchum & Haberly, 1993). Also, additional experiments using electrical stimulations (Honack *et al.*, 1991) or lesions in various parts of the PC (Wahnschaffe *et al.*, 1993) showed rostrocaudal differences in kindling rates and seizure susceptibility.

These findings are not limited to rodents only; studies in higher hierarchy animals also confirmed the structural and functional heterogeneity of the PC. For example, the primate PC is part of both frontal and temporal lobe with the LOT projecting at their junction (Zatorre *et al.*, 1992; Carmichael *et al.*, 1994). A functional divide was also noted, as different activation rates in frontal versus temporal PC was described in experiments involving either odor (Poellinger *et al.*,

2001; Gottfried *et al.*, 2002) or odorless stimulation (Zelano *et al.*, 2005). Although these studies shed light on several morpho-functional aspects along the rostrocaudal axis of PC, more studies are needed to fully understand the particularities of the PC subdivisions and their involvement in olfactory and memory processing.

1.1.2 Laminar organization of PC

Despite the anteroposterior axis heterogeneity, all parts of the PC contain the same three-layer laminar organization. Layer 1 (L1, or plexiform layer) contains few GABAergic neurons and is further divided into a superficial part (L1a) comprised of afferent fibers of the olfactory bulb; and a deep part (L1b) which contains dendrites from deeper cortical layers, as well as association fibers (Neville & Haberly, 2004). L2 consists of a high number of cell bodies of glutamatergic pyramidal and spiny semilunar cells as well as GABAergic cells with globular somata (Haberly & Price, 1978). Semilunar cells are commonly found in the superficial part of L2 and are characterised by a lack of basal dendrites but an extensive spiny apical dendritic arborisation in L1, similar to that of pyramidal cells. Although semilunar cells were shown to project to other areas (like pyramidal cells), their axons do not project back to the olfactory bulb (Haberly & Price, 1978). Superficial part of L3 contains a lower density of pyramidal cells as compared to L2, while in deep L3 both pyramidal and large GABAergic cells were described. GABAergic neurons were mostly found in L3, but their axons have an extensive arborisation in L2 where the pyramidal cells are concentrated (Ekstrand *et al.*, 2001).

1.1.3 Inhibitory processes in PC

Inhibitory neurons and their connections in the PC are thought to play a central role not only in olfactory and memory processing but also in epileptogenesis (McIntyre & Plant, 1989; Loscher & Ebert, 1996). Although several labs have studied PC interneuron localization and interconnections, only a few studies have focused on the electrophysiological properties of these interneurons. There is still a

lack of understanding of the exact involvement of specific interneuronal populations in information processing in PC, due to the interneuronal morphological variability, and especially to the lack of correspondence between their morphological features and their physiological properties. However, this situation is not limited to the PC; similar difficulties regarding correlation between structure and functional aspects of interneuronal populations have been described for other brain areas (see review, Markram *et al.*, 2004).

1.1.3.1 General characteristics of interneurons

Due to their high morpho-functional diversity, classification of interneuronal population is still a subject of debate and under constant review. In spite of this heterogeneity, there are some common traits among all types of interneurons.

Firstly, all interneurons are GABAergic, i.e. their main neurotransmitter released upon activation is represented by gamma aminobutyric acid (GABA). Release of GABA opens GABAergic receptors allowing chloride passage according to its electrochemical gradient. As the extracellular chloride concentration is usually higher than the intracellular compartment, opening of these channels leads to a transient hyperpolarization of the targeted membrane, hence the inhibitory effect of GABAergic transmission.

Second, unlike pyramidal cells, most interneuronal populations do not have dendritic spines; also they lack long apical dendrite and the projecting axon (Markram *et al.*, 2004), hence earning interneurons the name “local neuron”.

Third and lastly, as indicated by electron microscopy of neuronal synaptic ultrastructure, GABAergic synapses often have a distinct morphology: smaller active zone, narrower width of the synaptic cleft, reduced basement membrane, and flattened synaptic vesicles, as opposed to excitatory, glutamatergic synapses (Kandel & Siegelbaum, 2000). It is important to note that these ultrastructural traits of GABAergic synapses seem to be common in the adult cortex, however, in other parts of the brain such as the spinal cord, basal ganglia, cerebellum, substantia nigra as

well as during development there is a less marked correlation between synaptic morphology and their GABAergic content (Ribak & Roberts, 1990; Micheva & Beaulieu, 1996).

1.1.3.2 Molecular markers of PC interneurons

In addition to GABA, interneurons can also colocalize calcium-binding proteins (CBP), such as calretinin (CR), calbindin (CB) and parvalbumin (PV); and various neuropeptides such as somatostatin (SOM), neuropeptide Y (NPY), vasoactive intestinal peptide (VIP) and cholecystinin (CCK) which are used as reliable molecular markers to delineate interneuronal populations in the neocortex (Markram *et al.*, 2004) or hippocampal areas (Freund & Buzsaki, 1996). Distinct interneuronal populations expressing CBP were also shown to exist in PC. For example, pPC analysis of CBPs in mouse showed different morphologies and localization of PV, CB, and CR containing cells (Zhang *et al.*, 2006; Young & Sun, 2009). In rat, colocalization of PV, CB and GABA was studied by Kubota & Jones (1993) while a partial description of the CBP chemical content in piriform cortex basket cells was presented by Ekstrand *et al.* (2001). Although less well expressed than CBP, several neuropeptides (NPY, SOM, CCK and VIP) were also present in PC interneurons (Sanides-Kohlrausch & Wahle, 1990; Cummings, 1997). While these studies helped to define separate, non-overlapping interneuronal populations in the PC, there is still a lack in complete understanding of the distribution and wiring patterns of interneuronal populations in the PC.

1.1.3.3 Firing properties of PC interneurons.

Several studies examining passive and firing properties of PC interneurons located at the border between L2 and L3 showed that these cells have a higher firing rate, reduced firing adaptation and higher input resistance than PC pyramidal cells (Gellman & Aghajanian, 1994; Sheldon & Aghajanian, 1991; Protopapas & Bower, 2000). Distinct spiking pattern of interneurons in deep layers of PC were also noted

in rat (Tseng & Haberly, 1989b) and rabbit studies (Satou *et al.*, 1983a; Satou *et al.*, 1983b). In the mice pPC, various spiking patterns were described (fast spiking, late spiking, irregular spiking), however most interneurons displayed regular spiking behaviour that adapted to the stimulus (Young & Sun, 2009). A more recent study in the mouse PC (Suzuki & Bekkers, 2010) has also shown a number of differing spiking patterns. Together, these data suggest that distinct subpopulations of interneurons with specific functions could be located in all layers of rat PC; to date, a comprehensive examination of the repetitive firing properties of the interneurons in all layers of the rat anterior piriform cortex before and after kindling-induced epilepsy has not been conducted.

1.1.3.4 Feedback and feed-forward circuits in piriform cortex

As discussed in the above sections, GABAergic interneurons can be found in all layers of the PC, although most of them are located in L2 and L3. Interneurons participate in various inhibitory loops, according to their laminar location. For example, GABAergic cells provide both feed-forward inhibition (the LOT activates L1 interneurons or L2 interneurons with their dendritic tree expanded in L1, which give rise to inhibitory synapses on adjacent pyramidal cells), as well as feedback inhibition (pyramidal cell activation is spread along their collaterals exciting surrounding interneurons which in turn inhibit the pyramidal cell) controlling excitatory firings in piriform cortex (Haberly & Bower, 1984; Kanter *et al.*, 1996; Kapur *et al.*, 1997b; Ballain *et al.*, 1998; Ekstrand *et al.*, 2001). In the PC, inhibitory circuits, especially feedback inhibition, are thought to play an important role in preventing recurrent positive feedback mechanisms that could otherwise arise in this area (Neville & Haberly, 2004), due to the high pyramidal cell interconnectivity provided by the extensive association fiber system.

1.1.3.5 Dendritic and somatic inhibitory postsynaptic potentials in the piriform cortex

In addition to feed-forward and feedback circuits, inhibition in the PC can also be described in terms of localization and type of postsynaptic potentials generated in the postsynaptic neuron.

Studies where local stimulation was applied to either LOT or association fibers, have indicated that the excitatory postsynaptic potential (EPSP) evoked in pyramidal cells is followed by two GABA mediated inhibitory postsynaptic potentials (IPSPs). Thus, upon interneuronal activation, the subsequent GABA release is followed by: 1) activation of GABA_A receptors generating an early chloride IPSC, which originates in either the dendritic or somatic compartment of pyramidal cells, and 2) activation of GABA_B receptors generating a slower but longer lasting potassium -mediated IPSP in dendrites of pyramidal cells (Tseng & Haberly, 1988; Kanter *et al.*, 1996; Kapur *et al.*, 1997b). GABA_A mediated inhibitory postsynaptic currents (IPSCs) with different kinetics (GABA_{A,fast} with a decay time constant of 10ms and GABA_{A,slow} with a decay time of ~50 ms) and location (dendritic IPSCs have higher proportion of GABA_{A,slow} component than somatic IPSCs; Kapur *et al.*, 1997b) could indicate a different functional role of the dendritic and somatic inhibition. For example, a slower dendritic inhibition matching the time course of the N-methyl-D-aspartate (NMDA) component of an evoked EPSP, have shown to be more effective in blocking of NMDA- dependent long term potentiation than somatic IPSCs (Kapur *et al.*, 1997a). On the other hand, the location and kinetics of somatic IPSCs place them in a central position to inhibit and regulate the generation of action potentials, while allowing temporal processing of various inputs (afferent and/or associative) in dendritic compartments (Neville & Haberly, 2004).

1.2 Epilepsy

Epilepsy is one of the most common neurological diseases in humans, with a prevalence of about 0.5 - 1%, and a high incidence in young children and the elderly (Sundqvist, 2002; Chang & Lowenstein, 2003; Morimoto *et al.*, 2004). The epileptic seizure is by definition a paroxysmal and excessive electrical neuronal discharge in the brain that results from too much excitation or too little inhibition in the area in which the abnormal discharge starts (Chang & Lowenstein, 2003). This alteration in excitation/inhibition can lead to neuronal hyper-synchronization that then permits the seizure to fully develop and propagate throughout the brain.

All factors that can affect the brain: head traumas, degenerative diseases, infections, ischaemia and haemorrhages, can predispose a person to epilepsy (Vinters *et al.*, 1993). Also, genetic factors, mutations that cause abnormal brain development, progressive neurodegeneration, disturbed energy metabolism and abnormal function of ion channels, contribute to the aetiology in up to 40% of patients with epilepsy (Sander, 1996). Independent of the aetiology all epileptic seizures can be classified clinically into two major categories: 1) partial-seizures: those that originate in a small group of neurons that constitute a seizure focus, and 2) generalized-seizures: simultaneous disruption of normal brain activity in both cerebral hemispheres. Partial seizures are called secondary generalized when they spread to involve the majority of both cerebral hemispheres (Chabolla, 2002).

Of particular interest are seizures that develop from a local area that is the seizure focus. From the seizure focus, local paroxysmal depolarizing shifts (PDS) of membrane potential associated with high frequency bursts are thought to spread and may cause the seizure to generalize (Matsumoto & Marsan, 1964). PDS are inhibited by alpha-amino-3hydroxy-5methylsoxazole-4-propionate (AMPA) and NMDA channels receptor antagonists, underlying the importance of these channels in initiating and sustaining these long-lasting depolarizations. The afterhyperpolarizations that follow PDSs are called post-PDS hyperpolarizations and are mediated by GABA_A as well as voltage- and calcium dependent K⁺ channels,

reflecting the feedback and feed-forward inhibition of local neuronal circuits. However, these mechanisms are eventually overwhelmed and the spatial containment (surround inhibition) of the PDS activity is lost, permitting the seizure to spread and generalize (Lothman *et al.*, 1985). Nevertheless, it seems clear that the development of seizures that generalize often reflects the loss of balance between the magnitude and temporal summation of the excitation/inhibition within a relatively small region (Lothman & Collins, 1990). Most areas of the brain can be a seizure focus, but it was recognized that some areas are more seizurogenic than others. In particular, the limbic regions of the brain including: the hippocampus, entorhinal, piriform, and perirhinal cortex and their underlying structures such as the endopiriform nucleus, are highly seizurogenic (McIntyre & Poulter, 2001). They are often the site of foci in human epilepsy and thus these areas, particularly the hippocampus, have been scrutinized by researchers for many years as being central to partial complex seizure generation.

1.2.1 Temporal lobe epilepsy

Temporal lobe epilepsy (TLE) represents the most frequent type of epilepsy in humans often characterized by simple or complex partial seizures that usually arise in mesial temporal regions: amygdala, hippocampal and parahippocampal regions, and can secondarily generalize (Engel *et al.*, 1997; Chang & Lowenstein, 2003). Due to the involvement of mesial temporal lobe structures, the term mesial temporal lobe epilepsy (MTLE) is commonly used as opposed to lateral temporal lobe epilepsy (LTLE), which is linked to seizures originating in neocortical temporal lobe areas. However, the neocortical-induced seizures represent only a fraction, up to one third, of TLE cases (Williamson *et al.*, 1998; Panayiotopoulos, 2005). MTLE has a multifactorial aetiology including symptomatic causes such as brain injury/trauma, infections, brain tumours, (see review, Panayiotopoulos, 2005) or genetic (Berkovic *et al.*, 1996) and cryptogenic components, where no distinct aetiology can be determined (Engel, 1996).

To date, two MTLE syndromes with distinct neuropathological profiles, were described. In up to 70% cases, MTLE patients incurred hippocampal sclerosis (HS) (Bruton, 1988; Wolf *et al.*, 1993; Babb, 1999). The other neuropathological profile of MTLE is represented by lesions (malignant or benign tumours, vascular malformations, trauma, and cerebrovascular disease) without hippocampal sclerosis (Thom, 2004; Panayiotopoulos, 2005). Besides the obvious hippocampal pathological difference, studies comparing patients with and without HS, indicated that MTLE with HS cases are generally prone to cognitive deficits including impaired verbal and visual memory performance (Hermann *et al.*, 1997; Gleissner *et al.*, 1998; Helmstaedter, 2002; Wieser, 2004).

Although it is unclear if the HS is cause or the result of seizures (Jefferys, 1999), the morphological alterations in MTLE cases with HS are very well documented. These alterations include specific neuronal loss in cornus ammon 1 (CA₁), cornus ammon 3 (CA₃) and hillus, while cornus ammon 2 (CA₂) and dentate granule cells are preserved (Loscher & Brandt, 2010). Besides the neuronal loss and gliosis, a major reorganization of excitatory network, including mossy fiber sprouting (Sutula *et al.*, 1989; Babb *et al.*, 1991; Isokawa *et al.*, 1993; Isokawa, 1997) and neurogenesis (Blumcke *et al.*, 2001; Crespel *et al.*, 2005), are also described. Thus, by synapsing on adjacent granule cells, the new mossy fibers form a recurrent excitatory circuit, which together with abnormal connections from the newly formed granule cells (via neurogenesis), contribute to the imbalance between excitation and inhibition into the hippocampal/limbic system (Chang & Lowenstein, 2003). This imbalance is further deepened by alterations of glutamatergic and GABAergic hippocampal synaptic neurotransmission. For example, altered expression of NMDA receptors (Isokawa & Levesque, 1991; Mathern *et al.*, 1997; Mathern *et al.*, 1998b; de Lanerolle *et al.*, 1998), AMPA receptors (Babb *et al.*, 1996) and kainate receptors (Mathern *et al.*, 1998a) in the human epileptic hippocampus can alter the functional properties of these channels and promote hippocampal neuronal hyperexcitability. Altered expression of GABA_A receptor

subunits was also described in various hippocampal areas (CA₁- CA₃, dentate gyrus) of MTLE patients (Loup *et al.*, 2000). Other studies have indicated that GABAergic receptors subunit reorganization can be linked to increased zinc sensitivity (Shumate *et al.*, 1998; Brooks-Kayal *et al.*, 1999), and subsequent blockage of GABA_A receptors, leading to impaired inhibitory transmission in the hippocampus.

Besides all these mesial temporal lobe alterations, a common feature for most of MTLE patients is represented by their increased resistance to antiepileptic drugs (AEDs). This adds to the magnitude of epilepsy related health burden as most of the costs associated to epilepsy (as high as 80%) are linked to drug-resistant cases (Begley *et al.*, 2000). Thus, the need for new therapeutic avenues has prompted an increased interest in developing animal models of TLE that mimic human MTLE condition. The most important of these models are presented in the next section.

1.2.2 Animal models of temporal lobe epilepsy

Animal models of epilepsies play a pivotal role in understanding epileptogenesis mechanisms, which provide a solid platform in finding new therapeutic strategies and antiepileptic drugs (AEDs).

Rigorous selection criteria of animal models for various human epileptic disorders have been proposed, including: similar aetiology, age of onset, comparable electrographic and behavioural patterns, as well as equivalent AED mechanisms of action or pharmacological resistance (see review, Loscher, 1997; Sarkisian, 2001). Although many of the known models of epilepsy respect most of these criteria, no model seems to entirely recapitulate all aspects of seizures seen in humans. The most common animal models for TLE are post status epilepticus models, namely pilocarpine and kainate, and kindling models (Sharma *et al.*, 2007). Advantages and disadvantages of these models are presented in the following section.

1.2.3 Post status models

Most post status models are induced by systemic or local administration of pilocarpine (muscarinic acetylcholine receptor agonist), or kainate (an AMPA and kainate receptor agonist), which triggers acute but prolonged episodes of seizures, known as status epilepticus (SE). If the animal survives SE, spontaneous, secondarily generalized seizures are usually seen after a variable latency period. Most importantly, post-status induced alterations in hippocampal areas are similar to human MTLE including: CA₁ and CA₃ neuronal loss, gliosis, dentate gyrus neurogenesis, and mossy fiber sprouting (Turski *et al.*, 1984; Ben-Ari, 1985; Cronin & Dudek, 1988; Cavalheiro *et al.*, 1991; Okazaki *et al.*, 1995). However, the magnitude of necrosis is extensive and is often seen in extrahippocampal regions like neocortex, olfactory cortex, amygdala, thalamus and substantia nigra; this is especially true in the pilocarpine model (Sharma *et al.*, 2007).

Besides an alteration of the excitatory network, post status models also showed changes in the hippocampal inhibitory system, including expressional alterations of GABA_A receptor subunits (Schwarzer *et al.*, 1997; Brooks-Kayal *et al.*, 1998; Bouillere *et al.*, 2000), or downregulation of GABA_B receptors (Haas *et al.*, 1996). For example, in the pilocarpine model, network hyperexcitability can be further exacerbated by an increased expression of zinc sensitive GABA_A subunits in the epileptic hippocampus. Thus, the increased zinc, released from the sprouted mossy fibers overactivity, corroborated with newly zinc sensitive GABAergic receptors in dentate gyrus (DG) granule cells, will eventually lead to a failure of inhibition in the hippocampus (Coulter, 2000).

The main appeal of these models is the ease of SE induction, namely one treatment of pilocarpine or kainate, and the development of spontaneous seizures, which appear after a variable latent period. Generally, however, animals subjected to chemically induced SE have severe cognitive and behavioural deficits, as well as extensive widespread bilateral damage, including neocortical areas; while in many cases of human MTLE, neuronal death is more limited and usually localized in the

limbic system. Other weaknesses of post status models reside in high animal mortality during SE, as well as the variability of the age-dependent effects of pilocarpine and kainate. For example, when young rodents are used as post status models, via systemic administration of either pilocarpine or kainate, the extensive hippocampal damage and the behavioural deficits described in older animals are lacking (Wozniak *et al.*, 1991; Priel *et al.*, 1996; de Bruin *et al.*, 2000).

1.2.4 Kindling model of epilepsy

Kindling, the model used in our research, is a widely accepted model that produces complex partial seizures that secondarily generalize as in TLE. Kindling represents a progressive development of electrographic and convulsive motor seizures that follow daily electrical stimulation of a discrete brain area (Goddard, 1967).

1.2.4.1 Kindling model characteristics and classification of clinical manifestations

One important feature of kindling is the propagation of the epileptic wave to other sites and the recruitment of the new sites into the discharge, leading to enhanced sensitivity to the focal electrical stimulation. Thus the repeated electrical stimulation will gradually increase the seizure severity while the seizure threshold is reduced (Racine, 1972a). This progressive/gradual increase of seizure severity and epileptogenesis in kindling occurs in a slower temporal pace as compared to the post-status induced epileptogenesis and is considered to be relevant to various syndromes of human TLE (Sutula & Ockuly, 2006).

Based on severity of clinical manifestations, kindling induced seizures are rated between 1 and 5, according to a scale described by Racine (1972b): 1. Immobility and facial clonus; 2. Severe facial clonus; 3. Unilateral clonus of forelimb; 4. Rearing and bilateral forelimb clonus; 5. General tonic-clonic seizures. An animal is considered fully kindled when at least five consecutive stage 5

behavioural events are produced. However, if kindling is continued several weeks after stage 5 is reached, as in the over-kindling protocol, the animal will display spontaneous seizures (Pinel & Rovner, 1978). Although most kindling studies were done on rodents, this phenomenon can be seen in many other species from frogs to monkeys (see review, McNamara, 1986).

1.2.4.2 Kindling-induced structural brain changes

Kindling-induced alterations are similar to human MTLE, including gliosis (Hansen *et al.*, 1990), neurogenesis (Bengzon *et al.*, 1997; Parent *et al.*, 1998; Nakagawa *et al.*, 2000), mossy fiber sprouting (Represa *et al.*, 1989; Cavazos *et al.*, 1991) and memory dysfunction (Sutula *et al.*, 1995; Gilbert *et al.*, 2000; Hannesson *et al.*, 2001). Although the neuronal loss following kindling is limited (see review, Morimoto *et al.*, 2004), as compared to the extensive neuronal death induced by post status models, the pattern of neuronal loss (e.g. dentate gyrus, hillus, CA1 and CA3) resemble to that observed in human MTLE cases, especially in over-kindling models (Cavazos *et al.*, 1994).

1.2.4.3 Kindling-induced alterations of excitatory and inhibitory synaptic transmission

Besides these structural changes, kindling has been shown to induce alterations of both excitatory and inhibitory synaptic transmission. For example, increased NMDA dependent current, recorded on granule cells of DG (Mody & Heinemann, 1987) and lasting up to three months after last seizure (Sayin *et al.*, 1999), can lead to an increased discharge into the CA₃ region. Moreover, NMDA receptor activation increases calcium permeability, and thus subsequent activation of various second messenger systems can induce a plethora of intracellular events, including gene expression, which are responsible for the long-term functional changes in the hippocampus and limbic system after kindling (Sutula & Ockuly, 2006).

Besides altered glutamate transmission, kindling was also shown to induce changes in GABAergic system, which further contributes to the altered limbic neuronal network function. For example, GABAergic inhibition was found to be increased in dentate gyrus granule cells (Nusser *et al.*, 1998) and piriform cortex interneurons (Gavrilovici *et al.*, 2006) by an up-regulation of GABA_A receptors in response to amygdala/hippocampal kindling-induced seizures. Other studies (Kapur *et al.*, 1989; Zhao & Leung, 1991) showed that hippocampal or amygdala kindling could lead to a decreased GABAergic inhibition in CA₁, suggesting thus that the alteration in GABA_A synaptic transmission can vary from region to region. Kindling-induced reorganization of various GABA_A subunits was also reported in diverse pyramidal and interneuronal populations of the limbic system. For example, several reports indicated up-regulation of alpha1 (Nusser *et al.*, 1998) or beta3 (Kamphuis *et al.*, 1994) subunits on dentate granule cells after hippocampal kindling. Dentate gyrus mRNA levels for alpha4, beta1 and beta3 were also increased following amygdala kindling (Clark *et al.*, 1994). Meguro *et al.* (2004) showed that amygdala kindling induced an up-regulation of alpha2, alpha3 and alpha5 GABA_A subunits on CB-immunoreactive interneurons of the hilus and perirhinal cortex, while the PV-immunoreactive cells GABA_A subunit composition remained unchanged. This specific alteration suggests a selective reorganization of GABA_A receptors in response to seizures (Meguro *et al.*, 2004). Besides these GABA_A alterations, several studies have also shown that GABA_B receptor function can be impaired after kindling. For example, a reduced GABA_B function was noted in dentate granule cells (Buhl *et al.*, 1996) as well as in CA₁ neurons after kindling (Mangan & Lothman, 1996; Wu & Leung, 1997). Similar to post status models, GABAergic subunit reorganization after kindling can lead to enhanced zinc sensitivity followed by a zinc-induced collapse of inhibition in dentate gyrus (Buhl *et al.*, 1996).

1.2.4.4 Kindling-induced alterations in voltage gated receptor properties.

In addition to ligand-gated channel alterations, kindling was also shown to induce changes in the properties of several voltage-gated channels. As many voltage dependent channels can modulate the membrane excitability and their firing frequency and pattern (see review, McCormick, 2003), changes in the properties of these channels can have an important impact on “normal” brain network processing. For example, the sodium current was found to increase in CA₁ pyramidal cells but not in dentate cells following hippocampal kindling induced status epilepticus (Ketelaars *et al.*, 2001). Similar changes in the sodium current were also found in pilocarpine models; it is believed that this is linked to a change in the voltage gated subunit configuration (Ellerkmann *et al.*, 2003). Voltage-dependent Ca²⁺ currents were also increased in CA₁ pyramidal cell population following hippocampal kindling (Vreugdenhil & Wadman, 1994). Finally, several studies showed kindling-induced changes in expression of various voltage-gated potassium channels. For example, amygdala kindling induced an increased upregulation of Kv 7.2 immunoreactivity (Penschuck *et al.*, 2005) as well as increased expression of Kv 4.2 and Kv 4.3 (Chang *et al.*, 2006) in the amygdala region. Recently, Corcoran *et al.* (2011) showed that amygdala kindling induced an increased expression of KCNF1 and Kv 7.1 in the amygdala. Changing the site of kindling to the hippocampus, the same group (Corcoran *et al.*, 2011) found increased KCNF1 expression in the hippocampus and an increased Kv 3.4 while decreased KCNA3, Kv 7.1 and KCNF1 expression in the amygdala (Corcoran *et al.*, 2011).

1.2.4.5 Advantages and limitations of kindling model

The main advantage of the kindling model resides in its controlled and progressive development of epileptic events, thus avoiding the high rates of animal mortality and massive neuronal death seen in post-status epilepticus models. Depending on the type of kindling protocol (kindling versus over-kindling), kindling can model either MTLE with hippocampal sclerosis or the paradoxical model of

MTLE (MTLE without hippocampal sclerosis). Most of kindling disadvantages are related to the cumbersome nature of this method, specifically the requirement of stereotaxic brain surgery for electrode implantation and a longer induction time as repeated stimulation are required to reach stage 5 on the Racine scale. Overall, kindling has been proven as an excellent model for studying the progression of epileptic excitability and the role of various limbic regions in the generation and spread of epileptic waves. Also, the gradual increase in seizure strength allows testing of AED efficacy at different stages of epileptogenesis.

1.3 Piriform cortex involvement in limbic seizures

Various experiments ranging from anatomical studies of PC interconnection to other limbic regions, to metabolic mapping, markers of neuronal activity, as well as extra- or intracellular recordings of cell populations have indicated the involvement of the PC in limbic system seizure genesis, describing this area as having a great epileptogenic potential. A review of the representative research grouped by method of study is presented in the next sections.

1.3.1 Piriform cortex anatomical connection to other limbic structures

PC interconnections with other limbic structures, such as amygdala, entorhinal cortex, and hippocampus, might be relevant for the spread of limbic seizures. Anatomical studies of the PC input/output revealed two main circuits interconnecting PC with the amygdala (a reciprocal connection from the amygdala to the PC is made through endopiriform nuclei) and with the hippocampus (via entorhinal cortex and subiculum) (Luskin & Price, 1983). Also, due to the limbic output provided by the amygdala and subiculum, the seizure activity generated in the limbic system can easily spread to many other brain regions (Loscher & Ebert, 1996) underlining the role of PC in propagation of epileptogenic events in the limbic system.

1.3.2 Neuronal activation and metabolic rate studies in the piriform cortex

Expression of c-Fos or other immediate early gene products by neurons can be used as a marker of cell activation. By labeling recent activity in neuronal populations this method can provide important information regarding the involvement of various brain areas in the spread of epileptic events. For example, studies assessing the expression of c-fos indicated that the PC is activated very early during amygdala kindling (Dragunow *et al.*, 1988; Clark *et al.*, 1991; Ebert & Loscher, 1995), perirhinal kindling (Sato *et al.*, 1998; Ferland *et al.*, 1998) or perforant path electrical stimulations (Dragunow & Robertson, 1987). These findings, indicating early activation of the PC during kindling, were also confirmed by autoradiographic experiments using ¹⁴C-deoxyglucose (Engel *et al.*, 1978; Ackermann *et al.*, 1986) showing a high level of glucose utilization and thus an increased metabolic rate in the ipsilateral PC during amygdala kindling induced seizures.

1.3.3 Afterdischarge events, interictal spikes, spontaneous bursting in the piriform cortex

The importance of various brain regions in the spread of epileptic events can be assessed by their intrinsic kindling rates, afterdischarge threshold or appearance of interictal spikes (Loscher & Ebert, 1996). Although many brain regions can be the main site for kindling (Morimoto *et al.*, 2004), the PC was shown to kindle at a very high rate (Loscher & Ebert, 1996), exceeded only by the perirhinal and insular cortices (McIntyre *et al.*, 1993; Mohapel *et al.*, 2001). However it was also shown that kindling in other limbic areas such as amygdala induces broad afterdischarges (electrographic responses following electrical stimulation) not only in the amygdala, but also in the ipsilateral PC (Ebert & Loscher, 1995), suggesting a possible role of the PC in genesis and propagation of epileptiform afterdischarges (Loscher & Ebert, 1996).

Further evidence regarding the role of the PC in genesis of epileptiform activity was also provided by detection of interictal spikes, which appeared first and had the largest amplitude in the PC regardless of the limbic system kindling site (Kairiss *et al.*, 1984; Racine *et al.*, 1988a). However, spontaneous interictal events in the PC can also be elicited by chemical manipulations such as GABA_A receptors blockage. Under these conditions it was shown that spontaneous interictal events in brain slices have originated in the PC and spread to the neocortex (Rigas & Castro-Alamancos, 2004). Moreover, the application of convulsants, GABA antagonists and/or glutamate agonists, into the aPC was shown to lead to convulsive seizures, which could not be replicated in any other brain area (Piredda & Gale, 1985; Ebert *et al.*, 2000). On the other hand, pharmacological experiments have shown that microinjections of muscimol (a GABA_A receptor agonist) or 2-amino-5-phosphonovaleric acid (APV which is a NMDA antagonist) into the aPC reduced the afterdischarge duration of amygdala-kindled seizures by 20% (Morimoto *et al.*, 1986).

Interestingly, even in non-manipulated brain slices, the PC area was shown to display spontaneous bursting (Tseng & Haberly, 1989a; Tseng & Haberly, 1989b). Similarly, spontaneous spiking was also observed prior the onset of any electrical stimulus, indicating a lower spiking threshold and increased excitability of neurons in the PC (Loscher *et al.*, 1995).

1.3.4 Lesional studies underlying the importance of PC in epileptogenesis

Another set of techniques to study the role of PC in seizure genesis or spreading of epileptic events consisted of chemical, electrical or mechanical lesions of various parts of the PC. The assessment of the effect of these lesions on epileptogenic parameters such as afterdischarge duration, kindling rate, frequency of interictal events or spontaneous bursting, can provide valuable knowledge regarding the role of lesioned area in the seizure development.

Chemical lesions, produced by microinjections of neurotoxin ibotenate into the anterior, central or posterior PC, did not stop animals reaching kindling stage 5, but did decrease the amygdala kindling progression from stage 3 to 5 in rodents with central PC lesions (Schwabe *et al.*, 2000). Amygdala kindling progress in rodents from stage 1 to 2 was also decreased in rats with pPC lesions (Wahnschaffe *et al.*, 1993).

Electrical lesions involving larger parts of the PC (both anterior and posterior divisions) had different outcomes depending on the kindling site: it blocked the development of secondarily generalized seizures in hippocampal kindling (McIntyre & Kelly, 1990) but only decreased acquisition of septal kindling (Racine *et al.*, 1988b). Finally, more localized mechanical lesions in the transition zone between the aPC and the pPC leading to a disconnect between these areas had only a reduced effect on amygdala kindling rates (Racine *et al.*, 1988b). This suggests that different parts of the PC participate differently in spreading of epileptic events (see previous section). Overall these lesion studies indicate that the PC plays a facilitator role in development of kindling.

1.4 GABAergic system and epilepsy

Alterations of the GABAergic system, including GABA neurotransmission, changes in GABA_A receptor subunits, firing properties and connections of GABAergic neurons, has long been linked to epileptic disorders. These alterations are thought to induce a change in the very fine balance between excitation and inhibition processes in the brain that could lead to epileptogenesis in both experimental animal models and human condition (Olsen & Avoli, 1997; Morimoto *et al.*, 2004).

1.4.1 GABA receptors

GABA is the principal inhibitory neurotransmitter in the cerebral cortex. The action of GABA is mediated by ionotropic GABA_A and GABA_C (reviewed in

Barnard *et al.*, 1993) and metabotropic GABA_B receptors (reviewed in Bowery *et al.*, 2002). GABA_A receptors mediate fast inhibitory transmission by gating Cl⁻ ions which hyperpolarize the membrane and inhibit action potentials, but they are also involved in the maintenance of rhythmic activities in brain networks (Cobb *et al.*, 1995; Traub *et al.*, 1999).

Although GABA_A receptors are constructed from a large repertoire of subunits (alpha1-alpha6, beta1-beta3, gamma1-gamma3, delta, epsilon, theta and pi) only 5 subunits are used to form a pentameric heteroligomer comprised most usually from two alpha subunits, two beta subunits and one gamma (Bormann, 2000). GABA_B receptors are G protein-coupled receptors that hyperpolarize the neuron by increasing the potassium conductance, decreasing Ca²⁺ currents, having a slow inhibitory effect (Bowery *et al.*, 2002). Finally, GABA_C receptors, a relatively novel, but less well-characterized type of GABA ionotropic receptor, was also described (Chebib, 2004). GABA_C receptors are highly expressed in retina and although they have a pentameric subunit composition similar to that of GABA_A receptors, the identity of the subunits is entirely restricted to the rho (ρ) type (Chebib, 2004).

1.4.2 GABA_A receptor alterations in genetic models of epilepsy

Alterations in GABA_A receptor expression in epilepsy have been postulated almost since the heterogeneity of GABA_A receptor was first recognized. GABA_A receptor expression has been altered in various genetical/knockout mice models having varying impacts. For example a relatively severe effect was found in GABA beta3-deficient mice that displayed frequent myoclonus and occasional epileptic seizures, documented by electroencephalographic recording (Homanics *et al.*, 1997). Another model showed elevated levels of GABA alpha2 and beta1-subunit mRNA in the tottering cortex (Tehrani *et al.*, 1997). These mice display ataxia, sporadic focal myoclonic seizures and generalized cortical spike-wave discharges. Another animal model of seizure predisposition, which shows reduced responses to GABA_A receptor agonists and deficits in GABA function, is the genetically epilepsy-prone rat (GEPR,

Molnar *et al.*, 2000). Abnormal overexpression of GABA receptor subunits, observed in kindling-prone (alpha2, alpha3 and alpha5) and kindling-resistant (alpha1) rats, may result in the incapacity of the brain to prevent hypersynchrony in the neural networks (Poulter *et al.*, 1999). These seizure resistant and seizure prone rats do not display spontaneous seizures but do have other behavioural manifestations that are co-morbid with epilepsy like attention deficit hyperactive syndrome (McIntyre & Anisman, 2000).

Genetic evidence for the involvement of GABA_A receptors in human epilepsy has been shown by Baulac *et al.* (2001) who have reported a point mutation in the GABA_A receptor gamma2-subunit gene. This mutation segregates in a family with a phenotype closely related to generalized epilepsy with febrile seizures plus (GEFS+). Analysis of recombinant $\alpha_1\beta_2\gamma_2$ receptors expressed in *Xenopus laevis* oocytes confirmed the predicted effect of the mutation, a decrease in the amplitude of GABA-activated currents. Another mutation in a gene encoding a GABA_A receptor gamma2 subunit was found in two families with febrile seizures (FS) and childhood epilepsy. This mutation expressed in *Xenopus* oocytes suppressed diazepam potentiation of GABAergic currents (Wallace *et al.*, 2001).

GABAergic system alterations in human TLE and animal models of TLE have also been investigated in many labs (Brooks-Kayal *et al.*, 1998; Nusser *et al.*, 1998; Sperk *et al.*, 1998; Fritschy *et al.*, 1999; Loup *et al.*, 2000) and thought to be linked to epileptic mechanisms in the limbic system. These alterations were reviewed in detail in the previous sections.

1.4.3 GABAergic Interneurons and Epilepsy

Interneurons have morphological and functional characteristics that can be relevant for epilepsy. For example, the propensity of many interneurons to fire in higher frequency range as compared to pyramidal cells, their ability to activate at lower threshold levels, and their multiple interconnections with a large number of pyramidal cells (Buhl *et al.*, 1994), place them in a central role to control and

modulate the activity of pyramidal cells. Interneuronal activation, followed by GABA release at their terminals can provide both fast synaptic (phasic) and slow extra-synaptic (tonic) inhibition. In various models of epilepsy it was shown that altered phasic (Kobayashi & Buckmaster, 2003; Kobayashi *et al.*, 2003; Gavrilovici *et al.*, 2006; Trotter *et al.*, 2006) or tonic GABAergic currents (Zhang *et al.*, 2007) could disrupt the shunting of excitatory inputs and thus induce an imbalance between inhibition and excitation in targeted cells.

Moreover, in the larger context of a neuronal network, the interneurons can also control the timing of pyramidal cells firing, modulating their synchronization (Llinas, 1988; Cobb *et al.*, 1995) and generate oscillations (see review, Buzsaki & Chrobak, 1995). Due to the large number of pyramidal cells targeted by each interneuron, any change (decrease or increase) in the activity of interneurons can have major consequences for the neuronal network they are part of. These physiological and anatomical properties of interneurons point towards a link between altered interneuronal function and epilepsy. However, although some of the interneuronal alterations presented in previous chapters are believed to be the result of seizures, some inhibitory system changes preceded the onset of generalized seizures leading to a vivid debate regarding whether these changes are causal and/or part of a compensatory mechanism. Nonetheless, apart from the timing of these events it is apparent that an altered inhibitory system is linked to epilepsy.

1.5 Thesis outline

Despite much literature regarding the role and involvement of PC in temporal lobe epilepsy, the exact mechanisms through which the PC excitation-inhibition imbalance leads to pathological pyramidal cell synchronization, and thus to the generation and spreading of the epileptic wave throughout the limbic system are still unknown.

In our previous work (Gavrilovici *et al.*, 2006), we hypothesized that the high excitability of pyramidal neurons of the PC and their increased susceptibility for

epileptogenic activity after amygdala kindling is produced by an increased inhibition of the interneuronal population of PC. Indeed, by analyzing the miniature inhibitory post-synaptic currents (mIPSCs) collected from kindled and non-kindled brain slices on both pyramidal and non-pyramidal cell types, we concluded that increased inhibition of interneurons, produced by an increased number of GABA_A receptors in PC interneurons, predicts an enhanced disinhibition of pyramidal cells that might account for the kindling phenomena. Although this study (Gavrilovici *et al.*, 2006) shed some light on the mechanisms that can increase the activity of the excitatory cells in kindled PC, the epileptic phenomenon is associated not only with an increased excitatory output, but more importantly with a synchronous, pathological activity of these cells that can thus lead to epileptic waves.

My hypothesis for this thesis is that kindling induces changes in the firing pattern of interneuronal PC populations. An impaired interneuronal firing might lead to increased disinhibition and/or altered timing of network activities that could induce pathological synchronous events like those generated during epileptic seizures. In this view, a closer analysis of the neuronal network is needed to understand both the interneuronal firing patterns and neuronal interconnections for all three layers of PC before and after kindling. Thus the main objectives of the thesis are:

1. To quantify and characterize the interneuronal localization, dendritic arborizations and their innervation patterns in all three layers of PC
2. To assess the firing properties of identified PC interneuronal populations
3. To examine the changes in firing properties of PC interneurons after kindling-induced epilepsy.

Anatomical characterization of CBP interneurons in PC is presented in chapter 2, while electrophysiological properties of morphologically identified interneurons before kindling and after kindling are presented in chapter 3 and chapter 4. Lastly, the thesis concludes in chapter 5 with a general discussion of all the results and their relevance for PC links to epilepsy.

1.6 References

- Ackermann RF, Chugani HT, Handforth A, Moshe S, Caldecott-Hazard S, & Engel JJr (1986). Autoradiographic studies of cerebral metabolism and blood flow in rat amygdala kindling. In *Kindling*, ed. Wada JA, pp. 73-87. Raven Press, New York.
- Babb TL (1999). Synaptic reorganizations in human and rat hippocampal epilepsy. *Adv Neurol* **79**, 763-779.
- Babb TL, Kupfer WR, Pretorius JK, Crandall PH, & Levesque MF (1991). Synaptic reorganization by mossy fibers in human epileptic fascia dentata. *Neurosci* **42**, 351-363.
- Babb TL, Mathern GW, Leite JP, Pretorius JK, Yeoman KM, & Kuhlman PA (1996). Glutamate AMPA receptors in the fascia dentata of human and kainate rat hippocampal epilepsy. *Epilepsy Res* **26**, 193-205.
- Ballain T, Litaudon P, Martiel JL, & Cattarelli M (1998). Role of the net architecture in piriform cortex activity: analysis by a mathematical model. *Biol Cybern* **79**, 323-336.
- Barnard EA, Sutherland M, Zaman S, Matsumoto M, Nayeem N, Green T, Darlison MG, & Bateson AN (1993). Multiplicity, structure, and function in GABAA receptors. *Ann N Y Acad Sci* **707**, 116-125.
- Baulac S, Huberfeld G, Gourfinkel-An I, Mitropoulou G, Beranger A, Prud'homme JF, Baulac M, Brice A, Bruzzone R, & Leguern E (2001). First genetic evidence of GABA(A) receptor dysfunction in epilepsy: a mutation in the gamma2-subunit gene. *Nat Genet* **28**, 46-48.
- Begley CE, Famulari M, Annegers JF, Lairson DR, Reynolds TF, Coan S, Dubinsky S, Newmark ME, Leibson C, So EL, & Rocca WA (2000). The cost of epilepsy in the United States: an estimate from population-based clinical and survey data. *Epilepsia* **41**, 342-351.
- Ben-Ari Y (1985). Limbic seizure and brain damage produced by kainic acid: mechanisms and relevance to human temporal lobe epilepsy. *Neurosci* **14**, 375-403.
- Bengzon J, Kokaia Z, Elmer E, Nanobashvili A, Kokaia M, & Lindvall O (1997). Apoptosis and proliferation of dentate gyrus neurons after single and intermittent limbic seizures. *Proc Natl Acad Sci U S A* **94**, 10432-10437.
- Berkovic SF, McIntosh A, Howell RA, Mitchell A, Sheffield LJ, & Hopper JL (1996). Familial temporal lobe epilepsy: a common disorder identified in twins. *Ann Neurol* **40**, 227-235.

- Blumcke I, Schewe JC, Normann S, Brustle O, Schramm J, Elger CE, & Wiestler OD (2001). Increase of nestin-immunoreactive neural precursor cells in the dentate gyrus of pediatric patients with early-onset temporal lobe epilepsy. *Hippocampus* **11**, 311-321.
- Bormann J (2000). The 'ABC' of GABA receptors. *Trends Pharmacol Sci* **21**, 16-19.
- Bouillere V, Loup F, Kiener T, Marescaux C, & Fritschy JM (2000). Early loss of interneurons and delayed subunit-specific changes in GABA(A)-receptor expression in a mouse model of mesial temporal lobe epilepsy. *Hippocampus* **10**, 305-324.
- Bowery NG, Bettler B, Froestl W, Gallagher JP, Marshall F, Raiteri M, Bonner TI, & Enna SJ (2002). International Union of Pharmacology. XXXIII. Mammalian gamma-aminobutyric acid(B) receptors: structure and function. *Pharmacol Rev* **54**, 247-264.
- Brooks-Kayal AR, Shumate MD, Jin H, Lin DD, Rikhter TY, Holloway KL, & Coulter DA (1999). Human neuronal gamma-aminobutyric acid(A) receptors: coordinated subunit mRNA expression and functional correlates in individual dentate granule cells. *J Neurosci* **19**, 8312-8318.
- Brooks-Kayal AR, Shumate MD, Jin H, Rikhter TY, & Coulter DA (1998). Selective changes in single cell GABA_A receptor subunit expression and function in temporal lobe epilepsy. *Nature Medicine* **4**, 1166-1172.
- Bruton CJ (1988). The neuropathology of temporal lobe epilepsy. In *Maudsley monograph*, ed. Bruton CJ, Oxford University Press, Oxford.
- Buhl EH, Han ZS, Lorinczi Z, Stezhka VV, Karnup SV, & Somogyi P (1994). Physiological properties of anatomically identified axo-axonic cells in the rat hippocampus. *J Neurophysiol* **71**, 1289-1307.
- Buhl EH, Otis TS, & Mody I (1996). Zinc-induced collapse of augmented inhibition by GABA in a temporal lobe epilepsy model. *Science* **271**, 369-373.
- Buzsaki G & Chrobak JJ (1995). Temporal structure in spatially organized neuronal ensembles: a role for interneuronal networks. *Curr Opin Neurobiol* **5**, 504-510.
- Carmichael ST, Clugnet MC, & Price JL (1994). Central olfactory connections in the macaque monkey. *J Comp Neurol* **346**, 403-434.
- Cavalheiro EA, Leite JP, Bortolotto ZA, Turski WA, Ikonomidou C, & Turski L (1991). Long-term effects of pilocarpine in rats: structural damage of the brain triggers kindling and spontaneous recurrent seizures. *Epilepsia* **32**, 778-782.

- Cavazos JE, Das I, & Sutula TP (1994). Neuronal loss induced in limbic pathways by kindling: evidence for induction of hippocampal sclerosis by repeated brief seizures. *J Neurosci* **14**, 3106-3121.
- Cavazos JE, Golarai G, & Sutula TP (1991). Mossy fiber synaptic reorganization induced by kindling: time course of development, progression, and permanence. *J Neurosci* **11**, 2795-2803.
- Chabolla DR (2002). Characteristics of the epilepsies. *Mayo Clin Proc* **77**, 981-990.
- Chang BS & Lowenstein DH (2003). Epilepsy. *N Engl J Med* **349**, 1257-1266.
- Chang HH, Su T, Sun WW, Zhao QH, Qin B, & Liao WP (2006). Changes of potassium channels Kv4.2, Kv4.3 and Kv channel interacting protein 1 in amygdala kindling epilepsy: experiment with rats. *Zhonghua Yi Xue Za Zhi* **86**, 3315-3318.
- Chebib M (2004). GABAC receptor ion channels. *Clin Exp Pharmacol Physiol* **31**, 800-804.
- Clark M, Massenburg GS, Weiss SR, & Post RM (1994). Analysis of the hippocampal GABAA receptor system in kindled rats by autoradiographic and in situ hybridization techniques: contingent tolerance to carbamazepine. *Brain Res Mol Brain Res* **26**, 309-319.
- Clark M, Post RM, Weiss SR, Cain CJ, & Nakajima T (1991). Regional expression of c-fos mRNA in rat brain during the evolution of amygdala kindled seizures. *Brain Res Mol Brain Res* **11**, 55-64.
- Cobb SR, Buhl EH, Halasy K, Paulsen O, & Somogyi P (1995). Synchronization of neuronal activity in hippocampus by individual GABAergic interneurons. *Nature* **378**, 75-78.
- Corcoran ME, Kroes RA, Burgdorf JS, & Moskal JR (2011). Regional changes in gene expression after limbic kindling. *Cell Mol Neurobiol* **31**, 819-834.
- Coulter DA (2000). Mossy fiber zinc and temporal lobe epilepsy: pathological association with altered "epileptic" gamma-aminobutyric acid A receptors in dentate granule cells. *Epilepsia* **41 Suppl 6**, S96-S99.
- Crespel A, Rigau V, Coubes P, Rousset MC, de BF, Okano H, Baldy-Moulinier M, Bockaert J, & Lerner-Natoli M (2005). Increased number of neural progenitors in human temporal lobe epilepsy. *Neurobiol Dis* **19**, 436-450.

- Cronin J & Dudek FE (1988). Chronic seizures and collateral sprouting of dentate mossy fibers after kainic acid treatment in rats. *Brain Res* **474**, 181-184.
- Cummings SL (1997). Neuropeptide Y, somatostatin, and cholecystokinin of the anterior piriform cortex. *Cell Tissue Res* **289**, 39-51.
- Datiche F, Litaudon P, & Cattarelli M (1996). Intrinsic association fiber system of the piriform cortex: a quantitative study based on a cholera toxin B subunit tracing in the rat. *J Comp Neurol* **376**, 265-277.
- De Bruin VM, Marinho MM, De Sousa FC, & Viana GS (2000). Behavioral and neurochemical alterations after lithium-pilocarpine administration in young and adult rats: a comparative study. *Pharmacol Biochem Behav* **65**, 547-551.
- de Lanerolle NC, Eid T, von CG, Kovacs I, Spencer DD, & Brines M (1998). Glutamate receptor subunits GluR1 and GluR2/3 distribution shows reorganization in the human epileptogenic hippocampus. *Eur J Neurosci* **10**, 1687-1703.
- Dragunow M & Robertson HA (1987). Kindling stimulation induces c-fos protein(s) in granule cells of the rat dentate gyrus. *Nature* **329**, 441-442.
- Dragunow M, Robertson HA, & Robertson GS (1988). Amygdala kindling and c-fos protein(s). *Exp Neurol* **102**, 261-263.
- Ebert U & Loscher W (1995). Strong induction of c-fos in the piriform cortex during focal seizures evoked from different limbic brain sites. *Brain Res* **671**, 338-344.
- Ebert U, Wlaz P, & Loscher W (2000). High susceptibility of the anterior and posterior piriform cortex to induction of convulsions by bicuculline. *Eur J Neurosci* **12**, 4195-4205.
- Ekstrand JJ, Domroese ME, Feig SL, Illig KR, & Haberly LB (2001). Immunocytochemical analysis of basket cells in rat piriform cortex. *J Comp Neurol* **434**, 308-328.
- Ellerkmann RK, Remy S, Chen J, Sochivko D, Elger CE, Urban BW, Becker A, & Beck H (2003). Molecular and functional changes in voltage-dependent Na(+) channels following pilocarpine-induced status epilepticus in rat dentate granule cells. *Neurosci* **119**, 323-333.
- Engel JJr (1996). Introduction to temporal lobe epilepsy. *Epilepsy Res* **26**, 141-150.

- Engel JJr, Williamson PD, & Wieser HG (1997). Mesial temporal lobe epilepsy. In *Epilepsy: A comprehensive textbook*, eds. Engel JJr & Pedley TA, pp. 2417-2426. Lippincott-Raven, Philadelphia.
- Engel JJr, Wolfson L, & Brown L (1978). Anatomical correlates of electrical and behavioral events related to amygdaloid kindling. *Ann Neurol* **3**, 538-544.
- Ferland RJ, Nierenberg J, & Applegate CD (1998). A role for the bilateral involvement of perirhinal cortex in generalized kindled seizure expression. *Exp Neurol* **151**, 124-137.
- Freund TF & Buzsaki G (1996). Interneurons of the hippocampus. *Hippocampus* **6**, 347-470.
- Fritschy JM, Kiener T, Bouillere V, & Loup F (1999). GABAergic neurons and GABA(A)-receptors in temporal lobe epilepsy. *Neurochem Int* **34**, 435-445.
- Gavrilovici C, D'Alfonso S, Dann M, & Poulter MO (2006). Kindling-induced alterations in GABA_A receptor mediated inhibition and neurosteroid activity in the piriform cortex of rat. *Eur J Neurosci* **24**, 1373-1384.
- Gellman RL & Aghajanian GK (1994). Serotonin₂ receptor-mediated excitation of interneurons in piriform cortex: antagonism by atypical antipsychotic drugs. *Neuroscience* **58**, 515-525.
- Gilbert TH, Hannesson DK, & Corcoran ME (2000). Hippocampal kindled seizures impair spatial cognition in the Morris water maze. *Epilepsy Res* **38**, 115-125.
- Gleissner U, Helmstaedter C, & Elger CE (1998). Right hippocampal contribution to visual memory: a presurgical and postsurgical study in patients with temporal lobe epilepsy. *J Neurol Neurosurg Psychiatry* **65**, 665-669.
- Goddard GV (1967). Development of epileptic seizures through brain stimulation at low intensity. *Nature* **214**, 1020-1021.
- Gottfried JA, Deichmann R, Winston JS, & Dolan RJ (2002). Functional heterogeneity in human olfactory cortex: an event-related functional magnetic resonance imaging study. *J Neurosci* **22**, 10819-10828.
- Haas KZ, Sperber EF, Moshe SL, & Stanton PK (1996). Kainic acid-induced seizures enhance dentate gyrus inhibition by downregulation of GABA(B) receptors. *J Neurosci* **16**, 4250-4260.

- Haberly LB & Bower JM (1984). Analysis of association fiber system in piriform cortex with intracellular recording and staining techniques. *J Neurophysiol* **51**, 90-112.
- Haberly LB & Price JL (1978). Association and commissural fiber systems of the olfactory cortex of the rat. *J Comp Neurol* **178**, 711-740.
- Hannesson DK, Mohapel P, & Corcoran ME (2001). Dorsal hippocampal kindling selectively impairs spatial learning/short-term memory. *Hippocampus* **11**, 275-286.
- Hansen A, Jorgensen OS, Bolwig TG, & Barry DI (1990). Hippocampal kindling alters the concentration of glial fibrillary acidic protein and other marker proteins in rat brain. *Brain Res* **531**, 307-311.
- Helmstaedter C (2002). Effects of chronic epilepsy on declarative memory systems. *Prog Brain Res* **135**, 439-453.
- Hermann BP, Seidenberg M, Schoenfeld J, & Davies K (1997). Neuropsychological characteristics of the syndrome of mesial temporal lobe epilepsy. *Arch Neurol* **54**, 369-376.
- Herrick CJ (1933). The Functions of the Olfactory Parts of the Cerebral Cortex. *Proc Natl Acad Sci U S A* **19**, 7-14.
- Homanics GE, Delorey TM, Firestone LL, Quinlan JJ, Handforth A, Harrison NL, Krasowski MD, Rick CE, Korpi ER, Makela R, Brilliant MH, Hagiwara N, Ferguson C, Snyder K, & Olsen RW (1997). Mice devoid of gamma-aminobutyrate type A receptor beta3 subunit have epilepsy, cleft palate, and hypersensitive behavior. *Proc Natl Acad Sci U S A* **94**, 4143-4148.
- Honack D, Wahnschaffe U, & Loscher W (1991). Kindling from stimulation of a highly sensitive locus in the posterior part of the piriform cortex. Comparison with amygdala kindling and effects of antiepileptic drugs. *Brain Res* **538**, 196-202.
- Isokawa M (1997). Preservation of dendrites with the presence of reorganized mossy fiber collaterals in hippocampal dentate granule cells in patients with temporal lobe epilepsy. *Brain Res* **744**, 339-343.
- Isokawa M & Levesque MF (1991). Increased NMDA responses and dendritic degeneration in human epileptic hippocampal neurons in slices. *Neurosci Lett* **132**, 212-216.

- Isokawa M, Levesque MF, Babb TL, & Engel J, Jr. (1993). Single mossy fiber axonal systems of human dentate granule cells studied in hippocampal slices from patients with temporal lobe epilepsy. *J Neurosci* **13**, 1511-1522.
- Jefferys JG (1999). Hippocampal sclerosis and temporal lobe epilepsy: cause or consequence? *Brain* **122**, 1007-1008.
- Kairiss EW, Racine RJ, & Smith GK (1984). The development of the interictal spike during kindling in the rat. *Brain Res* **322**, 101-110.
- Kamphuis W, De Rijk TC, & Lopes da Silva FH (1994). GABAA receptor beta 1-3 subunit gene expression in the hippocampus of kindled rats. *Neurosci Lett* **174**, 5-8.
- Kandel ER & Siegelbaum SA (2000). Synaptic Integration. In *Principles of Neural Science*, eds. Kandel ER, Schwartz JH, & Jessell TM, pp. 207-228. McGraw Hill, New York.
- Kanter ED, Kapur A, & Haberly LB (1996). A dendritic GABAA-mediated IPSP regulates facilitation of NMDA-mediated responses to burst stimulation of afferent fibers in piriform cortex. *J Neurosci* **16**, 307-312.
- Kapur A, Lytton WW, Ketchum KL, & Haberly LB (1997a). Regulation of the NMDA component of EPSPs by different components of postsynaptic GABAergic inhibition: computer simulation analysis in piriform cortex. *J Neurophysiol* **78**, 2546-2559.
- Kapur A, Pearce RA, Lytton WW, & Haberly LB (1997b). GABAA-mediated IPSCs in piriform cortex have fast and slow components with different properties and locations on pyramidal cells. *J Neurophysiol* **78**, 2531-2545.
- Kapur J, Michelson HB, Buterbaugh GG, & Lothman EW (1989). Evidence for a chronic loss of inhibition in the hippocampus after kindling: electrophysiological studies. *Epilepsy Res* **4**, 90-99.
- Ketchum KL & Haberly LB (1993). Membrane currents evoked by afferent fiber stimulation in rat piriform cortex. I. Current source-density analysis. *J Neurophysiol* **69**, 248-260.
- Ketelaars SO, Gorter JA, van Vliet EA, Lopes da Silva FH, & Wadman WJ (2001). Sodium currents in isolated rat CA1 pyramidal and dentate granule neurones in the post-status epilepticus model of epilepsy. *Neurosci* **105**, 109-120.
- Kobayashi M & Buckmaster PS (2003). Reduced inhibition of dentate granule cells in a model of temporal lobe epilepsy. *J Neurosci* **23**, 2440-2452.

Kobayashi M, Wen X, & Buckmaster PS. Reduced inhibition and increased output of layer II neurons in the medial entorhinal cortex in a model of temporal lobe epilepsy. *J. Neurosci* **23**, 8471-8479. 2003.

Kubota Y & Jones EG (1993). Co-localization of two calcium binding proteins in GABA cells of rat piriform cortex. *Brain Res* **600**, 339-344.

Lehmann H, Ebert U, & Loscher W (1998). Amygdala-kindling induces a lasting reduction of GABA-immunoreactive neurons in a discrete area of the ipsilateral piriform cortex. *Synapse* **29**, 299-309.

Llinas RR (1988). The intrinsic electrophysiological properties of mammalian neurons: insights into central nervous system function. *Science* **242**, 1654-1664.

Loscher W & Brandt C (2010). Prevention or modification of epileptogenesis after brain insults: experimental approaches and translational research. *Pharmacol Rev* **62**, 668-700.

Loscher W & Ebert U (1996). The role of the piriform cortex in kindling. *Prog Neurobiol* **50**, 427-481.

Loscher W, Ebert U, Wahnschaffe U, & Rundfeldt C (1995). Susceptibility of different cell layers of the anterior and posterior part of the piriform cortex to electrical stimulation and kindling: comparison with the basolateral amygdala and "area tempestas". *Neurosci* **66**, 265-276.

Lothman EW & Collins RC (1990). Seizures and epilepsy. In *Neurobiology of Disease*, ed. Pearlman AL, pp. 276-298. Oxford Univ. Press, New York.

Lothman EW, Hatlelid JM, & Zorumski CF (1985). Functional mapping of limbic seizures originating in the hippocampus: a combined 2-deoxyglucose and electrophysiologic study. *Brain Res* **360**, 92-100.

Loup F, Wieser HG, Yonekawa Y, Aguzzi A, & Fritschy JM (2000). Selective alterations in GABAA receptor subtypes in human temporal lobe epilepsy. *J Neurosci* **20**, 5401-5419.

Luskin MB & Price JL (1983). The topographic organization of associational fibers of the olfactory system in the rat, including centrifugal fibers to the olfactory bulb. *J Comp Neurol* **216**, 264-291.

Mangan PS & Lothman EW (1996). Profound disturbances of pre- and postsynaptic GABAB-receptor-mediated processes in region CA1 in a chronic model of temporal lobe epilepsy. *J Neurophysiol* **76**, 1282-1296.

Markram H, Toledo-Rodriguez M, Wang Y, Gupta A, Silberberg G, & Wu C (2004). Interneurons of the neocortical inhibitory system. *Nat Rev Neurosci* **5**, 793-807.

Mathern GW, Pretorius JK, Kornblum HI, Mendoza D, Lozada A, Leite JP, Chimelli L, Born DE, Fried I, Sakamoto AC, Assirati JA, Peacock WJ, Ojemann GA, & Adelson PD (1998a). Altered hippocampal kainate-receptor mRNA levels in temporal lobe epilepsy patients. *Neurobiol Dis* **5**, 151-176.

Mathern GW, Pretorius JK, Kornblum HI, Mendoza D, Lozada A, Leite JP, Chimelli LM, Fried I, Sakamoto AC, Assirati JA, Levesque MF, Adelson PD, & Peacock WJ (1997). Human hippocampal AMPA and NMDA mRNA levels in temporal lobe epilepsy patients. *Brain* **120**, 1937-1959.

Mathern GW, Pretorius JK, Mendoza D, Lozada A, Leite JP, Chimelli L, Fried I, Sakamoto AC, Assirati JA, & Adelson PD (1998b). Increased hippocampal AMPA and NMDA receptor subunit immunoreactivity in temporal lobe epilepsy patients. *J Neuropathol Exp Neurol* **57**, 615-634.

Matsumoto H & Marsan CA (1964). Cortical cellular phenomena in experimental epilepsy: interictal manifestations. *Exp Neurol* **9**, 286-304.

McCormick DA (2003). Membrane potential and action potential. In *Fundamental Neuroscience*, eds. Squire LR, Bloom FE, McConnell SK, Roberts JL, Spitzer NC, & Zigmond MJ, pp. 139-161. Academic Press, San Diego.

McIntyre DC & Anisman H (2000). Anxiety and impulse control in rats selectively bred for seizure sensitivity. In *Contemporary Issues in Modeling Psychopathology*, eds. Myslobodsky M & Weiner I, pp. 29-43. Kluwer Academic, New York.

McIntyre DC & Kelly ME (1990). Is the pyriform cortex important for limbic kindling. In *Kindling*, ed. Wada JA, pp. 21-32. Plenum Press, New York.

McIntyre DC, Kelly ME, & Armstrong JN (1993). Kindling in the perirhinal cortex. *Brain Res* **615**, 1-6.

McIntyre DC & Plant JR (1989). Pyriform cortex involvement in kindling. *Neurosci Biobehav Rev* **13**, 277-280.

McIntyre DC & Poulter MO (2001). Kindling and the mirror focus. *Int Rev Neurobiol* **45**, 387-407.

McNamara JO (1986). Kindling model of epilepsy. *Adv Neurol* **44**, 303-318.

- Meguro R, Lu Z.W., Gavrilovici C, & Poulter MO (2004). Static, transient and permanent organisation of GABA_A receptor expression in calbindin positive interneurons in response to amygdala kindled seizures. *J Neurochem* **91**, 144-154.
- Micheva KD & Beaulieu C (1996). Quantitative aspects of synaptogenesis in the rat barrel field cortex with special reference to GABA circuitry. *J Comp Neurol* **373**, 340-354.
- Mody I & Heinemann U (1987). NMDA receptors of dentate gyrus granule cells participate in synaptic transmission following kindling. *Nature* **326**, 701-704.
- Mohapel P, Zhang X, Gillespie GW, Chlan-Fourney J, Hannesson DK, Corley SM, Li XM, & Corcoran ME (2001). Kindling of claustrum and insular cortex: comparison to perirhinal cortex in the rat. *Eur J Neurosci* **13**, 1501-1519.
- Molnar LR, Fleming WW, & Taylor DA (2000). Alterations in neuronal gamma-aminobutyric acid(A) receptor responsiveness in genetic models of seizure susceptibility with different expression patterns. *J Pharmacol Exp Ther* **295**, 1258-1266.
- Morimoto K, Dragunow M, & Goddard GV (1986). Deep prepyriform cortex kindling and its relation to amygdala kindling in the rat. *Exp Neurol* **94**, 637-648.
- Morimoto K, Fahnestock M, & Racine RJ (2004). Kindling and status epilepticus models of epilepsy: rewiring the brain. *Prog Neurobiol* **73**, 1-60.
- Nakagawa E, Aimi Y, Yasuhara O, Tooyama I, Shimada M, McGeer PL, & Kimura H (2000). Enhancement of progenitor cell division in the dentate gyrus triggered by initial limbic seizures in rat models of epilepsy. *Epilepsia* **41**, 10-18.
- Neville KR & Haberly LB (2004). Olfactory cortex. In *The Synaptic Organization of the Brain*, ed. Shepherd GM, pp. 415-454. Oxford University Press, New York.
- Nusser Z, Hajos N, Somogyi P, & Mody I (1998). Increased number of synaptic GABA(A) receptors underlies potentiation at hippocampal inhibitory synapses. *Nature* **395**, 172-177.
- Okazaki MM, Evenson DA, & Nadler JV (1995). Hippocampal mossy fiber sprouting and synapse formation after status epilepticus in rats: visualization after retrograde transport of biocytin. *J Comp Neurol* **352**, 515-534.
- Olsen RW & Avoli M (1997). GABA and epileptogenesis. *Epilepsia* **38**, 399-407.

- Panayiotopoulos CP (2005). Symptomatic and Probably Symptomatic Focal Epilepsies. In *The Epilepsies: Seizures, Syndromes and Management*, ed. Panayiotopoulos CP, Bladon Medical Publishing.
- Parent JM, Janumpalli S, McNamara JO, & Lowenstein DH (1998). Increased dentate granule cell neurogenesis following amygdala kindling in the adult rat. *Neurosci Lett* **247**, 9-12.
- Paxinos G & Watson PL (1986). *The rat brain in stereotaxic coordinates*, second ed. Academic Press, Sydney.
- Penschuck S, Bastlund JF, Jensen HS, Stensbol TB, Egebjerg J, & Watson WP (2005). Changes in KCNQ2 immunoreactivity in the amygdala in two rat models of temporal lobe epilepsy. *Brain Res Mol Brain Res* **141**, 66-73.
- Pinel JP & Rovner LI (1978). Experimental epileptogenesis: kindling-induced epilepsy in rats. *Exp Neurol* **58**, 190-202.
- Piredda S & Gale K (1985). A crucial epileptogenic site in the deep prepiriform cortex. *Nature* **317**, 623-625.
- Poellinger A, Thomas R, Lio P, Lee A, Makris N, Rosen BR, & Kwong KK (2001). Activation and habituation in olfaction--an fMRI study. *Neuroimage* **13**, 547-560.
- Poulter MO, Brown LA, Tynan S, Willick G, Williams R, & McIntyre DC (1999). Differential expression of alpha1, alpha2, alpha3, and alpha5 GABAA receptor subunits in seizure-prone and seizure-resistant rat models of temporal lobe epilepsy. *J Neurosci* **19**, 4654-4661.
- Price J (1990). Olfactory system. In *The Human Nervous System*, ed. Paxinos G, pp. 979-998. Academic Press, New York.
- Priel MR, dos Santos NF, & Cavalheiro EA (1996). Developmental aspects of the pilocarpine model of epilepsy. *Epilepsy Res* **26**, 115-121.
- Protopapas AD & Bower JM (2000). Physiological characterization of layer III non-pyramidal neurons in piriform (olfactory) cortex of rat. *Brain Res* **865**, 1-11.
- Racine RJ (1972a). Modification of seizure activity by electrical stimulation. I. After-discharge threshold. *Electroencephalogr Clin Neurophysiol* **32**, 269-279.
- Racine RJ (1972b). Modification of seizure activity by electrical stimulation. II. Motor seizure. *Electroencephalogr Clin Neurophysiol* **32**, 281-294.

Racine RJ, Mosher M, & Kairiss EW (1988a). The role of the pyriform cortex in the generation of interictal spikes in the kindled preparation. *Brain Res* **454**, 251-263.

Racine RJ, Paxinos G, Mosher JM, & Kairiss EW (1988b). The effects of various lesions and knife-cuts on septal and amygdala kindling in the rat. *Brain Res* **454**, 264-274.

Represa A, Le Gall La SG, & Ben-Ari Y (1989). Hippocampal plasticity in the kindling model of epilepsy in rats. *Neurosci Lett* **99**, 345-350.

Ribak CE & Roberts RC (1990). GABAergic synapses in the brain identified with antisera to GABA and its synthesizing enzyme, glutamate decarboxylase. *Journal of Electron Microscopy Technique* **15**, 34-48.

Rigas P & Castro-Alamancos MA (2004). Leading role of the pyriform cortex over the neocortex in the generation of spontaneous interictal spikes during block of GABA(A) receptors. *Neuroscience* **124**, 953-961.

Rowe TB, Macrini TE, & Luo ZX (2011). Fossil evidence on origin of the mammalian brain. *Science* **332**, 955-957.

Sander T (1996). The genetics of idiopathic generalized epilepsy: implications for the understanding of its aetiology. *Mol Med Today* **2**, 173-180.

Sanides-Kohlrausch C & Wahle P (1990). VIP- and PHI-immunoreactivity in olfactory centers of the adult cat. *J Comp Neurol* **294**, 325-339.

Sato T, Yamada N, Morimoto K, Uemura S, & Kuroda S (1998). A behavioral and immunohistochemical study on the development of perirhinal cortical kindling: a comparison with other types of limbic kindling. *Brain Res* **811**, 122-132.

Satou M, Mori K, Tazawa Y, & Takagi SF (1983a). Interneurons mediating fast postsynaptic inhibition in pyriform cortex of the rabbit. *J Neurophysiol* **50**, 89-101.

Satou M, Mori K, Tazawa Y, & Takagi SF (1983b). Neuronal pathways for activation of inhibitory interneurons in pyriform cortex of the rabbit. *J Neurophysiol* **50**, 74-88.

Sayin, Rutecki P, & Sutula T (1999). NMDA-dependent currents in granule cells of the dentate gyrus contribute to induction but not permanence of kindling. *J Neurophysiol* **81**, 564-574.

- Schwabe K, Ebert U, & Loscher W (2000). Bilateral lesions of the central but not anterior or posterior parts of the piriform cortex retard amygdala kindling in rats. *Neurosci* **101**, 513-521.
- Schwarzer C, Tsunashima K, Wanzenbock C, Fuchs K, Sieghart W, & Sperk G (1997). GABA_A receptor subunits in the rat hippocampus II: Altered distribution in kainic acid-induced temporal lobe epilepsy. *Neurosci* **80**, 1001-1017.
- Sharma AK, Reams RY, Jordan WH, Miller MA, Thacker HL, & Snyder PW (2007). Mesial temporal lobe epilepsy: pathogenesis, induced rodent models and lesions. *Toxicol Pathol* **35**, 984-999.
- Sheldon PW & Aghajanian GK (1991). Excitatory responses to serotonin (5-HT) in neurons of the rat piriform cortex: evidence for mediation by 5-HT_{1C} receptors in pyramidal cells and 5-HT₂ receptors in interneurons. *Synapse* **9**, 208-218.
- Shumate MD, Lin DD, Gibbs JW, III, Holloway KL, & Coulter DA (1998). GABA(A) receptor function in epileptic human dentate granule cells: comparison to epileptic and control rat. *Epilepsy Res* **32**, 114-128.
- Sperk G, Schwarzer C, Tsunashima K, & Kandlhofer S (1998). Expression of GABA(A) receptor subunits in the hippocampus of the rat after kainic acid-induced seizures. *Epilepsy Res* **32**, 129-139.
- Striedter GF (2003). Brain evolution. In *The Human Nervous System*, eds. Paxinos G & Mai JK, pp. 1-21. Academic Press, San Diego.
- Sundqvist A (2002). Epilepsy: a clinical diagnostic overview. *Eur J Pain* **6**, 21-25.
- Sutula T, Cascino G, Cavazos J, Parada I, & Ramirez L (1989). Mossy fiber synaptic reorganization in the epileptic human temporal lobe. *Ann Neurol* **26**, 321-330.
- Sutula T, Lauersdorf S, Lynch M, Jurgella C, & Woodard A (1995). Deficits in radial arm maze performance in kindled rats: evidence for long-lasting memory dysfunction induced by repeated brief seizures. *J Neurosci* **15**, 8295-8301.
- Sutula TP & Ockuly J (2006). Kindling, spontaneous seizures and the consequences of epilepsy: more than a model. In *Models of Seizures and Epilepsy*, eds. Pitkanen A, Schwartzkroin PA, & Moshe SL, pp. 395-406. Elsevier Academic Press, San Diego.
- Suzuki N & Bekkers JM (2010). Distinctive classes of GABAergic interneurons provide layer-specific phasic inhibition in the anterior piriform cortex. *Cereb Cortex* **20**, 2971-2984.

- Tehrani MH, Baumgartner BJ, Liu S-C, & Barnes EM (1997). Aberrant expression of GABA_A receptor subunits in the tottering mouse: an animal model for absence seizures. *Epilepsy Res* **28**, 213-223.
- Thom M (2004). Recent advances in the neuropathology of focal lesions in epilepsy. *Expert Rev Neurother* **4**, 973-984.
- Traub RD, Whittington MA, Buhl EH, Jefferys JG, & Faulkner HJ (1999). On the mechanism of the gamma --> beta frequency shift in neuronal oscillations induced in rat hippocampal slices by tetanic stimulation. *J Neurosci* **19**, 1088-1105.
- Trotter SA, Kapur J, Anzivino MJ, & Lee KS (2006). GABAergic synaptic inhibition is reduced before seizure onset in a genetic model of cortical malformation. *J Neurosci* **26**, 10756-10767.
- Tseng GF & Haberly LB (1988). Characterization of synaptically mediated fast and slow inhibitory processes in piriform cortex in an in vitro slice preparation. *J Neurophysiol* **59**, 1352-1376.
- Tseng GF & Haberly LB (1989a). Deep neurons in piriform cortex. I. Morphology and synaptically evoked responses including a unique high-amplitude paired shock facilitation. *J Neurophysiol* **62**, 369-385.
- Tseng GF & Haberly LB (1989b). Deep neurons in piriform cortex. II. Membrane properties that underlie unusual synaptic responses. *J Neurophysiol* **62**, 386-400.
- Turski WA, Cavalheiro EA, Bortolotto ZA, Mello LM, Schwarz M, & Turski L (1984). Seizures produced by pilocarpine in mice: a behavioral, electroencephalographic and morphological analysis. *Brain Res* **321**, 237-253.
- Vinters HV, Armstrong DL, Babb TL, Dumas-Duport C, Robitaille Y, Bruton CJ, & Farrel MA (1993). The neuropathology of human symptomatic epilepsy. In *Surgical treatment of the epilepsies* pp. 593-608. Raven Press, New York.
- Vreugdenhil M & Wadman WJ (1994). Kindling-induced long-lasting enhancement of calcium current in hippocampal CA1 area of the rat: relation to calcium-dependent inactivation. *Neurosci* **59**, 105-114.
- Wahnschaffe U, Ebert U, & Loscher W (1993). The effects of lesions of the posterior piriform cortex on amygdala kindling in the rat. *Brain Res* **615**, 295-303.
- Wallace RH, Marini C, Petrou S, Harkin LA, Bowser DN, Panchal RG, Williams DA, Sutherland GR, Mulley JC, Scheffer IE, & Berkovic SF (2001). Mutant

- GABA(A) receptor gamma2-subunit in childhood absence epilepsy and febrile seizures. *Nat Genet* **28**, 49-52.
- Wieser HG (2004). ILAE Commission Report. Mesial temporal lobe epilepsy with hippocampal sclerosis. *Epilepsia* **45**, 695-714.
- Williamson PD, Engel JJr, & Munari C (1998). Anatomic classification of localisation-related epilepsies. In *Epilepsy: A Comprehensive Textbook*, eds. Engel JJr & Pedley TA, pp. 2405-2416. Lippincott-Raven, Philadelphia.
- Wilson DA & Barkai E (2010). Olfactory cortex. In *Handbook of Brain Microcircuits*, eds. Shepherd G & Grillner S, pp. 263-273. Oxford University Press.
- Wolf HK, Campos MG, Zentner J, Hufnagel A, Schramm J, Elger CE, & Wiestler OD (1993). Surgical pathology of temporal lobe epilepsy. Experience with 216 cases. *J Neuropathol Exp Neurol* **52**, 499-506.
- Wozniak DF, Stewart GR, Miller JP, & Olney JW (1991). Age-related sensitivity to kainate neurotoxicity. *Exp Neurol* **114**, 250-253.
- Wu C & Leung LS (1997). Partial hippocampal kindling decreases efficacy of presynaptic GABAB autoreceptors in CA1. *J Neurosci* **17**, 9261-9269.
- Young A & Sun QQ (2009). GABAergic inhibitory interneurons in the posterior piriform cortex of the GAD67-GFP mouse. *Cereb Cortex* **19**, 3011-3029.
- Zatorre RJ, Jones-Gotman M, Evans AC, & Meyer E (1992). Functional localization and lateralization of human olfactory cortex. *Nature* **360**, 339-340.
- Zelano C, Bensafi M, Porter J, Mainland J, Johnson B, Bremner E, Telles C, Khan R, & Sobel N (2005). Attentional modulation in human primary olfactory cortex. *Nat Neurosci* **8**, 114-120.
- Zhang C, Szabo G, Erdelyi F, Rose JD, & Sun QQ (2006). Novel interneuronal network in the mouse posterior piriform cortex. *J Comp Neurol* **499**, 1000-1015.
- Zhang N, Wei W, Mody I, & Houser CR (2007). Altered localization of GABA(A) receptor subunits on dentate granule cell dendrites influences tonic and phasic inhibition in a mouse model of epilepsy. *J Neurosci* **27**, 7520-7531.
- Zhao D & Leung LS (1991). Effects of hippocampal kindling on paired-pulse response in CA1 in vitro. *Brain Res* **564**, 220-229.

Chapter 2. Diverse interneuron populations have highly specific interconnectivity in the rat piriform cortex

2.1 Introduction

The piriform cortex (PC) is part of the limbic system and is located in the paleocortex. In addition to olfactory sensation and memory processing, the PC has also been implicated in the development of seizures (Racine *et al.*, 1988; Rigas & Castro-Alamancos, 2004), displaying spontaneous epileptiform events under in vitro conditions (McIntyre & Wong, 1986; Haberly & Sutula, 1992). The PC has a distinct potential to generate spontaneous interictal (epileptiform) spikes (Rigas & Castro-Alamancos, 2004). This high-frequency activity is intrinsically generated in the posterior piriform cortex (pPC) and spreads to the neocortex (Rigas & Castro-Alamancos, 2004); therefore, the pPC appears to be responsible for the spread of excitatory waves in limbic epileptogenesis (Loscher & Ebert, 1996).

The γ -aminobutyric acid (GABA)-ergic interneuron system prevents excess excitation, playing an important role in the regulation of neuronal excitability (Mody, 2001) and the rhythmicity of the neural network (Freund, 2003; Whittington & Traub, 2003). An altered GABAergic system that shifts the inhibition–excitation network balance is thought to be relevant in epilepsy and epileptogenesis (Sloviter, 1987; Kamphuis *et al.*, 1994; Fritschy *et al.*, 1998; Cossart *et al.*, 2001; Dinocourt *et al.*, 2003; Gavrilovici *et al.*, 2006; Fritschy *et al.*, 1999; Fritschy *et al.*, 1999). It is commonly accepted that the inhibitory control in the PC is sustained by GABAergic interneurons that form feed-forward (Ballain *et al.*, 1998; Kanter *et al.*, 1996; Kapur *et al.*, 1997; Princivalle *et al.*, 2000; Ekstrand *et al.*, 2001a) and feedback (Haberly & Bower, 1984; Ballain *et al.*, 1998) circuits. Interneurons represent one of the most diverse populations in the mammalian central nervous system. Interneuron characterization based on neurochemical content, i.e., the presence of calcium-binding proteins (CBPs) or neuromodulators such as somatostatin, is considered to be one of the most useful characterization methods (Freund & Buzsaki, 1996);

Data presented in this chapter has been published as: Gavrilovici C, D'Alfonso S, & Poulter MO (2010). Diverse interneuron populations have highly specific interconnectivity in the rat piriform cortex. *J Comp Neurol* **518**, 1570-1588.

McBain & Fisahn, 2001; Markram *et al.*, 2004), as opposed to functional characterization, which has proved to be highly problematic, or anatomical classification, which tells little about interneuron function (McBain & Fisahn, 2001). Parvalbumin (PV), calbindin D28K (CB), and calretinin (CR) are calcium-binding proteins uniquely expressed in neurons that also express GABA and not in excitatory (glutamatergic) neurons (McBain & Fisahn, 2001). Thus, mapping CBP expression provides information on the location and morphology of different interneuronal subpopulations.

One problem associated with CBP characterization is that cells expressing the same CBP can possess surprisingly different functional and morphological properties; thus, using differential expression of a CBP may not necessarily be delineating strictly one particular subtype of interneuron. Also, because there is some overlap in CBP expression, especially between CB and PV (Kawaguchi & Kubota, 1997; Wang *et al.*, 2002) and to a lesser extent between CB and CR (Kubota & Jones, 1993; Kubota *et al.*, 1994; Kawaguchi & Kubota, 1997), the use of a single CBP to map any one subtype of interneuron is not precise. This, combined with the fact that there are more than three anatomical, electrical, and combined electrical–anatomical types of interneurons, makes the classification difficult. However, certain patterns of molecular, morphological, and functional attributes of interneurons are observed. If such patterns, expressed in a large number of combinations, are identified, then a number of discrete cell types or even a small number of nonoverlapping categories can be defined and thus the presence of several features can be used to predict a cell subtype (Ekstrand *et al.*, 2001a).

Although studies have been conducted regarding interneurons of the hippocampus (Freund & Buzsaki, 1996), neocortex (Markram *et al.*, 2004), and frontal cortex (Kawaguchi & Kondo, 2002), the PC has not been extensively studied. However, a partial characterization by (Ekstrand *et al.*, 2001a) investigated immunocytochemical characteristics of basket cells, providing detailed morphological descriptions of interneurons, including soma shape and axonal

arborization, but other cell types were not examined. Kubota & Jones (1993) undertook a pioneering study examining the colocalization of CBPs and investigating colocalization of PV, CB, and GABA. The study described the localization of the three proteins as well as some speculation on the source of immunoreactive (IR) terminals that surrounded the non-IR cell somata. Despite this literature, the foundation upon which to develop a complete picture of the interneuron wiring in the PC is still not available. Here we analyze the expression/coexpression of the three CBPs (PV, CB, and CR) and the colocalization of CBPs with the high-affinity GABA transporter-1 (GAT-1) for all PC cell types and layers. The data provide a unified view regarding the location of differing interneurons into the layers of PC, their dendritic arborization patterns, and the synaptic contacts that they make with other IR or non-IR neurons.

Understanding how and which interneurons are wired together provides the framework for subsequent functional work to determine the timing of neural patterns and is fundamental for comprehending the processing mechanisms of the PC, its role in central nervous function, and its activity as a potential seizurogenic area.

2.2 Methods

All experiments were conducted in accordance with the guidelines of the Canadian Council on Animal Care, and protocols were approved by The University of Western Ontario Animal Care Committee. Adult male Sprague Dawley rats (Charles River) weighing 200–250 g at the time of the study were used. Animals were individually housed with free access to food and water and maintained on a 12-hour/12-hour light/dark cycle.

2.2.1 Tissue preparation and fixation

Rats were deeply anesthetized with ketamine (100 mg/kg, i.p.)/xylazine (10 mg/kg, i.p.) and perfused intracardially with 0.1 M phosphate-buffered saline (PBS), pH 7.3, followed by 4% paraformaldehyde (PAF). The brain was then removed from

the skull and drop fixed in a solution of 10% glycerol and 2% dimethylsulfoxide (DMSO) dissolved in 4% PAF for 24 hours and then placed in a cryoprotectant solution of 20% glycerol and 2% DMSO dissolved in 0.1 M phosphate buffer (PB), pH 7.3, for 48 hours. The brains were then flash frozen in -50°C isopentane for 50 seconds and stored at -80°C until sectioning. The tissue was sectioned in a cryostat at -30°C in the coronal plane into 30- μm sections. The free-floating sections were placed in PBS-filled tissue culture dishes and were stored at -20°C in a 50:50 glycerol/PBS solution until they were ready to be processed.

2.2.2 Antigen retrieval and immunohistochemistry

Antigen retrieval procedures, based on microwave irradiation, were used to enhance the immunohistochemical staining via “unmasking” of subunit epitopes. Microwave irradiation of fixed tissue has been shown to produce a marked reduction of nonspecific staining, allowing improved detection of immunohistochemical signal (Fritschy et al., 1998).

Tissue sections were soaked overnight at 4°C in $1\times$ sodium citrate buffer, pH 4.5 for 24 hours. Sections were then microwaved at 90% power for 50 seconds in a 1,000-W microwave oven. The sections were allowed to cool and then were washed with PBS three times for 5 minutes, followed by PBS with 0.2% Triton-X three times for 5 minutes. The primary antibody solutions were pipetted into the tissue culture dish wells, and the sections were incubated overnight at 4°C . Sections were then washed with PBS with 0.2% Triton-X three times for 10 minutes, followed by application of secondary antibody solution and incubated for 2 hours at room temperature under low-light conditions. Sections were then washed with PBS with 0.2% Triton-X three times for 10 minutes.

To reduce autofluorescence, sections were placed in a solution of 1% Sudan black (Sigma, St. Louis, MO) dissolved in 70% ethanol for 2 minutes and then placed in 70% ethanol twice for 1 minute each, then again in 70% ethanol once for 2 minutes followed by two washes of PBS for 5 minutes each (Schnell *et al.*, 1999).

All washes and incubations took place on an agitator to ensure thorough washes and adequate antibody binding. Sections were wet mounted onto Fisher SuperFrost slides and mounted with glass coverslips in Prolong Gold Antifade mounting medium (Molecular Probes, Eugene, OR), allowed to cure overnight at room temperature, and sealed the next day with nail polish. Slides were stored at -20°C and protected from light until they were ready to be imaged.

2.2.3 Antibodies

Free-floating, 30- μm coronal rat sections were labelled with each of the following antibody combinations, in which all primary antibodies were diluted in antibody diluting buffer (Dako Diagnostics Canada, Mississauga, Ontario, Canada), and all secondary antibodies were diluted in PBS. Information on the primary antibodies used in our study is shown in Table 2.1. Further details regarding the specificity of each primary antibody are provided below. 1) Mouse monoclonal antiparvalbumin antibody specifically stains the $^{45}\text{Ca}^{2+}$ binding spot of PV in a two-dimensional immunoblot (manufacturer's data sheet) and specifically stains olfactory bulb PV interneurons (Parrish-Aungst *et al.*, 2007). 2) Rabbit polyclonal anticalbindin antibody stains a single band of 28 kD molecular weight on Western blots of mouse brain (Chalazonitis *et al.*, 2008). 3) Goat polyclonal anticalretinin antibody stains the expected band of 31 kD molecular weight on Western blots of rat posterior pituitary (Miyata *et al.*, 2000); the goat anticalretinin antibody recognizes a protein of the molecular mass and isoelectric point of CR in an immunoblot of a two-dimensional gel from rat cerebellum (Winsky *et al.*, 1996); rat brain staining is eliminated by preabsorption of anticalretinin antibody with purified rat recombinant calretinin (Winsky *et al.*, 1996). 4) Mouse monoclonal anticalbindin D28k antibody specifically stains the $^{45}\text{Ca}^{2+}$ binding spot (28 kD molecular weight) of calbindin D28k in a two-dimensional gel (manufacturer's data sheet). 5) Guinea pig polyclonal antiparvalbumin antibody recognizes both the calcium-bound and calcium-free forms of mammalian PV (manufacturer's technical information) and specifically stained PV

neurons in the rat hippocampus (Ferraguti *et al.*, 2004; Somogyi *et al.*, 2004). 6) Rabbit polyclonal anti-GABA transporter 1 (GAT-1) antibody recognized a single band of 67 kD molecular weight on immunoblots of rat diencephalon, consistent with the predicted size of GAT-1 (De Biasi *et al.*, 1998); this antibody stains GABAergic nerve terminals in rat cerebral cortex (Minelli *et al.*, 1995) and human brain (Woo *et al.*, 1998); rat brain staining is abolished when GAT-1 antibodies were preadsorbed with rat GAT-1₅₈₈₋₅₉₉ (Minelli *et al.*, 1995).

The list of the secondary antibodies used in each colocalization experiment is provided below: for the PV/CB colocalization: Alexa 555-conjugated donkey anti-mouse IgG (1:1,000) and Alexa 488-conjugated donkey anti-rabbit IgG (1:500); for PV/CR colocalization: Alexa 488-conjugated donkey anti-mouse IgG (1:1,000) and Alexa 546-conjugated donkey anti-goat IgG (1:1,000); for CB/CR colocalization: Alexa 488-conjugated donkey anti-mouse IgG (1:500) and Alexa 546-conjugated donkey anti-goat IgG (1:1,000); for PV/CB/GAT-1 colocalization: Alexa 488-conjugated donkey anti-mouse IgG (1:500), Alexa 546-conjugated goat anti-guinea pig IgG (1:4,000), and Alexa 647-conjugated donkey anti-rabbit IgG (1:2,000); for CR/GAT-1 colocalization: Alexa 546-conjugated donkey anti-goat IgG (1:1,000) and Alexa 647-conjugated donkey anti-rabbit IgG (1:2,000). The specificity of the secondary antibodies was verified in control sections in which the primary antibody was omitted. No staining was detected in omission control sections (data not shown).

Table 2.1 Primary Antibodies Used in the Study

| Co-localization | Primary antibody | Catalog # | Lot | Immunogen |
|---------------------------------|---|----------------|--------------|--|
| Parvalbumin/ Calbindin | <u>anti-Parvalbumin</u> mouse; 1:5000 Swant, Switzerland | 235 | 10-11(F) | Purified carp muscle parvalbumin |
| | <u>anti-Calbindin</u> rabbit; 1:500 Chemicon, Canada | AB1778 | 21071010 | Recombinant mouse calbindin |
| Parvalbumin/ Calretinin | <u>anti-Parvalbumin</u> mouse; 1:5000 Swant, Switzerland | 235 | 10-11(F) | Purified carp muscle parvalbumin |
| | <u>anti-Calretinin</u> goat; 1:4000 Chemicon, Canada | AB1550 | 23100764 | Recombinant guinea pig calretinin |
| Calbindin/ Calretinin | <u>anti-Calbindin</u> mouse; 1:1200 Research Diagnostics Inc., USA | RDI-Calbindabm | 18(f) | Calbindin D-28k purified from chicken gut |
| | <u>anti-Calretinin</u> goat; 1:4000 Chemicon, Canada | AB1550 | 23100764 | Recombinant guinea pig calretinin |
| Parvalbumin/ Calbindin/GAT-1 | <u>anti-Calbindin</u> mouse; 1:500 Research Diagnostics Inc., USA | RDI-Calbindabm | 18(f) | Calbindin D-28k purified from chicken gut |
| | <u>anti-Parvalbumin</u> guinea pig; 1:2000 Chemicon, Canada | AB9314 | Not provided | Purified rat muscle parvalbumin |
| | <u>anti-GABA plasma membrane transporter type-1 (GAT-1)</u> rabbit 1:75 Chemicon, Canada) | AB1570 | 24070738 | Synthetic GAT-1, aa 588-599 from C-terminus of rat |
| Calretinin/GAT-1 | <u>anti-Calretinin</u> goat; 1:4000 Chemicon, Canada | AB1550 | 23100764 | Recombinant guinea pig calretinin |
| | <u>anti-GABA plasma membrane transporter type-1(GAT-1)</u> rabbit; 1:75 Chemicon, Canada | AB1570 | 24070738 | Synthetic GAT-1, aa 588-599 from C-terminus of rat |

2.2.4 Image acquisition

Confocal images for Figure 2.1 and Figures 2.4–2.10 were taken on an Olympus IX 60 inverted microscope outfitted with a Perkin Elmer Spinning Disk Confocal attachment with a 20× (N.A. = 0.50) objective. Optical resolution for this objective was 490 nm at $\lambda = 490$ nm, 540 nm at $\lambda = 540$ nm, and 650 nm at $\lambda = 650$ nm. The microscope was equipped with a Hamamatsu Orca ER CCD camera (1,300 × 1,030 pixels), and images were acquired in Volocity software. Each image, unless otherwise indicated, represents a stack of 40–50 images 0.2 μm apart in the z-plane. This was performed for each wavelength channel.

Composite images (Fig. 2.2) were taken with an Olympus BX51 widefield fluorescence microscope with a 4× objective [numerical aperture (N.A.) = 0.13] having an optical resolution of 1,885 nm at $\lambda = 490$ nm and 2,077 nm at $\lambda = 540$ nm. The microscope was equipped with a Photometrics CoolSnap fx CCD camera (1,300 × 1,030 pixels), and images were acquired in ImagePro software.

The region of the PC that was examined was posterior to the caudal limit of the LOT (Luskin & Price, 1983). This pertains to approximately –2.30 Bregma from (Paxinos & Watson, 1986). Images were taken from the top of the PC just below the perirhinal cortex, to the end of the PC adjacent to the basolateral amygdala. Individual pictures were taken for L1–2 and L2–3. PC layer depth and demarcation between adjacent layers were set according to (Neville & Haberly, 2004) and (Ekstrand *et al.*, 2001a).

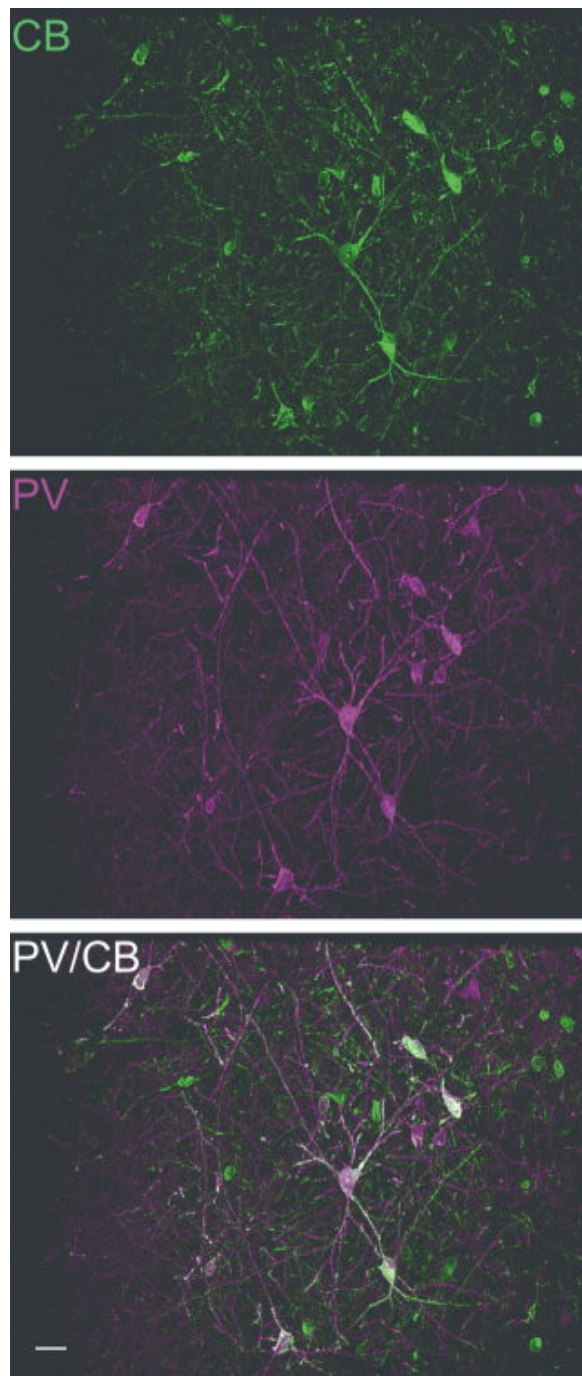


Figure 2.1 Example of the raw data showing two channels of images and the colocalized channel (white), which was added after appropriate thresholding of the magenta and green channels. For complete description see Materials and Methods. Scale bar = 20 μm .

2.2.5 Image processing and analysis

2.2.5.1 Interneuron localization in PC.

For each CBP, two stained slides from each animal were used to count the number of CBP-IR cells in each layer of the PC. To identify the number and distribution of particular CBP-expressing cells in each of the layers, stained slides were viewed under an Olympus BX51 widefield fluorescence microscope with a 20× objective (N.A. = 0.5). The individual images of Figure 2.2 were combined to make composite images in CorelDraw 12 software and visually adjusted for contrast.

2.2.5.2 CBP colocalization.

For the analysis of coexpression of the CBPs (Figs. 2.4, 2.5), the stacks of confocal images (10 μm thick with 0.2 μm z-spacing) were deconvolved with AutoQuant software (AutoQuant Imaging, Burnbury, Ontario, Canada) and then processed in Imaris software (Bitplane, Zurich, Switzerland). The images were analyzed with the colocalization module, which allows the pixels in each channel to be windowed according to a set of criteria and include only these pixels in the colocalization analysis.

Targets of interest are highly localized and intensely labelled; therefore, to isolate the high-intensity fluorescent signal from nonspecific or diffuse staining, an appropriate threshold for an image must be chosen. This threshold must separate the tail of the histogram of pixel intensities, containing specific high-intensity fluorescence, from the body of the intensity distribution. The different possible criteria for thresholding allow a choice regarding how rigorous elimination of nonspecific or diffuse staining should/can be. The procedure is subjective, but, once a suitable thresholding criterion is established, it is well defined and repeatable and allows comparison of different images on a common basis (see (Hutcheon *et al.*, 2000; Hutcheon *et al.*, 2004). The threshold used in this analysis was the 5% brightest pixels in each channel; thus, in order for CBPs to be considered colocalized, pixels from each channel that were juxtaposed also had to represent the

top 5% of each channel intensity. These pixels were turned to a different color, and the software created a separate colocalization channel depicted as white in all colocalization figures. The images were then processed with the Easy 3D module, which makes a projection of all the images of the stack. For contrast enhancement, background from each channel was subtracted, and the image was brightened while avoiding saturation. The difference between the raw and the processed data can be seen in Figure 2.1.

To quantify the frequency of CB-IR cells also expressing PV and the frequency of PV-IR cells expressing CB, two stacks of images from all animals were processed as described above. Then, for each image, the numbers of CB-IR cells were counted and the numbers of CB/PV colocalized cells were counted, and this was expressed as the percentage of CB-IR cells colocalized with PV. The same procedure was done for PV-IR cells. This technique was restricted to PV-IR and CB-IR, because our data indicated that these are the only CBP-IR cells that can be coexpressed in the PC interneurons.

Finally, Figures 2.4 and 2.5 show the bidimensional histogram of the channel in the x-axis and the y-axis. The histogram axes indicate the voxel intensities (0–4,095 levels of gray) occurring in each channel. The yellow box indicates the voxels included in the colocalization analysis, which pertains to the top 5% voxels from each channel. Voxels within the yellow box that are found along the center diagonal are positively correlated and thus are the colocalized pixels demonstrated by the white pixels in the picture (Fig. 2.4).

2.2.5.3 Dendritic arborization of interneurons defined by neurochemical content

For estimation of the morphological reconstruction of the dendritic arborization of interneurons (Figs. 2.6–8), the stacks of confocal images were deconvolved with AutoQuant software (AutoQuant Imaging) and then processed with Imaris Filament Tracer module in “Surpass mode” (Bitplane). Filament tracer creates dendritic arborization patterns based on an algorithm that predicts

arborization pathways. These pathways are set up by the user-set criteria of a start point, namely, the size of cell somata, and an end point representing minimum thickness of processes. Start points were set to 10 μm , and endpoints were set to 1 μm . The resultant filament lines were converted from lines to two-pixel-thick cones. To mark the cell bodies, an “Isosurface” was then created. This process creates a cell body from the stack of images that is then merged with the dendritic morphology.

To determine the predominant shape of the dendritic arborization among interneuron subtypes, the ratio of horizontal dendritic expanse to the vertical dendritic expanse was taken. Three sets of pictures for each CBP for each animal were processed as described above. Each cell in the picture was measured for its horizontal and vertical length. “Horizontal” was considered to be a parallel orientation to the layers, and “vertical” was considered to be a perpendicular orientation to the layers (see Figs. 2.6–8). For each cell, the maximal distribution covered by the dendrites in each direction was used as the measure of dendritic arborization. The data for each CBP and each layer were averaged, and a ratio was determined from the averages.

2.2.5.4 Innervation of interneurons defined by neurochemical content and coexpression

For image processing of colocalization of CBPs with GAT-1 (Figs. 2.9, 2.10), stacks of confocal images were deconvolved (AutoQuant Imaging) and processed in Imaris software (Bitplane). Similarly to the CBP colocalization analysis, the images were processed with the “Colocalization” module, and the threshold used in the analysis was also the 5% brightest pixels in each channel. A separate colocalization channel was again created, and the colocalized pixels were depicted as white in all figures. The images were then processed with the “Easy 3D” module. For contrast enhancement, background from each channel was subtracted, and the image was brightened while avoiding saturation.

To determine the percentage of inhibitory terminals from each CBP-expressing cell type in each layer, the stacks of confocal images were deconvolved (AutoQuant Imaging) and processed in IP Lab software (Scanalytics, Fairfax, VA). The stacks of images from each color channel were superimposed to create one frame from which the degree of colocalization of CBP and GAT-1 could be determined. Once again, the threshold used in this analysis was the 5% brightest pixels in each channel. These pixels were changed to a different color to visualize the colocalization, a procedure called *segmentation*. The program was then able to quantify the numbers of pixels that were colocalized (or segmented) within each region of interest (ROI), namely, L1, L2, and L3. The number of segmented pixels for each ROI was expressed as a percentage of the total number of GAT-1 pixels with intensity levels greater than or equal to the top 5% intensity levels. This analysis was done for two stacks of pictures from each animal.

Our analysis relies on some assumptions that limit our interpretation of the data. First, the analysis of the dendritic trees provides an estimate of the shape of the arborization pattern for a given subpopulation of interneurons; however, it cannot be considered to represent the entire dendritic tree. Nevertheless, it does provide a view of the bias with which different CBP-IR types of interneurons extend their dendritic processes. Second, the estimation of the terminal fields of these interneurons is limited by our ability to resolve the CBP signal at release sites. Although we can be reasonably sure that, when the CBP/GAT1 colocalization is detected, this represents a terminal or *bouton*, we are unsure whether every release site contains a CBP, so release sites without CBP might remain undetected. There is to our knowledge no evidence that interneurons can have a heterogeneous distribution of CBP at their release sites, so, at the very least, our analysis provides a detailed view of CBP/GAT-1-containing release sites within this region.

2.2.6 Cell nomenclature

The terminology describing interneuron soma and dendritic morphology in this report was similar to that used by Ekstrand *et al.* (2001a). The term *multipolar* was used to describe somata with a round to ovoid form with dendrites in many directions. The term *multiangular* was applied to multipolar cells whose dendrites had strongly tapering origins that distorted somatic shape. *Fusiform* described cells with elongated soma shapes that blended into thick dendritic trunks at opposing ends. *Globular* was applied to somata with a smooth, rounded contour whose dendrites originated abruptly. *Bipolar* was applied to cell bodies of globular form with two dendritic trunks at opposing ends. *Bitufted* defined cells with long apical and basal dendritic tufts that extended vertically through much of the depth of the cortex, regardless of whether individual dendrites originated directly from cell bodies or from bipolar stems.

2.3 Results

2.3.1 Interneuron localization in PC

Low-magnification widefield photomicrographs were examined to determine the anatomical distribution of the CBP-IR in the adult rat PC. We found that each CBP had a unique pattern of expression (Fig. 2.2). PV-IR somata were seen in L2–3. The highest density of PV-IR cell somata (~73%) was found in L3, whereas the remaining 27% of PV-IR cells was localized to L2 of PC (Table 2.2).

Figure 2.2 General distribution of calcium-binding protein (CBP) interneurons in the piriform cortex. **Left:** Low-power widefield photomicrographs of immunohistochemically stained coronal sections showing the distribution of CBP interneurons: parvalbumin (PV), calbindin (CB), and calretinin (CR). **Middle and right:** Magnified view of piriform cortex showing layer CBP distribution in layers 1–2 (middle) and 2–3 (right). Parvalbumin distribution (first row): PV immunoreactivity (PV-IR) is highly distributed in L1–3. Cell somata are most concentrated in L3, but some somata are also in L2. White arrow indicates cell somata in L3; red arrow indicates a cell soma with dendrites extending into L1. Calbindin distribution (second row): CB-IR is highly distributed in L3. Cell somata are almost exclusively found in L3. White arrow indicates cell soma in L3. Calretinin distribution (third row): CR-IR is highly distributed between L1 and L3. Cell somata are found in all three layers. White arrow indicates a cell soma in L3; red arrow indicates cell soma in L2; blue arrow indicates a cell soma in L1. Demarcation between piriform cortex layers is shown in the middle and right panels (dotted line). L1, layer 1; L2, layer 2; L3, layer 3 of piriform cortex. Scale bars = 100 μm in left panels; 25 μm in middle and right panels.

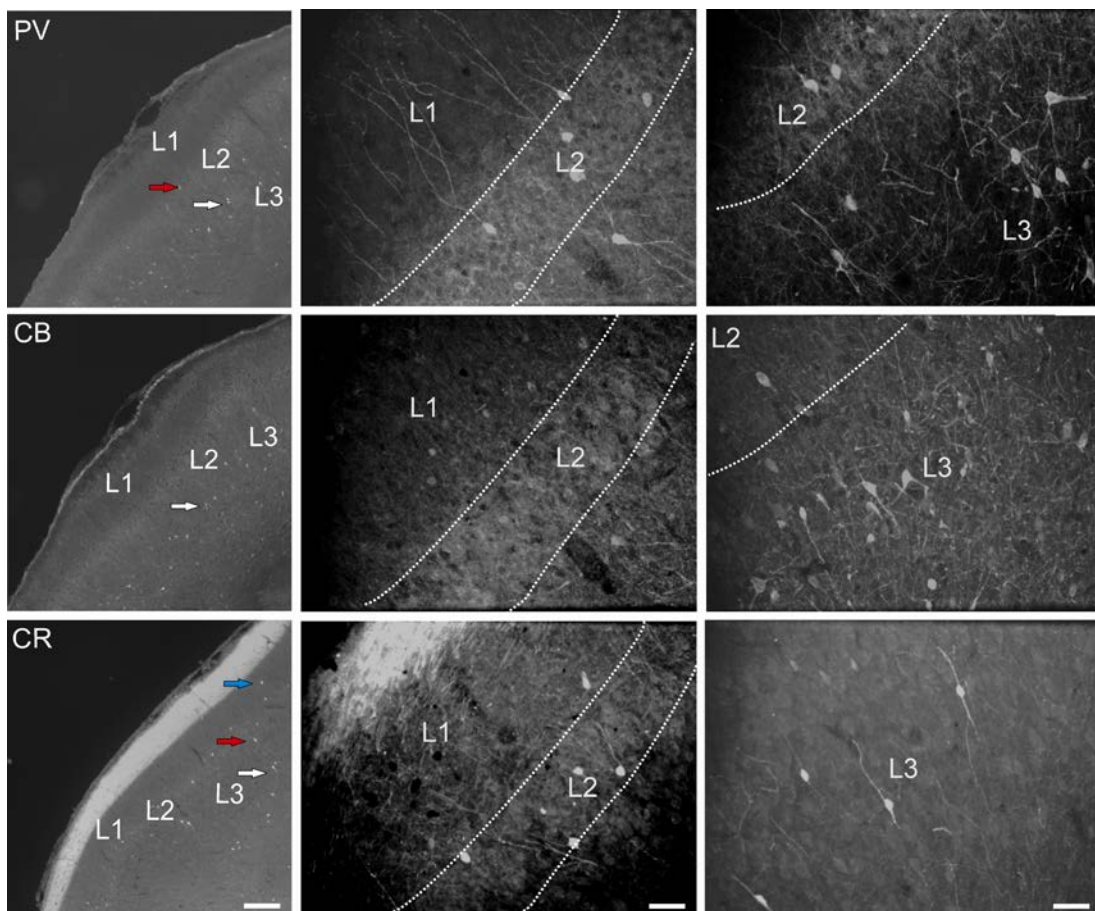


Table 2.2 Distribution of calcium-binding protein immunoreactive cells in the rat piriform cortex layers.

| CBP | CR % | CB % | PV/CB % | PV % |
|---------|--------------|------------|-------------|----------|
| Layer 1 | 4.85 ± 0.52 | - | - | - |
| Layer 2 | 40.03 ± 1.41 | 4.73 ± 0.7 | 19.94 ± 1 | 27 ± 1.5 |
| Layer 3 | 55.10 ± 1.22 | 95.27 ± 1 | 80.06 ± 1.1 | 73 ± 1.5 |
| ANOVA | L3>L2>>L1 | L3>>L2 | L3>>L2 | L3>>L2 |

Data are shown as means ± SE (n = 9). The numbers in the columns indicate the percentage of each CBP-IR cell population present in the three layers of piriform cortex. Statistical analysis (ANOVA) showing cell layer distribution differences for each CBP-IR cell population is indicated in the bottom row ($P < 0.001$; $P < < 0.0001$). CBP, calcium-binding protein; PV, parvalbumin-immunoreactive cells; CB, calbindin-immunoreactive cells; CR, calretinin-immunoreactive cells; PV/CB, colocalized parvalbumin/calbindin-immunoreactive cells; L1, layer 1; L2, layer 2; L3, layer 3.

In contrast to the PV distribution, CB-IR somata were almost entirely confined to L3 (~95%) and were rarely found in L2 (~5%; Table 2.2). Similarly to the PV-IR cell distribution, CB-IR somata were not found in L1 of the PC. CR-IR cell somata were distributed mainly in L3 (~55%) and L2 (~40%). However, unlike the case for PV-IR or CB-IR, ~5% of total CR-IR cell bodies were also found in L1 (Table 2.2).

Quantification of the cell somata indicates that the majority of CBP-expressing interneurons are found in L3 of the PC (~79%). L2 contains 19% of total CBP interneuronal population, whereas, for L1, we found a small population (~1%) of CR-IR cells (Fig. 2.3).

2.3.2 CBP colocalization

To determine whether any of the CBPs were coexpressed in the interneurons of the various layers of the PC, dual immunohistochemistry was conducted with combinations of the antisera against the three CBPs in tissue sections (see Materials and Methods for details). It was found that CB and PV colocalize both in cell somata of varying morphological types and in dendritic processes (Fig. 2.4). Colocalization of CB and PV was found mainly in L3 and L2 (Fig. 2.4, Table 2.2). Although PV/CB-IR cells had a layer distribution similar to that of PV-IR (80% in L3 and 20% in L2), the number of PV/CB cells across PC layers was the highest among all CBP⁺ types (42% of total CBP-IR cells were PV/CB compared with 30% CB, 21% CR, and only ~7% PV; Fig. 2.3). Our data also indicated that more PV-IR cells coexpress CB (81% ± 17%; n = 9) compared with CB-IR cells that coexpress PV (31% ± 12%; n = 9).

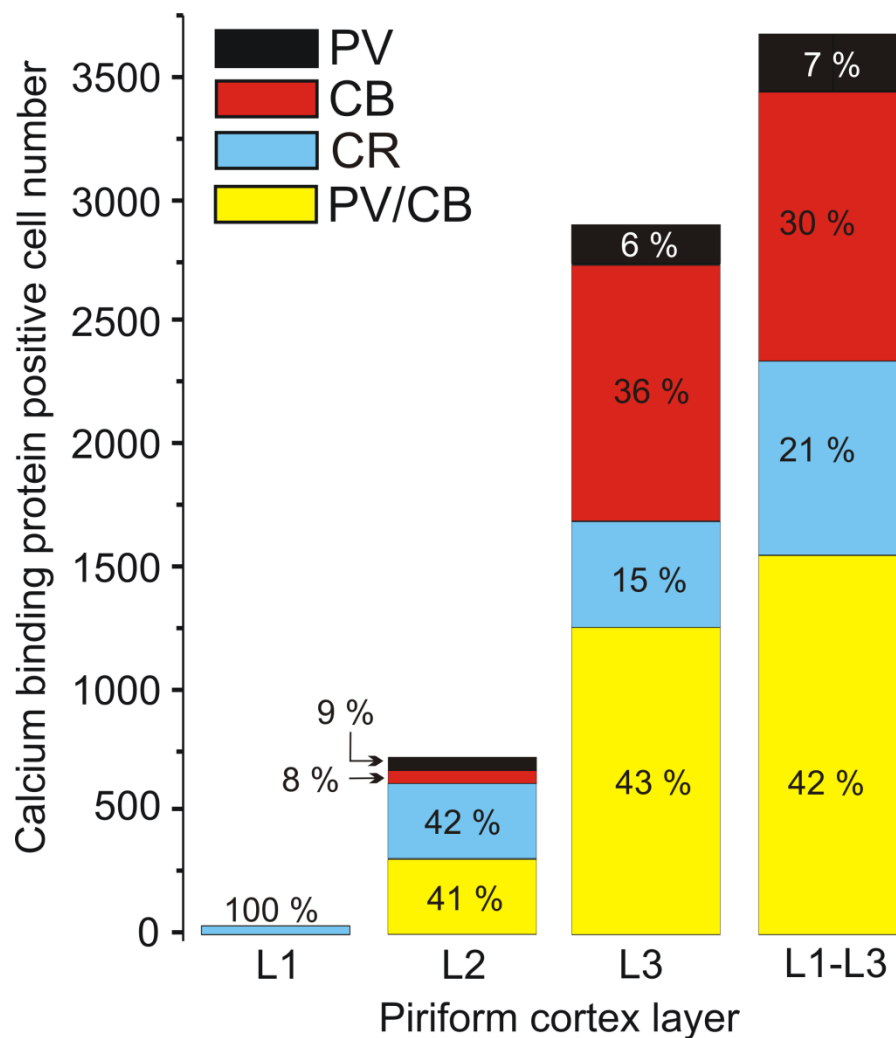


Figure 2.3 Calcium-binding protein immunoreactive (CBP-IR) cell distribution in each layer of the piriform cortex. The numbers represent the contribution (%) of each CBP-IR cell type, CR, CB, PV/CB, and PV, to the total number of CBP-IR cells present in each layer. PV, parvalbumin cells; PV/CB, colocalized parvalbumin/calbindin cells; CR, calretinin cells; L1, layer 1; L2, layer 2; L3, layer 3.

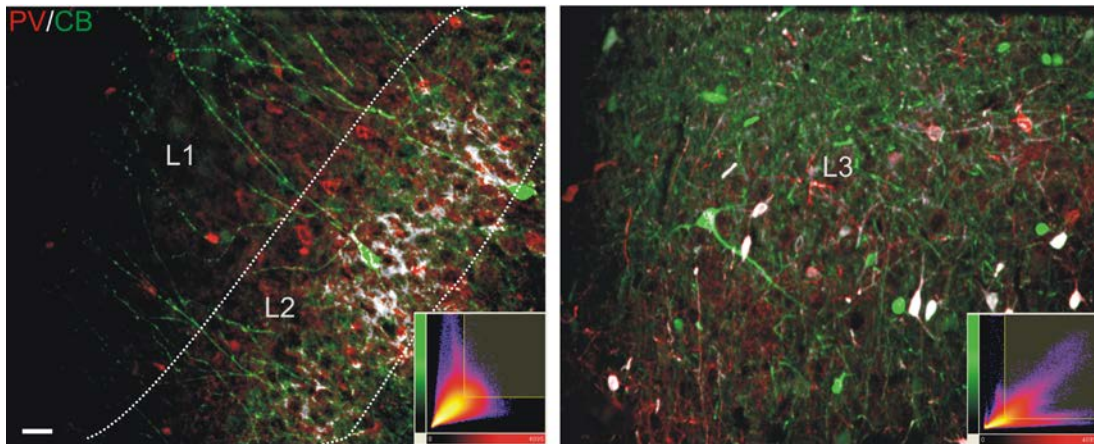


Figure 2.4 Parvalbumin/calbindin (PV/CB) colocalization in the piriform cortex.

Left: PV/CB colocalization in L1–2 of piriform cortex. Green channel represents calbindin immunoreactivity (CB-IR), magenta parvalbumin immunoreactivity (PV-IR), and white colocalized PV/CB-immunoreactive (PV/CB-IR) segments. Few PV-IR, CB-IR, and PV/CB-IR cells can be found in layer 2. Their dendrites traverse the L1–2 border. Most of the colocalized segments in L2 were seen around non-IR cell somata. The histogram indicates colocalization between PV and CB in layers 1–2, in that some voxels are found in the yellow area. **Right:** PV/CB colocalization in L3 of PC. Most of the CB-IR (green), PV-IR (magenta), and PV/CB-IR (white) somata are distributed in layer 3. Histogram indicates that most of the colocalization between PV-IR and CB-IR is found in layer 3, in that many voxels are found in the yellow area in a diagonal pattern, showing a strong positive correlation between the green (CB) and magenta (PV) channels. L1, layer 1; L2, layer 2; L3, layer 3. Scale bar = 15 μm .

Next, we examined whether PV and CR were coexpressed. Despite common localization of PV and CR somata and dendritic processes, there was no colocalization present in PC (Fig. 2.5). Finally, CB/CR coexpression analysis indicated that CB cells do not coexpress CR and that CR cells do not coexpress CB in the PC.

Our data indicated that each layer of PC has a unique CBP-IR cell distribution (Fig. 2.3). In L1, the only CBP-IR cells detected (1% of the total PC CBP-IR population; 38 cells; n = 9) were CR-IR. In L2, from a total of 725 CBP-IR cells (n = 9), 307 cells were CR-IR (42%), 54 cells expressed CB (8%), 300 cells coexpressed PV and CB (41%), and only 64 cells were PV-IR (9%). In L3, where most of the CBP cells were located (2,909 cells; n = 9), the distribution of the four types of CBP-IR cells was different: ~43% of total CBP-IR cells were PV/CB, ~36% CB, ~15% CR and only ~6% PV (Fig. 2.3).

2.3.3 Morphological characterization of interneurons defined by neurochemical content

From our observations, it was apparent that the patterns of dendritic immunoreactivity of the CBPs had distinct orientations. To estimate/quantify these observations, single and dual immunohistochemistry was conducted with antisera against the three CBPs in tissue sections (see Materials and Methods). The sections were then viewed with a confocal microscope and reconstructed with software. Figures 2.6–2.8 depict reconstructed dendritic arborizations in various layers of the PC. For simplicity, dendritic expansion perpendicular to the layers will be referred to as *vertical* expansion and dendritic expansion parallel to the layers will be referred to as *horizontal* expansion.

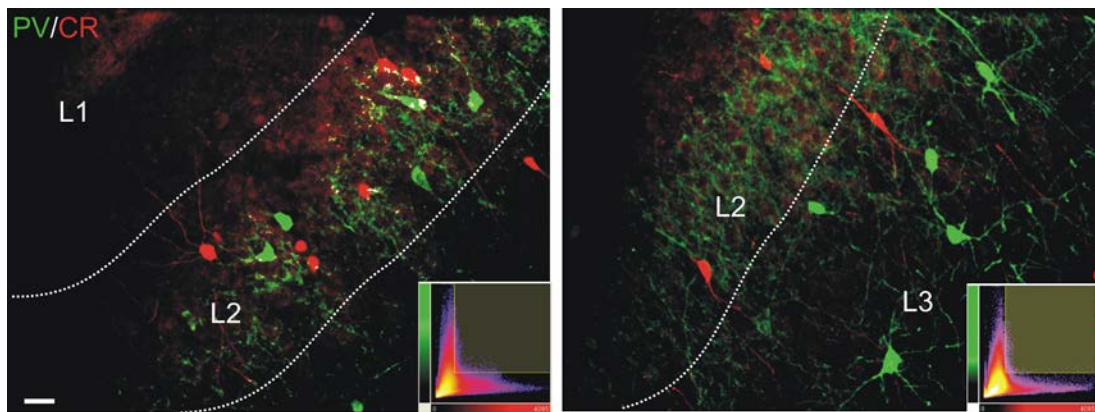


Figure 2.5 Parvalbumin/calretinin (PV/CR) colocalization in the piriform cortex. **Left:** PV/CR colocalization in L1–2 of piriform cortex. Green channel represents parvalbumin immunoreactivity (PV-IR). PV-IR somata are found at the L1–2 border, and thick varicose PV-IR dendritic processes extend into L1. Magenta channel represents calretinin immunoreactivity (CR-IR). Most of CR-IR somata are located in L2, and thin CR-IR dendritic processes can be seen extending into L1. White pixels are not found in this panel, suggesting that there is no colocalization between PV and CR in L1–2. **Right:** PV/CR colocalization in L3 of piriform cortex. PV-IR somata (green channel) are distributed throughout L3; PV-IR dendritic processes are oriented in many directions. CR-IR dendritic processes extend and run only in a specific orientation through the layers. No colocalization (no white pixels) is found in L3. The histograms (bottom right of each panel) indicate the lack of positive correlation between PV and CR channels (green and magenta channels), insofar as there are no voxels found in the yellow area or in the diagonal center of the plot. L1, layer 1; L2, layer 2; L3, layer 3. Scale bar = 15 μ m.

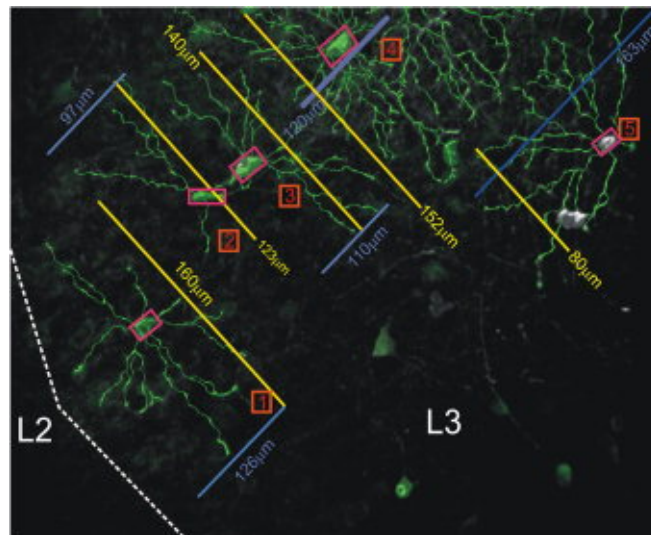


Figure 2.6 Calbindin dendritic arborization in L3 of the piriform cortex. Green signal indicates calbindin immunoreactive (CB-IR) cells in L3; white signal indicates cells that coexpress parvalbumin and calbindin (PV/CB). Blue lines and yellow lines indicate vertical and horizontal expansions; white dotted line represents the border between layers. It can be seen that, in general, CB-IR cells have a widespread dendritic tree in the horizontal direction but are more restricted in the vertical orientation. However, cell 5, which is coexpressing CB and PV, has the opposite pattern, with a greater expansion vertically than horizontally. Dendritic arborizations stop abruptly at the L2–3 border. Soma/dendritic morphology is variable: cells 1, 3, and 5 are multiangular; cell 2 is fusiform; and cell 5 is multipolar. L2, layer 2; L3, layer 3

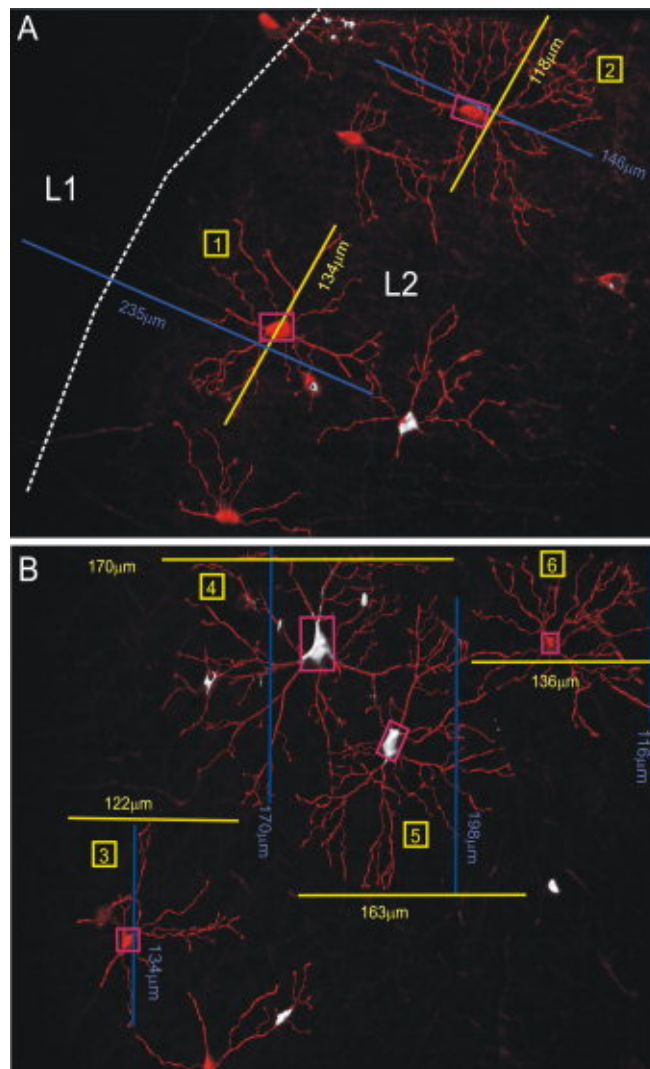


Figure 2.7 Parvalbumin dendritic arborization in the piriform cortex. Red signal indicates PV-IR cells; white signal indicates cells that are PV/CB-IR. Blue lines indicate vertical expansion; yellow lines indicate horizontal expansion. **A:** PV-IR cells with somata in L2 have a widespread dendritic tree in both the horizontal and the vertical orientations. Cell 1 has dendrites that extend into L1, whereas cell 2 has dendrites that stop abruptly at the L1–2 border. **B:** PV-IR cells with somata in L3 also have a widespread dendritic tree in the horizontal and vertical orientations. Soma/dendritic morphology is not variable: all PV-IR cells are multiangular, including those that coexpress CB. L1, layer 1; L2, layer 2; L3, layer 3.

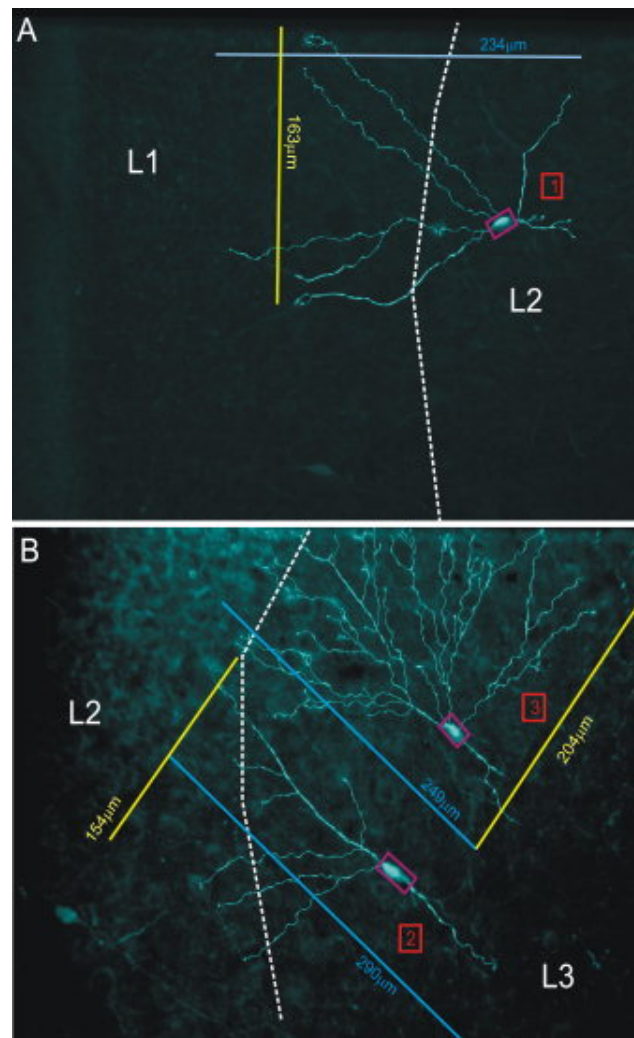
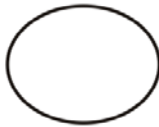
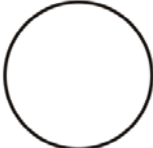

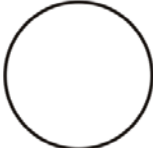


Figure 2.8 Calretinin dendritic arborization in the piriform cortex. Teal signal indicates CR-IR cells. Blue lines indicate vertical expansion; yellow lines indicate horizontal expansion; white dashed lines indicate the borders between layers. **A:** CR-IR cells with somata in L2 have a restricted conical arbor in the horizontal orientation and long vertically oriented dendrites. Cell 1 has dendrites that extend into from L2 into L1. Soma/dendritic morphology of cell 1 is bipolar/bitufted. **B:** CR-IR cells with somata in L3 have a restricted conical arbor in the horizontal orientation and long vertically oriented dendrites. Cells 2 and 3 have dendrites that traverse into L2. Soma/dendritic morphology is not variable: all cells are bipolar/bitufted. L1, layer 1; L2, layer 2; L3, layer 3.

Dendritic arborization reconstruction of CB-IR cells in L3 (where ~95% of all PC CB-IR cells are distributed; Table 2.2) indicated that they had a widespread dendritic tree in the horizontal direction and had a more restricted vertical expansion (1.3:1 ratio; see Table 2.3), giving the dendritic tree an oval shape. Dendrites of the CB-IR cells in L3 remained confined to the same layer (Fig. 2.6), whereas the dendrites of the smaller population of CB-IR cells in L2 (~3% of total CB-IR cells in PC; Table 2.2) traversed the L2 border into L1 (Fig. 2.4). CB-IR cells demonstrated various types of cell somata morphologies, specifically multiangular, fusiform, and globular cell shapes (Fig. 2.6).

PV-IR cell somata were present both in L2 and in L3 (Figs. 2.2, 2.7), so reconstructed dendritic arborizations for PV-IR cells were investigated in both layers. PV-IR cells in L3 (Fig. 2.7B) had a pattern of dendritic arborization different from that of CB-IR cells in L3. We found that PV-IR cells have widespread vertical and horizontal expansions as demonstrated by a 1:1 ratio (see Table 2.3), giving the dendritic tree a circular shape as opposed to an oval shape. Unlike CB-IR cells, PV-IR somata did not demonstrate very much variability in cell soma morphology, insofar as most had multiangular cell somata (Fig. 2.7B). PV-IR cells located in L2 demonstrated a vertical to horizontal dendritic expansion similar to that of PV-IR cells in L3. Some L2 dendrites traversed the layers and extended into L1; others stopped abruptly at the L1–2 border (Fig. 2.7A). PV-IR cell somata morphology is predominantly globular as opposed to the multiangular cell shape found in L3. Cells in L3 that coexpressed PV/CB demonstrated an arborization pattern that was similar to that of PV-IR cells, wherein horizontal expansion was similar to vertical expansion. However, PV/CB soma morphology showed large variability similar to that demonstrated by CB-IR cells.

Table 2.3 Mean ratio of horizontal to vertical dendritic arborization length and dendritic shape of calcium-binding protein cells in layer 2-3 of rat piriform cortex.

| CBP | CB | PV | CR | PV/CB |
|-------|---|---|--|---|
| Ratio | 1.3:1 | 1:1 | 1:1.5 | 1:1 |
| Shape |  |  |  |  |

CBP, calcium binding protein; PV, parvalbumin; CB, calbindin; CR, calretinin; PV/CB, co-localized parvalbumin/calbindin; (n=9).

CR-IR cells were present mainly in L2 and L3 (Fig. 2.2, Table 2.2). CR-IR cells demonstrated a pattern of arborization different from that of CB-IR and PV-IR cells. They were more restricted in the horizontal expansion than in the vertical one, as shown by the 1:1.5 ratio (see Table 2.3), giving the dendritic tree an oval shape, which extended through the layers. This pattern was similar in cells located in L2 and L3. CR-IR cell dendrites readily traversed into other layers: cells in L3 extended into L2, and cells in L2 extend into L1 (Fig. 2.8). In all layers of PC, CR-IR cells displayed a bipolar/bitufted morphology.

2.3.4 Innervation of interneurons defined by neurochemical content and coexpression

To determine the identity of the NTs in the various layers of the PC, dual and triple immunohistochemistry was conducted with combinations of the antisera against the three CBPs and antisera against GAT-1 in tissue sections (for details see Materials and Methods). GAT-1 has been shown to be enriched in GABAergic axons and terminals (Borden, 1996; Ribak *et al.*, 1996). For the PC, it has been previously shown that GAT-1 formed discrete puncta around cells in all layers (Ekstrand *et al.*, 2001b; Gavrilovici *et al.*, 2006). These puncta have been shown to be associated with GAD67 staining and are thought to represent interneuronal nerve terminals in the PC (Ekstrand *et al.*, 2001b). In the present study, when colocalized with a CBP, GAT-1 delineates GABAergic NTs belonging to that particular subset of interneurons. These terminals are referred to as CBP^+ instead of $CBP-IR$, because the CBP identity of the NTs is inferred via colocalization with GAT-1.

Our data showed very few CB^+ NTs in L1, with an even distribution in L2 and L3 (Table 2.4). In L1, CB^+ NTs surrounded non-IR and CB-IR dendrites, whereas, in L2, the CB^+ NTs were found along excitatory cell soma. In L3, CB^+ innervation was seen around cell bodies of non-IR cell bodies and on perisomatic

Table 2.4 Percent of GABA Transporter Type-1 (GAT-1) immunoreactive terminals co-localized with respective calcium-binding proteins in the rat piriform cortex.

| Co-localization | Layer 1 | Layer 2 | Layer 3 | ANOVA |
|-----------------|---------------|--------------|--------------|----------|
| PV/GAT-1 % | 13.63 ± 2.63 | 52.46 ± 2.22 | 33.89 ± 3.15 | L2>L3>L1 |
| CB/GAT-1 % | 18.74 ± 4.86 | 46.35 ± 5.57 | 34.90 ± 5.15 | L2,L3>L1 |
| CR/GAT-1 % | 59.21 ± 10.54 | 21.28 ± 6.36 | 19.49 ± 2.92 | L1>L2,L3 |
| PV/CB/GAT-1 % | 18.22 ± 2.59 | 35.74 ± 3.02 | 46.02 ± 5.41 | L2,L3>L1 |

Data are shown as means ± SE (n = 9). The numbers represent the percentages of GAT-1-IR terminals that are colocalized with the CBPs in each layer of the piriform cortex. Significant differences indicated by the use of Tukey test for multiple comparisons after analysis of variance ($P < 0.001$) are shown in the last column. CBP, calcium-binding protein; PV/GAT-1, colocalized parvalbumin/GAT-1 nerve terminals; CB/GAT-1, colocalized calbindin/GAT-1 nerve terminals; CR/GAT-1, calretinin/GAT-1 colocalized nerve terminals; PV/CB/GAT-1, parvalbumin/calbindin/GAT-1 nerve terminals; L1, layer 1; L2, layer 2; L3, layer 3.

regions of CB-IR cells as well as dendritic processes of CB-IR cells (Fig. 2.9A, Table 2.5).

PV⁺ NTs were found in all layers of the PC. In L1, PV⁺ NTs were found along PV-IR dendrites. In L2, PV⁺ NTs followed a pattern similar to that of CB⁺ NTs, in that they surrounded cell bodies of excitatory cells as well as perisomatic regions of PV-IR cell bodies located in L2 (Table 2.5). In L3, the pattern of innervation of PV⁺ NTs was found to be around cell somata, both non-IR and PV-IR, and PV-IR dendritic processes (Fig. 2.9B, Table 2.5). Unlike the CB⁺ NT distribution, PV⁺ NTs were expressed predominantly in L2 of PC (Table 2.4).

To investigate the innervation of NTs expressing both CB and PV, the resultant colocalized segments for CB/GAT-1 and PV/GAT-1 were analyzed. Any segments that showed up in this analysis were considered to be NTs expressing both CB and PV. The pattern of innervation of colocalized PV/CB⁺ NTs varied somewhat from the CB and PV innervations (Table 2.5). For example, in Figure 2.9D, PV/CB⁺ NTs in L1 can be seen along PV-IR dendrites. In L2, the pattern is similar to the PV-IR and CB-IR innervation pattern, where the innervation is so dense that a pyramidal shape is apparent. Presumably, these terminals innervate excitatory cell somata (Fig. 2.9D). In L3, PV/CB⁺ NTs were concentrated on the cell somata and processes of PV/CB cells (Fig. 2.9C).

Finally, CR⁺ NT distribution was investigated (Fig. 2.10). Most of the CR⁺ NTs were found in L1 around CR-IR dendrites. In L2 and L3, CR⁺ NTs were more evenly distributed (Table 2.4). In L2, CR⁺ NTs did not show the same pattern as CB⁺ NTs and PV⁺ NTs where they surround excitatory cell somata. As can be seen in Figure 2.10A, they innervate CR-IR dendritic processes, non-IR dendritic processes, and CR-IR somata. In L3, CR⁺ NTs can be seen along CR-IR dendritic processes (Fig. 2.10B, Table 2.5).

Figure 2.9. Calbindin-, parvalbumin-, and parvalbumin/calbindin-expressing nerve terminal distribution in the piriform cortex. **A:** Calbindin and GAT-1 distribution in layer 3 of piriform cortex. Green represents calbindin immunoreactivity (CB-IR); blue represents GABA transporter type-1 immunoreactivity (GAT1-IR); white represents CB and GAT-1 colocalized segments, which indicate CB⁺ NTs. CB⁺ NTs are found evenly distributed in L3. In this layer, CB⁺ innervation is seen around non-IR somata and perisomatic regions of CB-IR cells and dendritic processes. **B:** Parvalbumin and GAT-1 distribution in layer 3 of piriform cortex. Magenta represents PV-IR; blue represents GAT1-IR; white represents PV and GAT-1 colocalized segments, which indicate PV⁺ NTs. PV⁺ innervation is evenly distributed in L3. PV⁺ innervation is high around cell somata and along PV-IR dendritic processes. **C:** Parvalbumin/calbindin/GAT-1 distribution in layer 3 of piriform cortex. Green represents CB-IR; magenta represents PV-IR; blue represents GAT1-IR; white represents PV/CB-IR and GAT-1 colocalized segments, which indicate NTs that coexpress PV/CB. PV/CB⁺ innervation is found on cell somata, in perisomatic regions, and on dendritic processes of cells expressing both CBPs. **D:** Parvalbumin/calbindin/GAT-1 distribution in layer 2 of piriform cortex. Green represents CB-IR; magenta represents PV-IR; blue represents GAT1-IR; white represents PV/CB-IR and GAT-1 colocalized segments, which indicate NTs that coexpress PV/CB. In L1, PV/CB⁺ NTs are found along PV⁺ dendrites. In L2, PV/CB⁺ NTs are found highly innervating non-IR cell somata. L1, layer 1; L2, layer 2; L3, layer 3. Scale bars = 15 μ m in A (applies to A–C); 20 μ m in D.

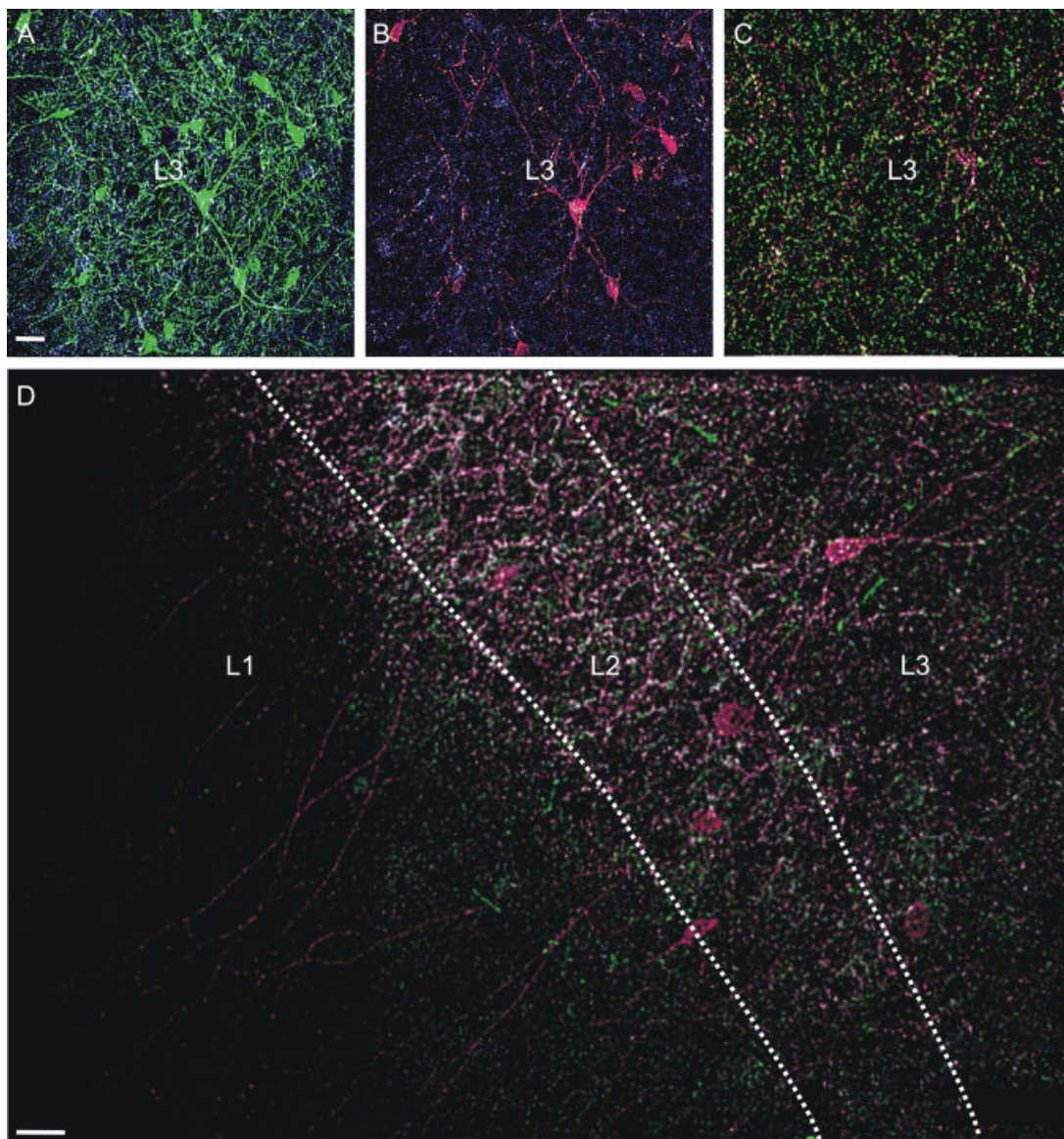


Table 2.5 Innervation target of calcium-binding protein immunoreactive interneurons of piriform cortex

| NTs | Target | Layer 1 | | Layer 2 | | Layer 3 | |
|-------|------------|-----------|------|-----------|------|-----------|------|
| | | Dendrites | Soma | Dendrites | Soma | Dendrites | Soma |
| PV | PV | + | - | + | + | + | + |
| | Non-IR/Pyr | - | - | - | + | - | + |
| CB | CB | + | - | - | - | + | + |
| | Non-IR/Pyr | + | - | - | + | - | + |
| CR | CR | + | - | + | + | + | - |
| | Non-IR/Pyr | - | - | + | - | - | - |
| PV/CB | PV/CB | - | - | + | + | + | + |
| | PV | + | - | - | - | - | - |
| | Non-IR/Pyr | - | - | - | + | - | - |

NTs, nerve terminals; PV, parvalbumin; CB, calbindin; PV/CB, colocalized parvalbumin/calbindin; CR, calretinin; Pyr, pyramidal cell; non-IR, nonimmunoreactive; plus and minus signs indicate the presence or the absence of the nerve terminals on the specified target. L1, layer 1; L2, layer 2; L3, layer 3.

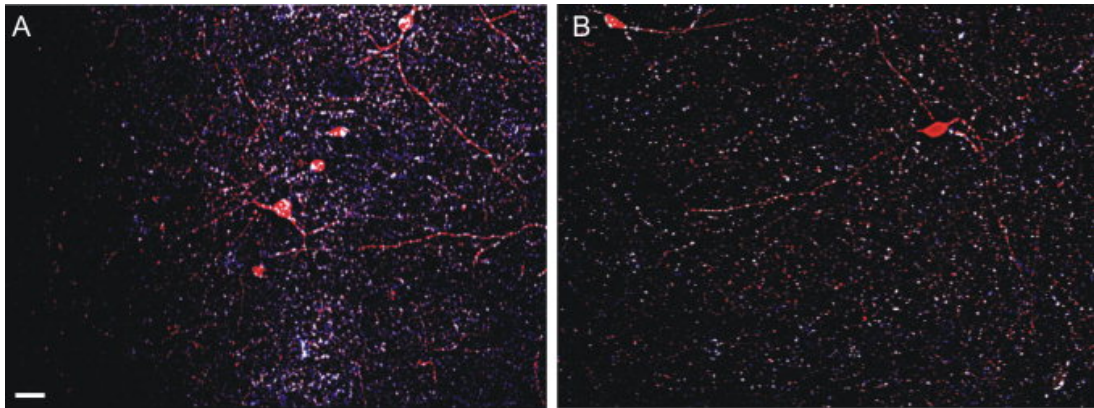


Figure 2.10 Calretinin nerve terminal distribution in the piriform cortex. Magenta channel shows calretinin immunoreactivity (CR-IR); blue signal represents GABA transporter type-1 immunoreactivity (GAT1-IR); white pixels indicate CR and GAT-1 colocalized segments, which represent CR⁺ NTs. **A**: In L1, CR⁺ NTs can be found along CR-IR dendritic processes. In L2, CR⁺ NTs are highly concentrated on CR-IR cell somata and dendritic processes as well as non-IR dendritic processes (**B**). In L3, CR⁺ NTs can be seen along CR-IR dendritic processes. L1, layer 1; L2, layer 2; L3, layer 3. Scale bar = 20 μ m.

As indicated in Table 2.4, the distribution of NTs in the layers of PC is different. PV⁺ NTs are expressed mostly in L2 (~52%), followed by L3 (~34%), whereas the lowest amount of terminals was found in L1 (14%). CB⁺ and PV/CB⁺ NTs showed a similar distribution, with most of the NTs evenly distributed between L2 and L3. Finally, CR⁺ NTs showed another pattern, with L1 containing most of this innervation (Table 2.4).

2.4 Discussion

The various interconnections of the PC coupled with mechanisms involved in olfactory sensation (Haberly, 2001) and its highly seizurogenic nature make the PC a suitable substrate for the development of widespread seizures in the cortex (Racine *et al.*, 1988; Rigas & Castro-Alamancos, 2004). The role of inhibitory cells in the cortex includes integrative processes, regulation of synaptic plasticity, shaping of spatial and temporal patterns of neuronal activity, and maintaining neurons and systems within their optimal dynamic ranges (Ekstrand *et al.*, 2001b). It has been suggested that the enhanced excitability of the PC in animal models of epilepsy may be related to a loss of GABAergic neurons (Lehmann *et al.*, 1998) or a change in interneuron wiring (Cossart *et al.*, 2005). However, insofar as interneuron wiring (both inhibitory connections on pyramidal cells and reciprocal connections with other interneurons) in the PC is still poorly understood, the impact of these changes on overall PC network activity remains unclear. Our study helps to fill this gap by investigating the wiring pattern distribution of CBP interneuronal populations of PC.

The results of our CBP coexpression study confirmed the findings of (Kubota & Jones, 1993) that subsets of interneurons coexpress PV and CB in cell somata in L3 as well as dendritic processes and NTs in all three layers. We found that ~81% of PV cells were IR for CB, a coexpression level similar to that previously reported (Kubota & Jones, 1993; Ekstrand *et al.*, 2001a). However, there had not been an investigation to determine whether the third CBP, CR, was coexpressed with PV, CB, or both in interneurons of the PC. We report here that CR was not coexpressed

with any other CBP in the PC (Curtis *et al.*, 2003; Jin *et al.*, 2001; Magloczky & Freund, 2005; Stroemer *et al.*, 1995; Stroemer *et al.*, 1998).

A specific laminar distribution for each type of CBP-expressing or CBP-coexpressing cell somata and NTs was found. As in previous studies (Kubota & Jones, 1993; Ekstrand *et al.*, 2001a), we found that L3 contained the highest PC interneuronal population. Compared with L2, the distribution of CBP-IR cells was different; most of the interneurons were PV/CB-IR, followed by CB-IR and CR-IR cells. This specific cell layer distribution suggests that there is a particular division of labor among the various CBP-IR interneurons. Our data indicated that, in addition to their distinct layer distribution, each CBP has a preferred dendritic arborization pattern. A broad horizontal extent of a dendritic tree suggests that a cell integrates inputs from a large volume of cortex, whereas a restricted conical arbor provides potential for more spatially specific integrative processes (Ekstrand *et al.*, 2001b).

Based on the dendritic arborizations, it appears that each cell type has a particular function. CB-IR dendritic trees, with their broad horizontal arbor that does not go beyond L3, most likely integrate inputs from a large volume of L3. PV-IR dendritic trees with equal vertical and horizontal expansions (1:1 ratio) can integrate intra- and interlayer inputs, because PV-IR arborizations do traverse into other layers. Insofar as the dendritic trees of cells coexpressing PV/CB have the same arborization pattern as PV-IR cells, they probably integrate in a similar manner; however, the PV-IR and CB-IR neurons were shown to have different firing patterns (Kawaguchi, 1995), so the additional presence of the CBP CB might cause PV/CB cells to behave differently from PV-only cells. CR cells with their restricted horizontal expansion and long vertical expansions extending through the layers probably integrate spatially specific processes between the layers.

The innervation targets of each CBP-expressing cell type indicated that the CBP⁺ NTs had distinct postsynaptic morphological targeting of non-IR cells and IR interneurons with patterns reminiscent of other limbic areas. In the hippocampus, PV-IR cells were shown to innervate perisomatic regions such as soma and axon

initial segments (AIS) of principal cells (Freund & Buzsaki, 1996). The present findings indicated that, in the PC, the PV⁺ NTs in L1 innervated PV⁺ dendrites. In L2 and L3, PV⁺ NTs were found surrounding non-IR, apparently pyramidal cell soma, along perisomatic regions of PV-IR cell bodies and PV-IR dendritic processes. Thus, the pattern of PV innervation of pyramidal cells was similar to that in the hippocampus. However, in the PC, PV innervation was also found on PV-IR somata and dendrites. CB-IR cells in the hippocampus were found to form synapses on dendrites of pyramidal cells and GABA⁺ dendrites (Gulyas *et al.*, 1996). In contrast, CB⁺ NTs in the PC were found in L1 along both CB and non-IR dendritic processes, in L2 surrounding non-IR cell soma, and in L3 also surrounding non-IR cell bodies as well as CB-IR cells. As in the hippocampus, CB⁺ NTs were found on dendrites of pyramidal cells and CB-IR dendrites. However, they were also found around CB-IR cell somata, which are not found in the hippocampus. Finally, the CR-IR cells in the hippocampus frequently form dendritic contacts with each other and non-CR GABAergic dendrites (Freund & Buzsaki, 1996; Gulyas *et al.*, 1996). In the PC, we showed that CR⁺ NTs in L1 were found along CR-IR processes and in L2 along CR-IR processes and non-IR processes and surrounding CR-IR cell somata. In L3 CR⁺ NTs were seen only along CR-IR processes. As in the hippocampus, CR⁺ NTs were found along CR-IR dendrites; however, they can also innervate perisomatic regions of CR-IR cells as well as non-IR processes. Coexpressed CBP NTs have not been investigated in the hippocampus. For the PC, however, we found that PV/CB⁺ NTs in L1 are found along PV-IR dendrites and in L2 are found surrounding non-IR cell somata as well as on the cell somata, perisomatic regions, and dendritic processes of cells expressing both CBPs. Finally, in L3 PV/CB⁺ NTs were found on the cell somata, perisomatic regions, and processes of PV/CB-IR cells.

There are two functional aspects that ought to be considered in relation to these data. They concern the implications of inhibitory input on pyramidal and nonpyramidal (interneuron) cells. Our results imply a specific pattern of innervation source and postsynaptic morphological targeting. Specifically, PV⁺ NTs and PV/CB⁺

NTs innervate perisomatic regions of principal cells; CR⁺ NTs innervate only dendrites of principal cells, whereas CB⁺ NTs innervate both somata and dendrites of principal cells. Interneuron types that innervate perisomatic regions, such as PV-IR, PV/CB-IR, and CB-IR in the PC, appear to have specific roles. Specifically, they are in a position to regulate the pyramidal cell output by inhibiting the initiation of action potentials in axons (Miles *et al.*, 1996). Cells that innervate perisomatic regions of pyramidal cells are also responsible for synchronizing large principal cell populations during network oscillations (Miles *et al.*, 1996). In PC, the CBP interneurons providing perisomatic innervation of the pyramidal cells are in position to modulate the oscillatory network activity and thus be relevant for the sensory information processing and odor representation in this area.

Our data provide insight into the involvement of CBP-IR interneurons in two main inhibitory pathways of PC: feed-forward and feedback inhibition processes. Feedback inhibition (Fig. 2.11) is provided by the interconnection between the pyramidal cells of L2 and inhibitory neurons located in adjacent layers (Ekstrand *et al.*, 2001a) for review, see (Suzuki & Bekkers, 2007). The axon collaterals of pyramidal cells in L2 are concentrated in L3 and make excitatory contacts onto these interneurons. In turn, the L3 interneurons then form inhibitory synapses back onto the pyramidal cells, either onto somata in L2 or onto the cells' apical dendrites in L1 (Neville & Haberly, 2004). Results from our study indicated that the frequency of interneuron somata in L3 were, in decreasing order, PV/CB, CB, CR, and PV cells. The PV/CB⁺ NTs, CB⁺ NTs, and PV⁺ NTs were found surrounding non-IR cell somata in L2. Thus any of these cell types could be responsible for that portion of the circuit (Fig. 2.11). In addition to perisomatic inhibition of L2 pyramidal cells, GABAergic L3 cells with long ascending axons could provide feedback inhibition on pyramidal cells apical dendrites (Neville & Haberly, 2004). In L1 the only NTs that were found along non-IR dendrites (apical dendrites of L2 pyramidal cells) were those that expressed CB. It is interesting to note, however, that L1 contains the lowest amount of CB⁺ NTs (compared with L2 and L3 CB⁺ NTs), suggesting that

CB-IR cell-mediated inhibition of non-IR apical dendrites in L1 is minimal. Finally, L2 bipolar/bitufted cells were also shown to mediate feedback inhibition in PC (Neville & Haberly, 2004). A large population of L2 CBP-IR cells with bipolar/bitufted morphology with long dendrites crossing the L2–3 border is represented by CR-IR cells (~42% of total L2 CBP-IR cells). CR⁺ NTs target only the dendritic tree (and not the perisomatic region) or pyramidal cells, suggesting that CR-IR cells (along with CB-IR interneurons) could provide another type of control over pyramidal cell activity.

The other PC inhibitory pathway, the feed-forward circuit (Fig. 2.12), starts from the afferent fibers from the olfactory bulb, which make direct synaptic contact on inhibitory interneurons in L1 (Haberly, 1983). These interneurons then make inhibitory synaptic contacts onto pyramidal cells, providing the feed-forward inhibition (Kelly *et al.*, 2002). The findings of this study suggest that the identities of L1 interneuron dendrites are PV/CB-IR, PV-IR (originating from L2 PV/CB and PV cells), and CR-IR (originating from L1 and L2 CR cells) dendrites. Although some CB-IR dendrites could be detected in L1, their expression is very low because of a very small CB-IR cell presence in L2 (only 8% of total number of L2 CBP-IR interneurons are CB-IR cells). Another difference among the cells participating in the feed-forward inhibition is that CR⁺ NTs were found only along dendrites of pyramidal cells (Nitsch *et al.*, 1990; Kawaguchi, 1993).

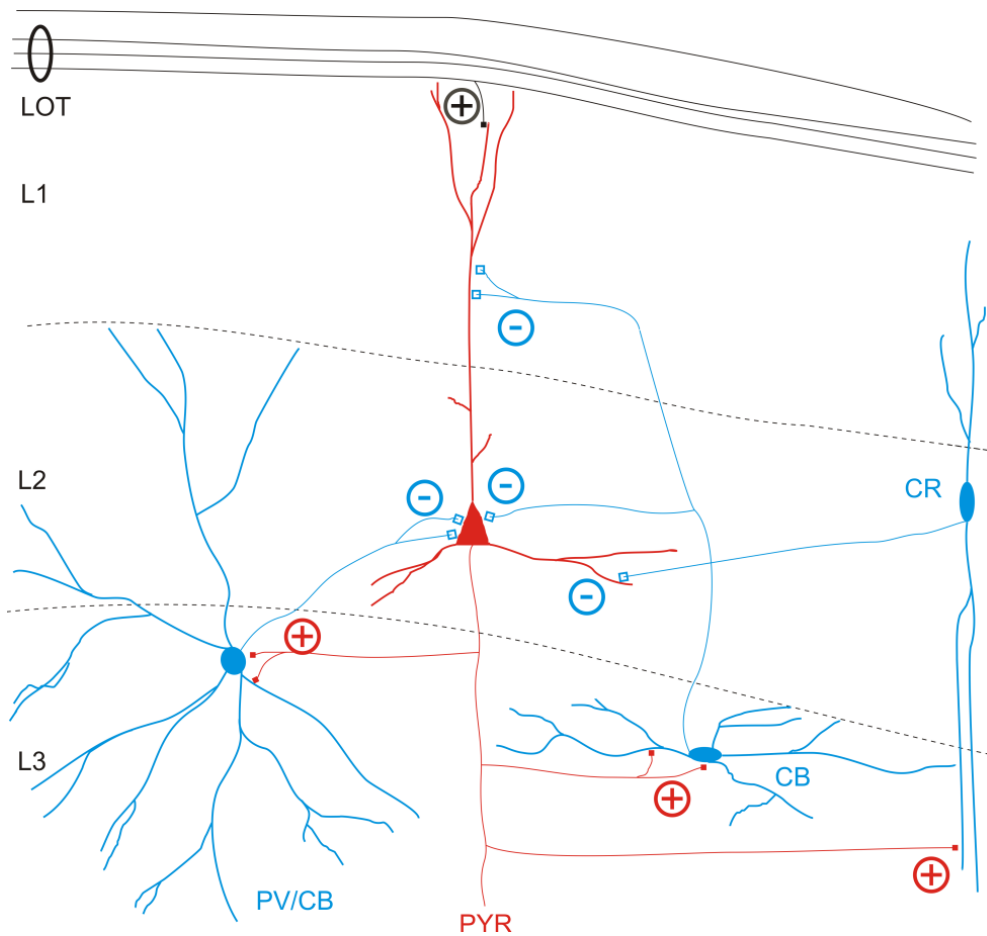


Figure 2.11 Hypothetical circuit indicating the contribution of calcium-binding protein immunoreactive (CBP-IR) interneurons to the feedback inhibition loop of piriform cortex. Lateral olfactory tract collaterals in layer 1 activate pyramidal cells of layer 2 with apical dendrites in layer 1. Pyramidal cell axon collaterals concentrate in layer 3, recruiting an interneuronal population of that layer or layer 2 interneurons with dendrites in layer 3. Here we indicate the feedback contribution of the most common CBP-IR cells in layer 3 (PV/CB and CB-IR cells) as well as layer 2 CR-IR cells with long dendrites crossing the L2–3 border. LOT, lateral olfactory tract; PV/CB, colocalized parvalbumin-calbindin cells; CB, calbindin cells; CR, calretinin cells. Plus signs indicate an excitatory input; minus signs represent an inhibitory input. L1, layer 1; L2, layer 2; L3, layer 3.

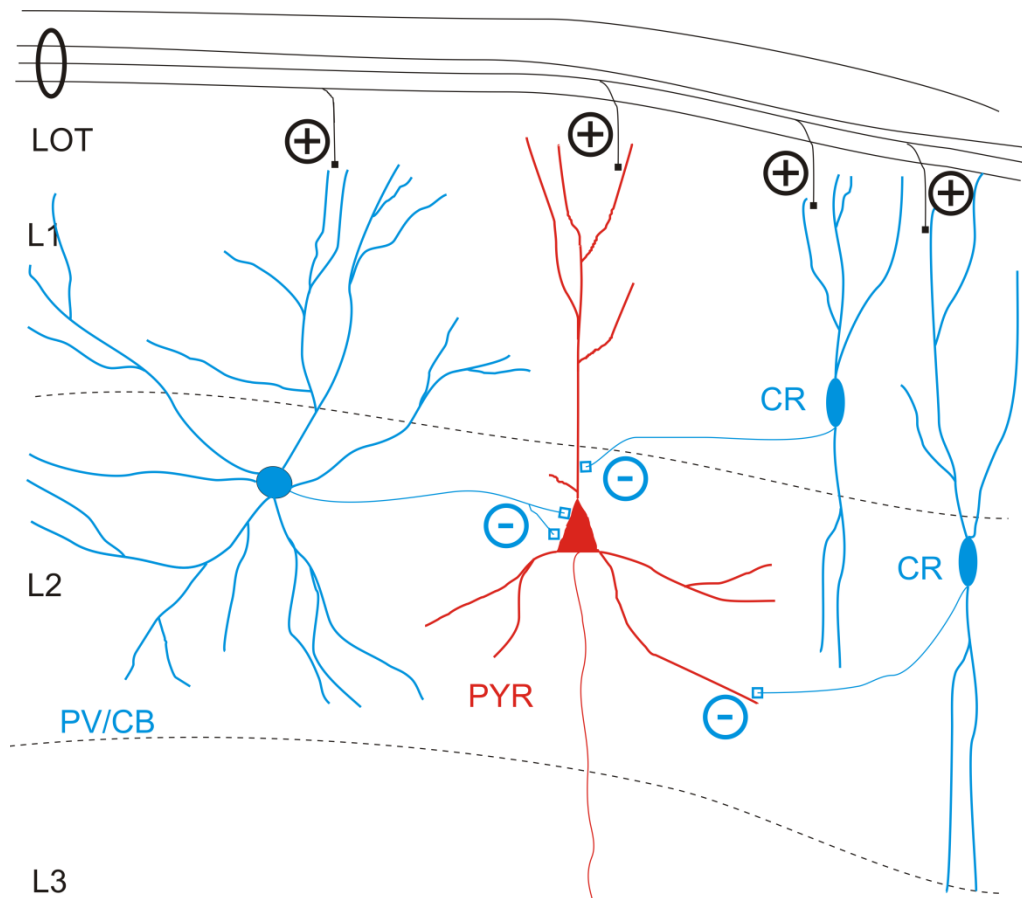


Figure 2.12 Hypothetical circuit indicating the contribution of calcium-binding protein immunoreactive (CBP-IR) interneurons to the feed-forward inhibition loop of piriform cortex. Lateral olfactory tract collaterals activate layer 1 interneurons or layer 2 interneurons with dendrites in layer 1. Our analysis indicated that the only CBP-IR interneurons in layer 1 were CR-IR. In layer 2, most of the CBP-IR cells with dendrites in layer 1 are CR-IR and PV/CB-IR cells. These cells could provide a different control on layer 2 pyramidal cell activity by either perisomatic innervations (PV/CB-IR) or dendritic innervation (CR-IR cells). LOT, lateral olfactory tract; PV/CB, colocalized parvalbumin-calbindin cells; CR, calretinin cells. Plus signs indicate an excitatory input; minus signs represent an inhibitory input. PYR, pyramidal cell; L1, layer 1; L2, layer 2; L3, layer 3.

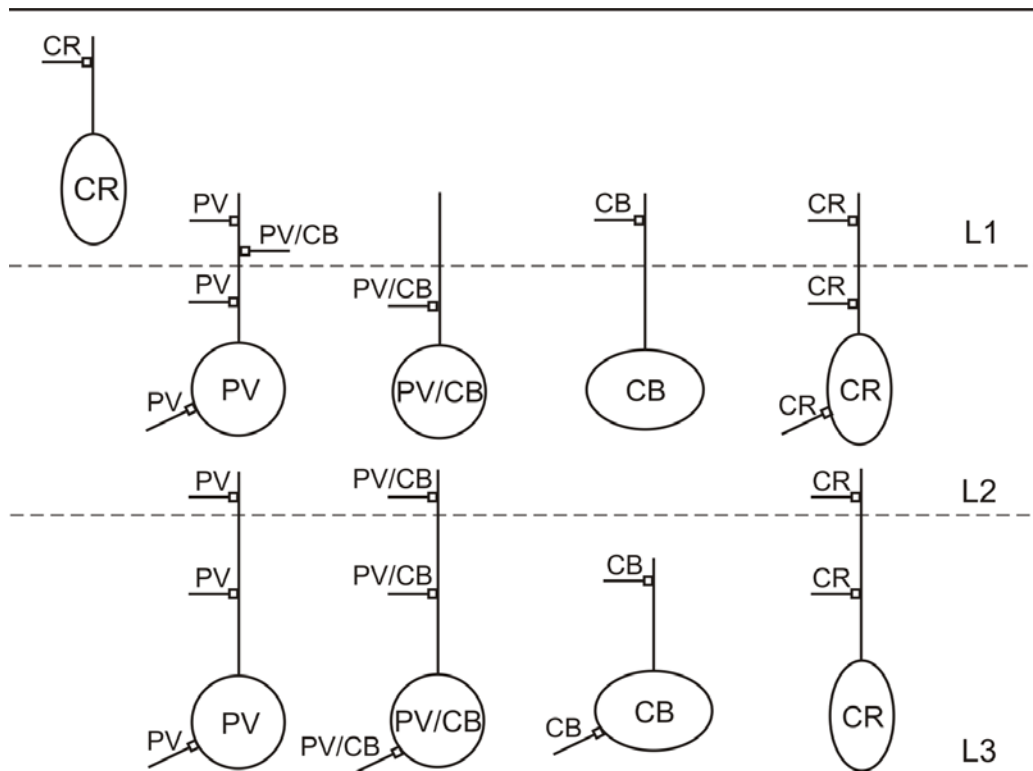


Figure 2.13 Inhibitory innervations on the calcium-binding protein immunoreactive (CBP-IR) interneurons of piriform cortex. CBP⁺ nerve terminals (NTs) innervate somata and dendrites positive for the same CBP, except for PV/CB⁺ NTs, which also innervate PV dendrites. CBP, calcium-binding protein; PV, parvalbumin cells; PV/CB, colocalized parvalbumin/calbindin cells; CR, calretinin cells; L1, layer 1; L2, layer 2; L3, layer 3.

The pattern of inhibitory innervation onto interneurons is also specific for the cell types (Table 2.5). We found that CBP⁺ NTs only innervate somata and dendrites positive for the same CBP, except for PV/CB⁺ NTs, which also innervate PV-IR dendrites (Figs. 2.9, 2.13). This pattern of innervation suggests that there are networks of interneurons that are connected only to one another and converge only via excitatory cell pathways. To take the notion of interneuronal networks one step further, interneurons that dendritically inhibit other interneurons, which inhibit the dendritic and somatic compartments of principal cells, play a role in the generation of synchronous rhythmic activity in the hippocampus (Miles *et al.*, 1996). In the PC, the only interneurons that fulfill these criteria are the CB-IR cells; however, it is not known whether they are involved in synchronous activity.

Because of the highly epileptogenic potential of PC, a very interesting avenue for future work will be to examine these parameters within an animal model of epilepsy. Our previous work (Gavrilovici *et al.*, 2006) indicated that the overall number of inhibitory synapses was not altered in kindled brain. However, a particular interneuron type might be more susceptible to death, and another cell type may compensate in its place. Thus, although the overall number of inhibitory synapses is not changing in the epileptic PC, the proportion of different CBP inhibitory inputs (PV, CB, PV/CB, and CR) within the PC layers might be altered. Because each type of CBP-IR interneurons has a specific innervation target (dendritic vs. perisomatic), any alteration in one CBP population could lead to a change in the timing activity of the PC network. These events could lead to altered intrinsic oscillatory network properties that may account for the seizurogenic tendency of the PC.

2.5 References

- Ballain T, Litaudon P, Martiel JL, & Cattarelli M (1998). Role of the net architecture in piriform cortex activity: analysis by a mathematical model. *Biol Cybern* **79**, 323-336.
- Borden LA (1996). GABA transporter heterogeneity: pharmacology and cellular localization. *Neurochem Int* **29**, 335-356.
- Chalazonitis A, Pham TD, Li Z, Roman D, Guha U, Gomes W, Kan L, Kessler JA, & Gershon MD (2008). Bone morphogenetic protein regulation of enteric neuronal phenotypic diversity: relationship to timing of cell cycle exit. *J Comp Neurol* **509**, 474-492.
- Cossart R, Bernard C, & Ben Ari Y (2005). Multiple facets of GABAergic neurons and synapses: multiple fates of GABA signalling in epilepsies. *Trends Neurosci* **28**, 108-115.
- Cossart R, Dinocourt C, Hirsch JC, Merchan-Perez A, De Felipe J, Ben Ari Y, Esclapez M, & Bernard C (2001). Dendritic but not somatic GABAergic inhibition is decreased in experimental epilepsy. *Nat Neurosci* **4**, 52-62.
- Curtis MA, Penney EB, Pearson AG, Roon-Mom WM, Butterworth NJ, Dragunow M, Connor B, & Faull RL (2003). Increased cell proliferation and neurogenesis in the adult human Huntington's disease brain. *Proc Natl Acad Sci U S A* **100**, 9023-9027.
- De Biasi S, Vitellaro-Zuccarello L, & Brecha NC (1998). Immunoreactivity for the GABA transporter-1 and GABA transporter-3 is restricted to astrocytes in the rat thalamus. A light and electron-microscopic immunolocalization. *Neuroscience* **83**, 815-828.
- Dinocourt C, Petanjek Z, Freund TF, Ben Ari Y, & Esclapez M (2003). Loss of interneurons innervating pyramidal cell dendrites and axon initial segments in the CA1 region of the hippocampus following pilocarpine-induced seizures. *J Comp Neurol* **459**, 407-425.
- Ekstrand JJ, Domroese ME, Feig SL, Illig KR, & Haberly LB (2001a). Immunocytochemical analysis of basket cells in rat piriform cortex. *J Comp Neurol* **434**, 308-328.
- Ekstrand JJ, Domroese ME, Johnson DM, Feig SL, Knodel SM, Behan M, & Haberly LB (2001b). A new subdivision of anterior piriform cortex and associated

- deep nucleus with novel features of interest for olfaction and epilepsy. *J Comp Neurol* **434**, 289-307.
- Ferraguti F, Cobden P, Pollard M, Cope D, Shigemoto R, Watanabe M, & Somogyi P (2004). Immunolocalization of metabotropic glutamate receptor 1alpha (mGluR1alpha) in distinct classes of interneuron in the CA1 region of the rat hippocampus. *Hippocampus* **14**, 193-215.
- Freund TF (2003). Interneuron Diversity series: Rhythm and mood in perisomatic inhibition. *Trends Neurosci* **26**, 489-495.
- Freund TF & Buzsaki G (1996). Interneurons of the hippocampus. *Hippocampus* **6**, 347-470.
- Fritschy JM, Kiener T, Bouilleret V, & Loup F (1999). GABAergic neurons and GABA(A)-receptors in temporal lobe epilepsy. *Neurochem Int* **34**, 435-445.
- Fritschy JM, Weinmann O, Wenzel A, & Benke D (1998). Synapse-specific localization of NMDA and GABA(A) receptor subunits revealed by antigen-retrieval immunohistochemistry. *J Comp Neurol* **390**, 194-210.
- Gavrilovici C, D'Alfonso S, Dann M, & Poulter MO (2006). Kindling-induced alterations in GABA_A receptor mediated inhibition and neurosteroid activity in the piriform cortex of rat. *Eur J Neurosci* **24**, 1373-1384.
- Gulyas AI, Hajos N, & Freund TF (1996). Interneurons containing calretinin are specialized to control other interneurons in the rat hippocampus. *J Neurosci* **16**, 3397-3411.
- Haberly LB (1983). Structure of the piriform cortex of the opossum. I. Description of neuron types with Golgi methods. *J Comp Neurol* **213**, 163-187.
- Haberly LB (2001). Parallel-distributed processing in olfactory cortex: new insights from morphological and physiological analysis of neuronal circuitry. *Chem Senses* **26**, 551-576.
- Haberly LB & Bower JM (1984). Analysis of association fiber system in piriform cortex with intracellular recording and staining techniques. *J Neurophysiol* **51**, 90-112.
- Haberly LB & Sutula TP (1992). Neuronal processes that underlie expression of kindled epileptiform events in the piriform cortex in vivo. *J Neurosci* **12**, 2211-2224.

- Hutcheon B, Brown LA, & Poulter MO (2000). Digital analysis of light microscope immunofluorescence: high-resolution co-localization of synaptic proteins in cultured neurons. *J Neurosci Methods* **96**, 1-9.
- Hutcheon B, Fritschy JM, & Poulter MO (2004). Organization of GABA receptor alpha-subunit clustering in the developing rat neocortex and hippocampus. *Eur J Neurosci* **19**, 2475-2487.
- Jin K, Minami M, Lan JQ, Mao XO, Bateur S, Simon RP, & Greenberg DA (2001). Neurogenesis in dentate subgranular zone and rostral subventricular zone after focal cerebral ischemia in the rat. *Proc Natl Acad Sci U S A* **98**, 4710-4715.
- Kamphuis W, De Rijk TC, & Lopes da Silva FH (1994). GABAA receptor beta 1-3 subunit gene expression in the hippocampus of kindled rats. *Neurosci Lett* **174**, 5-8.
- Kanter ED, Kapur A, & Haberly LB (1996). A dendritic GABAA-mediated IPSP regulates facilitation of NMDA-mediated responses to burst stimulation of afferent fibers in piriform cortex. *J Neurosci* **16**, 307-312.
- Kapur A, Pearce RA, Lytton WW, & Haberly LB (1997). GABAA-mediated IPSCs in piriform cortex have fast and slow components with different properties and locations on pyramidal cells. *J Neurophysiol* **78**, 2531-2545.
- Kawaguchi Y (1993). Groupings of nonpyramidal and pyramidal cells with specific physiological and morphological characteristics in rat frontal cortex. *J Neurophysiol* **69**, 416-431.
- Kawaguchi Y (1995). Physiological subgroups of nonpyramidal cells with specific morphological characteristics in layer II/III of rat frontal cortex. *J Neurosci* **15**, 2638-2655.
- Kawaguchi Y & Kondo S (2002). Parvalbumin, somatostatin and cholecystokinin as chemical markers for specific GABAergic interneuron types in the rat frontal cortex. *J Neurocytol* **31**, 277-287.
- Kawaguchi Y & Kubota Y (1997). GABAergic cell subtypes and their synaptic connections in rat frontal cortex. *Cereb Cortex* **7**, 476-486.
- Kelly ME, Staines WA, & McIntyre DC (2002). Secondary generalization of hippocampal kindled seizures in rats: examining the role of the piriform cortex. *Brain Res* **957**, 152-161.
- Kubota Y, Hattori R, & Yui Y (1994). Three distinct subpopulations of GABAergic neurons in rat frontal agranular cortex. *Brain Res* **649**, 159-173.

- Kubota Y & Jones EG (1993). Co-localization of two calcium binding proteins in GABA cells of rat piriform cortex. *Brain Res* **600**, 339-344.
- Lehmann H, Ebert U, & Loscher W (1998). Amygdala-kindling induces a lasting reduction of GABA-immunoreactive neurons in a discrete area of the ipsilateral piriform cortex. *Synapse* **29**, 299-309.
- Loscher W & Ebert U (1996). The role of the piriform cortex in kindling. *Prog Neurobiol* **50**, 427-481.
- Luskin MB & Price JL (1983). The topographic organization of associational fibers of the olfactory system in the rat, including centrifugal fibers to the olfactory bulb. *J Comp Neurol* **216**, 264-291.
- Magloczky Z & Freund TF (2005). Impaired and repaired inhibitory circuits in the epileptic human hippocampus. *Trends Neurosci* **28**, 334-340.
- Markram H, Toledo-Rodriguez M, Wang Y, Gupta A, Silberberg G, & Wu C (2004). Interneurons of the neocortical inhibitory system. *Nat Rev Neurosci* **5**, 793-807.
- McBain CJ & Fisahn A (2001). Interneurons unbound. *Nat Rev Neurosci* **2**, 11-23.
- McIntyre DC & Wong RK (1986). Cellular and synaptic properties of amygdala-kindled piriform cortex in vitro. *J Neurophysiol* **55**, 1295-1307.
- Miles R, Toth K, Gulyas AI, Hajos N, & Freund TF (1996). Differences between somatic and dendritic inhibition in the hippocampus. *Neuron* **16**, 815-823.
- Minelli A, Brecha NC, Karschin C, DeBiasi S, & Conti F (1995). GAT-1, a high-affinity GABA plasma membrane transporter, is localized to neurons and astroglia in the cerebral cortex. *J Neurosci* **15**, 7734-7746.
- Miyata S, Nakai S, Kiyohara T, & Hatton GI (2000). Calbindin-D28k and calretinin in the rat posterior pituitary; light and electron microscopic localization and upregulation with dehydration. *J Neurocytol* **29**, 5-17.
- Mody I (2001). Distinguishing between GABA(A) receptors responsible for tonic and phasic conductances. *Neurochem Res* **26**, 907-913.
- Neville KR & Haberly LB (2004). Olfactory cortex. In *The Synaptic Organization of the Brain*, ed. Shepherd GM, pp. 415-454. Oxford University Press, New York.
- Nitsch R, Soriano E, & Frotscher M (1990). The parvalbumin-containing nonpyramidal neurons in the rat hippocampus. *Anat Embryol (Berl)* **181**, 413-425.

- Parrish-Aungst S, Shipley MT, Erdelyi F, Szabo G, & Puche AC (2007). Quantitative analysis of neuronal diversity in the mouse olfactory bulb. *J Comp Neurol* **501**, 825-836.
- Paxinos G & Watson PL (1986). *The rat brain in stereotaxic coordinates*, second ed. Academic Press, Sydney.
- Princivalle A, Spreafico R, Bowery N, & de Curtis M (2000). Layer-specific immunocytochemical localization of GABA(B)R1a and GABA(B)R1b receptors in the rat piriform cortex. *Eur J Neurosci* **12**, 1516-1520.
- Racine RJ, Mosher M, & Kairiss EW (1988). The role of the pyriform cortex in the generation of interictal spikes in the kindled preparation. *Brain Res* **454**, 251-263.
- Ribak CE, Tong WM, & Brecha NC (1996). GABA plasma membrane transporters, GAT-1 and GAT-3, display different distributions in the rat hippocampus. *J Comp Neurol* **367**, 595-606.
- Rigas P & Castro-Alamancos MA (2004). Leading role of the piriform cortex over the neocortex in the generation of spontaneous interictal spikes during block of GABA(A) receptors. *Neuroscience* **124**, 953-961.
- Schnell SA, Staines WA, & Wessendorf MW (1999). Reduction of lipofuscin-like autofluorescence in fluorescently labeled tissue. *J Histochem Cytochem* **47**, 719-730.
- Sloviter RS (1987). Decreased hippocampal inhibition and a selective loss of interneurons in experimental epilepsy. *Science* **235**, 73-76.
- Somogyi J, Baude A, Omori Y, Shimizu H, El Mestikawy S, Fukaya M, Shigemoto R, Watanabe M, & Somogyi P (2004). GABAergic basket cells expressing cholecystinin contain vesicular glutamate transporter type 3 (VGLUT3) in their synaptic terminals in hippocampus and isocortex of the rat. *Eur J Neurosci* **19**, 552-569.
- Stroemer RP, Kent TA, & Hulsebosch CE (1995). Neocortical neural sprouting, synaptogenesis, and behavioral recovery after neocortical infarction in rats. *Stroke* **26**, 2135-2144.
- Stroemer RP, Kent TA, & Hulsebosch CE (1998). Enhanced neocortical neural sprouting, synaptogenesis, and behavioral recovery with D-amphetamine therapy after neocortical infarction in rats. *Stroke* **29**, 2381-2393.
- Suzuki N & Bekkers JM (2007). Inhibitory interneurons in the piriform cortex. *Clin Exp Pharmacol Physiol* **34**, 1064-1069.

Wang Y, Gupta A, Toledo-Rodriguez M, Wu CZ, & Markram H (2002). Anatomical, physiological, molecular and circuit properties of nest basket cells in the developing somatosensory cortex. *Cereb Cortex* **12**, 395-410.

Whittington MA & Traub RD (2003). Interneuron diversity series: inhibitory interneurons and network oscillations in vitro. *Trends Neurosci* **26**, 676-682.

Winsky L, Isaacs KR, & Jacobowitz DM (1996). Calretinin mRNA and immunoreactivity in the medullary reticular formation of the rat: colocalization with glutamate receptors. *Brain Res* **741**, 123-133.

Woo TU, Whitehead RE, Melchitzky DS, & Lewis DA (1998). A subclass of prefrontal gamma-aminobutyric acid axon terminals are selectively altered in schizophrenia. *Proc Natl Acad Sci U S A* **95**, 5341-5346.

Chapter 3. Diverse interneuron firing modes between layers of the rat piriform cortex

3.1 Introduction

The piriform cortex (PC) is a three-layered structure (paleocortex) that is part of the limbic system. In addition to olfactory sensation and memory processing (Haberly, 2001), the PC has also been implicated in the development of seizures (Loscher & Ebert, 1996; Racine *et al.*, 1988). As in all cortical networks, the GABAergic interneuron system within the PC is important for regulation of neuronal excitability and rhythmicity of the neural network, participating in both feed-forward and feedback inhibitory loops (Haberly, 1983; Kelly *et al.*, 2002; Neville & Haberly, 2004). These circuits have been shown to modulate associative long-term potentiation (Kanter & Haberly, 1993) and generate oscillatory activities (Neville & Haberly, 2003) in the PC. It has also been shown that the PC is a heterogeneous structure, with anatomical differences along the rostro-caudal axis, including differences in layer thickness (Haberly & Price, 1978), number of interneurons per layers (Haberly *et al.*, 1987; Loscher *et al.*, 1998) as well differences in the laminar distribution/orientation of associational fibers (Haberly & Price, 1978; Luskin & Price, 1983). These morphological traits are thought to reflect different functional roles along anteroposterior axis of the PC (Neville & Haberly, 2004). In light of this diverse functionality, the focus on morphological and electrophysiological characteristics of interneuronal subpopulations in the PC has increased. Immunohistochemically distinct interneurons, based on their differing expression of calcium-binding proteins and neuropeptides, have been shown to exist in PC (Ekstrand *et al.*, 2001; Young & Sun, 2009; Gavrilovici *et al.*, 2010; Suzuki & Bekkers, 2010b). There have also been a few studies on the firing patterns of PC interneurons. Two studies that examined interneurons expressing serotonin receptors, located in the border between L2-L3 rat piriform cortex (Sheldon & Aghajanian, 1991; Gellman & Aghajanian, 1994), revealed firing patterns with little or no firing

adaptation. Another set of studies showed distinct membrane properties and spiking patterns of pyramidal cells and interneurons in deep layers of PC (L3 and endopiriform nucleus) in rabbit (Satou *et al.*, 1983a; Satou *et al.*, 1983b) and rat (Tseng & Haberly, 1989). Young and Sun (2009), focused on morphological and electrophysiological properties of pPC in mice; this data indicated that most interneurons have regular spiking patterns that often adapt to the stimulus. Although infrequent, other firing types such as fast spiking, late spiking or irregular spiking were also described in the same study. A more recent study has also shown a number of differing spiking patterns in mouse PC (Suzuki & Bekkers, 2010a), but a similar study has not been done in all layers of rat PC. Although a study on rat (Protopapas & Bower, 2000) showed that PC L3 interneurons, located in the border between L2 and L3, have different spike shapes and spiking patterns. This might suggest that distinct subpopulations of interneurons with specific functions could be located in different layers of rat PC. As different types of feedback connections are at play in the three layers of the PC, unraveling the physiological properties of interneuronal populations in all three layers is crucial for understanding the function of this cortical region. PC oscillations and their possible involvement in the plasticity of this region, particularly during epileptogenesis, are an important process to understand as well.

To date, a comprehensive examination of the repetitive firing properties of the interneurons in all layers of the rat aPC has not been conducted. This is particularly important given that most kindling studies are done using rat models. Thus, the goal of the present study was to help elucidate the functional role of different groups of interneurons of rat PC. Using cluster analysis technique we found that three main interneuron morphological types have diverse firing patterns (five types of firing). These groups are not uniformly distributed throughout PC layers implying that precise interneuronal firing patterns are required to control olfactory and memory processing in this area.

3.2 Methods

Male Sprague Dawley rats (Charles River), weighing 300-350g at the time of the study ($n = 40$), were used. All experiments were conducted in accordance with the guidelines of the Canadian Council on Animal Care and protocols approved by The University of Western Ontario Animal Care Committee.

3.2.1 Tissue preservation, slicing procedures and maintenance

Coronal rat brain slices (350 μm ; 1.5 to -0.3 mm relative to bregma) were performed according to published methodology (McIntyre *et al.*, 2002; Gavrilovici *et al.*, 2006). Briefly, the anesthetized rats (Ketamine - Dormitor mixture; 0.1 ml/100 g; i.p.) were perfused through the heart with an ice-cold Ringer solution in which sodium was replaced by choline [containing (in mM): Choline Cl 110, KCl 2.5, NaH_2PO_4 1.2, NaHCO_3 25, CaCl_2 0.5, MgCl_2 7, Na pyruvate 2.4, ascorbate 1.3, dextrose 20]. After heart perfusion, the brain was removed and the temporal lobe was coronally sliced using a Vibratome. The slices were incubated at 37°C for 30 min and subsequently moved to a room-temperature (22°C) bath for at least 45 minutes. Slicing, incubation, and storage were all performed in the choline solution (see above). The ACSF solution used during electrical recordings was similar to the choline solution except that pyruvate and ascorbate were removed, equimolar NaCl replaced the choline Cl, MgCl_2 was used at a 2 mM concentration while CaCl_2 was present at 1mM concentration. All solutions were maintained at pH 7.4 and bubbled with 5% CO_2 / 95% O_2 (carbogen).

3.2.2 Electrophysiology

Patch electrodes were pulled from borosilicate glass capillaries and filled with K^+ -gluconate solution having a composition (in mM) of: K^+ gluconate 147, KCl 1, CaCl_2 2, HEPES 10, EGTA 1, Glucose 10, MgATP 2, GTP 0.3 (300 mOsm, pH 7.3-7.4). As this electrode solution has been shown to potentially block some potassium currents in hippocampus we also used an internal solution containing K^+ methanesulfonate ($n = 34$) to verify if the identified spiking patterns could be

influenced by the K^+ gluconate based internal solution (Zhang *et al.*, 1994). This electrode solution was not used throughout this study as we found that the long-term viability of patched cells was reduced as compared to those where the K^+ gluconate solution was employed. Whole-cell patch clamp recordings from neurons in layers 1-3 of anterior PC were made with an EPC 9/2 amplifier (HEKA, Lambrecht, Germany). Series resistance compensations were performed in all recordings. The initial access was $< 20 M\Omega$ and compensated by 50-70%. All experiments were performed at $32^\circ C$. Voltage-gated currents and excitability of the cell were monitored by means of voltage-clamp and current-clamp protocols (PulseFit v 8.0; Heka, Germany). Cell responses were obtained by injecting hyperpolarizing and depolarizing current steps (500 ms pulse; 50 pA increments). Neuronal resting membrane potential was measured only after the patch clamp recording was stable. Input resistance (R_I) was calculated by linear regression of the current-voltage relationship in response to hyperpolarizing steps (as described in Dietrich *et al.*, 2005) using Origin software (Microcal, Northampton, MA). Firing pattern analysis was performed at the current level that produced reliable repetitive firing (twice the firing threshold), in presence of NMDA, AMPA and kainate channel blockers (20 μm 2-amino phosphonovaleric acid, APV & 10 μm dinitroquinoxaline-2,3-dione, DNQX; Research Biochemicals, Natick, MA, USA). Interspike interval ratio (II_R) was obtained by dividing the last interspike interval (measured in milliseconds) by the duration of the first interval, as described in Kroner *et al.* (2007).

3.2.3 Cluster analysis & statistics

Unsupervised cluster analysis was performed on interneuronal populations of PC using Ward's method with z -score normalization and intervals calculated by Euclidian squared distances (SPSS 13, Chicago, Illinois, USA) according to described methodology (Cauli *et al.*, 2000). The analysis was based on their main electrophysiological parameters: input resistance, firing frequency and interspike interval ratio, providing five distinct firing groups (Fig. 3.1). Terminology for the five clusters was chosen according to their II_R (neurons with $II_R < 1.25$ were grouped

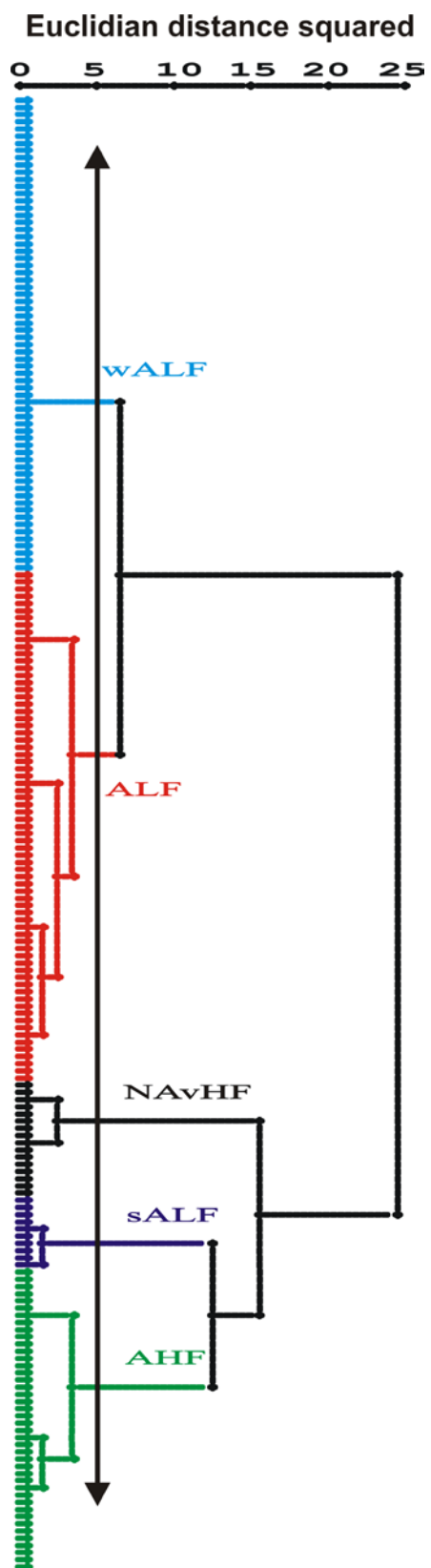
as non-adapting cells while neurons with $II_R > 1.25$ were classified as adapting cells; Fig. 3.2) and firing frequencies (FF > 50Hz – high frequency and FF < 50Hz as low frequency) as described in Kroner *et al.* (2007) and Ascoli *et al.* (2008).

Comparisons among different firing pattern groups were made by using ANOVA and a Tukey multiple comparison post-hoc test (SPSS 13, Chicago, Illinois, USA). All data are presented as means \pm standard error of the mean.

3.2.4 Histochemistry

In order to reconstruct the morphology and understand where the recordings were made, patch electrodes included 0.2% Biocytin. After the completion of a recording, the slice was removed from the microscope chamber and fixed in paraformaldehyde solution (4% paraformaldehyde in 0.1 phosphate buffer) for 5-7 days. The sections were washed for 15 min in PBS followed by a 30 min rinse in PBS-TX and 90 min incubation in streptavidin-conjugated Alexa Fluor-594 (5 μ g/ml; Molecular Probes) at room temperature. After rinsing in PB-TX for 30 min, the slices were mounted on slides for viewing on a confocal microscope.

Figure 3.1 Cluster analysis of electrophysiological properties of rat aPC interneuronal populations before kindling-induced epilepsy. The y -axis of dendrogram shows individual cells ($n = 205$) and the x -axis represents the linkage distance measured by Euclidean distance squared. Double arrow solid line represents the cut off showing five distinct clusters: Non-adapting very high frequency (NAvHF), adapting high frequency (AHF), adapting low frequency (ALF), strongly adapting low frequency (sALF), and weakly adapting low frequency (wALF).



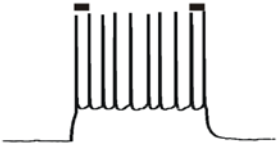
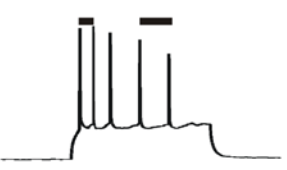
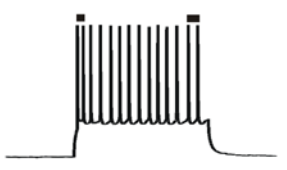
| Interspike Interval Ratio | Spiking pattern | Terminology |
|---|--|--------------|
| $\frac{\text{Last ISI}}{\text{First ISI}} < 1.25$ |  | Non-adapting |
| $\frac{\text{Last ISI}}{\text{First ISI}} > 1.25$ |  | Adapting |
| $\frac{\text{Last ISI}}{\text{First ISI}} > 1.25$ |  | |

Figure 3.2 Firing pattern classification and terminology.

Based on their spiking adaptation (interspike interval ratio), piriform cortex interneurons were classified in two main groups: non-adapting and adapting. Dark bars above each spiking pattern represent the first and the last interspike interval (ISI).

3.2.5 Image acquisition and morphological reconstruction of patched neurons

Confocal images were taken on an Olympus IX 60 inverted microscope outfitted with a Perkin Elmer Spinning Disk Confocal attachment with a 20X (N.A. = 0.50) objective. The microscope was equipped with a Hamamatsu Orca ER CCD camera (1,300 X 1,030 pixels), and images were acquired in Volocity software (Improvision, Lexington, MA). Each image represents a stack of 40–50 images, 0.2 μm apart in the z-plane. For morphological reconstruction of the dendritic arborization of patched neurons, the stacks of confocal images were deconvolved with Auto-Quant software (Auto quant X2, Media Cybernetics, Bethesda, MD) and then processed with Imaris Filament Tracer module in “Surpass mode” (Bitplane, Zurich, Switzerland). Filament tracer creates dendritic arborization patterns based on an algorithm that predicts arborization pathways. These pathways are set up by the user-set criteria of a start point, namely, the size of cell somata, and an end point representing minimum thickness of processes. Start points were set to 10 μm , and endpoints were set to 1 μm . The resultant filament lines were converted from lines to two-pixel-thick cones. To mark the cell bodies, an “Isosurface” was then created. This process creates a cell body from the stack of images that is then merged with the dendritic morphology (see also, Gavrilovici *et al.*, 2010).

We used criteria for classification of pyramidal versus non-pyramidal cells as previously described (McIntyre *et al.*, 2002; Gavrilovici *et al.*, 2006), based on: 1) soma morphology; 2) axonal projection to deeper layers for pyramidal cells; 3) presence of dendritic spines for pyramidal cells; and 4) spiking properties. A few cells that were spiny non-pyramidal were also found but not included in the analysis. Based on the morphologies that we have previously described (Gavrilovici *et al.*, 2010), interneurons were further grouped into three categories: 1) horizontal cells (usually calbindin immunoreactive; CB-IR) having extended dendrites in the horizontal plane – parallel to the PC layers; 2) multipolar cells (usually parvalbumin; PV-IR and PV-IR/CB-IR) having a round dendritic tree crossing into adjacent layers;

and 3) vertical/bipolar-bitufted cells (usually calretinin immunoreactive CR-IR) having extended dendrites in the vertical plane, perpendicular to PC layers.

PC layer depth and demarcation between adjacent layers were set according to Neville & Haberly (2004) and Ekstrand *et al.* (2001).

3.3 Results

The purpose of this study was to determine if distinct types of interneuronal firing patterns occur within the three cell layers of the aPC, or whether each layer has many differing firing patterns, originating from a diverse set of interneuron populations. A total of 205 recordings from aPC interneurons that were morphologically identified, according to the criteria indicated in Methods, are included in this study. First, we found that the resting membrane potential (RMP) of PC interneurons ranged from -60 mV to -82 mV, and no group of interneurons, described in detail below, were different from another based on RMP. All recordings could be broadly classified into two types of firings patterns: most cells (180 cells; ~88%) responded by firing tonically throughout the current injection, while the rest (25 cells; ~ 12%) fired phasically (i.e. they stopped firing before the end of the depolarizing step). Although adapting phasic firing was previously shown in some interneurons in L3 of PC and endopiriform nucleus (Tseng & Haberly, 1989), our study shows the presence of this firing in both L2 and L3 of PC.

The majority of the continuously firing interneurons (122 of 180 cells; ~68%) adapted to the stimulus. The occurrence of adaptation was defined by determining whether the last interspike firing interval was 25% longer than the first interval ($II_R > 1.25$). The rest (58 of 180 cells; ~32%), showed little or no firing adaptation ($II_R < 1.25$). We also found that adapting firing cells fired at both high (> 50 Hz) and low (< 50 Hz) frequencies. Although this broad classification can provide some interesting functional aspects of PC interneurons, a more exact (unbiased) functional grouping was provided by cluster analysis. Cluster analysis using interneuronal electrophysiological characteristics (see Methods), provided five distinct groups:

non-adapting very high frequency (NAvHF), adapting high frequency (AHF), adapting low frequency (ALF), strongly adapting low frequency (sALF), and weakly adapting low frequency (wALF).

We also classified the PC interneurons based on their dendritic arborization pattern. Three main morphological interneuronal classes have been previously described in rat aPC in our recent study (see Gavrilovici et al., 2010) and described in Methods). These include multipolar cells, bipolar/bifurcated (vertical) cells and horizontal cells.

3.3.1 High frequency spiking interneurons

High frequency spiking cells (firing frequency; FF > 50 Hz) accounted for about 28% of all recordings (58 of 205 cells; Fig. 3.3). In general, they were more excitable, having a significantly lower firing threshold than low frequency firing interneurons (see Table 3.1). In about 28% (16 of 58) of the high frequency spiking cells, the rate of firing did not change during the stimulus (II_R of 1.18 ± 0.06 ; Table 3.1; Fig. 3.4A & B). This behaviour was therefore termed as non-adapting very high frequency (NAvHF). Overall this type of firing pattern was observed in about 8% of all recordings (16 of 205; Table 3.1; Fig. 3.3). The average resting membrane potential was -76.1 ± 1.7 mV (Table 3.1) while the input resistance (R_i) was 179.1 ± 10.6 M Ω and threshold current was 103.1 ± 11.6 pA (Table 3.1). These cells also had the highest firing frequency among all PC interneuronal groups (118.8 ± 9.4 Hz; Table 3.1; Fig. 3.4A & B). The morphology of these cells was most often multipolar (12 of 16; 75%; see Fig. 3.4C and below for a more complete analysis).

The next class of high frequency firing contained interneurons that adapted to the stimulus. These are termed adapting high frequency (AHF). These cells had an II_R of 2.14 ± 0.10 (Table 3.1; Fig. 3.5A & B) and therefore a lower firing frequency at the end of a current stimulus (firing frequency of 54.7 ± 2.2 Hz; Table 3.1; Fig. 3.5A & B). This group accounted for about 72% of the HF interneurons (42 of 58 cells) and about 20% of all interneurons (42 of 205 cells; Fig.3.3). They were the

third largest group of interneurons in the aPC. Resting membrane potential and the threshold current of these cells were similar to the other high-frequency group (RMP = -76.2 ± 1.3 mV; threshold current = 119.0 ± 6.3 pA; Table 3.1).

3.3.2 Low firing frequency interneurons

The most common firing pattern found was the adapting low frequency (ALF) (FF = 38.8 ± 1.7 Hz; Table 3.1; Fig. 3.6A & B). They accounted for about 48% (71 of 147) of the LF cells and were 34.6% (71 of 205) of all recordings (Table 3.2; Fig. 3.3). The adaptation ratio of these cells was lower than the AHF group ($II_R = 1.7 \pm 0.06$; $P < 0.001$; Table 3.1). The average resting membrane potential of this group was -76.0 ± 0.9 mV (Table 3.1). The reduced excitability of ALF cells was accounted for by a lower R_I than the AHF group ($R_I = 174.2 \pm 5.8$ M Ω ; $P < 0.001$; Table 3.1).

The next type of firing pattern had the smallest representation of interneurons which fired at low frequency. They strongly adapted to the stimulus, therefore they are termed strongly adapting low frequency (sALF). They accounted for just 10 of 205 cells, representing only 4.8 % of the total number of recordings (Table 3.2; Fig. 3.3; Fig. 3.7). Although, the firing adaptation of these cells was the highest among all other PC interneurons ($II_R = 4.46 \pm 0.37$), the other electrophysiological parameters were similar to the ALF cells (the average resting membrane potential of this group was -70.6 ± 2.9 mV, $R_I = 134.4 \pm 15.9$ M Ω while FF was 43.5 ± 3.2 Hz; Table 3.1). These cells showed high threshold current, which differed significantly among the HF groups (threshold current = 190.0 ± 22.1 pA; Table 3.1).

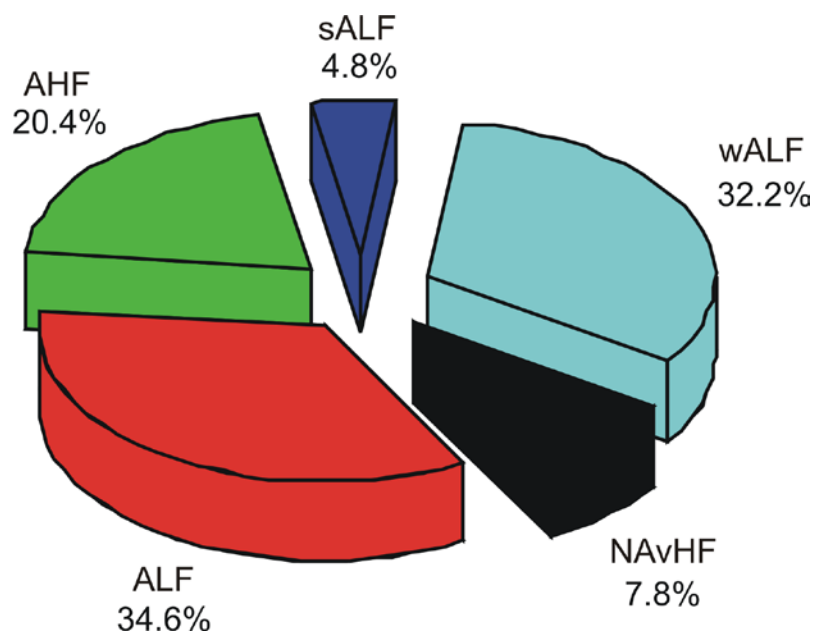


Figure 3.3 Distribution of the five types of firing patterns in the anterior piriform cortex of rat.

NAvHF, non-adapting very high frequency; AHF, adapting high frequency; ALF, adapting low frequency; sALF, strongly adapting low frequency; wALF, weakly adapting low frequency.

Table 3.1 Electrophysiological properties of the five types of interneuronal firing groups in the anterior piriform cortex.

| | Cluster 1 NAvHF (n = 16) | Cluster 2 AHF (n = 42) | Cluster 3 ALF (n = 71) | Cluster 4 sALF (n = 10) | Cluster 5 wALF (n = 66) |
|---|--------------------------------|------------------------------|------------------------------|-------------------------------|-------------------------------|
| RMP (mV) | -76.1 ± 1.7 | -76.2 ± 1.3 | -76.0 ± 0.9 | -70.6 ± 2.9 | -72.7 ± 0.8 |
| R _i (MΩ) | 179.1 ± 10.6 | 302.3 ± 12.5 | 174.2 ± 5.8 | 134.4 ± 15.9 | 97.2 ± 3.4 |
| Threshold current (pA) | 103.1 ± 11.6 | 119.0 ± 6.3 | 138.0 ± 7.6 | 190.0 ± 22.1 | 182.6 ± 10.0 |
| Interspike interval ratio (I _R) | 1.18 ± 0.06 | 2.14 ± 0.10 | 1.70 ± 0.06 | 4.46 ± 0.37 | 1.31 ± 0.44 |
| Frequency (Hz) | 118.8 ± 9.4 | 54.7 ± 2.2 | 38.8 ± 1.7 | 43.5 ± 3.2 | 26.6 ± 0.9 |
| Number of spikes per pulse | 53 ± 5 | 23 ± 1 | 18 ± 1 | 17 ± 2 | 13 ± 1 |

Values are means ± SE; n, number of cells; >, significantly greater with $P < 0.05$; >>, significantly greater with $P < 0.01$; Statistically significant comparisons were determined using Tukey post hoc analysis after performing ANOVA.

RMP, resting membrane potential; R_i input resistance; NAvHF, non-adapting very high frequency; AHF, adapting high frequency; ALF, adapting low frequency; sALF, strongly adapting low frequency; wALF, weakly adapting low frequency.

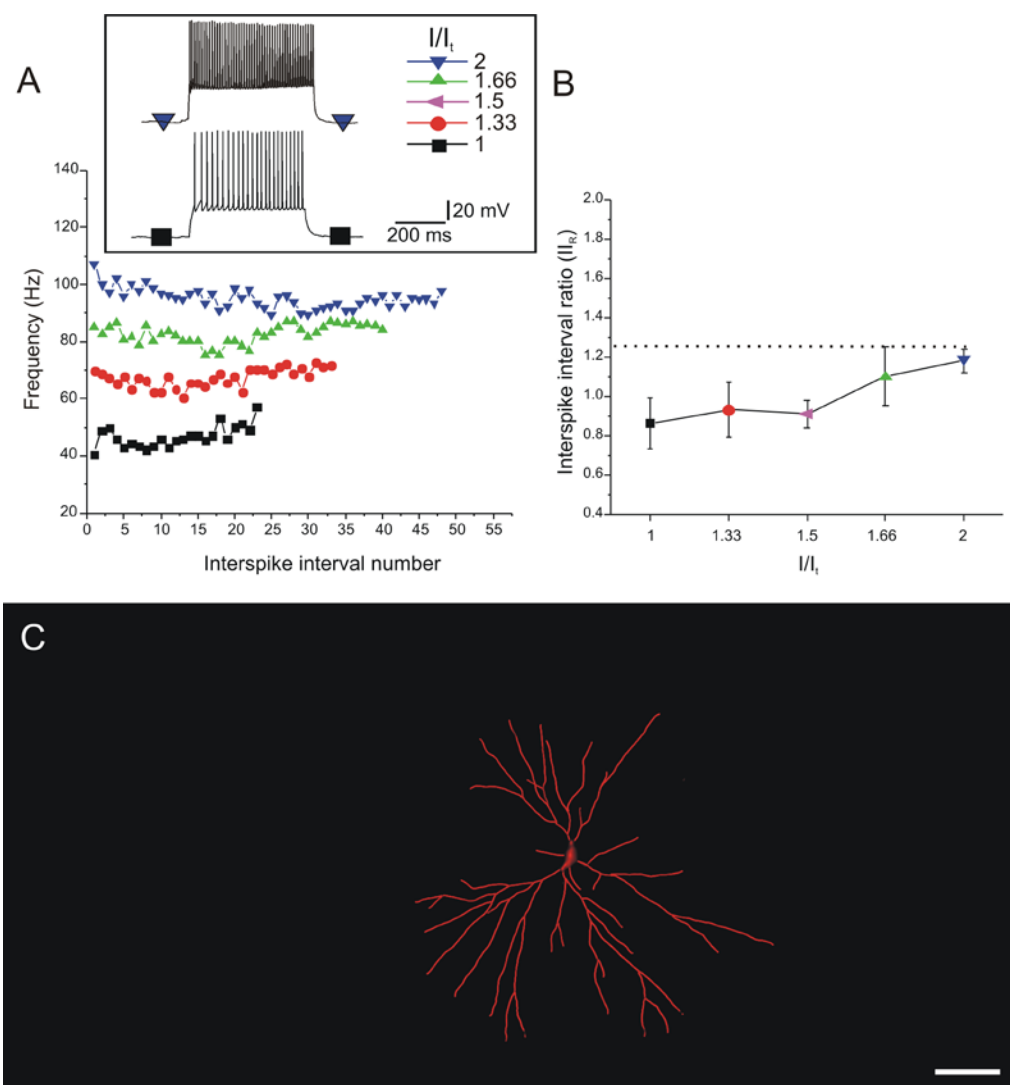


Figure 3.4 Electrophysiological properties of non-adapting very high frequency (NAvHF) cell type. **A.** Plot of firing frequency against interspike interval number in a typical NAvHF cell shows the lack of significant firing adaptation. **B.** The ratio between last and first interspike intervals (I_{I_R}) was plotted against level of injected current, showing absence of firing adaptation across NAvHF group ($I_{I_R} < 1.25$). **C.** Morphological reconstruction of NAvHF cell with firing pattern shown in panel A. Traces in the inset shows the response of NAvHF cell type to injection of depolarizing current steps at threshold ($I/I_t = 1$) and twice the firing threshold ($I/I_t = 2$) levels. Scale bar = 40 μm .

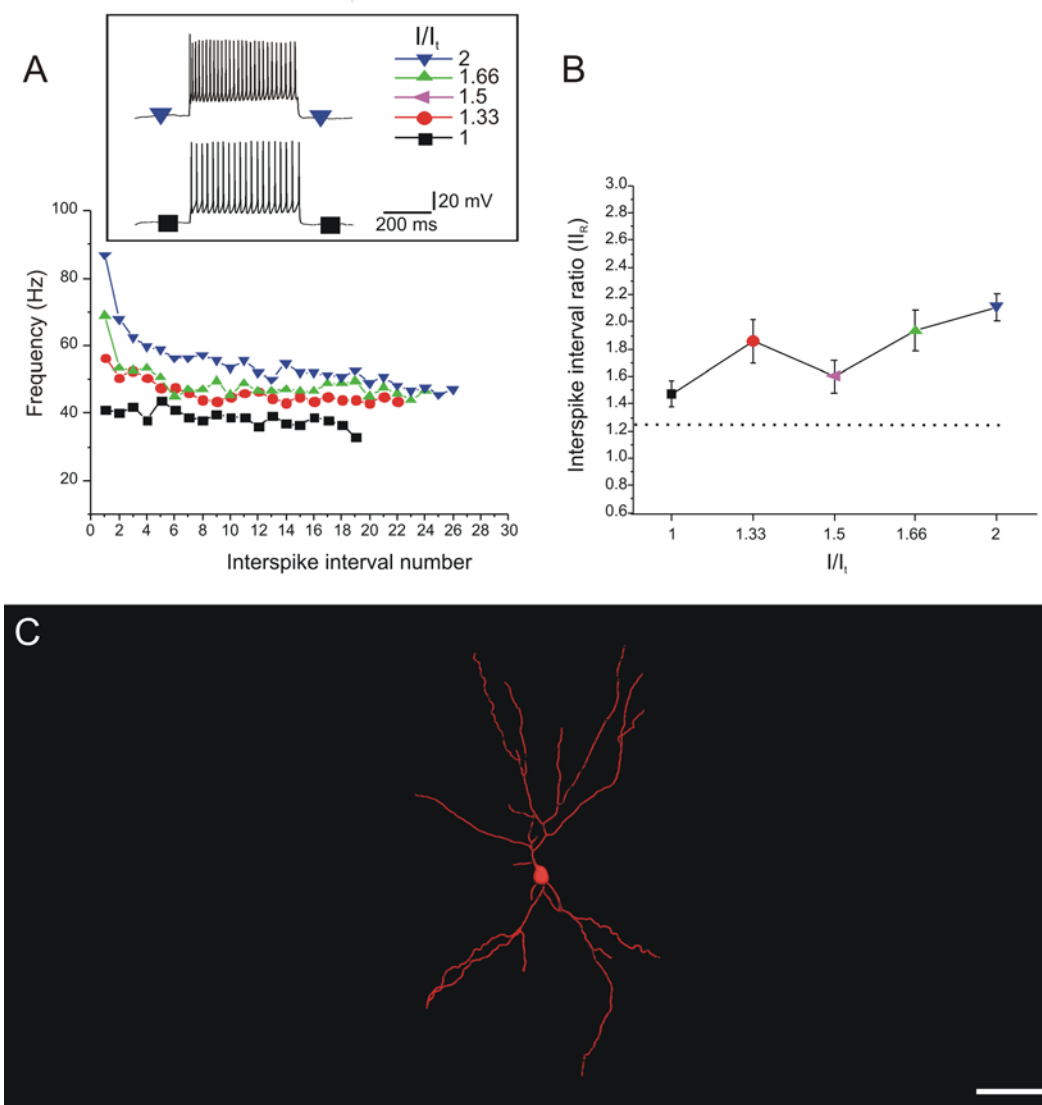


Figure 3.5 Electrophysiological properties of adapting high frequency (AHF) cell type. A. Plot of firing frequency against interspike interval number in a typical AHF cell. Note the moderate spike frequency adaptation. B. The ratio between last and first interspike intervals (II_R) was plotted against level of injected current, showing moderate level of firing adaptation across AHF group ($II_R > 1.25$). C. Morphological reconstruction of AHF cell firing pattern shown in panel A. Traces in the inset show the response of AHF cell type to injection of depolarizing current steps at threshold ($I/I_t = 1$) and twice the firing threshold ($I/I_t = 2$) levels. Scale bar = 40 μm .

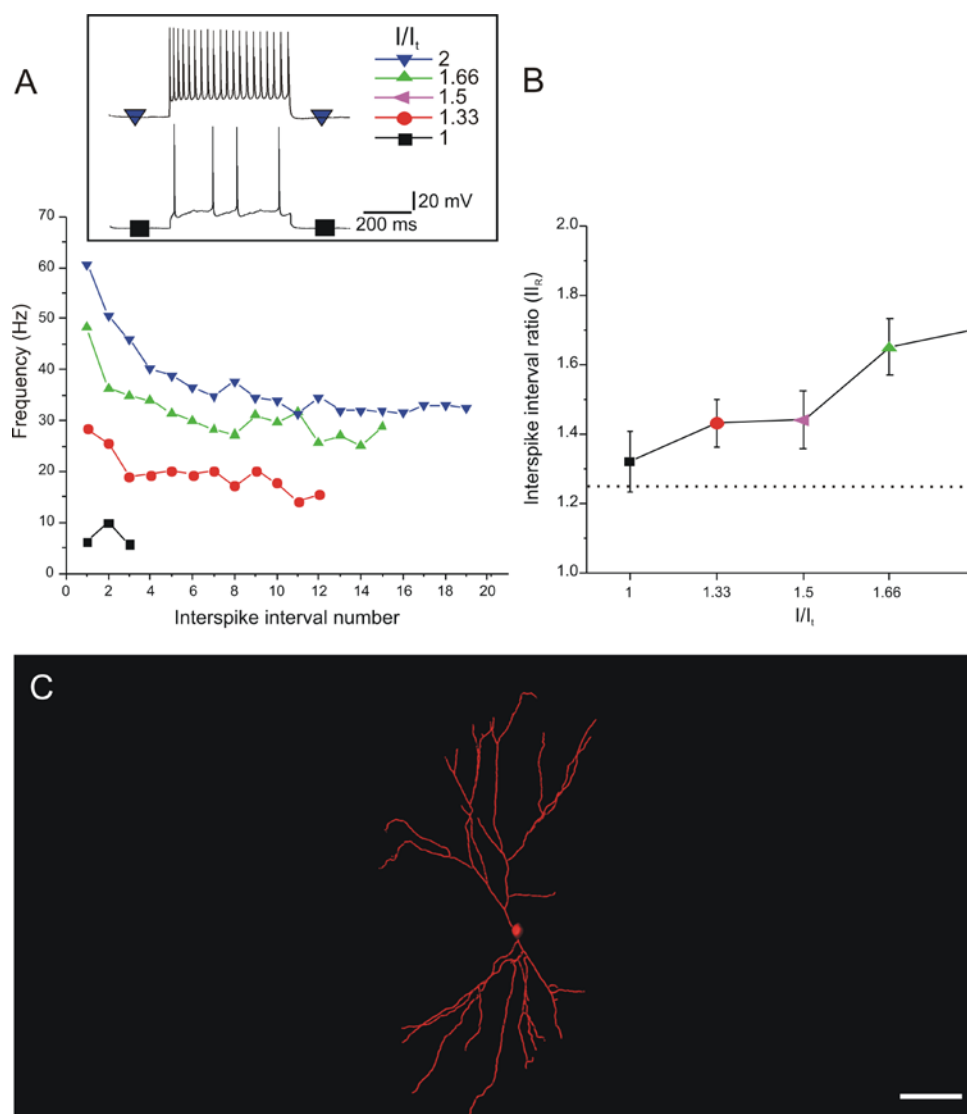


Figure 3.6 Firing properties of adapting low frequency (ALF) cell type.

A. Plot of firing frequency against interspike interval number in a typical ALF cell. Note the moderate spike frequency adaptation at higher depolarizing steps. B. The ratio between last and first interspike intervals (II_R) was plotted against level of injected current, showing moderate firing adaptation at currents higher than the firing threshold across ALF group. C. Morphological reconstruction of ALF cell with firing pattern shown in panel A. Traces in the inset show the response of ALF cell type to injection of depolarizing current steps at threshold ($I/I_t = 1$) and twice the firing threshold ($I/I_t = 2$) levels. Scale bar = 40 μm .

Table 3.2 Firing group distribution across the anterior piriform cortex layers

| Group | L1 % | L2 % | L3 % |
|----------------|------|------|------|
| NAvHF (n = 16) | 18.7 | 31.3 | 50.0 |
| AHF (n = 42) | 19.0 | 59.5 | 21.5 |
| ALF (n = 71) | 15.5 | 50.7 | 33.8 |
| sALF (n = 10) | 0.0 | 50.0 | 50.0 |
| wALF (n = 66) | 3.0 | 57.5 | 39.5 |

NAvHF, non-adapting very high frequency; AHF, adapting high frequency; ALF, adapting low frequency; sALF, strongly adapting low frequency; wALF, weakly adapting low frequency; L1, layer 1; L2, layer 2; L3, layer 3.

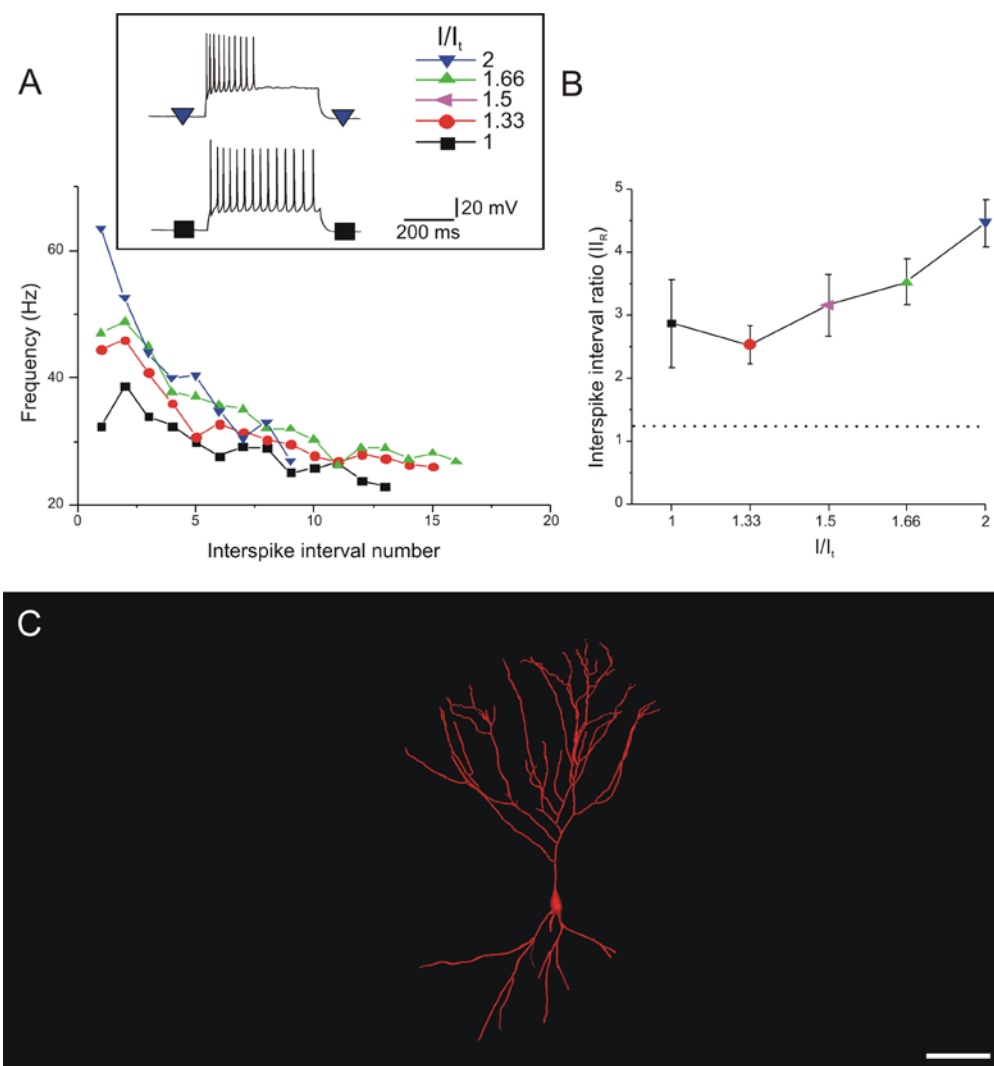


Figure 3.7 Firing properties of strongly adapting low frequency (sALF) cell type. A. Plot of firing frequency against interspike interval number in a typical sALF cell. Note the high spike frequency adaptation at higher depolarization levels (twice the firing threshold). B. The ratio between last and first interspike intervals (II_R) was plotted against level of injected current, showing increased firing adaptation across sALF group ($II_R > 1.25$). C. Morphological reconstruction of sALF cell with firing pattern shown in panel A. Traces in the inset show the response of sALF cell type to injection of depolarizing current steps at threshold ($I/I_t = 1$) and twice the firing threshold ($I/I_t = 2$) levels. Scale bar = 40 μm .

Finally, the last of the low frequency group was named weakly adapting low frequency (wALF) due to its slow adaptation to the stimulus. The wALF group represented about 45% of all LF cells (66 of 147) and 32.2% of all interneurons - the second largest group in the aPC (Table 3.2; Fig. 3.3; Fig. 3.8). The average resting membrane potential of this group was -72.7 ± 0.8 mV (Table 3.1). These cells fired in the lowest frequency range among all other interneurons (FF = 26.6 ± 0.9 Hz, Table 3.1). WALF cells had a lower R_I and a higher threshold current than those in the ALF group ($R_I = 97.2 \pm 3.4$ M Ω , $P < 0.001$; threshold current = 182.6 ± 10.0 pA; $P < 0.01$; Table 3.1).

3.3.3 Intra-layer localization analysis.

The next question to answer was “Where do these cells reside within the layers of the PC”? This is important to gain insight as to how these cells may participate in the inhibitory loops (feed-forward and feedback inhibition). We found that all firing patterns were present in every layer with the exception of L1 where sALF type was not seen. Our data showed that there is no dominant firing type in any of the three layers of PC (Fig. 3.9) indicating a large diversity of firing patterns in every layer of PC. However, following each interneuronal group distribution among PC layers, we found they had different layer preferences. For example, most of AHF cells (~ 60%) were found in L2 while the rest were equally distributed between L1 and L2 (Table 3.2). Most of the ALF group was also seen in L2 (~ 51%) followed by L3 and L1. NAvHF, sALF and wALF groups were mostly distributed in L2 and L3 (Table 3.2).

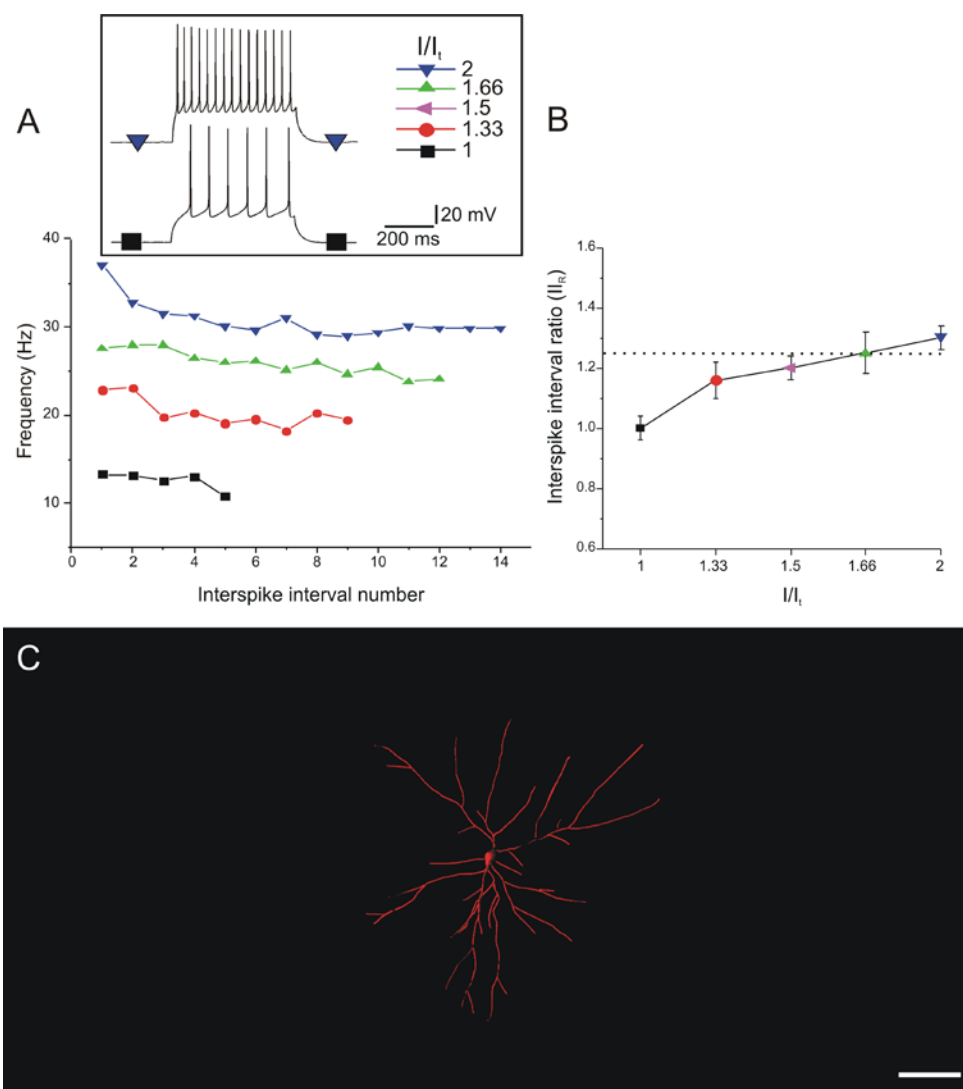


Figure 3.8 Firing properties of weakly adapting low frequency (wALF) cell type. A. Plot of firing frequency against interspike interval number in a typical wALF cell. Note the absence of spike frequency adaptation at lower depolarizing steps. B. The ratio between last and first interspike intervals (II_R) was plotted against level of injected current, showing small firing adaptation across wALF group ($II_R \leq 1.25$). C. Morphological reconstruction of wALF cell with firing pattern shown in panel A. Traces in the inset show the response of wALF cell type to injection of depolarizing current steps at threshold ($I/I_t = 1$) and twice the firing threshold ($I/I_t = 2$) levels. Scale bar = 40 μm .

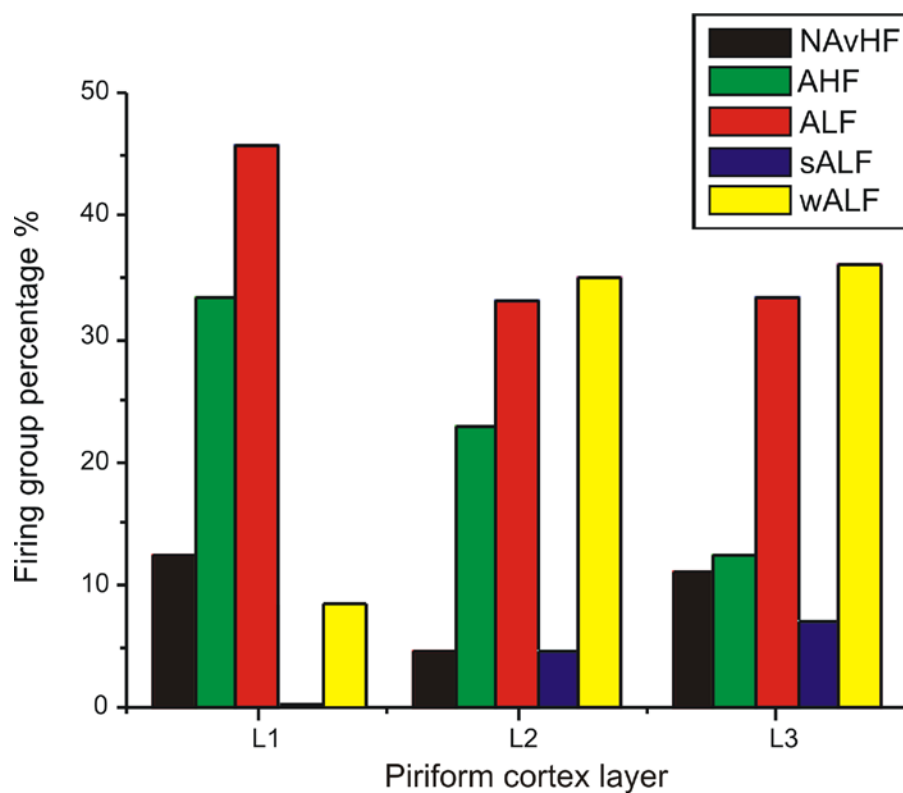


Figure 3.9 Layer distribution of the five firing groups in the anterior piriform cortex. The columns represent the contribution (%) of each firing group to the total number of firing types recorded in each PC layer. NAvHF, non-adapting very high frequency; AHF, adapting high frequency; ALF, adapting low frequency; sALF, strongly adapting low frequency; wALF, weakly adapting low frequency.

3.3.4 Comparison of firing patterns with morphological attributes

Although the spiking patterns were not consistently predictive of a specific interneuronal morphology, we found that most of the cells displaying non-adapting firing pattern were multipolar (see Fig. 3.10; 12 of 16 NAvHF cells were multipolar, 75%; $P < 0.05$). However, the other four clusters did not show a preference towards any of the detected morphological types, multipolar, horizontal and vertical cells were similarly distributed into the AHF, ALF, sALF and wALF groups (Fig. 3.10). Examples of different interneurons pertaining to the five firing groups within the aPC layers were shown in Fig. 3.11.

A broad morphological classification of PC interneurons in three groups: horizontal, vertical and multipolar interneurons; and a subsequent analysis of their firing behaviour also showed a large variability of firing patterns (Table 3.3). Most vertical cells fired in ALF mode (~42%), while least of them had NAvHF and sALF behaviour (~3% of total vertical cells for each of these two groups). About 36% of all multipolar cells had wALF firing while only 5% pertained to sALF group. Finally, almost 40% of horizontal cells were AHF interneurons while at the lower end of firing preference only 5% of total horizontal cell population had NAvHF firing (Table 3.3).

As noted in the Methods section all these recordings were done with K^+ gluconate electrodes to maintain the Cl^- ion gradient at physiological levels. K^+ gluconate electrode recording have been shown in the past to attenuate the activity of calcium activated potassium channels (Storm, 1990; Zhang *et al.*, 1994). This may have a potential impact on the firing properties of cells. To check this possibility we did some recordings using electrodes that had K^+ methanesulfonate as part of the internal solution. We found that all five patterns of firing were represented in similar proportions as in the K^+ gluconate recordings ($n = 34$). In Fig. 3.12 we show an example of a ALF interneuron with vertical morphology. Note that in this recording there is no afterhyperpolarizing potential that one would expect if calcium activated potassium conductances were active in these cells.

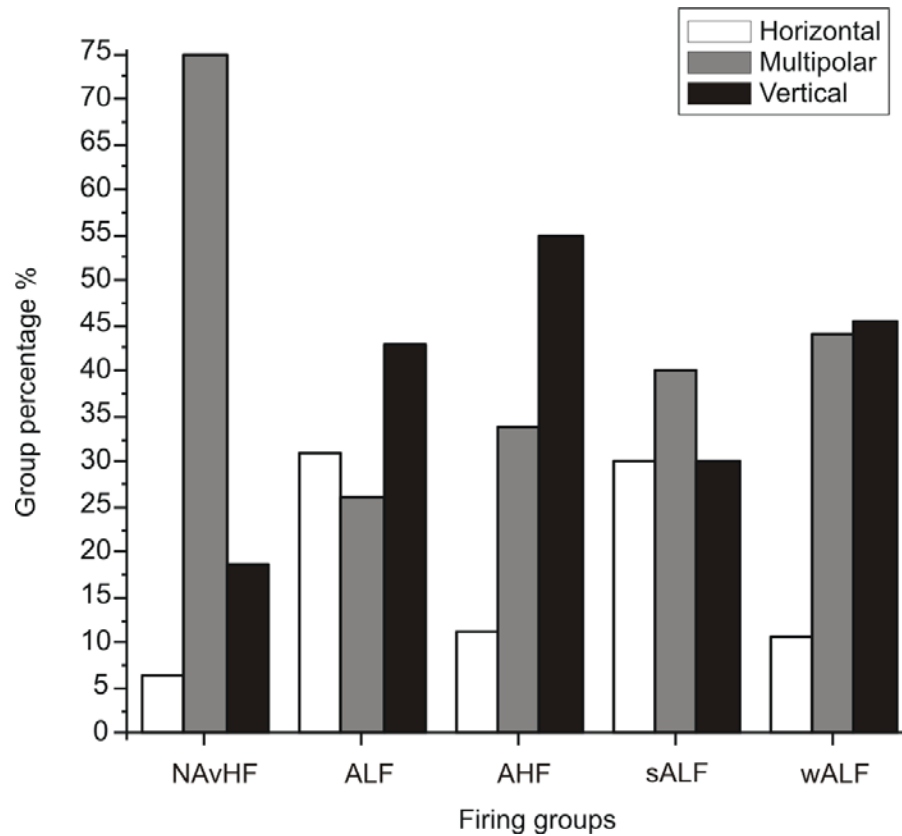


Figure 3.10 Correlation between the firing pattern types and interneuronal morphology in the anterior piriform cortex. NAvHF, non-adapting very high frequency; AHF, adapting high frequency; ALF, adapting low frequency; sALF, strongly adapting low frequency; wALF, weakly adapting low frequency.

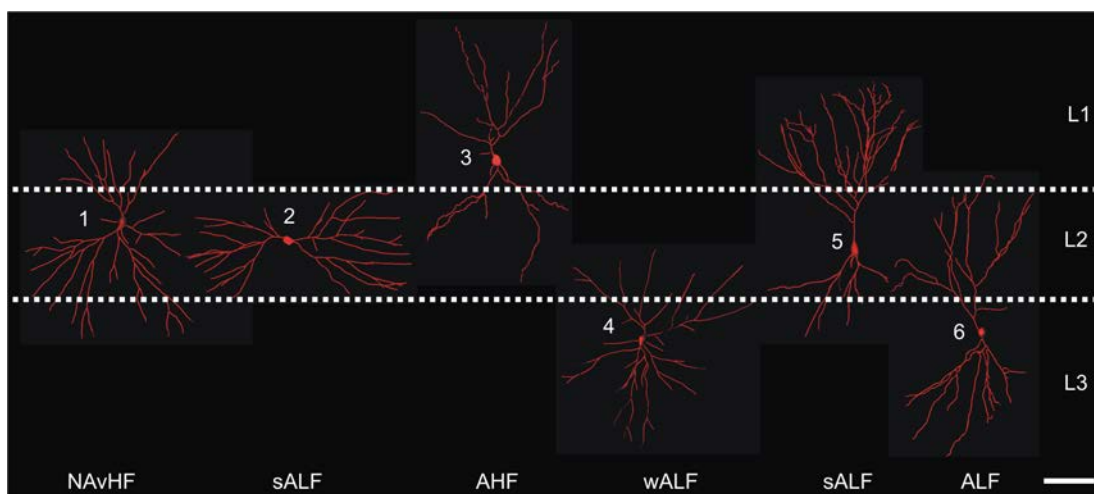


Figure 3.11 Localization and morphologies of predominant firing patterns groups within the anterior piriform cortex. Examples of interneurons with NAvHF (cell 1, multipolar), AHF (cell 3, vertical), ALF (cell 6, vertical), sALF (cell 2, horizontal; cell 5 vertical) and wALF (cell 4, multipolar) firing characteristics. Demarcation between piriform cortex layers is shown as dotted lines. NAvHF, non-adapting very high frequency; AHF, adapting high frequency; ALF, adapting low frequency; sALF, strongly adapting low frequency; wALF, weakly adapting low frequency; L1, layer 1; L2, layer 2; L3, layer 3; Scale bar = 40 μm .

Table 3.3 Layer distribution of the three main morphological interneuronal types of piriform cortex.

| Morphology | Firing type | L1 % | L2 % | L3 % | L1-L3 % |
|------------------------|-------------|------|------|------|---------|
| Horizontal (n = 32) | NAvHF | 0.0 | 4.5 | 0.0 | 3.1 |
| | AHF | 0.0 | 54.6 | 10.0 | 40.6 |
| | ALF | 0.0 | 22.7 | 30.0 | 25.0 |
| | sALF | 0.0 | 4.5 | 20.0 | 9.4 |
| | wALF | 0.0 | 13.7 | 40.0 | 21.9 |
| | Total | 0.0 | 100 | 100 | 100 |
| | | | | | |
| Morphology | Firing type | L1 % | L2 % | L3 % | L1-L3 % |
| Multipolar (n = 80) | NAvHF | 0 | 9.0 | 22.9 | 15.0 |
| | AHF | 0 | 13.3 | 14.3 | 13.7 |
| | ALF | 0 | 33.3 | 25.7 | 30.0 |
| | sALF | 0 | 4.4 | 5.7 | 5.0 |
| | wALF | 0 | 40.0 | 31.4 | 36.3 |
| | Total | 0 | 100 | 100 | 100 |
| | | | | | |
| Morphology | Firing type | L1 % | L2 % | L3 % | L1-L3 % |
| Vertical (n = 93) | NAvHF | 12.5 | 0.0 | 0.0 | 3.2 |
| | AHF | 33.3 | 16.6 | 11.1 | 19.4 |
| | ALF | 45.9 | 38.1 | 44.5 | 41.9 |
| | sALF | 0.0 | 4.8 | 3.7 | 3.2 |
| | wALF | 8.3 | 40.5 | 40.7 | 32.2 |
| | Total | 100 | 100 | 100 | 100 |

Data in columns represent the contribution (%) of each morphological type to the five firing clusters in each layer of PC.

NAvHF, non-adapting very high frequency; AHF, adapting high frequency; ALF, adapting low frequency; sALF, strongly adapting low frequency; wALF, weakly adapting low frequency; L1, layer 1; L2, layer 2; L3, layer 3.

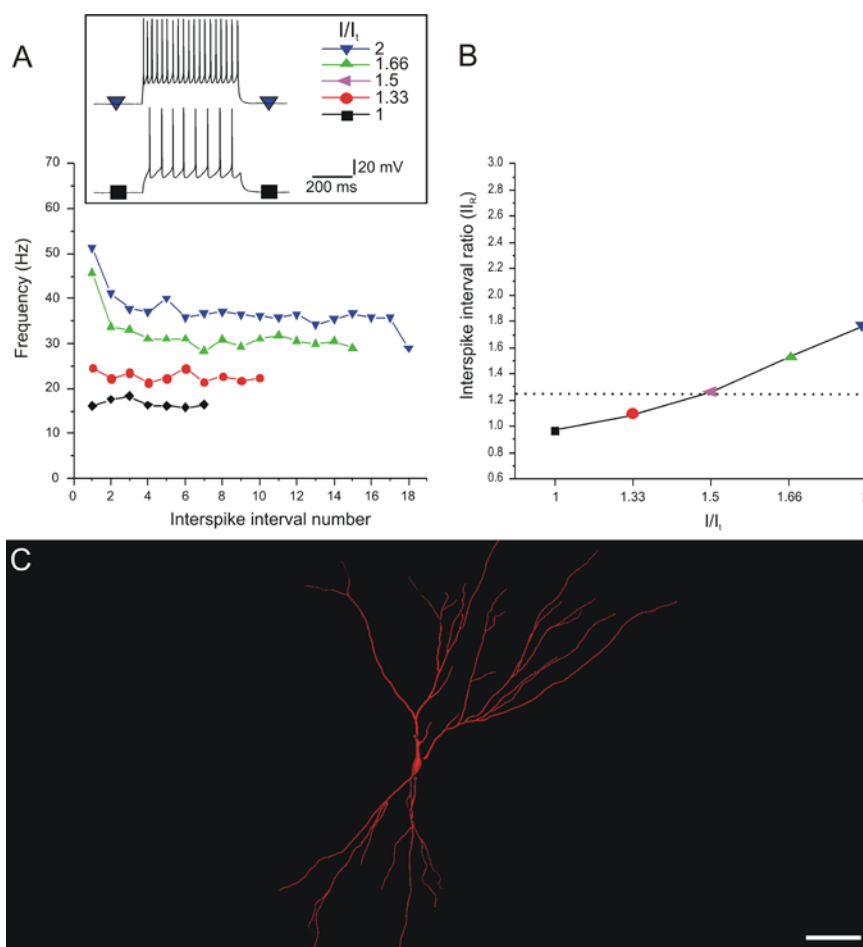


Figure 3.12 Firing properties of cells recorded using K^+ methanesulfonate are similar to those recorded in K^+ gluconate electrode solution. Here we show a recording from a vertical cell in layer 3 with a typical adapting low frequency (ALF) firing pattern. Note the absence of the slow afterhyperpolarization at the end of the action potential train. A. Plot of firing frequency against interspike interval number in a typical ALF cell. Note the moderate spike frequency adaptation at higher depolarizing steps. B. The ratio between last and first interspike intervals (I/I_t) was plotted against level of injected current, showing moderate firing adaptation at currents higher than the threshold. C. Morphological reconstruction of ALF cell with firing pattern shown in panel A. Traces in the inset show the response of ALF cell type to injection of depolarizing current steps at threshold ($I/I_t = 1$) and twice the firing threshold ($I/I_t = 2$) levels. Scale bar = 40 μm .

3.4 Discussion

Our study identifies multiple subpopulations of interneurons with different firing patterns and membrane properties in all three layers of rat aPC. Interneurons were classified in five clusters based on their firing frequency, firing adaptation and their input resistance; and labeled in concordance with criteria developed by Ascoli *et al.* (2008) (high or low firing frequency: $50\text{Hz} < \text{FF} > 50\text{ Hz}$; non-adapting vs. adapting; $1.25 < \text{II}_R > 1.25$). Although this classification system may not fully describe all the fine details of the firing patterns, it does describe the predominant behaviours that can often be associated with interneuron morphology and location within the layers. Although we have identified five firing groups in L2 and L3, in L1 only four firing groups were found (NAvHF: 12.5%; AHF: 33.3%; ALF: 45.8% and wALF: 8.3%).

Overall, it was found that low frequency groups (e.g. ALF, sALF and wALF) predominated especially in L2 and L3. In L2, these groups accounted for about 72% of all types, whereas in L3 the occurrence of this pattern was 76%; this suggests that the most important mode of firing within the PC is the low frequency adapting type. These attributes undoubtedly control the feed-forward and feedback inhibition, however how this predominant firing mode and how the others participate in more complex network activity is not known. This latter uncertainty is important to resolve since it is well established that interneuron activity generates and sustains oscillatory activities (see review, Whittington & Traub, 2003; Klausberger & Somogyi, 2008).

3.4.1 Comparison of aPC spiking patterns to those found in other cortical and limbic regions.

The spiking patterns observed in aPC relate to other firings patterns described in the CNS, albeit being termed by differing nomenclature. For example, NAvHF group, due to their high firing frequency ($\text{FF} > 50\text{ Hz}$) and the limited/lack of firing adaptation ($\text{II}_R < 1.25$), resemble the fast spiking interneuronal cell type described in cortex of rodents (Kawaguchi, 1993; Kawaguchi & Kubota, 1997; Young & Sun,

2009) and primates (Kroner *et al.*, 2007). Phasic firing, which is discontinuation of firing before the end of stimulation, was previously detected in deep layers of PC (L3 and endopiriform nucleus) (Tseng & Haberly, 1989) but also in lamina I of the spinal dorsal horn (Prescott & De Koninck, 2002; Dougherty *et al.*, 2005). Finally, adapting firing type resemble the spiking type previously described as regular spiking (RS) non-pyramidal firing mode (Connors & Gutnick, 1990) or as adapting non-pyramidal (ANP) firing (Kroner *et al.*, 2007). Thus, the spiking patterns described in the PC are very similar to those found in both cortical, hippocampal and spinal cord regions of the CNS.

3.4.2 How do these firing patterns control the activity of the aPC?

We found that in L1 almost all firing patterns recorded (87.5%) were adapting. The only other firing pattern recorded was NAvHF (12.5%). L1 cells are thought to be involved in feed-forward inhibitory loops, receiving excitatory stimulus from LOT and providing inhibition to L2 pyramidal cells (Haberly & Bower, 1984; Kapur *et al.*, 1997; Ekstrand *et al.*, 2001; Gavrilovici *et al.*, 2010). Neurons in L1 are uniquely calretinin positive but GAT-1/CR-IR puncta, presumably representing release sites, are located throughout L1-L3. Most of the puncta are found in L1 (60%) with only about 20 % being found in each of the other layers. Little GAT-1/CR-IR puncta were associated with cell soma in L1 but some puncta were associated with other CR-IR soma. Thus, the bulk of the inhibition provided by this class of cell is presumed to be primarily axo-dendritic (Gavrilovici *et al.*, 2010). Interestingly we also noted that these interneurons also make synaptic connections with each other and so the patterning of their inhibition may also be spatially controlled by lateral inhibition between adjacent CR-IR cells. However, we should also note that this mode of inhibition seems to play only small role in the total inhibition of the aPC, compared to the density and innervation provided from other layers and that this is fairly consistent across a number of species including opossum (Haberly *et al.*, 1987), mouse (Suzuki & Bekkers, 2010b) and rat (Loscher *et al.*,

1998; Gavrilovici *et al.*, 2010). Interestingly, the firing patterns in rat aPC only partially overlapped the firing found in mouse pPC (Young & Sun, 2009), namely the adapting tonic type (described as RSNP) and NAvHF (similar to fast spiking type: FS). We did not find late spiking or irregular spiking in our recordings in L1 or in the other layers of rat aPC.

In L2 and L3, all types of firing patterns were present, however with a slightly different distribution. In each of these layers more than 72% of all firing behaviour was represented by ALF interneurons, mostly grouped in wALF and ALF clusters. In L3 the next most frequent group was represented by AHF interneurons (~23% of all L3 recordings) followed by sALF and NAvHF with similar distributions (4.6%). However in L2, AHF, sALF and NAvHF clusters had similar distributions (12.5%, 11.1% and 7% respectively).

In L3, adapting firing mode (both low and high frequency) represents more than 87% of total firing types. This correlates with other findings in PC (Protopapas & Bower, 2000) where the interneurons of L3 showed a repetitive firing pattern, i.e. continuously throughout the depolarization steps, that increases in adaptation from the threshold to higher levels of depolarization. This variability of interneuronal firing types might be correlated with involvement of these cells in both feedback and feed-forward inhibition. Such firing variability might suggest different ways the interneurons of both layers could modulate the activity of pyramidal cells through feedback inhibitory loops in L2-L3 and feed-forward inhibition provided by L2 interneurons with long dendrites that cross L1-L2 border.

Indeed it has been established that certain types of interneurons targeting specific pyramidal cell compartments (perisomatic or dendritic) participate in differing network oscillations in hippocampal area (Maccaferri & McBain, 1996; Chapman & Lacaille, 1999; Pike *et al.*, 2000) and in entorhinal cortex (Middleton *et al.*, 2008). The firing patterns of the various interneurons are often well matched to the oscillations in which they participate. For example, Lacunosum-moleculare interneurons that would be classified as ALF cells have been shown to be important

in generating theta rhythms in the hippocampus (Chapman & Lacaille, 1999; Maccaferri *et al.*, 2000). Similarly, fast spiking basket cells are important for the generation of gamma rhythms (Pike *et al.*, 2000) while bistratified interneurons are involved in theta rhythms (Klausberger *et al.*, 2004). A third type of interneuron innervation, the oriens-lacunosum moleculare (O-LM), participates in theta rhythm but is silent during ripple episodes (Klausberger *et al.*, 2003). In PC, although oscillatory activities are considered part of olfactory processing and memory coding (Neville & Haberly, 2004), less is known about the identity of different classes of interneurons that might participate in PC oscillatory behaviour. Based on our recent findings that multipolar cells provide the bulk of pyramidal cell (somatic) inhibition (Gavrilovici *et al.*, 2010), it seems that they would be obvious candidates for being involved in gamma rhythms. The activation of the interneurons in L2 and L3 are however activated in two very different ways. As L2 cells have dendrites that extend into L1, they are activated by olfactory axons, while those in L3 rely on activation by the pyramidal cells output (Neville & Haberly, 2004; Gavrilovici *et al.*, 2010). Thus the participation of these neurons in ongoing oscillatory activity is fundamentally different; one relies on feed-forward activation while the other is within a feedback loop. Finally, we should note that the PC is a highly interconnected structure and the activation of L2 and L3 interneurons will also occur from excitation arising from numerous other brain regions including, but not limited to, amygdala, endopiriform nucleus and hippocampus (Loscher & Ebert, 1996).

3.4.3 Morphological and functional correlations.

Our morphological reconstructions were classified in three main groups previously shown to exist in rat aPC, and was based on the tendency of interneurons to have a particular dendritic arborization pattern (Gavrilovici *et al.*, 2010). Although the biocytin morphological reconstructions might not reconstitute the entire CBP arborization a number of interneuronal types: multipolar, vertical and horizontal cells were identified (Gavrilovici *et al.*, 2010). However, none of our five interneuronal

clusters were limited to one morphological type. With the exception of NAvHF cluster where most of the interneurons had multipolar morphology (previously described as PV-like and PV/CB-like types), the other clusters contained all three morphological types in similar distributions. This is not surprising, as a reduced correspondence between morphological and electrophysiological characteristics of interneurons was previously described in neocortex (see review, Markram *et al.*, 2004) and in hippocampus, where cells with the same morphological type had different membrane properties and firing patterns (Mott *et al.*, 1997; Parra *et al.*, 1998). This increased firing heterogeneity is thought to result from different distribution/expression of various ionic channels on a cell's membrane, and/or morphological features (Llinas, 1988; Mainen & Sejnowski, 1996). In spite of this diversity, we were able to find that some firing patterns tend to be more often represented in specific neuronal morphologies than others.

In previous studies it was found that L1 contains interneurons that co-express CR- IR (Young & Sun, 2009; Gavrilovici *et al.*, 2010; Suzuki & Bekkers, 2010b). Accordingly, in the present study, all our morphological reconstructions in L1 matched the previously described CR-IR type cells as having bipolar/bitufted dendritic morphologies that cross the border between L1-L2 (Gavrilovici *et al.*, 2010). These cells, located in L1, had either an adapting or a FS firing (non-adapting very high frequency) and most likely participate in feed-forward inhibition loops.

The aPC NAvHF firing patterns matched with the multipolar morphology (75%) which correlates with previous observations that multipolar cells co-express PV (Freund & Buzsaki, 1996; Gavrilovici *et al.*, 2010) and with their tendency towards non-adapting, fast spiking firing mode (Kawaguchi, 1993; Kawaguchi & Kubota, 1997). L2 multipolar PV-IR cells, with dendrites that cross L1-L2 border, are a very interesting cell group as they are in a position to play an effective role in the feed-forward inhibition of main excitatory pathways. This is due to several reasons: 1) the extrinsic excitatory afferent fibers (LOT) terminate both on dendrites of pyramidal cells and of GABAergic interneurons (Haberly, 1983); 2) the ability of

PV containing neurons to fire repetitively at a high frequency (Kawaguchi, 1993; Kawaguchi & Kubota, 1997); and 3) the tendency of PV-IR interneurons to synapse along perisomatic regions (Nitsch *et al.*, 1990; Freund & Buzsaki, 1996; Gavrilovici *et al.*, 2010). These morpho-physiological characteristics that confer PV cells a strong inhibitory effect are also thought to confer them the ability to modulate the synchrony of pyramidal cells (Cobb *et al.*, 1995; Miles *et al.*, 1996).

As previously described, vertical cells (CR-like phenotype) in L1 or in L2 with dendrites that cross the L1-L2 border, could also be involved in feed-forward inhibition (Haberly & Bower, 1984; Kapur *et al.*, 1997; Ekstrand *et al.*, 2001; Gavrilovici *et al.*, 2010). However their specific postsynaptic targeting (CR-NTs were found only on the dendrites of pyramidal cells (Kawaguchi, 1993; Gavrilovici *et al.*, 2010) coupled with the lack of NA_vHF firing pattern in L2, where most of the CBP-IR cells (~42%) are CR-IR (Gavrilovici *et al.*, 2010), suggest the existence of different types of control of pyramidal cells through feed-forward inhibition loops.

Interneurons in L3, receiving synaptic input from L2 pyramidal cell axon collaterals, are thought to be involved in feedback inhibitory loops (Neville & Haberly, 2004; Ekstrand *et al.*, 2001). It has also been shown that L2 bipolar/bitufted cells could also mediate feedback inhibition in PC (Neville & Haberly, 2004). In our previous work (Gavrilovici *et al.*, 2010), it was shown that multipolar and horizontal cells in L2, or bipolar/bitufted interneurons located in L2, could be involved in this inhibitory loop. Again, differences in postsynaptic targeting: PV cells- perisomatic, CR – dendritic and CB- dendritic and perisomatic (Gavrilovici *et al.*, 2010), and their firing pattern bias might serve to differently modulate the activity of pyramidal cells.

Overall, these findings may help elucidate the functional role of different groups of interneurons of the PC. Understanding the electrophysiological properties of interneurons provides the foundation for further explorations of how the timing of neural patterns in the PC is controlled, and perhaps why this region is particularly seizurogenic.

3.5 References

Ascoli GA, Alonso-Nanclares L, Anderson SA, Barrionuevo G, Benavides-Piccione R, Burkhalter A, Buzsaki G, Cauli B, DeFelipe J, Fairen A, Feldmeyer D, Fishell G, Fregnac Y, Freund TF, Gardner D, Gardner EP, Goldberg JH, Helmstaedter M, Hestrin S, Karube F, Kisvarday ZF, Lambolez B, Lewis DA, Marin O, Markram H, Munoz A, Packer A, Petersen CC, Rockland KS, Rossier J, Rudy B, Somogyi P, Staiger JF, Tamas G, Thomson AM, Toledo-Rodriguez M, Wang Y, West DC, & Yuste R (2008). Petilla terminology: nomenclature of features of GABAergic interneurons of the cerebral cortex. *Nat Rev Neurosci* **9**, 557-568.

Cauli B, Porter JT, Tsuzuki K, Lambolez B, Rossier J, Quenet B, & Audinat E (2000). Classification of fusiform neocortical interneurons based on unsupervised clustering. *Proc Natl Acad Sci U S A* **97**, 6144-6149.

Chapman CA & Lacaille JC (1999). Intrinsic theta-frequency membrane potential oscillations in hippocampal CA1 interneurons of stratum lacunosum-moleculare. *J Neurophysiol* **81**, 1296-1307.

Cobb SR, Buhl EH, Halasy K, Paulsen O, & Somogyi P (1995). Synchronization of neuronal activity in hippocampus by individual GABAergic interneurons. *Nature* **378**, 75-78.

Connors BW & Gutnick MJ (1990). Intrinsic firing patterns of diverse neocortical neurons. *Trends Neurosci* **13**, 99-104.

Dietrich D, Podlogar M, Ortmanns G, Clusmann H, & Kral T (2005). Calbindin-D28k content and firing pattern of hippocampal granule cells in amygdala-kindled rats: a perforated patch-clamp study. *Brain Res* **1032**, 123-130.

Dougherty KJ, Sawchuk MA, & Hochman S (2005). Properties of mouse spinal lamina I GABAergic interneurons. *J Neurophysiol* **94**, 3221-3227.

Ekstrand JJ, Domroese ME, Feig SL, Illig KR, & Haberly LB (2001). Immunocytochemical analysis of basket cells in rat piriform cortex. *J Comp Neurol* **434**, 308-328.

Freund T & Buzsaki G (1996). Interneurons of the hippocampus. *Hippocampus* **6**, 345-371.

Gavrilovici C, D'Alfonso S, Dann M, & Poulter MO (2006). Kindling-induced alterations in GABA_A receptor mediated inhibition and neurosteroid activity in the piriform cortex of rat. *Eur J Neurosci* **24**, 1373-1384.

- Gavrilovici C, D'Alfonso S, & Poulter MO (2010). Diverse interneuron populations have highly specific interconnectivity in the rat piriform cortex. *J Comp Neurol* **518**, 1570-1588.
- Gellman RL & Aghajanian GK (1994). Serotonin₂ receptor-mediated excitation of interneurons in piriform cortex: antagonism by atypical antipsychotic drugs. *Neuroscience* **58**, 515-525.
- Haberly LB (1983). Structure of the piriform cortex of the opossum. I. Description of neuron types with Golgi methods. *J Comp Neurol* **213**, 163-187.
- Haberly LB (2001). Parallel-distributed processing in olfactory cortex: new insights from morphological and physiological analysis of neuronal circuitry. *Chem Senses* **26**, 551-576.
- Haberly LB & Bower JM (1984). Analysis of association fiber system in piriform cortex with intracellular recording and staining techniques. *J Neurophysiol* **51**, 90-112.
- Haberly LB, Hansen DJ, Feig SL, & Presto S (1987). Distribution and ultrastructure of neurons in opossum piriform cortex displaying immunoreactivity to GABA and GAD and high-affinity tritiated GABA uptake. *J Comp Neurol* **266**, 269-290.
- Haberly LB & Price JL (1978). Association and commissural fiber systems of the olfactory cortex of the rat. *J Comp Neurol* **178**, 711-740.
- Kanter ED & Haberly LB (1993). Associative long-term potentiation in piriform cortex slices requires GABA_A blockade. *J Neurosci* **13**, 2477-2482.
- Kapur A, Pearce RA, Lytton WW, & Haberly LB (1997). GABA_A-mediated IPSCs in piriform cortex have fast and slow components with different properties and locations on pyramidal cells. *J Neurophysiol* **78**, 2531-2545.
- Kawaguchi Y (1993). Groupings of nonpyramidal and pyramidal cells with specific physiological and morphological characteristics in rat frontal cortex. *J Neurophysiol* **69**, 416-431.
- Kawaguchi Y & Kubota Y (1997). GABAergic cell subtypes and their synaptic connections in rat frontal cortex. *Cereb Cortex* **7**, 476-486.
- Kelly ME, Staines WA, & McIntyre DC (2002). Secondary generalization of hippocampal kindled seizures in rats: examining the role of the piriform cortex. *Brain Res* **957**, 152-161.

- Klausberger T, Magill PJ, Marton LF, Roberts JD, Cobden PM, Buzsaki G, & Somogyi P (2003). Brain-state- and cell-type-specific firing of hippocampal interneurons in vivo. *Nature* **421**, 844-848.
- Klausberger T, Marton LF, Baude A, Roberts JD, Magill PJ, & Somogyi P (2004). Spike timing of dendrite-targeting bistratified cells during hippocampal network oscillations in vivo. *Nat Neurosci* **7**, 41-47.
- Klausberger T & Somogyi P (2008). Neuronal diversity and temporal dynamics: the unity of hippocampal circuit operations. *Science* **321**, 53-57.
- Kroner S, Krimer LS, Lewis DA, & Barrionuevo G (2007). Dopamine increases inhibition in the monkey dorsolateral prefrontal cortex through cell type-specific modulation of interneurons. *Cereb Cortex* **17**, 1020-1032.
- Llinas RR (1988). The intrinsic electrophysiological properties of mammalian neurons: insights into central nervous system function. *Science* **242**, 1654-1664.
- Loscher W & Ebert U (1996). The role of the piriform cortex in kindling. *Prog Neurobiol* **50**, 427-481.
- Loscher W, Lehmann H, & Ebert U (1998a). Differences in the distribution of GABA- and GAD-immunoreactive neurons in the anterior and posterior piriform cortex of rats. *Brain Res* **800**, 21-31.
- Luskin MB & Price JL (1983). The topographic organization of associational fibers of the olfactory system in the rat, including centrifugal fibers to the olfactory bulb. *J Comp Neurol* **216**, 264-291.
- Maccaferri G & McBain CJ (1996). The hyperpolarization-activated current (I_h) and its contribution to pacemaker activity in rat CA1 hippocampal stratum oriens-alveus interneurons. *J Physiol* **497**, 119-130.
- Maccaferri G, Roberts JD, Szucs P, Cottingham CA, & Somogyi P (2000). Cell surface domain specific postsynaptic currents evoked by identified GABAergic neurones in rat hippocampus in vitro. *J Physiol* **524 Pt 1**, 91-116.
- Mainen ZF & Sejnowski TJ (1996). Influence of dendritic structure on firing pattern in model neocortical neurons. *Nature* **382**, 363-366.
- Markram H, Toledo-Rodriguez M, Wang Y, Gupta A, Silberberg G, & Wu C (2004). Interneurons of the neocortical inhibitory system. *Nat Rev Neurosci* **5**, 793-807.

McIntyre DC, Hutcheon B, Schwabe K, & Poulter MO (2002). Divergent GABA(A) receptor-mediated synaptic transmission in genetically seizure-prone and seizure-resistant rats. *J Neurosci* **22**, 9922-9931.

Middleton S, Jalics J, Kispersky T, LeBeau FE, Roopun AK, Kopell NJ, Whittington MA, & Cunningham MO (2008). NMDA receptor-dependent switching between different gamma rhythm-generating microcircuits in entorhinal cortex. *Proc Natl Acad Sci U S A* **105**, 18572-18577.

Miles R, Toth K, Gulyas AI, Hajos N, & Freund TF (1996). Differences between somatic and dendritic inhibition in the hippocampus. *Neuron* **16**, 815-823.

Mott DD, Turner DA, Okazaki MM, & Lewis DV (1997). Interneurons of the dentate-hilus border of the rat dentate gyrus: morphological and electrophysiological heterogeneity. *J Neurosci* **17**, 3990-4005.

Neville KR & Haberly LB (2004). Olfactory cortex. In *The Synaptic Organization of the Brain*, ed. Shepherd GM, pp. 415-454. Oxford University Press, New York.

Neville KR & Haberly LB (2003). Beta and gamma oscillations in the olfactory system of the urethane-anesthetized rat. *J Neurophysiol* **90**, 3921-3930.

Parra P, Gulyas AI, & Miles R (1998). How many subtypes of inhibitory cells in the hippocampus? *Neuron* **20**, 983-993.

Pike FG, Goddard RS, Suckling JM, Ganter P, Kasthuri N, & Paulsen O (2000). Distinct frequency preferences of different types of rat hippocampal neurons in response to oscillatory input currents. *J Physiol* **529**, 205-213.

Prescott SA & De Koninck Y (2002). Four cell types with distinctive membrane properties and morphologies in lamina I of the spinal dorsal horn of the adult rat. *J Physiol* **539**, 817-836.

Protopapas AD & Bower JM (2000). Physiological characterization of layer III non-pyramidal neurons in piriform (olfactory) cortex of rat. *Brain Res* **865**, 1-11.

Racine RJ, Mosher M, & Kairiss EW (1988). The role of the pyriform cortex in the generation of interictal spikes in the kindled preparation. *Brain Res* **454**, 251-263.

Satou M, Mori K, Tazawa Y, & Takagi SF (1983a). Interneurons mediating fast postsynaptic inhibition in pyriform cortex of the rabbit. *J Neurophysiol* **50**, 89-101.
Satou M, Mori K, Tazawa Y, & Takagi SF (1983b). Neuronal pathways for activation of inhibitory interneurons in pyriform cortex of the rabbit. *J Neurophysiol* **50**, 74-88.

Sheldon PW & Aghajanian GK (1991). Excitatory responses to serotonin (5-HT) in neurons of the rat piriform cortex: evidence for mediation by 5-HT_{1C} receptors in pyramidal cells and 5-HT₂ receptors in interneurons. *Synapse* **9**, 208-218.

Storm JF (1990). Potassium currents in hippocampal pyramidal cells. *Prog Brain Res* **83**, 161-187.

Suzuki N & Bekkers JM (2010a). Distinctive classes of GABAergic interneurons provide layer-specific phasic inhibition in the anterior piriform cortex. *Cereb Cortex* **20**, 2971-2984.

Suzuki N & Bekkers JM (2010b). Inhibitory neurons in the anterior piriform cortex of the mouse: classification using molecular markers. *J Comp Neurol* **518**, 1670-1687.

Tseng GF & Haberly LB (1989). Deep neurons in piriform cortex. II. Membrane properties that underlie unusual synaptic responses. *J Neurophysiol* **62**, 386-400.

Whittington MA & Traub RD (2003). Interneuron diversity series: inhibitory interneurons and network oscillations in vitro. *Trends Neurosci* **26**, 676-682.

Young A & Sun QQ (2009). GABAergic inhibitory interneurons in the posterior piriform cortex of the GAD67-GFP mouse. *Cereb Cortex* **19**, 3011-3029.

Zhang L, Weiner JL, Valiante TA, Velumian AA, Watson PL, Jahromi SS, Schertzer S, Pennefather P, & Carlen PL (1994). Whole-cell recording of the Ca²⁺-dependent slow afterhyperpolarization in hippocampal neurones: effects of internally applied anions. *Pflugers Arch* **426**, 247-253.

Chapter 4. Kindling-induced alterations of interneuronal firing pattern in the piriform cortex

4.1 Introduction

The piriform cortex, also known as the paleocortex, is three-layered structure specialized in olfactory processing. Besides its involvement in olfactory coding and olfactory memory, this area has a great epileptogenic potential. The role of PC in generation, facilitation and/or spreading the epileptic seizures was observed in several clinical and experimental studies. In kindled animals, the amygdala and PC showed the earliest onset of interictal discharges regardless of the site of stimulation (Loscher & Ebert, 1996). It has also been shown that amygdala stimulation in amygdala – PC slices from kindled animals increased the duration of evoked burst events in PC as compared to non-kindled animals (McIntyre & Wong, 1986). Generalized seizures were elicited by administration (microinjections) of low doses of bicuculline in anterior, central and posterior PC (Ebert *et al.*, 2000); in contrast, these same drugs were relatively ineffective when injected into the amygdala. Other lines of evidence linking the PC to seizure genesis mechanisms were provided by autoradiographic studies measuring the cerebral metabolic activity during the progression of seizures. In early stages elicited by amygdala kindling, increased ^{14}C -2-deoxyglucose (2-DG) uptake was observed in ipsilateral PC, entorhinal cortex, frontal limbic field (sulcal area) and medial septal area, suggesting the early contribution of these structures in the spreading and amplification of the excitatory waves (Engel *et al.*, 1978; Ackermann *et al.*, 1986). Thus, with a great epileptogenic potential, strong interconnection with other limbic structures (amygdala, entorhinal cortex, hippocampus) and a relative simple three-layered structure, PC qualifies as an important candidate for studying and understanding the epileptic mechanisms in the temporal lobe epilepsy (TLE).

Kindling, the model used in our study, is a widely accepted animal model of epilepsy that produces complex partial seizures that secondarily generalize, as in TLE (Morimoto *et al.*, 2004). In our previous work (Gavrilovici *et al.*, 2006), it was

hypothesized that the high excitability of pyramidal neurons of the PC, and their increased susceptibility for epileptogenic activity after amygdala kindling is produced by an increased inhibition of the interneuronal population of PC by an increase in the number of GABA_A receptors of PC interneurons. Although this study shed some light on the mechanisms that can increase the activity of the excitatory cells in kindled PC, the epileptic phenomena are associated not only with an increased excitatory output, but more importantly with a synchronous, pathological activity of these cells that can thus lead to epileptic waves. As the GABAergic network was found to be involved in timing of pyramidal cells firing (Cobb *et al.*, 1995; Freund & Buzsaki, 1996; Whittington & Traub, 2003), a closer analysis of the interneuronal network is relevant to epilepsy research as a change of interneuronal firing patterns might lead to alteration of normal processing activity in PC and it could account for increased epileptogenic potential of this area. However, up to date, it is not known whether the interneuronal excitability and their firing patterns are altered in PC after kindling. Thus, the goal of this study is to investigate the electrophysiological properties of rat interneurons in all layers of aPC using whole-cell patch clamp recordings and immunohistochemistry techniques for morphological reconstitution of patched interneurons. Intracellular, whole-cell patch clamp recordings of aPC neurons were made in brain slices of amygdala-kindled rats (2 weeks after their last stage 5 seizure), or non-kindled (control) rats of the same age. Our study showed, for the first time, kindling-induced alterations in firing patterns of aPC interneurons. These alterations were represented by a lack of non-adapting and weakly adapting firing patterns after kindling. Further experiments indicated that these changes were linked to an up-regulation of Kv 1.6 channels in the aPC. Indeed, an increased K⁺ current can effectively reduce the neuronal excitability/firing (see review, Misonou, 2010) and thus it could account for the shift of non-adapting and weakly adapting behaviours towards firing patterns with increased adaptation ratios. These kindling-induced alterations of interneuronal firing properties, especially the lack of non-adapting very high frequency (fast spiking)

firing behaviour, could change the intrinsic oscillatory properties of PC network, thus leading to pathological synchronous events like those generated during epileptic seizures.

Overall, the present study is important for better understanding of kindling-induced alterations in PC network, providing a foundation for further explorations of how the timing of neural patterns in the PC is controlled and perhaps why this region is particularly seizurogenic.

4.2 Methods

4.2.1 Animals and surgery

Male Sprague Dawley rats weighing 200 g at the time of the initial surgery were used. They were housed individually with free access to food and water under a continuous 12-h/12-h light/dark cycle.

4.2.1.1 Electrode implantation

Animals were anaesthetized with Ketamine - Dormitor mixture (0.1 ml/100g; i.p.) and implanted with two bipolar stimulating/recording electrodes bilaterally in the basolateral amygdala with the following coordinates: 2.6 mm posterior to Bregma, 4.5 mm lateral to midline and 8.0 mm ventral (Paxinos & Watson, 1986). The electrodes were constructed of two twisted strands of 0.127-mm diameter Diamel-insulated Nichrome wire and were attached to male Amphenol pins. The electrodes were implanted and secured to the skull with jeweller's screws. The electrode assembly was fixed to the skull by dental acrylic cement (McIntyre & Molino, 1972).

4.2.1.2 Kindling and slice preparation

The experimental group began kindling protocol 1 week after the surgery. The afterdischarge threshold (ADT) was determined in each amygdala by delivering a 2-s 60-Hz sine wave stimulus of progressively increasing intensity (15, 25, 35, 50,

75, 100, 150, 200, 250, 300 and 350 μ A) until an ADT was triggered (McIntyre & Plant, 1993; Gavrilovici *et al.*, 2006). The rats were stimulated daily until six generalized stage 5 convulsions on the Racine's scale were elicited. Seizure severity and duration were recorded daily during the kindling acquisition. Fully kindled rats were allowed to recover for 2 weeks after the last seizure. To obtain brain slices, rats were deeply anaesthetized with Ketamine - Dormitor mixture (0.1 ml/100 g; i.p.) and then perfused through the heart with an ice-cold Ringer's solution in which sodium was replaced by choline [containing (in mM): choline Cl, 110; KCl, 2.5; NaH₂PO₄, 1.2; NaHCO₃, 25; CaCl₂, 0.5; MgCl₂, 7; Na pyruvate, 2.4; ascorbate, 1.3; dextrose, 20] (as described in McIntyre *et al.*, 2002b). After perfusion, the brain was rapidly removed and the temporal lobe area was excised as a block. The block was sliced coronally with a Vibratome (350- μ m-thick sections). The slices were obtained from 1.5 to -0.3 mm relative to bregma. The slices were then incubated at 37°C for 30 min and subsequently moved to a room-temperature (22° C) bath for at least 45 min. Slicing, incubation and storage were all performed in the choline solution. The ACSF solution used during electrical recordings was similar to the choline solution except that pyruvate and ascorbate were removed, equimolar NaCl replaced the choline Cl, MgCl₂ was used at a concentration of 2 mM while CaCl₂ was present at 1 mM (Gavrilovici *et al.*, 2006). All solutions were maintained at pH 7.4 and bubbled with 5%CO₂/ 95%O₂ (carbogen).

4.2.2 Electrophysiology

Patch electrodes were pulled from borosilicate glass capillaries and filled with K⁺-gluconate solution having a composition (in mM) of: K⁺ gluconate 147, KCl 1, CaCl₂ 2, HEPES 10, EGTA 1, Glucose 10, MgATP 2, GTP 0.3 (300 mOsm, pH 7.3-7.4). Whole-cell patch clamp recordings from neurons in layers 1-3 of anterior PC were made with an EPC 9/2 amplifier (HEKA, Lambrecht, Germany). Series resistance compensations were performed in all recordings. The initial access was < 20 M Ω and compensated by 50-70%. All experiments were performed at 32°C.

Voltage-gated currents and excitability of the cell were monitored by means of voltage-clamp and current-clamp protocols (PulseFit v 8.0; Heka, Germany). Cell responses were obtained by injecting hyperpolarizing and depolarizing current steps (500 ms pulse; 50 pA increments). Neuronal resting membrane potential was measured only after the patch clamp recording was stable. Input resistance (R_i) was calculated by linear regression of the current-voltage relationship in response to hyperpolarizing steps, as described in Dietrich *et al.* (2005), using Origin software (Microcal, Northampton, MA). Firing pattern analysis was performed at the current level that produced reliable repetitive firing (twice the firing threshold), in presence of NMDA, AMPA and kainate channel blockers (20 μ M 2-amino phosphonovaleric acid, APV & 10 μ M dinitroquinoxaline-2,3-dione, DNQX; Research Biochemicals, Natick, MA, USA). Interspike interval ratio (II_R) was obtained by dividing the last interspike interval (measured in milliseconds) by the duration of the first interval, as described in (Kroner *et al.*, 2007). In a small number of recordings ($n = 35$) blocking GABA_A receptors with gabazine (10 μ M; added to the perfusion bath) did not affect the firing pattern. The blocking effect of gabazine (10 μ M) on GABAergic currents recorded on interneurons ($n = 9$) was assessed using KCl electrode solution in presence of TTX, APV and DNQX, as described in Gavrilovici *et al.* (2006).

Also, in a number of recordings ($n = 72$) to evaluate the K⁺ current, before and after kindling, sodium and calcium channel blockers (250 nM TTX, and 1mM NiCl₂) were added into the bath perfusion (alongside with the above mentioned NMDA, AMPA, kainate and GABA_A blockers). Potassium outward currents were evoked by depolarizing steps between -50 and +10 mV and were measured at the end of each pulse.

Finally, a small number of current clamp recordings ($n = 15$) were performed on sham rats (electrode implanted, but never kindled) of the same age as kindled and control group rats, using identical protocols. The five firing patterns observed (NAvHF, AHF, ALF, sALF and wALF), corresponded to the firing patterns seen in control rats.

4.2.3 Cluster analysis & statistics

Unsupervised cluster analysis was performed on interneuronal populations of PC using Ward's method with z -score normalization and intervals calculated by Euclidian squared distances (SPSS 13, Chicago, Illinois, USA), according to described methodology (Cauli *et al.*, 2000). The analysis was based on their main electrophysiological parameters: input resistance; firing frequency; and interspike interval ratio; providing three distinct firing groups.

Terminology for the five clusters was chosen according to their Π_R (neurons with $\Pi_R < 1.25$ were grouped as non-adapting cells while neurons with $\Pi_R > 1.25$ were classified as adapting cells) and firing frequencies (FF > 50Hz – high frequency and FF < 50Hz as low frequency) as described in Kroner *et al.* (2007) and Ascoli *et al.* (2008).

Comparisons among different firing pattern groups in were made by using ANOVA and a Tukey multiple comparison post-hoc test as appropriate (SPSS 13, Chicago, Illinois, USA). All data are presented as means \pm standard error of the mean.

4.2.4 Histochemistry

4.2.4.1 Image acquisition and morphological reconstruction of patched neurons

In order to reconstruct the morphology and understand where the recordings were made, patch electrodes included 0.2% Biocytin. After the completion of a recording, the slice was removed from the microscope chamber and fixed in paraformaldehyde solution (4% paraformaldehyde in 0.1 phosphate buffer) for 5-7 days. The sections were washed for 15 min in PBS followed by a 30 min rinse in PBS-TX and 90 min incubation in streptavidin-conjugated Alexa Fluor-594 (5 μ g/ml; Molecular Probes) at room temperature. After rinsing in PB-TX for 30 min, the slices were mounted on slides for viewing on a confocal microscope.

Confocal images were taken on an Olympus IX 60 inverted microscope outfitted with a Perkin Elmer Spinning Disk Confocal attachment with a 20X (N.A. = 0.50) objective. The microscope was equipped with a Hamamatsu Orca ER CCD camera (1,300 X 1,030 pixels), and images were acquired in Volocity software (Improvision, Lexington, MA). Each image represents a stack of 40–50 images 0.2 μm apart in the z-plane. For morphological reconstruction of the dendritic arborization of patched neurons, the stacks of confocal images were deconvolved with Auto-Quant software (Auto quant X2, MediaCybernetics, Bethesda, MD) and then processed with Imaris Filament Tracer module in “Surpass mode” (Bitplane, Zurich, Switzerland). Filament tracer creates dendritic arborization patterns based on an algorithm that predicts arborization pathways. These pathways are set up by the user-set criteria of a start point, namely, the size of cell somata, and an end point representing minimum thickness of processes. Start points were set to 10 μm , and endpoints were set to 1 μm . The resultant filament lines were converted from lines to two-pixel-thick cones. To mark the cell bodies, an “Isosurface” was then created. This process creates a cell body from the stack of images that is then merged with the dendritic morphology (see also Gavrilovici *et al.*, 2010).

We used criteria for classification of pyramidal versus non-pyramidal cells as previously described (McIntyre *et al.*, 2002; Gavrilovici *et al.*, 2006) and were based on: 1) soma morphology; 2) axonal projection to deeper layers for pyramidal cells; 3) presence of dendritic spines for pyramidal cells; and 4) spiking properties. A few cells that were spiny non-pyramidal were also found but not included in the analysis. Based on the morphologies that we have previously described (Gavrilovici *et al.*, 2010), interneurons were further grouped into three categories: 1) horizontal cells, usually CB-IR, having extended dendrites in the horizontal plane – parallel to the PC layers; 2) multipolar cells, usually PV-IR and PV-IR/CB-IR, having a round dendritic tree crossing into adjacent layers and 3) vertical/bipolar-bitufted cells, usually CR-IR, having extended dendrites in the vertical plane, perpendicular to PC

layers. PC layer depth and demarcation between adjacent layers were set according to Neville & Haberly (2004) and Ekstrand *et al.* (2001).

4.2.4.2 Parvalbumin/Kv1.6 colocalization

Tissue preparation and fixation

Rats were deeply anesthetized with Ketamine - Dormitor mixture (0.1 ml/100 g; i.p.) and perfused intracardially with 0.1 M phosphate-buffered saline (PBS), pH 7.3, followed by Lana's solution (4% paraformaldehyde and 14% picric acid in phosphate-buffered saline). The brain was then removed from the skull and drop fixed in Lana's solution for 24 hours and then placed in a cryoprotectant solution of 20% glycerol and 2% DMSO dissolved in 0.1 M phosphate buffer (PB), pH 7.3, for 48 hours. The brains were then flash frozen in -80°C isopentane for 50 seconds and stored at -80°C until sectioning. The tissue was sectioned in a cryostat at -15°C in the coronal plane into 60- μm sections. The free-floating sections were placed in cryoprotectant-filled tissue culture dishes and were stored at -20°C in glycerol/PBS solution until they were ready to be processed.

Immunohistochemistry

The sections were washed with TBS plus 0.025% Triton-X two times for 5 minutes. The primary antibodies were diluted in TBS with 1% BSA and then pipetted into the tissue culture dish wells; the sections were incubated overnight at 4°C . Sections were then washed with PBS with 0.025% Triton-X two times for 10 minutes, followed by application of secondary antibody solution (secondary antibodies were diluted in TBS with 1% BSA) and incubated for 1 hour at room temperature under low-light conditions. Sections were then rinsed with TBS three times for 5 minutes. Sections were wet mounted onto Fisher SuperFrost slides and mounted with glass coverslips in Prolong Gold Antifade mounting medium (Molecular Probes, Eugene, OR), allowed to cure overnight at room temperature, and

sealed the next day with nail polish. Slides were stored at -20°C and protected from light until they were ready to be imaged.

Antibodies

The list of the primary and secondary antibodies used for PV/Kv1.6 colocalization experiment is provided below: Primary antibody monoclonal antiparvalbumin (mouse), 1:2,500, Swant, Switzerland, catalog code 235, lot 10-11(F); primary antibody polyclonal anti KV1.6 (rabbit), 1:10,000, Abcam, US, catalog code ab210089. Secondary antibodies: donkey anti mouse Alexa 488, (1:1,000), and goat anti rabbit Alexa 594 (1:1,000). The specificity of the secondary antibodies was verified in control sections in which the primary antibody was omitted. No staining was detected in omission control sections (data not shown).

Image acquisition and processing

Confocal images for Figure 4.11 were acquired on a Zwiss laser-scanning microscope (LSM 510) with a $40\times$ objective, using Zeiss LSM software. Each image represents a stack of 10-15 images $1\ \mu\text{m}$ apart in the z-plane. This was performed for each wavelength channel. The stacks of confocal images were processed in Imaris software (Bitplane, Zurich, Switzerland). The images were analyzed with the colocalization module, which allows the pixels in each channel to be windowed according to a set of criteria and include only these pixels in the colocalization analysis (see Gavrilovici *et al.*, 2010).

4.2.5 RT-QPCR

The same animals used in the electrophysiology experiments were used as a source of cellular RNA. Tissue not used for electrophysiology was immediately frozen at -80°C until further use. Frozen rat brain tissue was placed in Trizol (Invitrogen) and homogenized. RNA was extracted from the homogenate following the manufacturer's protocol. RNA purity and quantity was analyzed using a NanoDrop 1000 spectrometer. RNA (1-5 μg) with a 260/280 above 1.80 was reverse

transcribed using the Invitrogen Superscript II protocol with oligo(dT) primers. QPCR reactions were performed in duplicate for each sample using BioRad MyIQ single-color real-time PCR detection system. DNA abundance was detected using SYBR Green (Bio Rad iQ SYBR Green Supermix) following the manufacturer's protocol. An initial screen of more than 80 genes that code for ion channels in the rat nervous system was done using RT² ProfilerTM rat PCR array (PARN-036, Qiagen; see Appendix 1). This was done by pooling equal amounts of RNA from 5 control and 5 kindled rat brains. Genes shown to be up regulated were further analyzed to confirm the results. This was done by analyzing expression individually, using 11 control and 9 kindled rats. For these experiments primers were designed in house. QPCR primer efficiency was quantified using a five point 10x dilution series of rat brain cDNA at 55°C (100ng – 10pg). PCR primer sets with efficiency between 90-110% were used for subsequent experiments. Neuron specific enolase was chosen as a reference gene, which was used to normalize gene expression levels.

We used the following primer sequences:

Gene Kv 2.1- Forward: 5`-TGAGCTGCAGAGCCTAGACGAGT-3`,
Reverse: 5`- ACCTCAGCAAGTACTCCATGGTGA-3`;

Gene Kv 9.3-Forward: 5`-GTGGATCAGAGTACACTCCTGCGG-3`,
Reverse: 5`-AGAATGGCCTCCTCAGAGTGGCAG-3`;

Gene Kv 1.2- Forward: 5`-ATGACAGTGGCTACCGGAGACC-3`,
Reverse: 5`- TCGTGGTCTGCCTCTGGGTCATA-3`;

Gene Kv 1.6 -Forward: 5`- TGTGAGTGGTGGCAGTGGTCAGAA-3`,
Reverse: 5`- TGAAGATCCGAAACACCCGGACCA-3`.

The ΔC_t method was used to quantify the mRNA expression. Cycle threshold (C_t) values represent the cycle number at which fluorescence emission data exceeded a threshold limit (20X baseline). ΔC_t is expressed as (C_t (reference gene) – C_t (gene of interest)) and represents the difference in threshold cycles between reference gene and gene of interest. The data was statistically analyzed using ANOVA (SPSS 13, Chicago, Illinois, USA). Data is expressed as mean \pm standard error of the ΔC_t values.

4.3 Results

The purpose of this study was to investigate the electrophysiological properties of interneuronal populations across PC layers after kindling-induced epilepsy. A total of 108 recordings from aPC interneurons that were morphologically identified according to the criteria indicated in Methods are included in this study.

Similar to control rats (chapter 3), the resting membrane potential (RMP) of PC interneurons after kindling ranged from -61 mV to -86 mV and no group of interneurons, described in detail below, were different from another based on RMP. Several other electrophysiological parameters were unchanged after kindling: input resistance (R_I) was $189.8 \pm 10.2 \text{ M}\Omega$ (control $I_R = 174.1 \pm 6.2 \text{ M}\Omega$), threshold current $152.3 \pm 7.1 \text{ pA}$ (control threshold current = $148.3 \pm 4.9 \text{ pA}$) while the firing frequency (FF) was $41.4 \pm 2.1 \text{ Hz}$ (control FF = $44.6 \pm 1.9 \text{ Hz}$). However, after kindling, we found that firing adaptation was increased ($II_R = 2.1 \pm 0.08$ in kindled as compared to $II_R = 1.7 \pm 0.06$ in control group, $P < 0.001$) while the number of spikes was reduced to 15.9 ± 0.9 (control group: 20.0 ± 0.9 , $P < 0.001$).

Two broad classes of firings (tonic and phasic) were present after kindling. The distribution of these firing patterns was similar to that observed in control rats (81.5% tonic and 18.5% phasic). Most of the interneurons (75%) fired in a low frequency rate (FF < 50 Hz) virtually identical to the control group (~ 72% of interneurons had low frequency firing patterns). However we found that after kindling all interneurons adapted to the stimulus. Thus, all interneurons firing continuously throughout the depolarization pulse adapted to the stimulus having an $II_R > 1.25$ while in control rats tonically firing interneurons had both adapting ($II_R > 1.25$; ~68%) and non-adapting behaviours ($II_R < 1.25$; ~ 32%).

As shown in control group, interneurons of kindled rats were also classified based on their morphological arborization pattern: vertical, horizontal and vertical cells (Gavrilovici *et al.*, 2010). We found that their distribution was similar before and after kindling, suggesting absence of a specific morphological interneuron loss due to kindling (control rats contained 16% horizontal cells, 38% multipolar and

46% vertical cells while in kindled animals we found 11% horizontal, 35% multipolar and 54% vertical cells).

As we indicated in the previous chapter (chapter 3), we chose the cluster analysis as a classification system as it does not primarily depend on arbitrary cut-off points ($1.25 < I_{R} > 1.25$; $50 \text{ Hz} < FF > 50 \text{ Hz}$). Classification of interneurons, using cluster analysis, indicated that only three firing groups are present after kindling, namely: AHF, ALF and sALF (Fig. 4.1). Thus, after kindling two firing patterns are absent: wALF and NAvHF.

Adapting high frequency firing behaviour was recorded in ~25% of kindled interneurons (27 of 108 cells; Fig. 4.2), similar to control group distribution of AHF interneurons (~20.4%). These interneurons had the highest firing frequency ($FF = 70.5 \pm 3.9 \text{ Hz}$), largest input resistance ($R_{I} = 301.2 \pm 28.1 \text{ M}\Omega$) and highest number of spikes (22 ± 3) among all other kindled groups (see Table 4.1; Fig. 4.3). AHF interneurons in kindled rats differ from control AHF interneurons by having a greater firing frequency ($70.5 \pm 3.9 \text{ Hz}$ in kindled vs. $54.7 \pm 2.1 \text{ Hz}$ in control groups; $P < 0.001$).

Lower frequency firing interneurons were represented by two clusters: ALF and sALF. Similar to control rats, where ALF was one of the most representative firing patterns, in kindled rats ALF behaviour was observed in half of all interneuronal recordings (54 of 108 cells; Fig. 4.2). They had the smallest firing frequency ($FF = 29.1 \pm 1.3 \text{ Hz}$) and smallest number of spikes (13 ± 1) among all kindled interneuronal groups (see Table 4.1; Fig. 4.4). They also differ from AHF neurons by having a lower input resistance (152.1 ± 7.1 ; $P < 0.01$).

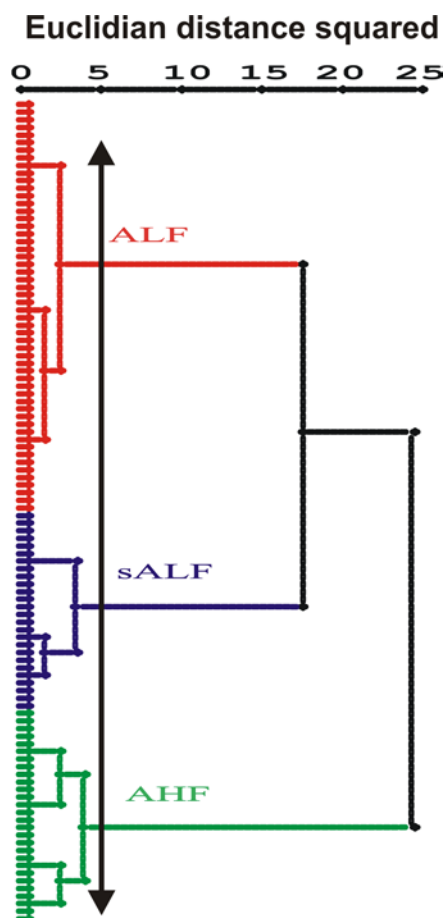


Figure 4.1 Cluster analysis of electrophysiological properties of rat aPC interneuronal populations after kindling-induced epilepsy. The y -axis of dendrogram shows individual cells ($n = 108$) and the x -axis represents the linkage distance measured by Euclidean distance squared. Double arrow solid line represents the cut off showing three distinct clusters: Adapting high frequency (AHF), adapting low frequency (ALF) and strongly adapting low frequency (sALF).

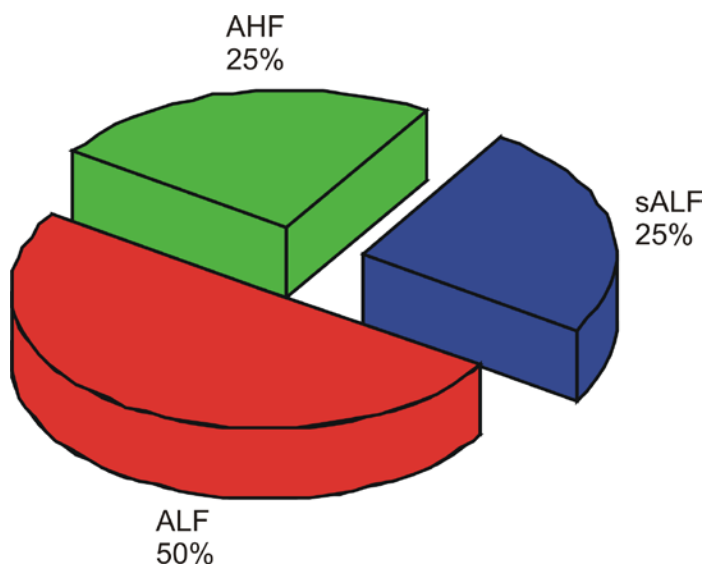


Figure 4.2 Distribution of the three types of firing patterns in the anterior piriform cortex of rat after kindling-induced epilepsy. AHF, adapting high frequency; ALF, adapting low frequency; sALF, strongly adapting low frequency.

Table 4.1 Electrophysiological properties of the five types of interneuronal firing groups in the anterior piriform cortex in amygdala kindled rats.

| | Cluster 1 AHF (n = 27) | Cluster 2 ALF (n = 54) | Cluster 3 sALF (n = 27) |
|---|------------------------------|------------------------------|-------------------------------|
| RMP (mV) | -76.7 ± 1.1 | -76.8 ± 0.7 | -76.8 ± 1.1 |
| R _I (MΩ) | 301.2 ± 28.1 | 152.1 ± 7.1 | 153.9 ± 9.3 |
| | 1 >> 2,3 | | |
| Threshold current (pA) | 131.4 ± 13.6 | 153.7 ± 10.4 | 170.3 ± 13.1 |
| Interspike interval ratio (I _R) | 1.86 ± 0.07 | 1.66 ± 0.05 | 3.47 ± 0.13 |
| | 1,2 << 3 | | |
| Frequency (Hz) | 70.5 ± 3.9 | 29.1 ± 1.3 | 37.0 ± 2.2 |
| | 1 >> 2,3; 2 < 3 | | |
| Number of spikes per pulse | 22 ± 3 | 13 ± 1 | 15 ± 1 |
| | 1 >> 2; 1 > 3 | | |

Values are means ± SE; n, number of cells; >, significantly greater with $P < 0.01$; >> significantly greater with $P < 0.001$. Statistically significant comparisons were determined using Tukey post hoc analysis after performing ANOVA.

RMP, resting membrane potential; R_I input resistance; AHF, adapting high frequency; ALF, adapting low frequency; sALF, strongly adapting low frequency.

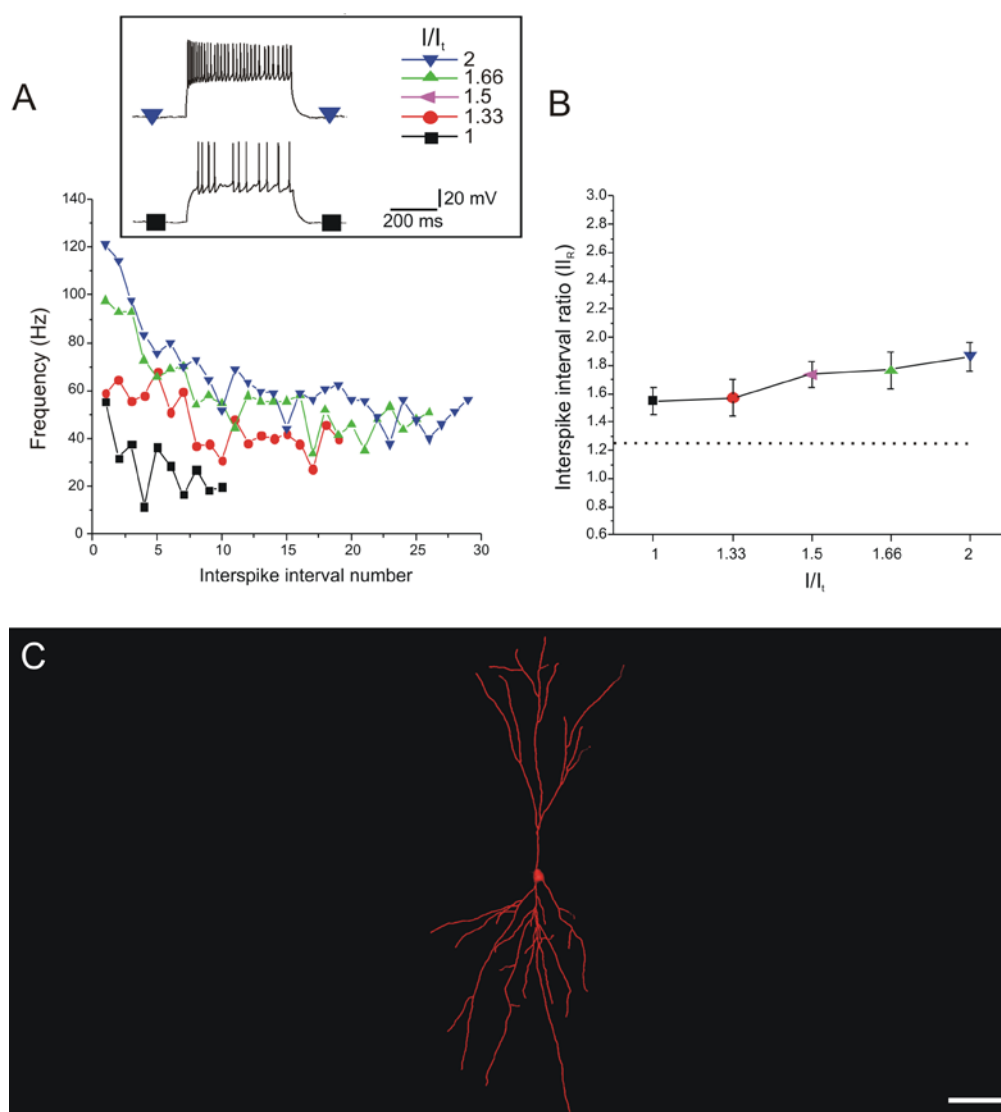


Figure 4.3 Electrophysiological properties of adapting high frequency (AHF) cell type.

A. Plot of firing frequency against interspike interval number in a typical AHF cell. Note the moderate spike frequency adaptation. B. The ratio between last and first interspike intervals (I_R) was plotted against level of injected current, showing moderate level of firing adaptation across AHF group ($I_R > 1.25$). C. Morphological reconstruction of AHF cell firing pattern shown in panel A. Traces in the inset show the response of AHF cell type to injection of depolarizing current steps at threshold ($I/I_t = 1$) and twice the firing threshold ($I/I_t = 2$) levels. Scale bar = 40 μm .

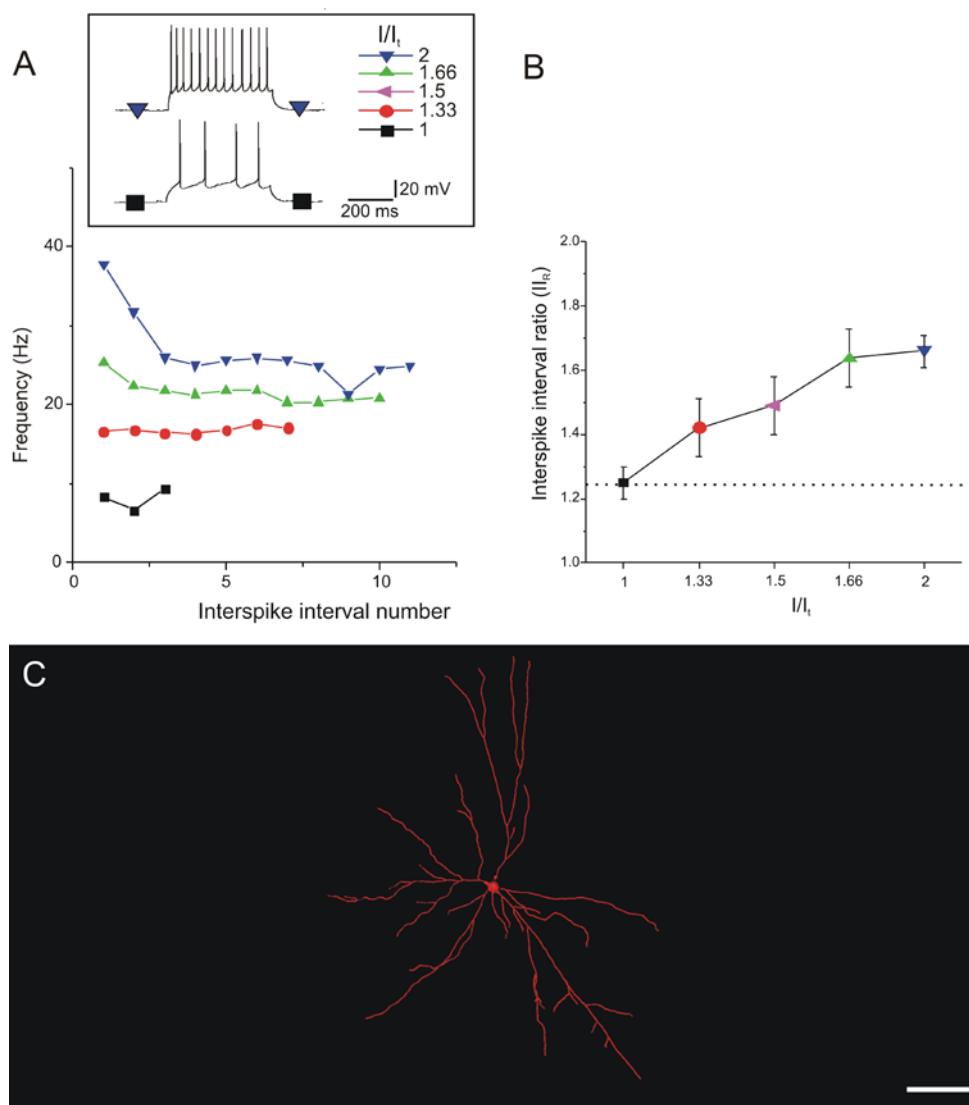


Figure 4.4 Firing properties of adapting low frequency (ALF) cell type.

A. Plot of firing frequency against interspike interval number in a typical ALF cell.

Note the moderate spike frequency adaptation at higher depolarizing steps. B. The ratio between last and first interspike intervals (I_{I_R}) was plotted against level of injected current, showing moderate firing adaptation at currents higher than the firing threshold across ALF group. C. Morphological reconstruction of ALF cell with firing pattern shown in panel A. Traces in the inset show the response of ALF cell type to injection of depolarizing current steps at threshold ($I/I_t = 1$) and twice the firing threshold ($I/I_t = 2$) levels. Scale bar = 40 μm .

Our data indicated that ALF interneurons in kindled rats have a lower firing frequency and number of spikes as compared to control ALF group (29.1 ± 1.3 Hz and 13 ± 0.7 spikes in kindled vs. 38.8 ± 1.7 Hz and 18 ± 0.8 spikes in control; $P < 0.001$).

Finally, sALF behaviour was recorded in 25% of kindled interneuronal population (27 of 108 cells; Fig. 4.2), similar to AHF distribution. This group had the highest adaptation ratio among all kindled interneurons (3.47 ± 0.14 ; $P < 0.001$; Table 4.1). They also differ from ALF group by firing at a higher frequency (37.0 ± 2.2 Hz; $P < 0.05$; Table 4.1; Fig. 4.5). When compared to sALF interneurons in control rats, it was found that after kindling, sALF interneurons have a lower interspike interval ratio ($\Pi_R = 3.4 \pm 0.1$ in kindled vs. $\Pi_R = 4.4 \pm 0.3$ in control group; $P < 0.01$).

4.3.1 Intra-layer localization analysis

We found all three firing patterns (AHF, ALF and sALF) in every layer of aPC but no firing type was dominant in any of PC layer (Fig. 4.6). However there was a layer preference for each of the firing clusters: AHF and sALF cells were mostly distributed in L2 (over 51%), while the rest were equally divided between L1 and L3 (Table 4.2). However ALF distribution on aPC was different: ~68% in L2 followed by ~22% in L3 and just 9% in L1 (see Table 4.2).

As seen in control group, none of the firing pattern was dominant over the other in any of aPC layers. After kindling AHF and ALF group kept their L1-L3 distribution, however a few sALF interneurons (~ 9%) are now present in L1.

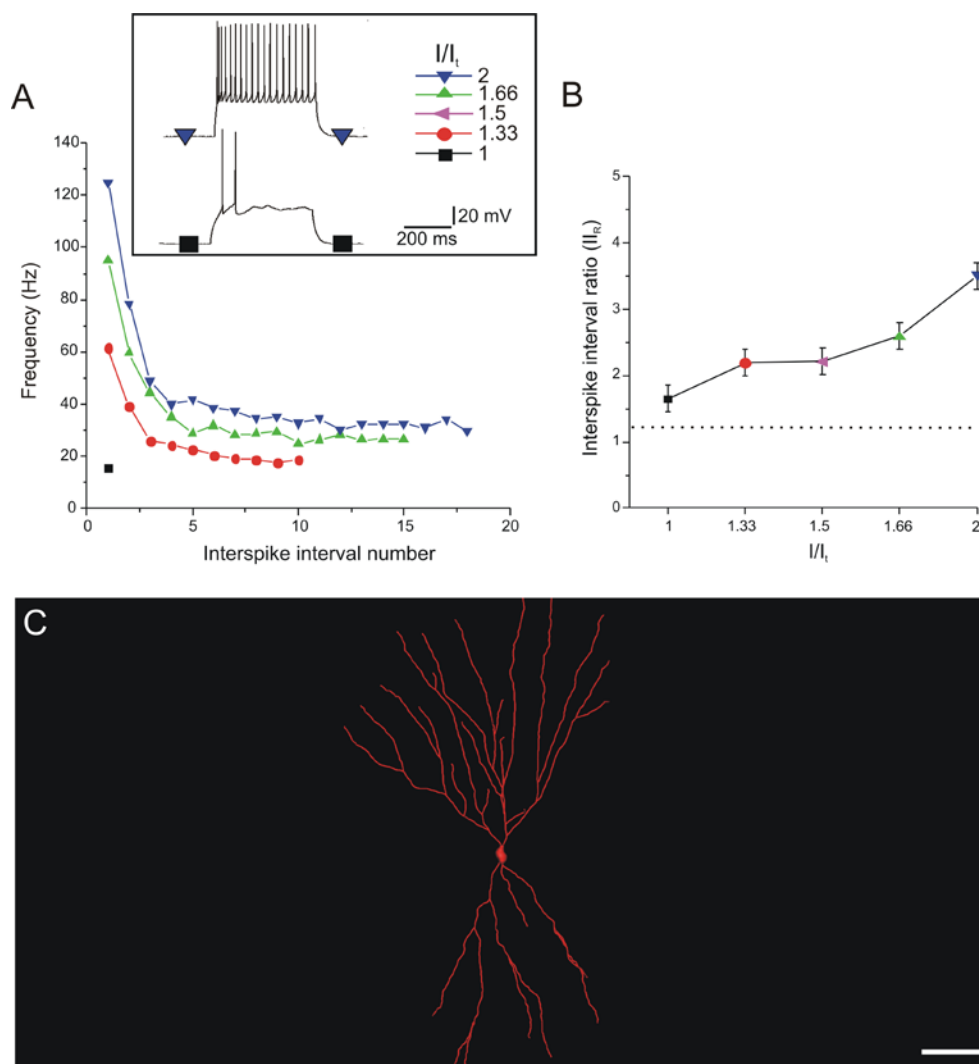


Figure 4.5 Firing properties of strongly adapting low frequency (sALF) cell type. A. Plot of firing frequency against interspike interval number in a typical sALF cell. Note the high spike frequency adaptation at higher depolarization levels (twice the firing threshold). B. The ratio between last and first interspike intervals (II_R) was plotted against level of injected current, showing increased firing adaptation across sALF group ($II_R > 1.25$). C. Morphological reconstruction of sALF cell with firing pattern shown in panel A. Traces in the inset show the response of a sALF cell type to injection of depolarizing current steps at threshold ($I/I_t = 1$) and twice the firing threshold ($I/I_t = 2$) levels. Scale bar = 40 μm .

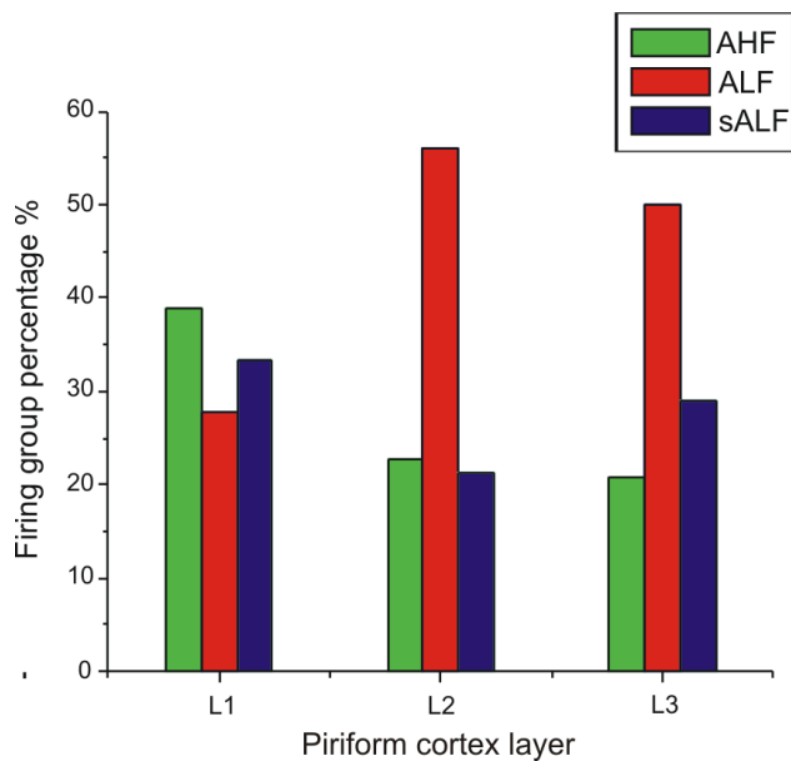


Figure 4.6 Layer distribution of the three firing groups in the anterior piriform cortex.

The columns represent the contribution (%) of each firing group to the total number of firing types recorded in each PC layer. AHF, adapting high frequency; ALF, adapting low frequency; sALF, strongly adapting low frequency.

Table 4.2 Firing group distribution across the anterior piriform cortex layers in amygdala kindled rats.

| Group | L1 % | L2 % | L3 % |
|---------------|------|------|------|
| AHF (n = 27) | 25.9 | 55.6 | 18.5 |
| ALF (n = 54) | 9.2 | 68.5 | 22.3 |
| sALF (n = 27) | 22.2 | 51.8 | 26.0 |

Data in rows represent the distribution (%) of each firing cluster in the three layers of aPC. AHF, adapting high frequency; ALF, adapting low frequency; sALF, strongly adapting low frequency; L1, layer 1; L2, layer 2; L3, layer 3.

4.3.2 Comparison of firing patterns with morphological attributes

Our data indicated a lack of correspondence between firing clusters and cell morphology, none of the three clusters (AHF, ALF and sALF) having a preference towards any of the morphological types (multipolar, horizontal and vertical cells) in the aPC (Fig. 4.7).

Morphological based classification of PC interneurons (multipolar, vertical and horizontal) also showed a high variability of firing patterns (Table 4.3). However, we found a reduced excitability of multipolar cells after kindling as revealed by an increased Π_R (2.04 ± 0.14 in kindled versus 1.6 ± 0.18 in control; $P < 0.05$) and a reduced firing frequency (37.3 ± 2.5 Hz in kindled versus 48.6 ± 1.8 Hz in control, $P < 0.05$).

4.3.3 Kindling-induced alteration voltage-gated K^+ channels.

The absence of two firing behaviours (NAvHF and wALF) after kindling is not due to a specific interneuronal loss as similar distribution were seen before and after kindling (control rats contained 16% horizontal cells, 38% multipolar and 46% vertical cells while in kindled animals we found 11% horizontal, 35% multipolar and 54% vertical cells). Thus a possible explanation for the lack of the two behaviours resides in a change in the firing pattern of interneurons after kindling that can be the result of several factors including altered GABA_A and/or voltage-gated receptor function. However, gabazine (a GABA_A blocker; see methods) did not change the firing pattern of interneurons (Fig. 4.8) so we excluded a possible relationship between kindling-alteration of GABA_A function (see Gavrilovici *et al.*, 2006) and the absence of the non-adapting firing patterns.

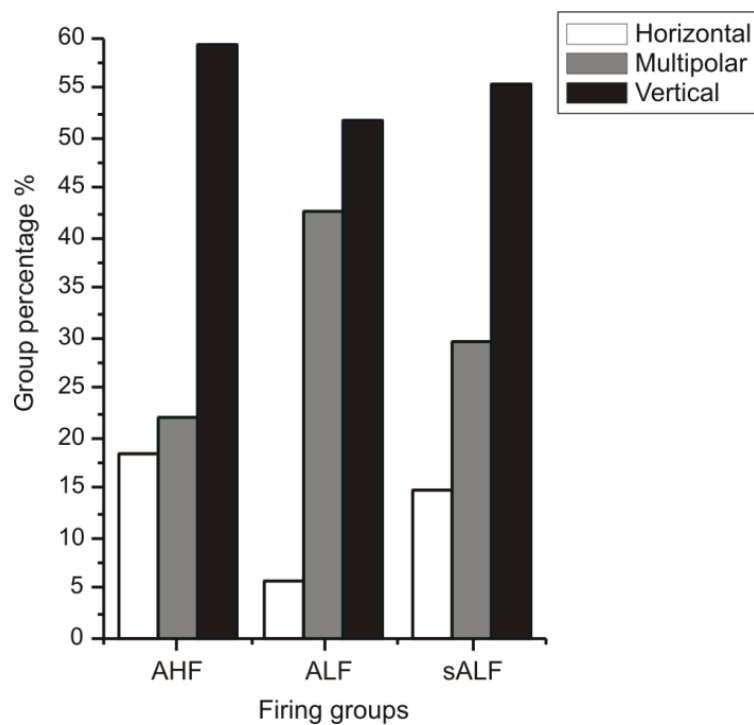


Figure 4.7 Correlation between the firing pattern types and interneuronal morphology in the anterior piriform cortex. AHF, adapting high frequency; ALF, adapting low frequency; sALF, strongly adapting low frequency.

Table 4.3 Firing distribution of the three main morphological interneuronal types of piriform cortex in amygdala kindled rats.

| Morphology | Firing type | | | Total % |
|------------------------|-------------|-------|--------|---------|
| | AHF % | ALF % | sALF % | |
| Horizontal (n = 12) | 42 | 25 | 33 | 100 |
| Multipolar (n = 37) | 16 | 62 | 22 | 100 |
| Vertical (n = 59) | 27 | 48 | 25 | 100 |

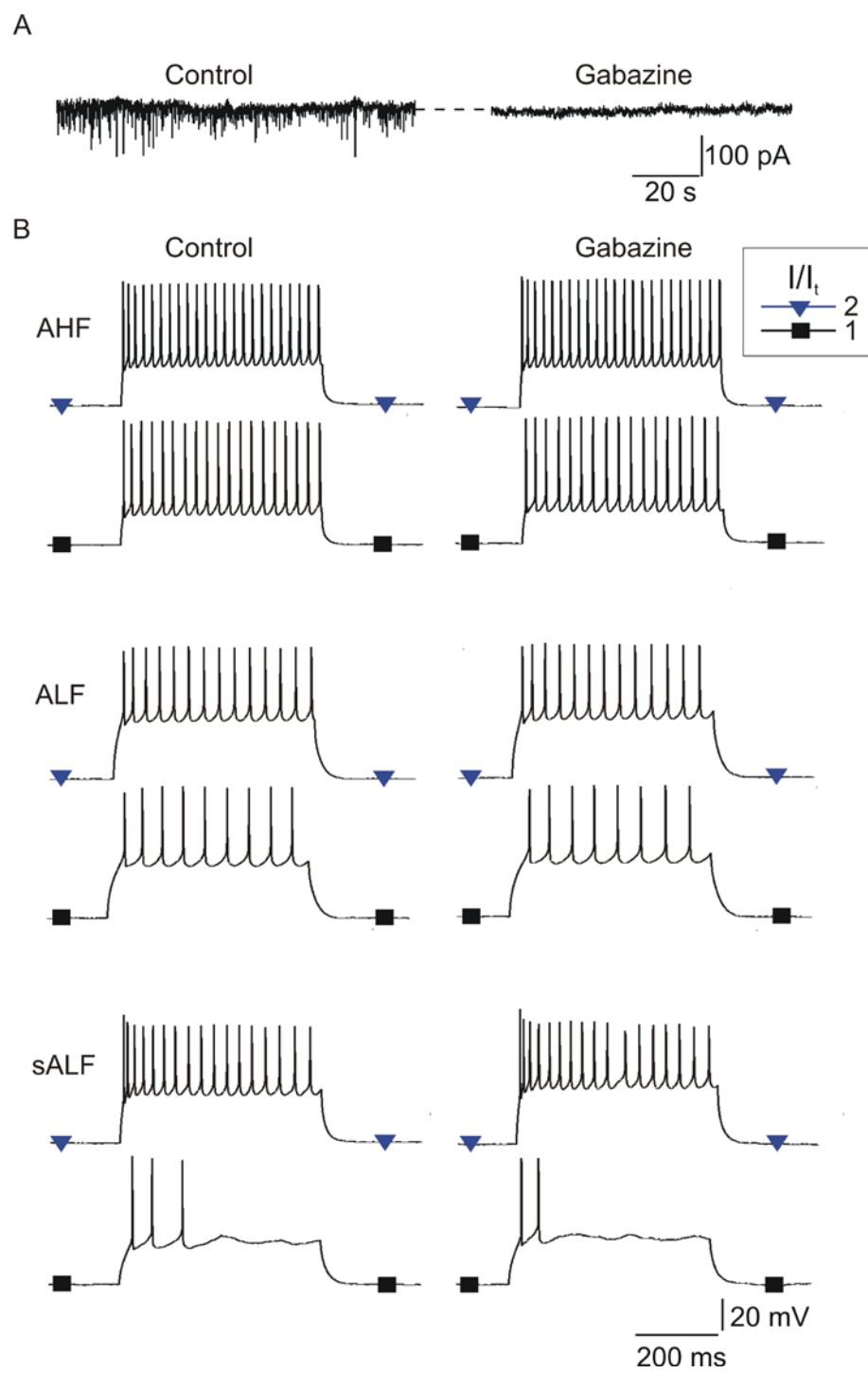
Data in rows represent the contribution (%) of each morphological type to the three firing clusters of PC. AHF, adapting high frequency; ALF, adapting low frequency; sALF, strongly adapting low frequency.

In another set of experiments we assessed the possible involvement of K⁺ channels in shaping the interneuronal firing pattern after kindling by electrophysiological and molecular biology experiments. As most of the NAvHF cells in control rats were multipolar cells, we assessed K⁺ current of interneurons based on their morphological traits. As described in methods, K⁺ currents before and after kindling were evoked by depolarizing steps between -50 and 10 mV by blocking all other ionic channels. Increased K⁺ current after kindling was observed in multipolar cells at every step of depolarizing pulse between -35 mV and +10 mV (see Fig. 4.9A). However no significant alteration in K⁺ current was seen on vertical cells or horizontal cells after kindling (Fig. 4.9B& C). This increased K⁺ current suggests an up-regulation of K⁺ channels after kindling which was further assessed by QPCR and immunohistochemistry experiments. Using pooled RNA from control and kindled rats, we screened using QPCR arrays representing 80 neuronal ion channels to see what K⁺ channel(s) mRNA may be increased (four candidates were identified: Kv 1.2, Kv 1.6, Kv 2.1, Kv 9.3). However, using individual samples, we found an increased expression of one voltage-gated K⁺ channel mRNA (Kv 1.6) in kindled aPC samples (Fig. 4.10), as expressed by significant changes in ΔC_t values ($\Delta C_t = -10.1 \pm 0.3$ in control vs. -8.5 ± 0.1 in kindled samples; $P < 0.05$). Also, immunohistochemical assessment of coexpression of parvalbumin and Kv 1.6 (see methods) in aPC indicated a higher expression of colocalized PV/Kv 1.6 after kindling (Fig. 4.11).

This increased voltage-gated channel expression and increased K⁺ current can decrease neuronal excitability by altering firing adaptation ratios and could therefore explain the lack of non-adapting/weakly adapting firing patterns in aPC interneurons after kindling.

Figure 4.8 Gabazine effect on firing patterns of piriform cortex interneurons.

A. Gabazine (10 μ M) blocked GABAergic currents on PC interneurons (n = 9). In B, we show that gabazine (10 μ M) did not alter the firing pattern of interneurons (n = 35). Here we show one example for each firing cluster: AHF (top traces), ALF (middle) and sALF (bottom) interneuron response to injection of depolarizing current at threshold ($I/I_t = 1$) and twice the firing threshold ($I/I_t = 2$) levels. AHF, adapting high frequency; ALF, adapting low frequency; sALF, strongly adapting low frequency.



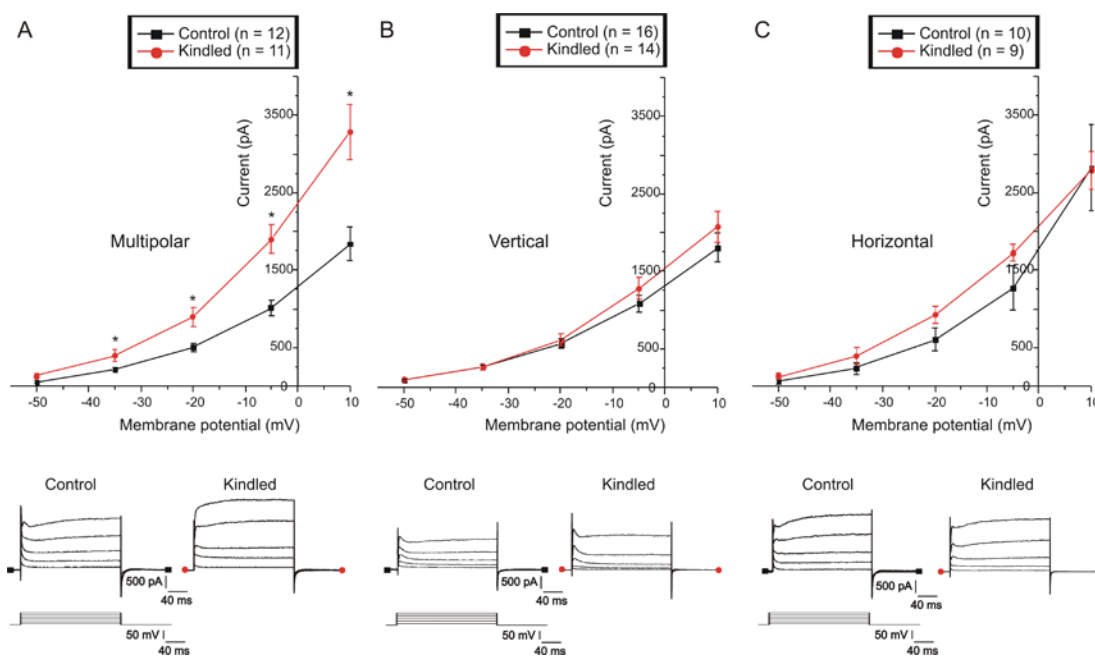


Figure 4.9 The voltage-dependent K^+ current in PC interneurons before and after kindling. Potassium outward currents were evoked by depolarizing steps between -50 and +10 mV in multipolar (A), vertical (B) and horizontal (C) piriform cortex interneurons. The current-voltage ($I-V$) relationships showing increased K^+ current after kindling in multipolar but no change was seen in vertical and horizontal cells. Outward currents were measured at the end of each depolarizing voltage pulse (bottom traces). Error bars represent the standard error of the mean. Statistically significant comparisons were determined using t -test, $*P < 0.05$.

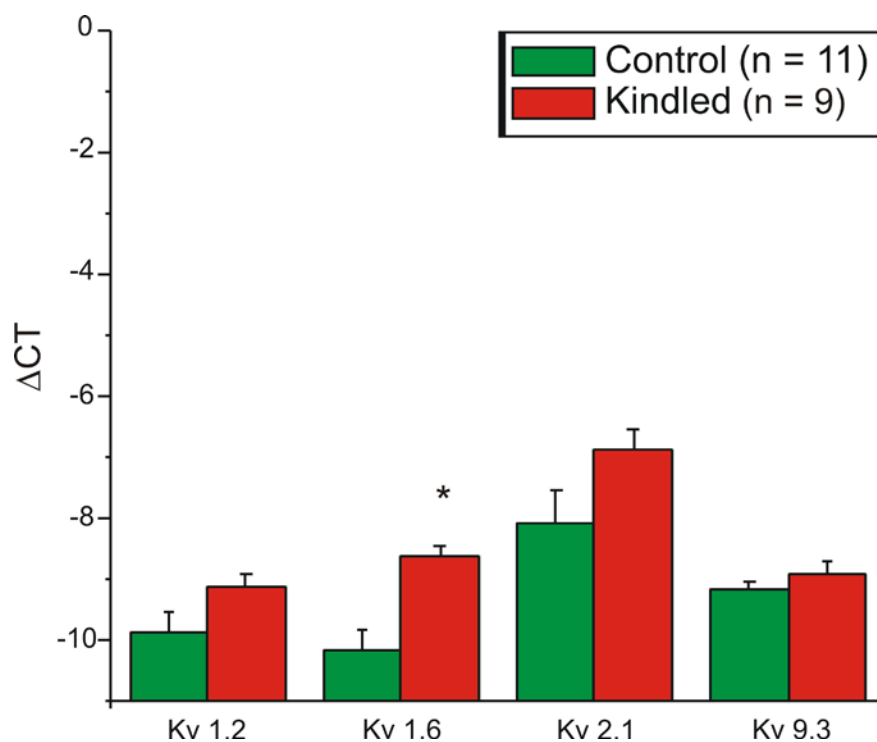


Figure 4.10 Delta C_t analysis of four voltage-gated potassium channels mRNA expression in rat anterior piriform cortex before and after kindling-induced epilepsy. Comparison between control and kindled groups indicate increased expression of Kv 1.6 after kindling. Test genes are listed on x axis while ΔC_t values are shown on y axis. Significant differences ($*P < 0.05$) are listed with an asterisk.

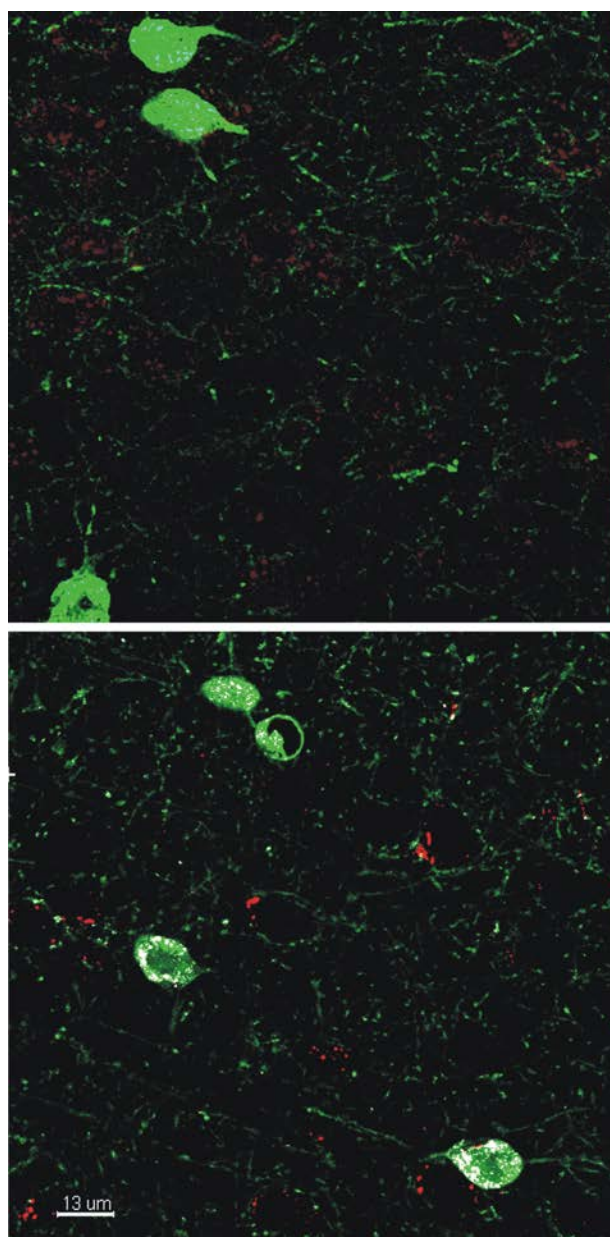


Fig. 4.11 Parvalbumin/Kv 1.6 colocalization in rat anterior piriform cortex before and after kindling-induced epilepsy. Green channel shows parvalbumin immunoreactivity (PV-IR); red signal represents Kv1.6 (KV1.6-IR); white pixels indicate PV and Kv1.6 colocalized segments. Low level of PV/Kv1.6 colocalization is found in control tissue (**top**), while higher expression of PV/Kv1.6 is seen in PV interneurons after kindling (**bottom**).

4.4 Discussion

The main finding of the present study is that amygdala kindling induces an alteration in the firing pattern of interneuronal populations of aPC, shifting interneuronal firing patterns towards adapting firing modes at the expense of non-adapting and weakly adapting firing. Thus it is shown that there is a loss of complexity in the interneuron firing patterns. These alterations in firing pattern are not linked to a change of passive membrane properties, as RMP and input resistance were unchanged after kindling. This is in line with other reports indicating unchanged passive membrane properties after kindling (Mody & Staley, 1994).

The absence of two firing behaviours, NAvHF and wALF, after kindling is not due to a specific interneuronal loss as a similar distribution of multipolar, vertical and horizontal cells before and after kindling was found (see results). This correlates with previous findings showing no GABAergic cell death in aPC and pPC after amygdala kindling (Lehmann *et al.*, 1998). Thus, as no interneuronal death is present after kindling in aPC, it implies that interneurons previously pertaining to NAvHF and wALF clusters are now part of the remaining clusters (AHF, ALF, sALF). These additions could explain why several interneuronal parameters (adaptation ratio, firing frequency and /or number of spikes) in kindled clusters (AHF, ALF and sALF) are not identical to the same clusters in control groups.

As passive membrane properties of interneuronal population are unchanged after kindling, other possible factors that could modulate the firing pattern might be represented by changes in GABA_A and/or voltage-gated ion channel function. As previously shown (Gavrilovici *et al.*, 2006), there was an increased inhibitory drive onto aPC interneurons following amygdala kindling. Increased inhibition in aPC was shown to be produced by an increased number of GABA_A receptors on interneuronal populations of aPC but not on pyramidal cells. However the impact of this increased inhibition on the firing patterns on differing interneuronal populations was not known. By using a GABA_A blocker (gabazine) we did not obtain any changes in the firing pattern of interneurons thus excluding a possible link between kindling-

alteration of GABA_A function and the lack of non-adapting and weakly adapting firing behaviour.

Many voltage-dependent channels can modulate membrane excitability and firing frequency and pattern (see review, McCormick, 2003). Moreover, alterations in the expression of gene encoding voltage-gated ion channels are widely reported in human epilepsies and animal model of epilepsies (see review, Lukasiuk *et al.*, 2007). However there are only a few electrophysiology studies showing changes of sodium, calcium and potassium currents in animal models of epilepsy. For example, sodium current was found to be increased in CA1 pyramidal cells but not in dentate cells following hippocampal electrically induced status epilepticus (Ketelaars *et al.*, 2001). Other studies indicated increased T-type calcium current in CA1 pyramidal cell dendrites in lithium-pilocarpine-induced status epilepticus animal models (Su *et al.*, 2002; Yaari *et al.*, 2007). Calcium current enhancement was not limited to pilocarpine model as similar alterations were found in CA1 pyramidal cells after hippocampal kindling (Vreugdenhil & Wadman, 1994), as well as in dentate granule cells in kainate model of epilepsy (Beck *et al.*, 1998). Similar to other neuronal types, where T-type calcium channels have been linked to bursting behaviour (see review Perez-Reyes, 2003), the upregulation of this type of calcium channel in animal models of epilepsy changed CA1 pyramidal cells firing from regular to burst firing (Sanabria *et al.*, 2001; Su *et al.*, 2002).

However, in our study, the nature of firing pattern change, namely increased firing adaptation, pointed towards a change in potassium current. Indeed, our assessment of K⁺ current before and after kindling showed an increased K⁺ current in multipolar cells, suggesting an up regulation of voltage-gated K⁺ channels in these cells. These results were confirmed by QPCR and immunohistochemistry experiments, indicating a significant up regulation of Kv 1.6 in aPC after kindling. Although kindling-increased K⁺ current and increased expressional change of a voltage-gated K⁺ channel in the PC is shown here for the first time, kindling-induced alterations of various voltage-gated K⁺ channels were also described in other limbic

areas. For example, in a similar model to ours, amygdala kindling induced an increased of Kv 7.2 immunoreactivity (Penschuck *et al.*, 2005) as well as increased expression of Kv 4.2, Kv 4.3 (Chang *et al.*, 2006) in the amygdala region. Recently (Corcoran *et al.*, 2011) showed that amygdala kindling induced an increase in the expression of KCNF1, Kv 7.1 in amygdala. Changing the site of kindling to hippocampus, the same group (Corcoran *et al.*, 2011) found increased KCNF1 expression in hippocampus and Kv 3.4 in amygdala and decreased KCNA3, Kv 7.1 and KCNF1 expression in amygdala (Corcoran *et al.*, 2011).

In another animal model of epilepsy, Kv 1.4 immunoreactivity was shown to be increased in the dentate molecular layer, while Kv 4.2 expression was decreased in stratum radiatum of CA₁ post pilocarpine-induced SE (Monaghan *et al.*, 2008). Similarly, pilocarpine-decreased expression of Kv 4.2 in CA₁ region, leading to a Kv 4.2-dependent enhanced excitability, was also confirmed by others (Bernard *et al.*, 2004; Su *et al.*, 2008).

These studies showed a plethora of voltage-gated K⁺ channel alterations following chemical or electrical induced epilepsy. Thus, depending on the type of the alteration (down- or upregulation), and the type of voltage-gated K⁺ channel affected, neuronal excitability can be effectively changed (see review, Misonou, 2010). In our case, the upregulation of Kv 1.6 and the subsequent increase in K⁺ current is correlated to the firing pattern changes observed after kindling. These voltage-gated K⁺ channels were previously reported in the limbic system (olfactory bulb, hippocampus), but they were also found in other areas of rat CNS including: cerebellar Purkinje and granular cell layers; deep cerebellar nuclei; and spinal cord (Kues & Wunder, 1992; Veh *et al.*, 1995). Kv1.6 channels were shown to be part of the delayed rectifier class (Kv1 class, shaker-related subfamily), mediating the voltage-dependent potassium ion permeability of neurons (Hille, 2001; Gutman *et al.*, 2005). As opposed to Kv 1.4 which mediates transient (A-type) outward K⁺ current, Kv 1.6 channels, along with Kv 1.1-1.3 and Kv 1.5 members of shaker

related subfamily, generate sustained outward Kv currents (Vacher *et al.*, 2008), similar to those recorded by us in multipolar cells following kindling.

The important question to be answered here is the impact of these changes leading to decreased excitability and altered interneuronal firing pattern population after kindling on the aPC network information processing and oscillatory activities. Understanding the participation of specific types of interneurons in local PC circuits and their firing behaviours can bring further insights on the role played by CBP interneurons in the epileptogenic mechanisms of this region. The fact that multipolar PV-IR nerve terminals provide perisomatic innervation to pyramidal cells in the aPC corroborated with our electrophysiology findings that the majority of NAvHF (FS-like firing) interneurons (75%) matched PV-IR phenotype, suggests that multipolar PV-IR cells could play a major role in pyramidal cell disinhibitory mechanisms in the epileptic PC. However, after kindling, the increased firing adaptation and especially the lack of the fast spiking behaviour (NAvHF), might alter disinhibitory mechanisms and the timing of pyramidal cells firing, that could lead to pathological synchronous events like those generated during epileptic seizures.

The present study provides the foundation for further explorations of how the timing of neural patterns in the PC is controlled and perhaps why this region is particularly seizurogenic. These findings are important for better understanding of kindling-induced alterations in PC network and could lead to new therapeutic targets for TLE.

4.5 References

- Ackermann RF, Chugani HT, Handforth A, Moshe S, Caldecott-Hazard S, & Engel JJr (1986). Autoradiographic studies of cerebral metabolism and blood flow in rat amygdala kindling. In *Kindling*, ed. Wada JA, pp. 73-87. Raven Press, New York.
- Ascoli GA, Alonso-Nanclares L, Anderson SA, Barrionuevo G, Benavides-Piccione R, Burkhalter A, Buzsaki G, Cauli B, DeFelipe J, Fairen A, Feldmeyer D, Fishell G, Fregnac Y, Freund TF, Gardner D, Gardner EP, Goldberg JH, Helmstaedter M, Hestrin S, Karube F, Kisvarday ZF, Lambolez B, Lewis DA, Marin O, Markram H, Munoz A, Packer A, Petersen CC, Rockland KS, Rossier J, Rudy B, Somogyi P, Staiger JF, Tamas G, Thomson AM, Toledo-Rodriguez M, Wang Y, West DC, & Yuste R (2008). Petilla terminology: nomenclature of features of GABAergic interneurons of the cerebral cortex. *Nat Rev Neurosci* **9**, 557-568.
- Beck H, Steffens R, Elger CE, & Heinemann U (1998). Voltage-dependent Ca²⁺ currents in epilepsy. *Epilepsy Res* **32**, 321-332.
- Bernard C, Anderson A, Becker A, Poolos NP, Beck H, & Johnston D (2004). Acquired dendritic channelopathy in temporal lobe epilepsy. *Science* **305**, 532-535.
- Cauli B, Porter JT, Tsuzuki K, Lambolez B, Rossier J, Quenet B, & Audinat E (2000). Classification of fusiform neocortical interneurons based on unsupervised clustering. *Proc Natl Acad Sci U S A* **97**, 6144-6149.
- Chang HH, Su T, Sun WW, Zhao QH, Qin B, & Liao WP (2006). [Changes of potassium channels Kv4.2, Kv4.3 and Kv channel interacting protein 1 in amygdala kindling epilepsy: experiment with rats]. *Zhonghua Yi Xue Za Zhi* **86**, 3315-3318.
- Cobb SR, Buhl EH, Halasy K, Paulsen O, & Somogyi P (1995). Synchronization of neuronal activity in hippocampus by individual GABAergic interneurons. *Nature* **378**, 75-78.
- Corcoran ME, Kroes RA, Burgdorf JS, & Moskal JR (2011). Regional changes in gene expression after limbic kindling. *Cell Mol Neurobiol* **31**, 819-834.
- Dietrich D, Podlogar M, Ortmanns G, Clusmann H, & Kral T (2005). Calbindin-D28k content and firing pattern of hippocampal granule cells in amygdala-kindled rats: a perforated patch-clamp study. *Brain Res* **1032**, 123-130.
- Ebert U, Wlaz P, & Loscher W (2000). High susceptibility of the anterior and posterior piriform cortex to induction of convulsions by bicuculline. *Eur J Neurosci* **12**, 4195-4205.

- Ekstrand JJ, Domroese ME, Feig SL, Illig KR, & Haberly LB (2001). Immunocytochemical analysis of basket cells in rat piriform cortex. *J Comp Neurol* **434**, 308-328.
- Engel JJr, Wolfson L, & Brown L (1978). Anatomical correlates of electrical and behavioral events related to amygdaloid kindling. *Ann Neurol* **3**, 538-544.
- Freund TF & Buzsaki G (1996). Interneurons of the hippocampus. *Hippocampus* **6**, 347-470.
- Gavrilovici C, D'Alfonso S, Dann M, & Poulter MO (2006). Kindling-induced alterations in GABA_A receptor mediated inhibition and neurosteroid activity in the piriform cortex of rat. *Eur J Neurosci* **24**, 1373-1384.
- Gavrilovici C, D'Alfonso S, & Poulter MO (2010). Diverse interneuron populations have highly specific interconnectivity in the rat piriform cortex. *J Comp Neurol* **518**, 1570-1588.
- Gutman GA, Chandy KG, Grissmer S, Lazdunski M, McKinnon D, Pardo LA, Robertson GA, Rudy B, Sanguinetti MC, Stuhmer W, & Wang X (2005). International Union of Pharmacology. LIII. Nomenclature and molecular relationships of voltage-gated potassium channels. *Pharmacol Rev* **57**, 473-508.
- Hille B (2001). Potassium channels and chloride channels. In *Ion Channels of Excitable Membranes*, ed. Sunderland MA, Sinauer Associates.
- Ketelaars SO, Gorter JA, van Vliet EA, Lopes da Silva FH, & Wadman WJ (2001). Sodium currents in isolated rat CA1 pyramidal and dentate granule neurones in the post-status epilepticus model of epilepsy. *Neurosci* **105**, 109-120.
- Kroner S, Krimer LS, Lewis DA, & Barrionuevo G (2007). Dopamine increases inhibition in the monkey dorsolateral prefrontal cortex through cell type-specific modulation of interneurons. *Cereb Cortex* **17**, 1020-1032.
- Kues WA & Wunder F (1992). Heterogeneous Expression Patterns of Mammalian Potassium Channel Genes in Developing and Adult Rat Brain. *Eur J Neurosci* **4**, 1296-1308.
- Lehmann H, Ebert U, & Loscher W (1998). Amygdala-kindling induces a lasting reduction of GABA-immunoreactive neurons in a discrete area of the ipsilateral piriform cortex. *Synapse* **29**, 299-309.
- Loscher W & Ebert U (1996). The role of the piriform cortex in kindling. *Prog Neurobiol* **50**, 427-481.

- Lukasiuk K, Dingledine R, Lowenstein D, & Pitkanen A (2007). Gene expression underlying changes in network excitability. In *Epilepsy: A Comprehensive Textbook*, eds. Engel J & Pedley T, pp. 307-322. Lippincott Williams and Wilkins, Philadelphia.
- McCormick DA (2003). Membrane potential and action potential. In *Fundamental Neuroscience*, eds. Squire LR, Bloom FE, McConnell SK, Roberts JL, Spitzer NC, & Zigmond MJ, pp. 139-161. Academic Press, San Diego.
- McIntyre DC, Hutcheon B, Schwabe K, & Poulter MO (2002). Divergent GABA(A) receptor-mediated synaptic transmission in genetically seizure-prone and seizure-resistant rats. *J Neurosci* **22**, 9922-9931.
- McIntyre DC & Molino A (1972). Amygdala lesions and CER learning: long term effect of kindling. *Physiol Behav* **8**, 1055-1058.
- McIntyre DC & Plant JR (1993). Long-lasting changes in the origin of spontaneous discharges from amygdala-kindled rats: piriform vs. perirhinal cortex in vitro. *Brain Res* **624**, 268-276.
- McIntyre DC & Wong RK (1986). Cellular and synaptic properties of amygdala-kindled piriform cortex in vitro. *J Neurophysiol* **55**, 1295-1307.
- Misonou H (2010). Homeostatic regulation of neuronal excitability by K(+) channels in normal and diseased brains. *Neuroscientist* **16**, 51-64.
- Mody I & Staley KJ (1994). Cell properties in the epileptic hippocampus. *Hippocampus* **4**, 275-280.
- Monaghan MM, Menegola M, Vacher H, Rhodes KJ, & Trimmer JS (2008). Altered expression and localization of hippocampal A-type potassium channel subunits in the pilocarpine-induced model of temporal lobe epilepsy. *Neurosci* **156**, 550-562.
- Morimoto K, Fahnstock M, & Racine RJ (2004). Kindling and status epilepticus models of epilepsy: rewiring the brain. *Prog Neurobiol* **73**, 1-60.
- Neville KR & Haberly LB (2004). Olfactory cortex. In *The Synaptic Organization of the Brain*, ed. Shepherd GM, pp. 415-454. Oxford University Press, New York.
- Paxinos G & Watson PL (1986). *The rat brain in stereotaxic coordinates*, second ed. Academic Press, Sydney.

- Penschuck S, Bastlund JF, Jensen HS, Stensbol TB, Egebjerg J, & Watson WP (2005). Changes in KCNQ2 immunoreactivity in the amygdala in two rat models of temporal lobe epilepsy. *Brain Res Mol Brain Res* **141**, 66-73.
- Perez-Reyes E (2003). Molecular physiology of low-voltage-activated t-type calcium channels. *Physiol Rev* **83**, 117-161.
- Sanabria ER, Su H, & Yaari Y (2001). Initiation of network bursts by Ca²⁺-dependent intrinsic bursting in the rat pilocarpine model of temporal lobe epilepsy. *J Physiol* **532**, 205-216.
- Su H, Sochivko D, Becker A, Chen J, Jiang Y, Yaari Y, & Beck H (2002). Upregulation of a T-type Ca²⁺ channel causes a long-lasting modification of neuronal firing mode after status epilepticus. *J Neurosci* **22**, 3645-3655.
- Su T, Cong WD, Long YS, Luo AH, Sun WW, Deng WY, & Liao WP (2008). Altered expression of voltage-gated potassium channel 4.2 and voltage-gated potassium channel 4-interacting protein, and changes in intracellular calcium levels following lithium-pilocarpine-induced status epilepticus. *Neurosci* **157**, 566-576.
- Vacher H, Mohapatra DP, & Trimmer JS (2008). Localization and targeting of voltage-dependent ion channels in mammalian central neurons. *Physiol Rev* **88**, 1407-1447.
- Veh RW, Lichtinghagen R, Sewing S, Wunder F, Grumbach IM, & Pongs O (1995). Immunohistochemical localization of five members of the Kv1 channel subunits: contrasting subcellular locations and neuron-specific co-localizations in rat brain. *Eur J Neurosci* **7**, 2189-2205.
- Vreugdenhil M & Wadman WJ (1994). Kindling-induced long-lasting enhancement of calcium current in hippocampal CA1 area of the rat: relation to calcium-dependent inactivation. *Neurosci* **59**, 105-114.
- Whittington MA & Traub RD (2003). Interneuron diversity series: inhibitory interneurons and network oscillations in vitro. *Trends Neurosci* **26**, 676-682.
- Yaari Y, Yue C, & Su H (2007). Recruitment of apical dendritic T-type Ca²⁺ channels by backpropagating spikes underlies de novo intrinsic bursting in hippocampal epileptogenesis. *J Physiol* **580**, 435-450.

Chapter 5. General discussion

The piriform cortex, an area involved in perception, discrimination and memory coding of olfactory signals, has been the subject of recent interest in the study of epileptogenesis. The PC qualifies as an important candidate for studying and understanding the epileptic mechanisms in TLE (Loscher & Ebert, 1996) for several reasons, namely: the PC has great epileptogenic potential with seizures spreading easily as strong interconnections with other limbic structures, such as the amygdala, entorhinal cortex and hippocampus (Luskin & Price, 1983) easily spread an epileptic event. On the other hand, lesions to the PC attenuate seizure genesis (de Guzman *et al.*, 2004; Schwabe *et al.*, 2004). From a practical point of view the PC is a relatively simple three-layered organization, with afferent and associational fiber system orderly distributed. Thus it is an excellent model for studying network dynamics as compared to the more complex six-layered neocortical structure. Nevertheless, despite this simpler structure the exact mechanisms through which the PC leads to pathological pyramidal cell synchronization and to the generation and spread of epileptic waves throughout the limbic system are not fully understood.

My previous research (Gavrilovici *et al.*, 2006) focused on understanding how and to what magnitude GABA_A receptor-mediated transmission was altered in the PC epileptic network. Although we found that increased inhibition on interneurons of PC suggests disinhibitory mechanisms, the impact of these alterations on the PC cortex processing was hampered by a limited understanding of the functional and morphological diversity of interneuronal populations. Moreover, we hypothesized that altered interneuronal firing patterns might also be at play in the PC after kindling-induced seizures. Thus, the working hypothesis in this work is that kindling induces alterations in the firing properties of PC interneuronal populations. If so, it may imply a role in disinhibitory mechanisms and/or a change in oscillatory network activities in the PC.

To understand the involvement of the interneurons in PC epileptogenesis it was important to first identify and describe their morpho-functional properties in unkindled brain and then to assess the electrophysiological parameters following kindling. Therefore, the present thesis addressed the following questions:

1. What kinds of interneurons are in the PC and what are their wiring patterns?
2. What are the firing patterns of interneuronal population in the PC?
3. How do interneurons change their firing behavior after kindling?

This section focuses on the main findings of these studies, and analyzes the consequences of kindling induced alterations in the firing behavior of interneurons in the PC.

5.1 Morphological analysis of PC interneuronal populations

Distinct interneurons expressing differing CBPs: PV, CB, and CR, have been shown to exist in PC. However, a comprehensive examination of the distribution and innervation patterns of these neurons was still needed. Thus the purpose of our study was to combine the analysis of the CBP cell localization with analysis of their innervation patterns. Each type was differentially localized in the three layers of the PC. Only CR-IR neurons were found in L1. PV and CB are found in L2-L3, most of them expressing both PV and CB. A morphological estimate of the dendritic extent for each subtype showed that PV-IR and PV/CB-IR cells demonstrated equally wide, horizontal and vertical arborizations (multipolar cells), whereas CB cells had wide horizontal and restricted vertical arborizations (horizontal cells). CR cells had restricted horizontal and very long vertical arborizations (vertical cells). These dendritic arborization tendencies help us understand how these separate interneuronal populations process information in the layers of PC. Thus, long dendritic trees which cross adjacent layers as seen for CR-IR and PV-IR cells, suggest a role in the integration of information between PC layers; whereas the

restricted dendritic arborization of CB cells suggest an increased intralayer integration of signals.

Postsynaptic morphological targeting was also found to be specific, namely, PV-IR and PV/CB-IR NTs innervate perisomatic regions of principal cells. CR-IR NTs innervate only dendrites of principal cells while CB-IR NTs innervate both somata and dendrites of principal cells. Taken together, these dendritic and axonal attributes of the CBP interneurons are important not only to delineate separate morphological classes of interneurons in the three layers of the PC, but also to understand how they are interconnected with the pyramidal cells and other interneurons. This sheds light on the participation of different CBP populations in the main inhibitory circuits: feed-forward and feedback inhibition loops. Thus, due to their specific localization on L1, CR-IR cells with vertical morphology are easily activated by LOT and thus are in central position to provide feed-forward inhibition to L2 pyramidal cells. As well, L2 cells with long dendritic trees crossing in L1 like CR-IR, PV-IR cells can also be integrated in this circuit. This heterogeneous participation of various CBP interneurons in this circuit, and more importantly their different targeting of pyramidal cell compartments (CR – dendritic inhibition versus PV perisomatic inhibition) suggest different ways to control and modulate the activity of the postsynaptic target, the pyramidal cell. CB-IR cells, with their restricted dendritic arbor, are not likely to be innervated by the excitatory output of the LOT (which runs only into the superficial part of L1) and thus do not participate in feed-forward inhibition. In the other main inhibitory circuit, feedback inhibition, all types of interneurons can be activated by collaterals from pyramidal cells in L3 (Neville & Haberly, 2004; Ekstrand *et al.*, 2001). Most of these interneurons were PV/CB-IR and CB-IR followed by CR-IR cells. However, CR-IR cells which are highly distributed in L2 and have elongated dendritic trees crossing in L3 could also connect to pyramidal cell collaterals in L3 and therefore might be involved in this circuit.

The relevance of such diverse interconnections between interneuronal populations and pyramidal cells, indicating a high degree of control over pyramidal cell firing behavior, may be required to balance the activity of highly interconnected pyramidal populations which are heavily connected by collaterals from other pyramidal cells in the PC (Neville & Haberly, 2004). At the same time, the connections between differing interneurons and pyramidal cells and their specific postsynaptic targeting (dendritic versus perisomatic compartments of pyramidal cells) could link PC interneurons to distinct network oscillations as was shown in other brain areas (Maccaferri & McBain, 1996; Chapman & Lacaille, 1999; Pike *et al.*, 2000; Middleton *et al.*, 2008). For example, perisomatic inhibitory neurons (basket cells) in the entorhinal cortex (Middleton *et al.*, 2008) or in hippocampus (Pike *et al.*, 2000) are involved in generation of gamma oscillations while dendritic targeting interneurons like bistratified and oriens-lacunosum moleculare in hippocampus participate in theta rhythms (Klausberger *et al.*, 2004).

Overall, morphological analysis of PC interneurons show highly complex innervation patterns for all of the CBP interneurons of the PC and form a basis for further studies in the plasticity of this region.

5.2 Electrophysiological study of PC interneuronal populations

Morphological analysis of interneurons provided us the necessary framework to pursue the next step in unraveling their role in PC network activity. Thus, the goal of this study was to analyze the aPC interneuronal electrophysiological properties and correlate these properties to their morphological features. Based on their firing frequency (FF), interspike interval ratio (II_R), and their input resistance (R_I) we were able to classify the firing behavior of PC interneurons into five distinct clusters. Non-adapting very high frequency (NAvHF) interneurons did not adapt at any depolarizing steps, showing maximal firing frequency compared to the other groups. The other 4 groups showed different levels of firing adaptation as well as different firing frequencies: adapting high frequency (AHF), adapting low frequency (ALF),

strongly adapting low frequency (sALF), and weakly adapting low frequency (wALF). Lower frequency groups had a lower excitability, i.e. higher threshold current and/or lower input resistance, than the higher frequency interneurons.

Although the spiking pattern was not consistently predictive of a specific interneuronal morphology, we found that most of the cells displaying non-adapting very high frequency firing pattern were multipolar (PV-IR morphological type). These firing properties of multipolar PV interneurons are not limited to rat aPC as high frequency trains of action potentials fired in non-adapting manner (fast spiking behavior) were also correlated with PV-IR interneuronal phenotype in other studies in mouse pPC (Young & Sun, 2009), mouse aPC (Suzuki & Bekkers, 2010), as well as in other brain areas (Kawaguchi & Kubota, 1997; Kawaguchi & Kondo, 2002; Toledo-Rodriguez *et al.*, 2004; Zaitsev *et al.*, 2005).

However, the other firing groups did not show a preference towards a specific morphological type, indicating a very high diversity of firing behaviors among different morphological types. The weak correlation between the rest of the firing clusters (AHF, ALF, sALF and wALF), and morphological characteristics is not a unique situation, as similar lack of correspondence between morpho-functional characteristics is also seen in neocortex (Markram *et al.*, 2004) and hippocampal interneurons (Parra *et al.*, 1998). Overall, firing pattern heterogeneity of aPC interneurons suggests different ways to control and regulate the olfactory network processing, memory coding and/or generation of oscillatory activities.

5.3 Kindling induced alterations in the firing pattern of interneuronal populations.

Electrophysiological analysis of PC interneurons after kindling induced epilepsy, revealed important changes in the firing behaviors of PC interneurons. The main finding of this study was the absence of NAvHF and wALF patterns in interneuronal populations of kindled brain, indicating a loss of firing diversity and a shift from non-adapting to adapting firing behaviour after kindling. The lack of non-

adapting behaviour, especially the NAvHF, is most interesting as our study linked this firing behavior to multipolar cells (PV-IR interneurons) in the PC of un-kindled brain. After kindling, despite preservation of multipolar cells in the PC, these cells had decreased excitability, as revealed by an increased firing adaptation and reduced firing frequency. We also found that multipolar cells were the only type showing an increased K^+ current due to a specific up regulation of voltage-gated potassium channels (Kv 1.6). Similar changes in the expression of voltage-gated potassium channels resulting in decreased firing have been shown to occur after increased neuronal activity (Misonou, 2010). What is particularly interesting here is that the up-regulation and loss of excitability occurs on cells (interneurons) that would tend to dampen the excitation. Thus this outcome would seem to be a maladaptive one that exacerbates the seizure genesis. This argues against the idea that these alterations might be part of a compensatory mechanism to protect against the increased kindling-driven excitatory network activity.

In light of these alterations, the question to be answered is: “What are the specific consequences of this firing pattern change and might they be linked to increased excitability in the PC?” First, due to reduced firing properties of multipolar PV cells, their activation by input of similar strength would result in a decreased action potential output, hence an impaired inhibition of the pyramidal cells. Second, our immunohistochemical analysis of multipolar PV-IR NTs indicated their placement on perisomatic compartment of pyramidal cells (Gavrilovici *et al.*, 2010) may make this loss of inhibition even more important. This conclusion is supported by similar findings showing perisomatic inhibition provided by the PV cells on pyramidal cells is also confirmed by other studies in neocortical areas (DeFelipe, 1997), and hippocampus (Kosaka *et al.*, 1987; Nitsch *et al.*, 1990; Ribak *et al.*, 1993). This perisomatic inhibition was shown to have a potent effect on pyramidal cells output, as compared to a modulatory role in integrating the glutamatergic input provided by dendritic inhibition (Miles *et al.*, 1996). Third, considering the unique structure of the PC, with a high level of associational fibers

interconnecting pyramidal populations along its anterior-posterior axis, reduction of perisomatic inhibition might create an even greater imbalance between excitation and inhibition by allowing the excitatory recurrent activity between pyramidal cells to predominate, and thus to generate aberrant epileptiform events. The sum of these effects predicts a disinhibitory mechanism that produces seizures.

Although here we present, for the first time, an altered function of multipolar (PV-IR) cells in the PC in a kindling model, other evidence suggesting the involvement of PV interneurons in epileptogenesis were shown in other animal models of epilepsy. For example, in knockout PV mice, the severity of seizures induced by a convulsant drug (pentylenetetrazol) was enhanced while the seizure threshold was decreased (Schwaller *et al.*, 2004). As PV has been implicated in buffering intracellular Ca^{2+} (Heizmann, 1992), it may be that increased Ca^{2+} loading in these interneurons may excessively activate Ca^{2+} -dependent currents which would reduce interneuron excitability. In another mouse genetic model, increased seizure susceptibility was correlated with a decline of PV-IR interneurons (Powell *et al.*, 2003). Finally, in the status epilepticus model of epilepsy, reduction of PV cells was correlated to the severity of SE, suggesting that they might play a role in progression of epileptic events (van Vliet *et al.*, 2004). Finally, in a recent study of malformed epileptogenic cortex (George & Jacobs, 2011), it was found that fast spiking PV interneurons had an altered firing pattern, with a decreased firing frequency, which reduced their effectiveness in inhibitory mechanism in the neuronal network and thus promoting epileptogenesis. Overall, these studies revealed that a decreased PV interneuronal function can facilitate the development of seizurogenic activities.

Besides increased disinhibition, altered interneuronal firing behavior is also likely to induce changes in the timing of neuronal network activities (Cobb *et al.*, 1995). Very interestingly, PV-IR cells with fast spiking properties were shown to be linked to gamma oscillations. Recent studies provided evidence for the involvement of fast spiking PV cells in generation and modulation of gamma oscillations in hippocampus (Fuchs *et al.*, 2007; Gulyas *et al.*, 2010) and neocortex (Cardin *et al.*,

2009). In the PC, gamma, beta and theta oscillations are common, as they are linked with the respiratory cycle and various olfactory processing and odor discrimination mechanisms (Neville & Haberly, 2004; Kay *et al.*, 2009). Although it is believed that interneuronal populations are involved in these activities (Neville & Haberly, 2004; Poo & Isaacson, 2009), a correlation between a specific interneuronal type and a particular oscillatory activity remain to be determined. Nonetheless, the presence of PV-IR cells, with a fast spiking behavior and their perisomatic inhibition might indicate a similar involvement (as seen in other areas) in these activities. However, a change in the firing pattern of interneurons, leading to increased disinhibition, could alter the oscillatory properties of the PC network. The question here is whether a change in oscillatory properties of a network can lead to epileptiform events. In hippocampus, it was shown that depending on the strength of recurrent inhibition, two different oscillations might arise: strong excitation of interneurons favor gamma network oscillations while reduced excitation of interneurons will favor population bursts (Traub *et al.*, 2005). In PC, where gamma oscillations are common, reduced firing pattern of perisomatic interneurons (PV cells) after kindling (e.g. a reduced inhibitory output) might favor the emergence of faster oscillations and/or epileptiform events. Interestingly, very fast oscillations (>80 Hz) were shown to emerge before and in association with seizures in humans (see review, Traub & Whittington, 2010). In this view, a further investigation of the PC oscillatory network activities after kindling is needed to determine if similar abnormal oscillations could arise in this network (see next section).

Overall, these findings may help elucidate the functional role of different groups of interneurons of PC. Kindling-induced alteration of interneuronal firing properties, especially the lack of fast spiking firing behavior, could lead to an imbalance between excitation and inhibition and/or change intrinsic oscillatory properties of PC network, leading to pathological synchronous events like those generated during epileptic seizures. The present study provides the foundation for

further explorations of how the timing of neural patterns in the PC is controlled and perhaps why this region is particularly seizurogenic.

5.4 Further studies.

Multiple cell recordings (whole-cell patch clamp recordings) can provide important information regarding the connectivity and synchronicity of a neuronal network. Our data suggests an increased disinhibition resulting in the hyperexcitability of the pyramidal cells. However further studies are needed to determine whether the disinhibition of pyramidal cells could lead to hypersynchrony and thus epileptogenic events in the PC. For example, cross-correlation analysis of neuronal firing pattern could reveal the temporal coupling and interactions of neurons and represent an important method to decode how neurons act together to represent various biological signals (Tam, 1998; Okatan *et al.*, 2005). Multiple whole cell patch clamp recording method (two to four neurons/trial) could be used to collect the evoked responses of patched cells to electrical stimulations of LOT delivered in frequencies resembling physiological inputs into the PC. Subsequent cross-correlation analysis of these firing patterns could therefore indicate the level of synchrony of the pyramidal cells before and after kindling-induced epilepsy.

Similarly, voltage sensitive dye recordings method can be used to study whether kindling alters the oscillatory activities over larger groups of neurons in the PC. These studies can be coupled with pharmacological manipulations targeting voltage-gated potassium channels (Kv 1.6), to revert firing pattern of multipolar cells to fast spiking and subsequent analysis of oscillatory activities in the PC.

Finally, although previous work (Gavrilovici *et al.*, 2006) indicated that the overall number of inhibitory synapses after kindling is not altered, the proportion of various CBP synapses in different layers of PC might change. Therefore, an immunohistochemical analysis of nerve terminals coexpressing each CBP after kindling-induced epilepsy is still needed. Due to specific targeting provided by

different CBP interneuronal populations, an altered distribution of these synapses could provide more insights on the network alterations induced by kindling.

5.5 References

- Cardin JA, Carlen M, Meletis K, Knoblich U, Zhang F, Deisseroth K, Tsai LH, & Moore CI (2009). Driving fast-spiking cells induces gamma rhythm and controls sensory responses. *Nature* **459**, 663-667.
- Chapman CA & Lacaille JC (1999). Intrinsic theta-frequency membrane potential oscillations in hippocampal CA1 interneurons of stratum lacunosum-moleculare. *J Neurophysiol* **81**, 1296-1307.
- Cobb SR, Buhl EH, Halasy K, Paulsen O, & Somogyi P (1995). Synchronization of neuronal activity in hippocampus by individual GABAergic interneurons. *Nature* **378**, 75-78.
- de Guzman P, D'antuono M, & Avoli M (2004). Initiation of electrographic seizures by neuronal networks in entorhinal and perirhinal cortices in vitro. *Neurosci* **123**, 875-886.
- DeFelipe J (1997). Types of neurons, synaptic connections and chemical characteristics of cells immunoreactive for calbindin-D28K, parvalbumin and calretinin in the neocortex. *J Chem Neuroanat* **14**, 1-19.
- Fuchs EC, Zivkovic AR, Cunningham MO, Middleton S, LeBeau FE, Bannerman DM, Rozov A, Whittington MA, Traub RD, Rawlins JN, & Monyer H (2007). Recruitment of parvalbumin-positive interneurons determines hippocampal function and associated behavior. *Neuron* **53**, 591-604.
- Gavrilovici C, D'Alfonso S, Dann M, & Poulter MO (2006). Kindling-induced alterations in GABA_A receptor mediated inhibition and neurosteroid activity in the piriform cortex of rat. *Eur J Neurosci* **24**, 1373-1384.
- Gavrilovici C, D'Alfonso S, & Poulter MO (2010). Diverse interneuron populations have highly specific interconnectivity in the rat piriform cortex. *J Comp Neurol* **518**, 1570-1588.
- George AL & Jacobs KM (2011). Altered intrinsic properties of neuronal subtypes in malformed epileptogenic cortex. *Brain Res* **1374**, 116-128.
- Gulyas AI, Szabo GG, Ulbert I, Holderith N, Monyer H, Erdelyi F, Szabo G, Freund TF, & Hajos N (2010). Parvalbumin-containing fast-spiking basket cells generate the field potential oscillations induced by cholinergic receptor activation in the hippocampus. *J Neurosci* **30**, 15134-15145.

- Heizmann CW (1992). Calcium-binding proteins: basic concepts and clinical implications. *Gen Physiol Biophys* **11**, 411-25.
- Kawaguchi Y & Kondo S (2002). Parvalbumin, somatostatin and cholecystinin as chemical markers for specific GABAergic interneuron types in the rat frontal cortex. *J Neurocytol* **31**, 277-287.
- Kawaguchi Y & Kubota Y (1997). GABAergic cell subtypes and their synaptic connections in rat frontal cortex. *Cereb Cortex* **7**, 476-486.
- Kay LM, Beshel J, Brea J, Martin C, Rojas-Libano D, & Kopell N (2009). Olfactory oscillations: the what, how and what for. *Trends Neurosci* **32**, 207-214.
- Kosaka T, Katsumaru H, Hama K, Wu JY, & Heizmann CW (1987). GABAergic neurons containing the Ca²⁺-binding protein parvalbumin in the rat hippocampus and dentate gyrus. *Brain Res* **419**, 119-130.
- Loscher W & Ebert U (1996). The role of the piriform cortex in kindling. *Prog Neurobiol* **50**, 427-481.
- Luskin MB & Price JL (1983). The topographic organization of associational fibers of the olfactory system in the rat, including centrifugal fibers to the olfactory bulb. *J Comp Neurol* **216**, 264-291.
- Maccaferri G & McBain CJ (1996). The hyperpolarization-activated current (I_h) and its contribution to pacemaker activity in rat CA1 hippocampal stratum oriens-alveus interneurons. *J Physiol* **497**, 119-130.
- Markram H, Toledo-Rodriguez M, Wang Y, Gupta A, Silberberg G, & Wu C (2004). Interneurons of the neocortical inhibitory system. *Nat Rev Neurosci* **5**, 793-807.
- Middleton S, Jalics J, Kispersky T, LeBeau FE, Roopun AK, Kopell NJ, Whittington MA, & Cunningham MO (2008). NMDA receptor-dependent switching between different gamma rhythm-generating microcircuits in entorhinal cortex. *Proc Natl Acad Sci U S A* **105**, 18572-18577.
- Miles R, Toth K, Gulyas AI, Hajos N, & Freund TF (1996). Differences between somatic and dendritic inhibition in the hippocampus. *Neuron* **16**, 815-823.
- Misonou H (2010). Homeostatic regulation of neuronal excitability by K(+) channels in normal and diseased brains. *Neuroscientist* **16**, 51-64.
- Neville KR & Haberly LB (2004). Olfactory cortex. In *The Synaptic Organization of the Brain*, ed. Shepherd GM, pp. 415-454. Oxford University Press, New York.

- Nitsch R, Soriano E, & Frotscher M (1990). The parvalbumin-containing nonpyramidal neurons in the rat hippocampus. *Anat Embryol (Berl)* **181**, 413-425.
- Okatan M, Wilson MA, & Brown EN (2005). Analyzing functional connectivity using a network likelihood model of ensemble neural spiking activity. *Neural Comput* **17**, 1927-1961.
- Parra P, Gulyas AI, & Miles R (1998). How many subtypes of inhibitory cells in the hippocampus? *Neuron* **20**, 983-993.
- Pike FG, Goddard RS, Suckling JM, Ganter P, Kasthuri N, & Paulsen O (2000). Distinct frequency preferences of different types of rat hippocampal neurones in response to oscillatory input currents. *J Physiol* **529**, 205-213.
- Poo C & Isaacson JS (2009). Odor representations in olfactory cortex: "sparse" coding, global inhibition, and oscillations. *Neuron* **62**, 850-861.
- Powell EM, Campbell DB, Stanwood GD, Davis C, Noebels JL, & Levitt P (2003). Genetic disruption of cortical interneuron development causes region- and GABA cell type-specific deficits, epilepsy, and behavioral dysfunction. *J Neurosci* **23**, 622-631.
- Ribak CE, Seress L, & Leranth C (1993). Electron microscopic immunocytochemical study of the distribution of parvalbumin-containing neurons and axon terminals in the primate dentate gyrus and Ammon's horn. *J Comp Neurol* **327**, 298-321.
- Schwabe K, Ebert U, & Loscher W (2004). Bilateral microinjections of vigabatrin in the central piriform cortex retard amygdala kindling in rats. *Neurosci* **129**, 425-429.
- Schwaller B, Tetko IV, Tandon P, Silveira DC, Vreugdenhil M, Henzi T, Potier MC, Celio MR, & Villa AE (2004). Parvalbumin deficiency affects network properties resulting in increased susceptibility to epileptic seizures. *Mol Cell Neurosci* **25**, 650-663.
- Suzuki N & Bekkers JM (2010). Distinctive classes of GABAergic interneurons provide layer-specific phasic inhibition in the anterior piriform cortex. *Cereb Cortex* **20**, 2971-2984.
- Tam DC (1998). A cross-interval spike train analysis: the correlation between spike generation and temporal integration of doublets. *Biol Cybern* **78**, 95-106.

- Toledo-Rodriguez M, Blumenfeld B, Wu C, Luo J, Attali B, Goodman P, & Markram H (2004). Correlation maps allow neuronal electrical properties to be predicted from single-cell gene expression profiles in rat neocortex. *Cereb Cortex* **14**, 1310-1327.
- Traub RD, Pais I, Bibbig A, LeBeau FE, Buhl EH, Garner H, Monyer H, & Whittington MA (2005). Transient depression of excitatory synapses on interneurons contributes to epileptiform bursts during gamma oscillations in the mouse hippocampal slice. *J Neurophysiol* **94**, 1225-1235.
- Traub RD & Whittington MA (2010). Epilepsy. In *Cortical Oscillations in Health and Disease*, eds. Traub RD & Whittington MA, pp. 70-104. Oxford University Press, New York.
- van Vliet EA, Aronica E, Tolner EA, Lopes da Silva FH, & Gorter JA (2004). Progression of temporal lobe epilepsy in the rat is associated with immunocytochemical changes in inhibitory interneurons in specific regions of the hippocampal formation. *Exp Neurol* **187**, 367-379.
- Young A & Sun QQ (2009). GABAergic inhibitory interneurons in the posterior piriform cortex of the GAD67-GFP mouse. *Cereb Cortex* **19**, 3011-3029.
- Zaitsev AV, Gonzalez-Burgos G, Povysheva NV, Kroner S, Lewis DA, & Krimer LS (2005). Localization of calcium-binding proteins in physiologically and morphologically characterized interneurons of monkey dorsolateral prefrontal cortex. *Cereb Cortex* **15**, 1178-1186.

APPENDIX A: Gene table for RT² Profiler™ rat PCR Array

| Position | Unigene | GeneBank | Symbol | Description | Gene Name |
|----------|-----------|--------------|---------|---|--|
| A01 | Rn.37523 | NM_012892 | Accn1 | Amiloride-sensitive cation channel 1, neuronal | MDEG1, MDEG2 |
| A02 | Rn.37385 | NM_024154 | Accn2 | Amiloride-sensitive cation channel 2, neuronal | Asic1 |
| A03 | Rn.24225 | NM_173135 | Accn3 | Amiloride-sensitive cation channel 3 | Asic3 |
| A04 | Rn.2992 | NM_012504 | Atp1a1 | ATPase, Na ⁺ /K ⁺ transporting, alpha 1 polypeptide | Nkaa1b |
| A05 | Rn.8925 | NM_013113 | Atp1b1 | ATPase, Na ⁺ /K ⁺ transporting, beta 1 polypeptide | ATPBS |
| A06 | Rn.10624 | NM_012507 | Atp1b2 | ATPase, Na ⁺ /K ⁺ transporting, beta 2 polypeptide | ATPB2, ATPB2S, Amog, MGC93648, RATATPB2S |
| A07 | Rn.218029 | NM_058213 | Atp2a1 | ATPase, Ca ⁺⁺ transporting, cardiac muscle, fast twitch 1 | Serca1 |
| A08 | Rn.214529 | NM_012509 | Atp4a | ATPase, H ⁺ /K ⁺ exchanging, alpha polypeptide | Hka, Hkatpc |
| A09 | Rn.92965 | NM_134364 | Atp5b | ATP synthase, H ⁺ transporting, mitochondrial F1 complex, beta polypeptide | - |
| A10 | Rn.93045 | NM_031785 | Atp6ap1 | ATPase, H ⁺ transporting, lysosomal accessory protein 1 | Atp6s1, C7-1 |
| A11 | Rn.19803 | NM_001106681 | Atp6v0b | ATPase, H ⁺ transporting, lysosomal V0 subunit B | - |
| A12 | Rn.87769 | NM_012918 | Cacna1a | Calcium channel, voltage-dependent, P/Q type, alpha 1A subunit | BccA1, Cav2.1, rBA-1 |
| B01 | Rn.85880 | NM_147141 | Cacna1b | Calcium channel, voltage-dependent, N type, alpha 1B subunit | BIII |
| B02 | Rn.9827 | NM_012517 | Cacna1c | Calcium channel, voltage-dependent, L type, alpha 1C subunit | RATIVS302 |
| B03 | Rn.86960 | NM_031601 | Cacna1g | Calcium channel, voltage-dependent, T type, alpha 1G subunit | - |
| B04 | Rn.49178 | NM_153814 | Cacna1h | Calcium channel, voltage-dependent, T type, alpha 1H subunit | - |
| B05 | Rn.10738 | NM_053873 | Cacna1s | Calcium channel, voltage-dependent, L type, alpha 1S subunit | Cchl1a3 |
| B06 | Rn.9417 | NM_017346 | Cacnb1 | Calcium channel, voltage-dependent, beta 1 subunit | - |
| B07 | Rn.10739 | NM_053851 | Cacnb2 | Calcium channel, voltage-dependent, beta 2 subunit | Cacnb2 |
| B08 | Rn.2808 | NM_012828 | Cacnb3 | Calcium channel, voltage-dependent, beta 3 subunit | CACH3B |
| B09 | Rn.9863 | NM_001105733 | Cacnb4 | Calcium channel, voltage-dependent, beta 4 subunit | - |
| B10 | Rn.72939 | NM_053351 | Cacng2 | Calcium channel, voltage-dependent, gamma subunit 2 | Ipr328 |
| B11 | Rn.124539 | NM_031506 | Cftr | Cystic fibrosis transmembrane conductance regulator homolog (human) | RGD1561193 |
| B12 | Rn.10440 | NM_013147 | Clcn1 | Chloride channel 1 | SMCC |
| C01 | Rn.11073 | NM_017137 | Clcn2 | Chloride channel 2 | CIC-2 |

| | | | | | |
|-----|-----------|--------------|---------|--|-------------------------------|
| C02 | Rn.4175 | NM_053363 | Clcn3 | Chloride channel 3 | CIC-3 |
| C03 | Rn.44406 | NM_022198 | Clcn4-2 | Chloride channel 4-2 | Clcn4, MGC105433 |
| C04 | Rn.10337 | NM_017106 | Clcn5 | Chloride channel 5 | CLC5 |
| C05 | Rn.7226 | NM_001106479 | Clcn6 | Chloride channel 6 | - |
| C06 | Rn.10338 | NM_031568 | Clcn7 | Chloride channel 7 | CIC-7 |
| C07 | Rn.203139 | NM_001002807 | Clic1 | Chloride intracellular channel 1 | - |
| C08 | Rn.103254 | NM_001009651 | Clic2 | Chloride intracellular channel 2 | MGC108828 |
| C09 | Rn.9769 | NM_173095 | Kcna1 | Potassium voltage-gated channel, shaker-related subfamily, member 1 | Kcna, Kcpvd, Kv1.1 |
| C10 | Rn.10298 | NM_012970 | Kcna2 | Potassium voltage-gated channel, shaker-related subfamily, member 2 | BK2, NGK1 |
| C11 | Rn.44292 | NM_019270 | Kcna3 | Potassium voltage-gated channel, shaker-related subfamily, member 3 | - |
| C12 | Rn.207159 | NM_012971 | Kcna4 | Potassium voltage-gated channel, shaker-related subfamily, member 4 | KCHAN, Kv1.4, Kv4, RHK1, RK3 |
| D01 | Rn.162789 | NM_012972 | Kcna5 | Potassium voltage-gated channel, shaker-related subfamily, member 5 | Kv1, Kv1.5 |
| D02 | Rn.162791 | NM_023954 | Kcna6 | Potassium voltage gated channel, shaker related subfamily, member 6 | Kv1.6 |
| D03 | Rn.26724 | NM_013186 | Kcna1 | Potassium voltage gated channel, Shab-related subfamily, member 1 | DRK1PC, Kcr1-1, Kv2.1, Shab |
| D04 | Rn.33095 | NM_012856 | Kcnc1 | Potassium voltage gated channel, Shaw-related subfamily, member 1 | KShIIIB, Kv3.1, Kv4, NGK2-KV4 |
| D05 | Rn.9885 | NM_053997 | Kcnc3 | Potassium voltage gated channel, Shaw-related subfamily, member 3 | KShIIID |
| D06 | Rn.9458 | NM_001105748 | Kcnd1 | Potassium voltage-gated channel, Shal-related subfamily, member 1 | Kv4.1 |
| D07 | Rn.87841 | NM_031730 | Kcnd2 | Potassium voltage-gated channel, Shal-related subfamily, member 2 | Kv4.2, RK5, Shall1 |
| D08 | Rn.10540 | NM_031739 | Kcnd3 | Potassium voltage-gated channel, Shal-related subfamily, member 3 | Kv4.3 |
| D09 | Rn.9734 | NM_012973 | Kcne1 | Potassium voltage-gated channel, Isk-related family, member 1 | Isk, m |
| D10 | Rn.91148 | NM_001169104 | Kcnf1 | Potassium voltage-gated channel, subfamily F, member 1 | Kh1, Kv5.1 |
| D11 | Rn.11071 | NM_031742 | Kcnh1 | Potassium voltage-gated channel, subfamily H (eag-related), member 1 | - |
| D12 | Rn.10970 | NM_053949 | Kcnh2 | Potassium voltage-gated channel, subfamily H (eag-related), member 2 | ERG1 |
| E01 | Rn.144567 | NM_017108 | Kcnh3 | Potassium voltage-gated channel, subfamily H (eag-related), member 3 | Bec1, Elk2 |
| E02 | Rn.22609 | NM_017023 | Kcnj1 | Potassium inwardly-rectifying channel, subfamily J, member 1 | Kcnj, ROMK1 |
| E03 | Rn.3985 | NM_031358 | Kcnj11 | Potassium inwardly rectifying channel, subfamily J, member 11 | Kir6.2 |
| E04 | Rn.81018 | NM_133321 | Kcnj15 | Potassium inwardly-rectifying channel, subfamily J, member 15 | Kir4.2 |
| E05 | Rn.9809 | NM_031610 | Kcnj3 | Potassium inwardly-rectifying channel, subfamily J, member 3 | - |
| E06 | Rn.10197 | NM_053870 | Kcnj4 | Potassium inwardly-rectifying channel, subfamily J, member 4 | Hirk2 |
| E07 | Rn.10047 | NM_017297 | Kcnj5 | Potassium inwardly-rectifying channel, subfamily J, member 5 | MGC93525 |

| | | | | | |
|-----|-----------|-----------|---------|---|----------------------------------|
| E08 | Rn.10185 | NM_013192 | Kcnj6 | Potassium inwardly-rectifying channel, subfamily J, member 6 | - |
| E09 | Rn.118306 | NM_017099 | Kcnj8 | Potassium inwardly-rectifying channel, subfamily J, member 8 | Kir6.1, UKATP1, uKATP-1 |
| E10 | Rn.10820 | NM_019273 | Kcnmb1 | Potassium large conductance calcium-activated channel, subfamily M, beta member 1 | - |
| E11 | Rn.44422 | NM_019313 | Kcnn1 | Potassium intermediate/small conductance calcium-activated channel, subfamily N, member 1 | KCa2.1 |
| E12 | Rn.44421 | NM_019314 | Kcnn2 | Potassium intermediate/small conductance calcium-activated channel, subfamily N, member 2 | KCa2.2 |
| F01 | Rn.10840 | NM_019315 | Kcnn3 | Potassium intermediate/small conductance calcium-activated channel, subfamily N, member 3 | KCa2.3, SK3 |
| F02 | Rn.44212 | NM_023021 | Kcnn4 | Potassium intermediate/small conductance calcium-activated channel, subfamily N, member 4 | KCa3.1, MGC156636, rKCNN4c, rSK4 |
| F03 | Rn.9779 | NM_032073 | Kcnq1 | Potassium voltage-gated channel, KQT-like subfamily, member 1 | Kvlqt1 |
| F04 | Rn.33317 | NM_133322 | Kcnq2 | Potassium voltage-gated channel, KQT-like subfamily, member 2 | - |
| F05 | Rn.205060 | NM_031597 | Kcnq3 | Potassium voltage-gated channel, KQT-like subfamily, member 3 | - |
| F06 | Rn.144875 | XM_233477 | Kcnq4 | Potassium voltage-gated channel, KQT-like subfamily, member 4 | - |
| F07 | Rn.30012 | NM_053954 | Kcns1 | Potassium voltage-gated channel, delayed-rectifier, subfamily S, member 1 | Kv9.1 |
| F08 | Rn.64498 | NM_023966 | Kcns2 | Potassium voltage-gated channel, delayed-rectifier, subfamily S, member 2 | - |
| F09 | Rn.10878 | NM_031778 | Kcns3 | Potassium voltage-gated channel, delayed-rectifier, subfamily S, member 3 | - |
| F10 | Rn.32079 | NM_030875 | Scn1a | Sodium channel, voltage-gated, type I, alpha | - |
| F11 | Rn.4958 | NM_017288 | Scn1b | Sodium channel, voltage-gated, type I, beta | - |
| F12 | Rn.88636 | NM_012877 | Scn2b | Sodium channel, voltage-gated, type II, beta | SCNB2 |
| G01 | Rn.87394 | NM_013119 | Scn3a | Sodium channel, voltage-gated, type III, alpha | Nav1.3, SCIII, Scn2a |
| G02 | Rn.9700 | NM_013178 | Scn4a | Sodium channel, voltage-gated, type IV, alpha subunit | NCHVS, Nav1.4, microI |
| G03 | Rn.32074 | NM_013125 | Scn5a | Sodium channel, voltage-gated, type V, alpha subunit | SCAL |
| G04 | Rn.54541 | NM_031686 | Scn7a | Sodium channel, voltage-gated, type VII, alpha | Na-G, Scn6a |
| G05 | Rn.91216 | NM_019266 | Scn8a | Sodium channel, voltage gated, type VIII, alpha subunit | - |
| G06 | Rn.88082 | NM_133289 | Scn9a | Sodium channel, voltage-gated, type IX, alpha | Nav1.7, PN1, Scn2a |
| G07 | Rn.9987 | NM_031663 | Slc18a3 | Solute carrier family 18 (vesicular acetylcholine), member 3 | VACht, rVAT |
| G08 | Rn.6384 | NM_013032 | Slc1a1 | Solute carrier family 1 | Eaac1, Eaat3, |

| | | | | | |
|-----|-----------|--------------|---------|---|----------------------------|
| | | | | (neuronal/epithelial high affinity glutamate transporter, system Xag), member 1 | REAAC1 |
| G09 | Rn.11352 | NM_017335 | Slc6a12 | Solute carrier family 6 (neurotransmitter transporter, betaine/GABA), member 12 | BGT1, Gat1, RNU28927, VGAT |
| G10 | Rn.10093 | NM_012694 | Slc6a3 | Solute carrier family 6 (neurotransmitter transporter, dopamine), member 3 | Dat1 |
| G11 | Rn.32110 | NM_053818 | Slc6a9 | Solute carrier family 6 (neurotransmitter transporter, glycine), member 9 | GLYT-1, GLYT-1b, Glyt1 |
| G12 | Rn.54594 | NM_031353 | Vdac1 | Voltage-dependent anion channel 1 | - |
| H01 | Rn.973 | NM_001007604 | Rplp1 | Ribosomal protein, large, P1 | MGC72935 |
| H02 | Rn.47 | NM_012583 | Hprt1 | Hypoxanthine phosphoribosyltransferase 1 | Hgpptase, Hprt, MGC112554 |
| H03 | Rn.92211 | NM_173340 | Rpl13a | Ribosomal protein L13A | - |
| H04 | Rn.107896 | NM_017025 | Ldha | Lactate dehydrogenase A | Ldh1 |
| H05 | Rn.94978 | NM_031144 | Actb | Actin, beta | Actx |
| H06 | N/A | U26919 | RGDC | Rat Genomic DNA Contamination | RGDC |
| H07 | N/A | SA_00104 | RTC | Reverse Transcription Control | RTC |
| H08 | N/A | SA_00104 | RTC | Reverse Transcription Control | RTC |
| H09 | N/A | SA_00104 | RTC | Reverse Transcription Control | RTC |
| H10 | N/A | SA_00103 | PPC | Positive PCR Control | PPC |
| H11 | N/A | SA_00103 | PPC | Positive PCR Control | PPC |
| H12 | N/A | SA_00103 | PPC | Positive PCR Control | PPC |

APPENDIX B: ETHICS APPROVAL (Rat)



AUP Number: 2010-017

PI Name: Poulter, Michael

AUP Title: Electrophysiological and Genetic Studies of the Kindled Central Nervous System

The YEARLY RENEWAL to Animal Use Protocol (AUP) 2010-017 has been approved.

1. This AUP number must be indicated when ordering animals for this project.
2. Animals for other projects may not be ordered under this AUP number.
3. Purchases of animals other than through this system must be cleared through the ACVS office.

Health certificates will be required.

REQUIREMENTS/COMMENTS

Please ensure that individual(s) performing procedures on live animals, as described in this protocol, are familiar with the contents of this document.

The holder of this Animal Use Protocol is responsible to ensure that all associated safety components (biosafety, radiation safety, general laboratory safety) comply with institutional safety standards and have received all necessary approvals. Please consult directly with your institutional safety officers.

Submitted by: Thompson, Sharla H
on behalf of the Animal Use Subcommittee

APPENDIX C: COPYRIGHT LICENSE AGREEMENT

JOHN WILEY AND SONS LICENSE TERMS AND CONDITIONS

Sep 30, 2011

This is a License Agreement between Cezar Gavrilovici ("You") and John Wiley and Sons ("John Wiley and Sons") provided by Copyright Clearance Center ("CCC"). The license consists of your order details, the terms and conditions provided by John Wiley and Sons, and the payment terms and conditions.

All payments must be made in full to CCC. For payment instructions, please see information listed at the bottom of this form.

| | |
|------------------------------|---|
| License Number | 2758870791755 |
| License date | Sep 30, 2011 |
| Licensed content publisher | John Wiley and Sons |
| Licensed content publication | Journal of Comparative Neurology |
| Licensed content title | Diverse interneuron populations have highly specific interconnectivity in the rat piriform cortex |
| Licensed content author | Cezar Gavrilovici,Sabrina D'Alfonso,Michael O. Poulter |
| Licensed content date | May 1, 2010 |
| Start page | 1570 |
| End page | 1588 |
| Type of use | Dissertation/Thesis |
| Requestor type | Author of this Wiley article |
| Format | Print and electronic |
| Portion | Full article |

Terms and Conditions

TERMS AND CONDITIONS

This copyrighted material is owned by or exclusively licensed to John Wiley & Sons, Inc. or one of its group companies (each a "Wiley Company") or a society for whom a Wiley Company has exclusive publishing rights in relation to a particular journal (collectively WILEY"). By clicking "accept" in connection with completing this licensing transaction, you agree that the following terms and conditions apply to this

transaction (along with the billing and payment terms and conditions established by the Copyright Clearance Center Inc., ("CCC's Billing and Payment terms and conditions"), at the time that you opened your Rightslink account (these are available at any time at <http://myaccount.copyright.com>)

Terms and Conditions

1. The materials you have requested permission to reproduce (the "Materials") are protected by copyright.
2. You are hereby granted a personal, non-exclusive, non-sublicensable, non-transferable, worldwide, limited license to reproduce the Materials for the purpose specified in the licensing process. This license is for a one-time use only with a maximum distribution equal to the number that you identified in the licensing process. Any form of republication granted by this licence must be completed within two years of the date of the grant of this licence (although copies prepared before may be distributed thereafter). The Materials shall not be used in any other manner or for any other purpose. Permission is granted subject to an appropriate acknowledgement given to the author, title of the material/book/journal and the publisher. You shall also duplicate the copyright notice that appears in the Wiley publication in your use of the Material. Permission is also granted on the understanding that nowhere in the text is a previously published source acknowledged for all or part of this Material. Any third party material is expressly excluded from this permission.
3. With respect to the Materials, all rights are reserved. Except as expressly granted by the terms of the license, no part of the Materials may be copied, modified, adapted (except for minor reformatting required by the new Publication), translated, reproduced, transferred or distributed, in any form or by any means, and no derivative works may be made based on the Materials without the prior permission of the respective copyright owner. You may not alter, remove or suppress in any manner any copyright, trademark or other notices displayed by the Materials. You may not license, rent, sell, loan, lease, pledge, offer as security, transfer or assign the Materials, or any of the rights granted to you hereunder to any other person.
4. The Materials and all of the intellectual property rights therein shall at all times remain the exclusive property of John Wiley & Sons Inc or one of its related companies (WILEY) or their respective licensors, and your interest therein is only that of having possession of and the right to reproduce the Materials pursuant to Section 2 herein during the continuance of this Agreement. You agree that you own no right, title or interest in or to the Materials or any of the intellectual property rights therein. You shall have no rights hereunder other than the license as provided for above in Section 2. No right, license or interest to any trademark, trade name, service mark or other branding ("Marks") of WILEY or its licensors is granted hereunder, and you agree that you shall not assert any such right, license or interest with respect thereto.
5. NEITHER WILEY NOR ITS LICENSORS MAKES ANY WARRANTY OR REPRESENTATION OF ANY KIND TO YOU OR ANY THIRD PARTY,

EXPRESS, IMPLIED OR STATUTORY, WITH RESPECT TO THE MATERIALS OR THE ACCURACY OF ANY INFORMATION CONTAINED IN THE MATERIALS, INCLUDING, WITHOUT LIMITATION, ANY IMPLIED WARRANTY OF MERCHANTABILITY, ACCURACY, SATISFACTORY QUALITY, FITNESS FOR A PARTICULAR PURPOSE, USABILITY, INTEGRATION OR NON-INFRINGEMENT AND ALL SUCH WARRANTIES ARE HEREBY EXCLUDED BY WILEY AND ITS LICENSORS AND WAIVED BY YOU.

6. WILEY shall have the right to terminate this Agreement immediately upon breach of this Agreement by you.

7. You shall indemnify, defend and hold harmless WILEY, its Licensors and their respective directors, officers, agents and employees, from and against any actual or threatened claims, demands, causes of action or proceedings arising from any breach of this Agreement by you.

8. IN NO EVENT SHALL WILEY OR ITS LICENSORS BE LIABLE TO YOU OR ANY OTHER PARTY OR ANY OTHER PERSON OR ENTITY FOR ANY SPECIAL, CONSEQUENTIAL, INCIDENTAL, INDIRECT, EXEMPLARY OR PUNITIVE DAMAGES, HOWEVER CAUSED, ARISING OUT OF OR IN CONNECTION WITH THE DOWNLOADING, PROVISIONING, VIEWING OR USE OF THE MATERIALS REGARDLESS OF THE FORM OF ACTION, WHETHER FOR BREACH OF CONTRACT, BREACH OF WARRANTY, TORT, NEGLIGENCE, INFRINGEMENT OR OTHERWISE (INCLUDING, WITHOUT LIMITATION, DAMAGES BASED ON LOSS OF PROFITS, DATA, FILES, USE, BUSINESS OPPORTUNITY OR CLAIMS OF THIRD PARTIES), AND WHETHER OR NOT THE PARTY HAS BEEN ADVISED OF THE POSSIBILITY OF SUCH DAMAGES. THIS LIMITATION SHALL APPLY NOTWITHSTANDING ANY FAILURE OF ESSENTIAL PURPOSE OF ANY LIMITED REMEDY PROVIDED HEREIN.

9. Should any provision of this Agreement be held by a court of competent jurisdiction to be illegal, invalid, or unenforceable, that provision shall be deemed amended to achieve as nearly as possible the same economic effect as the original provision, and the legality, validity and enforceability of the remaining provisions of this Agreement shall not be affected or impaired thereby.

10. The failure of either party to enforce any term or condition of this Agreement shall not constitute a waiver of either party's right to enforce each and every term and condition of this Agreement. No breach under this agreement shall be deemed waived or excused by either party unless such waiver or consent is in writing signed by the party granting such waiver or consent. The waiver by or consent of a party to a breach of any provision of this Agreement shall not operate or be construed as a waiver of or consent to any other or subsequent breach by such other party.

11. This Agreement may not be assigned (including by operation of law or otherwise) by you without WILEY's prior written consent.

12. Any fee required for this permission shall be non-refundable after thirty (30) days from receipt.

13. These terms and conditions together with CCC's Billing and Payment terms and conditions (which are incorporated herein) form the entire agreement between you and WILEY concerning this licensing transaction and (in the absence of fraud) supersedes all prior agreements and representations of the parties, oral or written. This Agreement may not be amended except in writing signed by both parties. This Agreement shall be binding upon and inure to the benefit of the parties' successors, legal representatives, and authorized assigns.

14. In the event of any conflict between your obligations established by these terms and conditions and those established by CCC's Billing and Payment terms and conditions, these terms and conditions shall prevail.

15. WILEY expressly reserves all rights not specifically granted in the combination of (i) the license details provided by you and accepted in the course of this licensing transaction, (ii) these terms and conditions and (iii) CCC's Billing and Payment terms and conditions.

16. This Agreement will be void if the Type of Use, Format, Circulation, or Requestor Type was misrepresented during the licensing process.

17. This Agreement shall be governed by and construed in accordance with the laws of the State of New York, USA, without regards to such state's conflict of law rules. Any legal action, suit or proceeding arising out of or relating to these Terms and Conditions or the breach thereof shall be instituted in a court of competent jurisdiction in New York County in the State of New York in the United States of America and each party hereby consents and submits to the personal jurisdiction of such court, waives any objection to venue in such court and consents to service of process by registered or certified mail, return receipt requested, at the last known address of such party.

Wiley Open Access Terms and Conditions

All research articles published in Wiley Open Access journals are fully open access: immediately freely available to read, download and share. Articles are published under the terms of the Creative Commons Attribution Non Commercial License, which permits use, distribution and reproduction in any medium, provided the original work is properly cited and is not used for commercial purposes. The license is subject to the Wiley Open Access terms and conditions:

Wiley Open Access articles are protected by copyright and are posted to repositories and websites in accordance with the terms of the Creative Commons Attribution Non Commercial License. At the time of deposit, Wiley Open Access articles include all changes made during peer review, copyediting, and publishing. Repositories and websites that host the article are responsible for incorporating any publisher-supplied amendments or retractions issued subsequently.

Wiley Open Access articles are also available without charge on Wiley's publishing platform, Wiley Online Library or any successor sites.

Use by non-commercial users

For non-commercial and non-promotional purposes individual users may access, download, copy, display and redistribute to colleagues Wiley Open Access articles,

as well as adapt, translate, text- and data-mine the content subject to the following conditions:

- The authors' moral rights are not compromised. These rights include the right of "paternity" (also known as "attribution" - the right for the author to be identified as such) and "integrity" (the right for the author not to have the work altered in such a way that the author's reputation or integrity may be impugned).
- Where content in the article is identified as belonging to a third party, it is the obligation of the user to ensure that any reuse complies with the copyright policies of the owner of that content.
- If article content is copied, downloaded or otherwise reused for non-commercial research and education purposes, a link to the appropriate bibliographic citation (authors, journal, article title, volume, issue, page numbers, DOI and the link to the definitive published version on Wiley Online Library) should be maintained. Copyright notices and disclaimers must not be deleted.
- Any translations, for which a prior translation agreement with Wiley has not been agreed, must prominently display the statement: "This is an unofficial translation of an article that appeared in a Wiley publication. The publisher has not endorsed this translation."

Use by commercial "for-profit" organisations

Use of Wiley Open Access articles for commercial, promotional, or marketing purposes requires further explicit permission from Wiley and will be subject to a fee. Commercial purposes include:

- Copying or downloading of articles, or linking to such articles for further redistribution, sale or licensing;
- Copying, downloading or posting by a site or service that incorporates advertising with such content;
- The inclusion or incorporation of article content in other works or services (other than normal quotations with an appropriate citation) that is then available for sale or licensing, for a fee (for example, a compilation produced for marketing purposes, inclusion in a sales pack)
- Use of article content (other than normal quotations with appropriate citation) by for-profit organisations for promotional purposes
- Linking to article content in e-mails redistributed for promotional, marketing or educational purposes;
- Use for the purposes of monetary reward by means of sale, resale, licence, loan, transfer or other form of commercial exploitation such as marketing products
- Print reprints of Wiley Open Access articles can be purchased from: corporatesales@wiley.com

CURRICULUM VITAE

- Name:** Cezar Gavrilovici
- Post-secondary Education and Degrees:**
- Alexandru Ioan Cuza University
Iasi, Romania, 1991-1996 BSc in Biology
 - Alexandru Ioan Cuza University
Iasi, Romania, 1996-1997 MSc in Biology
 - Carleton University
Ottawa, Ontario, Canada, 2002- 2004 MSc in Neuroscience
- Honours and Awards:**
- Governmental Undergraduate Scholarship, 1992 – 1996
 - Graduate Studies Scholarship, 2002 - 2005
 - Schulich Graduate Scholarship, 2006 - 2010
 - Ontario Graduate Scholarship, 2009- 2010
- Related Work Experience:**
- University Instructor
Alexandru Ioan Cuza University, 1998- 2001
 - Assistant Professor
Alexandru Ioan Cuza University, 2001- 2002
 - Teaching Assistant
Carleton University, 2003- 2006
University of Western Ontario, 2006- 2010
- Publications:**
- Gavrilovici C, D'Alfonso S, Poulter MO.** (2010) Diverse interneuron populations have highly specific interconnectivity in the rat piriform cortex. *J Comp Neurol.* **518**(9): 1570-1588
- Gavrilovici C, D'Alfonso S, Dann M, Poulter MO.** (2006) Kindling-induced alterations in GABA_A receptor mediated inhibition and neurosteroid activity in the piriform cortex of rat. *Eur J. Neurosci.* **24**(5): 1373-1384

Schwabe K, **Gavrilovici C**, McIntyre DC, Poulter MO. (2005) Neurosteroids exhibit differential effects on mIPSCs recorded from normal and seizure prone rats. *J Neurophysiol.* **94**(3): 2171-81.

Meguro R, Lu J, **Gavrilovici C**, Poulter MO. (2004) Static, transient and permanent organization of GABA receptor expression in calbindin-positive interneurons in response to amygdala kindled seizures. *J Neurochem.* **91**(1): 144-54.